ROLE OF MICRORNAs IN REGULATING MITOCHONDRIAL BIOGENESIS AND FUNCTION

Thesis Submitted
in Partial Fulfilment of the Requirement for the
Degree of

DOCTOR OF PHILOSOPHY

by

Kritika Sharma
(2K19/PHDBT/12)

Under the Supervision of

Supervisor
Prof. Yasha Hasija, PhD
Department of Biotechnology,
Delhi Technological University

Joint-Supervisor
Dr. Neeru Saini, PhD
Chief Scientist, CSIR-IGIB
Professor, AcSIR

To the
Department of Biotechnology

DELHI TECHNOLOGICAL UNIVERSITY
(Formerly Delhi College of Engineering)
Shahbad Daulatpur, Main Bawana Road, Delhi-110042, India

November 2024

DELHI TECHNOLOGICAL UNIVERSITY

(Formerly Delhi College of Engineering)

Shahbad Daulatpur, Main Bawana Road, Delhi-110042, India

CANDIDATE'S DECLARATION

I **Kritika Sharma** hereby declare that the work being presented in the thesis entitled **"Role of MicroRNAs in Regulating Mitochondrial Biogenesis and Function"** in the partial fulfillment of the requirement for the award of degree of Doctor of Philosophy submitted in the **Department of Biotechnology**, Delhi Technological University is an authentic record of my work carried out during the period **from 2019 to 2024** under the supervision of **Prof. Yasha Hasija (Supervisor) and Dr. Neeru Saini (Joint- Supervisor).**

The matter presented in the thesis has not been submitted for the award of this or any other institute.

Kritika Sharma

Candidate's Signature

This is to certify that the student has incorporated all the corrections suggested by the examiners in the thesis and the statement made by the candidate is correct to the best of our knowledge.

17.12.24

Signature of Supervisor(s)

17.12.24

Signature of External Examiner

17/12/24

DELHI TECHNOLOGICAL UNIVERSITY

(Formerly Delhi College of Engineering)

Shahbad Daulatpur, Main Bawana Road, Delhi-110042, India

CERTIFICATE

Certified that **Kritika Sharma (2K19/PhD/BT12)** has carried out her research work in this thesis entitled "**Role of MicroRNAs in Regulating Mitochondrial Biogenesis and Function**" for the award of **Doctor of Philosophy** from the Department of Biotechnology to Delhi Technological University, Delhi, under our supervision. The thesis embodies the results of the original work, and studies carried out by the student herself and the contents of the thesis do not form the basis for the award of any other degree to the candidate or to anybody else from this or any other university/institute.

Supervisor

Prof. Yasha Hasija, PhD

Department of Biotechnology,

Delhi Technological University

Place: Delhi

Joint-Supervisor

Dr. Neeru Saini, PhD

Chief Scientist, CSIR-IGIB

Professor, AcSIR

Place: Delhi

Date: 17-12-24

Abstract

Coordination between energy intake, storage, and expenditure is necessary for energy homeostasis. Variations in one of these processes are often balanced out in healthy individuals by control of the other two. On the other hand, metabolic disorders result from deviations from the improper balance of the caloric equation. A comprehensive investigation over the following century identified two key roles of mitochondria: producing ATP, the cell's energy currency, and creating biosynthetic intermediates to maintain energy homeostasis. This abstract summarized the findings from three independent studies linking the pivotal role of microRNA-128 (miR-128) in mitochondrial biogenesis and function as well as its implications for metabolic disorders. First, we had established a direct link between miR-128 and extensively described as a master regulator of mitochondrial biogenesis and oxidative phosphorylation PGC1α *in vitro and in vivo*. Overexpression of miR-128 in C2C12 myoblasts reduced mitochondrial biogenesis, altered dynamics, and impaired ATP production leading to mitochondrial dysfunction. Conversely, Inhibition of miR-128 expression improved mitochondrial health and oxidative phosphorylation. Second, we have tried to identify the key genes associated with mitochondrial function and their mRNA-miRNA network by employing an integrated approach of machine learning-based feature selection and explainable artificial intelligence. We found BAX, a target of the miR-128 gene, as one of the top features in the study. We have previously shown the role of miR-128 in mitochondrial dysfunction by directly targeting BAX. In addition, the interaction network highlighted the regulatory role of miR-375, miR-30a-5p, miR-16-5p, miR-129-5p, miR-1229-3p, and miR-1224-3p, offering insights into novel therapeutic targets. Third, we have identified miR-128's potential as a regulator of BICD1 as a target, impacting intracellular transportation of HIF1α which correlates with reduced activity and affects mitochondrial metabolism. In summary, these studies collectively contributed to our understanding of the molecular mechanisms linked to miR-128, mitochondrial function, and metabolic disorders, offering insights into potential therapeutic targets and early intervention strategies for metabolic disorders like obesity and T2DM.

Acknowledgment

I am pleased to thank the people who made this research work possible.

First and foremost, I would like to express my deepest gratitude to my supervisor, **Prof. Yasha Hasija**, and joint supervisor, **Dr. Neeru Saini**, for their invaluable guidance, unwavering support, and constant encouragement throughout this project. Their expertise and insightful feedback have been crucial in shaping the direction and quality of this research. I am sincerely thankful for their extensive knowledge and critical suggestions, which have enriched this work significantly. Their combined mentorship has been the key driving force behind the successful completion of this endeavor.

I want to express my heartfelt gratitude to my supervisor**, Prof. Yasha Hasija**, for giving me the invaluable opportunity to work under her guidance. Her constant support and encouragement have been instrumental in my academic growth. This opportunity has introduced me to the fascinating world of Artificial Intelligence and allowed me to explore it in ways I never imagined. Her expertise, insights, and unwavering belief in my potential have been crucial in shaping my research journey, and for that, I am deeply thankful.

I want to extend my deepest gratitude to **Dr. Neeru Saini**, whose invaluable support and guidance have been instrumental in shaping my academic journey. Her encouragement to think critically and approach challenges like a true PhD scholar has had a profound impact on my intellectual growth. I am incredibly grateful for the first hands-on platform she provided me, which allowed me to explore, experiment, and develop essential research skills. Throughout this journey, she has demonstrated remarkable patience, always providing thoughtful feedback and mentorship as I navigated new concepts and challenges. Her unwavering belief in my potential has not only helped me develop academically, but she has also been a pillar of personal support during times of need. Her kindness, understanding, and encouragement have meant the world to me, and I am forever thankful for the positive impact she has had on both my academic and personal development.

I extend my sincere gratitude to the **Vice Chancellor of Delhi Technological University (DTU)**, and the **Director of CSIR-IGIB**, their leadership has fostered an environment of innovation and collaboration, enabling me to excel in my work. The opportunities provided by CSIR-IGIB and DTU have been critical to my research and academic development. I also extend my sincerest thanks to my DRC members, **Dr. Prof Jaigopal Sharma** (DTU), **Dr. Shilpa Pal** (DTU), **Dr. Seema Kashyap** (AIIMS), **Dr. Tapsaya Srivastava** (Delhi University) for critically reviewing my work and making insightful suggestions. I also acknowledge the other scientists at IGIB for letting me use their lab facilities in the phase of COVID-19.

I consider myself incredibly fortunate to have had seniors like **Dr. Ravindresh** and **Dr. Yogita,** whose work I had the privilege of carrying forward. **Dr. Richa Singh** taught me the valuable lesson of never repeating the same mistake but always striving to make new ones and grow from them. **Dr. Richa Dubey,** the sweetest of all, and **Dr. Pallavi,** who not only taught me technicalities but also asked the most thought-provoking questions about experiments, have been crucial to my learning. **Dr. Shruti** and **Sachin** exemplified good lab practices and profoundly impacted my professional growth. Each was a great source of inspiration and encouragement, always ready to help when needed.

I would also like to thank my lab members from both labs **Raj Kumar** for helping me whether day or night with my queries and the SHAP paper**. Neha**, **Richa**, **Jaishree**, **Kushi**, **Nakul**, **Mansi**, **Himani**, **Amit**, **Bharat**, **Raj Rajeshwar**, **Partibha**, and **Sneha** for their continuous support and cooperation. A special thanks goes to **Harshi and Anushka**, who walked miles for me in times of need. They helped maintain a positive, cheerful atmosphere in the lab, making this long, challenging PhD journey even more pleasant.

I would also like to extend a special thanks to **Dr. Arun Nandwani**, my rakhi brother, and **Dr. Manoj**, **Dr. Ahmed**, **Dr. Shakti**, **Dr. Shagun**, **Dr. Neha Kanojia**, **Dr. Amit Yadav**, **Dr. Devesh**, **Dr. Rukhsar**, **Manish, Dr. Naresh, Priyanka, Dr. Shweta** and **Ashima**. They have been incredibly helpful in my work and experiments, taking mock presentations, ensuring I wasn't left alone during late time points, and always sharing

lab chemicals, for the Mall Road Badminton group and coffee table fun in the canteen. A special mention goes to **Dr Neha Kanojia**, who supported me immensely when I first moved out, with her kindness and the delicious lunches and dinners she made for me.

I would like to express my heartfelt gratitude to my wonderful roommate, **Jyoti Sain**, who has played an irreplaceable role in my journey. She helped me maintain a balance between work and life, fun nights, and the healing she so effortlessly brought into my life. Even though she is now miles away, I am still thankful for all the ways she has supported me. Jyoti has truly become like a sister to me, and I am forever grateful to the universe for bringing such a remarkable person into my life. I would also like to extend my thanks to **Dr. Sanyogita, Jyoti**, **Aashna**, **Aashna's mother, Amit Bhaiya, and Bhabhi**. They ensured that I never had to make food for myself, and it never felt like I was living away from home. Their warmth and kindness made this journey so much more comforting. I am deeply appreciative of the love, support, and care that each of them has shown me.

I would like to extend my heartfelt thanks to my childhood friends, **Ridhima Suri**, **Dr. Piya Patra**, **Sampurna Rudra**, and **Dr. Suvankar Ghosh**, for their constant support and for persistently nagging me about when I was going to register and then submit—it truly kept me on track! Their encouragement and companionship have meant the world to me throughout this journey. A special mention goes to **Dr Usha Sankhla** for her incredible help during the times of my life and when I had to move to different places. Her presence made life and those transitions so much easier and less stressful. I am truly grateful for the unwavering support and love my friends have given me, and I cherish their role in this journey.

I owe my deepest gratitude to my parents, **my mother and father**, for their unwavering support and for always allowing me to be myself. Their dedication to my education has been invaluable, and I am profoundly thankful for their belief in me. I am incredibly blessed to have parents who never pressured or troubled me about my studies, but instead, provided me with the freedom to pursue my path at my own pace. I would also like to thank **my brother** for his constant support and for taking care of

the family while I was away. His presence and responsibility gave me peace of mind to focus on my journey.

Special thanks to my aunt, **Asha Sharma**, and my cousins, **Meenakshi and Atul**, for their support. Their love and encouragement have been a great source of strength for me throughout this journey. I am truly grateful to the universe for giving me such wonderful, understanding parents, a supportive brother, and a loving extended family, all of whom have been the foundation of my growth.

I would like to extend my heartfelt thanks to the street animals, both pets and strays, who have brought me immense joy and comfort during challenging times, especially throughout the pandemic. Their presence took away so much of my stress and filled my heart with love. I am deeply grateful to these wonderful souls for coming to me for help and for offering their companionship without asking for anything in return. A special mention goes to the **Late Burbon, Late Tiger, Heroine, Bhura, Duggu, Tomu, and Tiger**—each of them have had left a lasting imprint on my heart. Their unconditional love and presence have been a source of healing, and I will always cherish the memories they've given me. They have reminded me of the simple yet profound joy of caring and being cared for, and for that, I am eternally grateful.

Lastly, I would like to express my deepest gratitude to the almighty Ganesh Ji for his divine guidance, blessings, and presence throughout this journey. His grace has provided me with strength, wisdom, and clarity, especially during the most challenging times. With folded hands, I offer my sincere thanks to Ganesh Ji.

I would also like to extend my heartfelt thanks to everyone who has played a part in this journey. Whether mentioned by name or not, each of you has made a difference in your special way.

List of Publications

1. Sharma K, Chandra A, Hasija Y, Saini N. MicroRNA-128 inhibits mitochondrial biogenesis and function via targeting PGC1α and NDUFS4. Mitochondrion. 2021 Sep;60:160-169. doi: 10.1016/j.mito.2021.08.008. Epub 2021 Aug 9. PMID: 34384932.
2. Sharma K, Saini N, Hasija Y. Identifying the mitochondrial metabolism network by integration of machine learning and explainable artificial intelligence in skeletal muscle in type 2 diabetes. Mitochondrion. 2024 Jan;74:101821. doi: 10.1016/j.mito.2023.11.004. Epub 2023 Nov 29. PMID: 38040172.

List of Tables

List of Figures

List of Abbreviations

AMPK: AMP-Activated Catalytic Protein Kinase

ATP: Adenosine Triphosphate

ATF2: Activating Transcription Factor 2

CAMK2: Ca2+/Calmodulin-Dependent Protein Kinase 2

CCT3: Chaperonin Containing TCP1 Subunit 3

cDNA: Complementary DNA

COX1: Cytochrome c oxidase subunit

COX2: Cytochrome c oxidase subunit 2

DMSO: Dimethylsulphoxide

ETC: Electron Transport Chain

FCS: Fetal calf serum

FGF19: Fibroblast Growth Factor 19

FOXO3: Forkhead Box O3

GSK3β: Glycogen Synthase Kinase 3 Beta

IGF-1: Insulin Like Growth Factor 1

miRNA: microRNA

mtDNA: Mitochondrial DNA

MEF2: Myocyte Enhancer Factor 2

nDNA: nuclear DNA

ND1: NADH Dehydrogenase Subunit 1

OCR: Oxygen Consumption Rate

OXPHOS: Oxidative Phosphorylation

3’UTR: 3’ Untranslated region

PCR: Polymerase chain reaction

PDK1: Pyruvate Dehydrogenase Kinase 1

RICTOR: RPTOR Independent Companion of MTOR Complex 2

ROS: Reaction Oxygen Species

S.E.M.: Standard Error Mean

SHAP: SHapley Additive exPlanations

T2DM: Type 2 Diabetes

TCA cycle - Tricarboxylic Acid Cycle

TMZ: Trimetazidine

TRAIL: Tumor necrosis factor-related apoptosis-inducing ligand

TFB1M: Transcription Factor B1, Mitochondrial

TFB2M: Transcription Factor B2, Mitochondrial

TOMM34: Translocase of Outer Mitochondrial Membrane 34

TRBP: Transactivating response RNA-binding protein

UCP1: Uncoupling Protien

XGBoost: Extreme Gradient Boosting

XAI: Explainable artificial intelligence

Chapter 1

Thesis Overview

1.1 Rationale of the study

The mitochondria are an endosymbiont double-membrane active and dynamic organelle and a significant energy producer (Picard, Wallace, and Burelle 2016). In addition to 22 tRNAs and 2 rRNAs, the mitochondria's ~16.6 kb genome also contains the genes for 13 proteins involved in oxidative phosphorylation (Peng et al. 2022). The control of intracellular pathways such as the tricarboxylic acid cycle, electron transport chain, intracellular ion homeostasis, oxidative stress, lipid metabolism, and amino acid metabolism depends on mitochondria as it actively transduces biological signaling (Friedman and Nunnari 2014).

Mitochondrial biogenesis is highly flexible in response to cellular energy needs, developmental cues, and environmental influences (Dorn and Kitsis 2015). The primary regulator of mitochondrial biogenesis is peroxisome proliferator-activated receptor gamma coactivator 1 (PGC1α) (Rodgers et al. 2005). The nuclear respiratory factors NRF1 and NRF2 are then activated by PGC1α. These nuclear respiratory regulators regulate the signaling of mitochondrial DNA replication-related transcriptional regulators including TFAM (mitochondrial transcription factor A) and genes responsible for oxidative phosphorylation (Cardanho-Ramos and Morais 2021). Mitochondria undergo physical interactions that facilitate the brief exchange of information to cater to the need for cellular energy and homeostasis.

Recent discoveries have highlighted the dynamic nature of mitochondria, undergoing fission, fusion, transport, and degradation for fine-tuning mitochondrial health and cellular homeostasis (Detmer and Chan 2007; Liesa, Palacín, and Zorzano 2009). A state of flux is maintained between these processes to meet the energy demands of the cell. Any impairment of mitochondria is also correlated with secondary diseases such as obesity, cardiovascular diseases, and respiratory ailments leading to increased morbidity and mortality either directly or indirectly (Mengeste, Rustan, and Lund 2021; Prasun 2020). Mitofusin 1 and Mitofusin 2 (MFN1 and MFN2, localized in the outer membrane of the mitochondria) and optic atrophy 1 (OPA1, localized in the inner membrane of the

mitochondria), help in the fusion of the outer membrane and inner membrane of the mitochondria respectively. The fusion helps in increased ATP synthesis capacity and sharing of the metabolites, as well as aid in the biogenesis to produce newly formed organelles. Conversely, the division of the mitochondria into two mitochondria is known as fission and is regulated by dynamin-related protein 1 (DRP1, localized in the cytoplasm). Fission occurs usually to remove the damaged part of the mitochondria when overabundant damaged mitochondria or/ dysfunctional mitochondria are present within the cell. Therefore, there is a need for a greater understanding of these pathway and functions that would lead to novel clinical approaches as well as a better understanding of disease molecular mechanisms.

MicroRNAs are single-stranded small noncoding RNAs that are ~22 nucleotides long. MicroRNA is transcribed in the nucleus as a long primary RNA transcript and then cleaved into a ~70 nucleotide precursor RNA (pre-RNA) with the help of the enzyme drosha. The pre-miRNA is then transported into the cytosol with the help of exportin-5 and Ran-GTP-dependent pathway and further processed by the complex of RNase III, Dicer, and TRBP to form the mature miRNA (O'Brien et al. 2018). miRNAs can target and affect more than one gene by the process of translational repression or mRNA degradation. Each miRNA has a specific 2-8 bases of seed sequence which align according to the Watson-Crick base pairing and bind to the 3'UTR of the target gene (Huang, Xiang, and Song 2022). This makes them a potential key to understanding the role of miRNA in modulating mitochondrial biogenesis and function. Recent studies have shown evidence that miRNA also binds to the gene's intronic region, exonic region, and 5'UTR (Kotagama and McJunkin 2023). Earlier, miR-494-3p, miR-133, and miR-149 have been found to play a role in maintaining mitochondrial homeostasis in skeletal muscle during metabolic disorders (Mohamed et al. 2014; Yin et al. 2013).

Previously, our laboratory has shown that miR-128 targets BAX which in turn leads to mitochondrial dysfunction by regulating the membrane potential (Yogita K. Adlakha and Saini 2011). In addition, our laboratory has established that miR-128 targets SIRT1, an NAD^+ dependent deacetylase exerts the regulation of that gene expression through histone deacetylation. It also plays role in pro-apoptotic effect in a p53 transcription-dependent and independent manner via PUMA-BAK axis (Y. K. Adlakha and Saini 2013). The literature strongly suggests that SIRT1 directly interacts with and deacetylates the master regulator PGC1α causes mitochondrial malfunction by inducing apoptosis through the release of cytochrome c (Zhou et al. 2018).

Prelimnary, *in silico* analysis of microarray expression data (Control vs miR-128 overexpression in HEK cells) led us to identify various target genes of miR-128 involved in mitochondrial biogenesis and function. This list included the extensively researched key regulator PGC1α and various genes in oxidative phosphorylation such as NDUFS4, and NDUFS7. PGC1α and NDUFS4 are the direct targets of miR-128 as predicted by the miRNA target prediction databases such as TargetScan, miRDB, and miRTarbase. Luciferase reporter assay revealed that miR-128 directly targets PGC1α by binding in its 3'UTR.

Based on our preliminary findings, we hypothesized that miR-128 might play a role in the regulation of mitochondrial biogenesis and function. To this end, we framed our objectives to examine the possibility of a coordinated regulation of mitochondrial biogenesis and function by miR-128.

1.2 Objectives

1.2.1 To investigate the role of miR-128 in regulating mitochondrial biogenesis.

1.2.2 To understand the role of miR-128 in regulating networks involved in mitochondrial function.

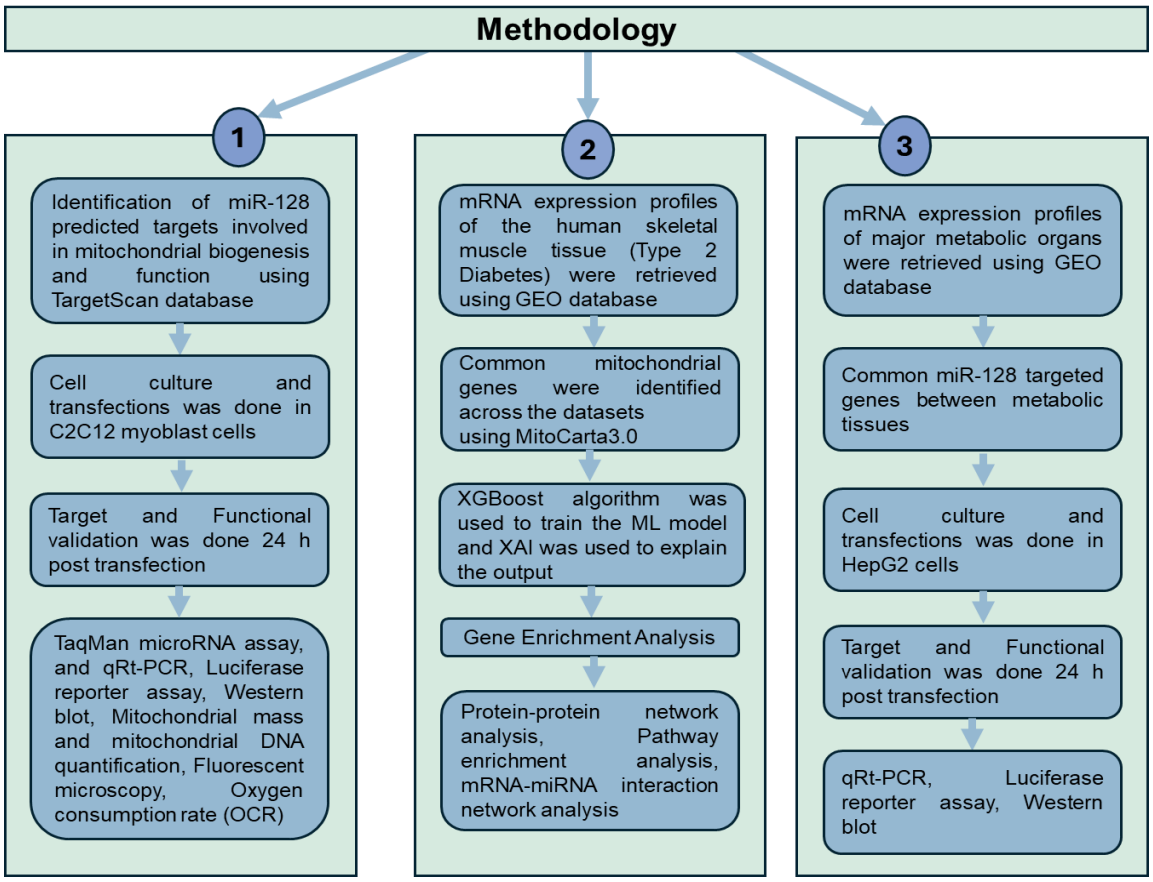

***Figure 1.1**: Flowchart represents the methodology used for the studies.*

Chapter 2

Review of Literature

2.1 Mighty Mitochondria

Mitochondria are central to the production of energy as they have been known as the powerhouse of the cells and are crucial to the homeostasis of life (Al Amir Dache and Thierry 2023). This organelle is supposed to have evolved from *Alphaproteo* bacteria. The theory of the evolution of mitochondria is known as the endo-symbiotic theory (Hill 2020; Wallace 2018). They have evolved certain transcriptional and translational machinery alongside the nuclear genome over the millennia as they have incorporated their mitochondrial DNA (mtDNA). Preserving the double membraned structure from their ancestors, the circular mtDNA (~16 KB for humans) encodes 37 genes. Thirteen proteins code for the respiratory complex subunits (I-V), twenty-two genes code for tRNAs necessary for the translation of the mtDNA-encoded proteins, and two for 12S and 16S rRNAs (El-Hattab, Craigen, and Scaglia 2017).

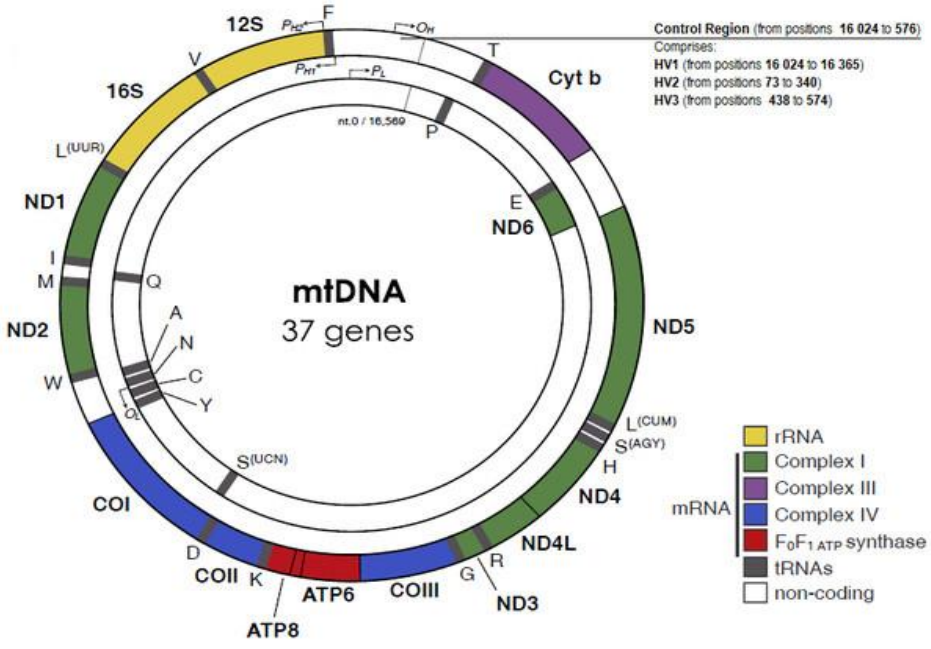

Figure 2.1*: Labelled gene and regulatory areas on the human mitochondrial DNA genome* (Picard, Wallace, and Burelle 2016).

The mtDNA polymerase γ (POLG), which consists of the catalytic subunit expressed by the POLG gene. The RNA Polymerase Mitochondrial (POLRMT) mitochondrial RNA polymerase transcribes the mtDNA (Do et al. 2020). TFAM (transcription factor A, mitochondrial), which ensures mtRNA unwinding and flexing necessary for the POLRMT binding to the mtDNA promoters, is the essential enhancer protein. The unique dissociation factor TFB2M (transcription factor B2, mitochondrial) facilitates interaction between POLRMT and TFAM. TFB1M and TFB2M can both act as rRNA modifiers because they attach to rRNA di-methyltransferases. It has been proposed that rather than acting as a transcription factor, TFB1M's main function is rRNA methylation (Ramachandran et al. 2017). Additionally essential to mtDNA transcription, TFAM's expression regulates the amount of mtDNA copies, therefore serving as a key component in mtDNA maintenance and transmission (Ekstrand et al. 2004).

Nuclei are host to additional proteins that are essential for maintaining the integrity of mtDNA. About 1500 mitochondrial proteins are delivered into the mitochondria encoded by nuclear genes to maintain their homeostasis. These comprise ribosomal proteins, DNA replication and transcription-related proteins, and citric acid cycle-related enzymes. The electron transport chain complexes are composed of proteins encoded by both nucleus and mitochondria genes (Peng et al. 2022). Energy conversion is one of the salient functions of mitochondria. Adenosine triphosphate (ATP), which is produced by aerobic respiration in the mitochondrion, is necessary to maintain bioenergetics and cell energy metabolism. The two primary series of processes that contribute to the production of ATP are the TCA cycle and oxidative phosphorylation (OXPHOS) (Brand et al. 2013). The integration of many metabolic pathways, controlling cellular death, and maintaining the calcium homeostasis mechanism are just a few examples of the molecular systems that control cellular metabolism, which requires the consumption and production of energy. Mitochondria produces metabolic building blocks for macromolecules like lipids, proteins, DNA, and RNA. Therefore, any potential disruption of the mitochondrial system has an impact on the energy equilibrium and controls cellular metabolism (Spinelli and Haigis 2018).

The primary requisite for healthy mitochondria requires dynamic activities including mitochondrial biogenesis, transportation, fission, fusion, and mitophagy. The two healthy, identical mitochondria can be produced from an pre-existing one through biogenesis, which occurs after full growth and successful mitochondrial DNA replication (Das, Sauceda, and Webster 2021). Although the dynamics of mitochondria vary depending on the kind of cell and the tissue, the essential protein machinery that powers the process has been surprisingly maintained over time (Glancy et al. 2020). Each dynamic process is necessary to maintain a healthy mitochondrial population, which is important in normal physiology and organism conditions (W. Chen, Zhao, and Li 2023). The inability of the mitochondria to provide and maintain the required ATP for the needs of the cell. An imbalance affecting mitochondrial function is caused by the reduction and acceleration of any of these dynamic processes because of pathological or physiological stressors, ultimately causing numerous illnesses in cardiovascular, neurological, metabolic, and cancer diseases (Jomova et al. 2023). Controlled regulation of nuclear-encoded and mitochondrial transcription factors is required. It is said that PGC1α is the main regulator of mitochondrial biogenesis and function.

2.2 Regulation of the Key modulator: PGC1α

PGC1α is a transcriptional regulator that is part of the PGC family. PGC1β and PRC (PGC1-related coactivator) are further members of the family (Puigserver et al. 1998). PGC1α family lacks a DNA-binding domain. Furthermore, PGC1α lacks the intrinsic histone acetyltransferase activity that triggers chromatin remodeling and gene activation in other transcriptional coactivators. PGC1α functions more like a transcriptional regulator by giving proteins a docking platform. Consequently, transcription is indirectly promoted by PGC1α (Bost and Kaminski 2019).

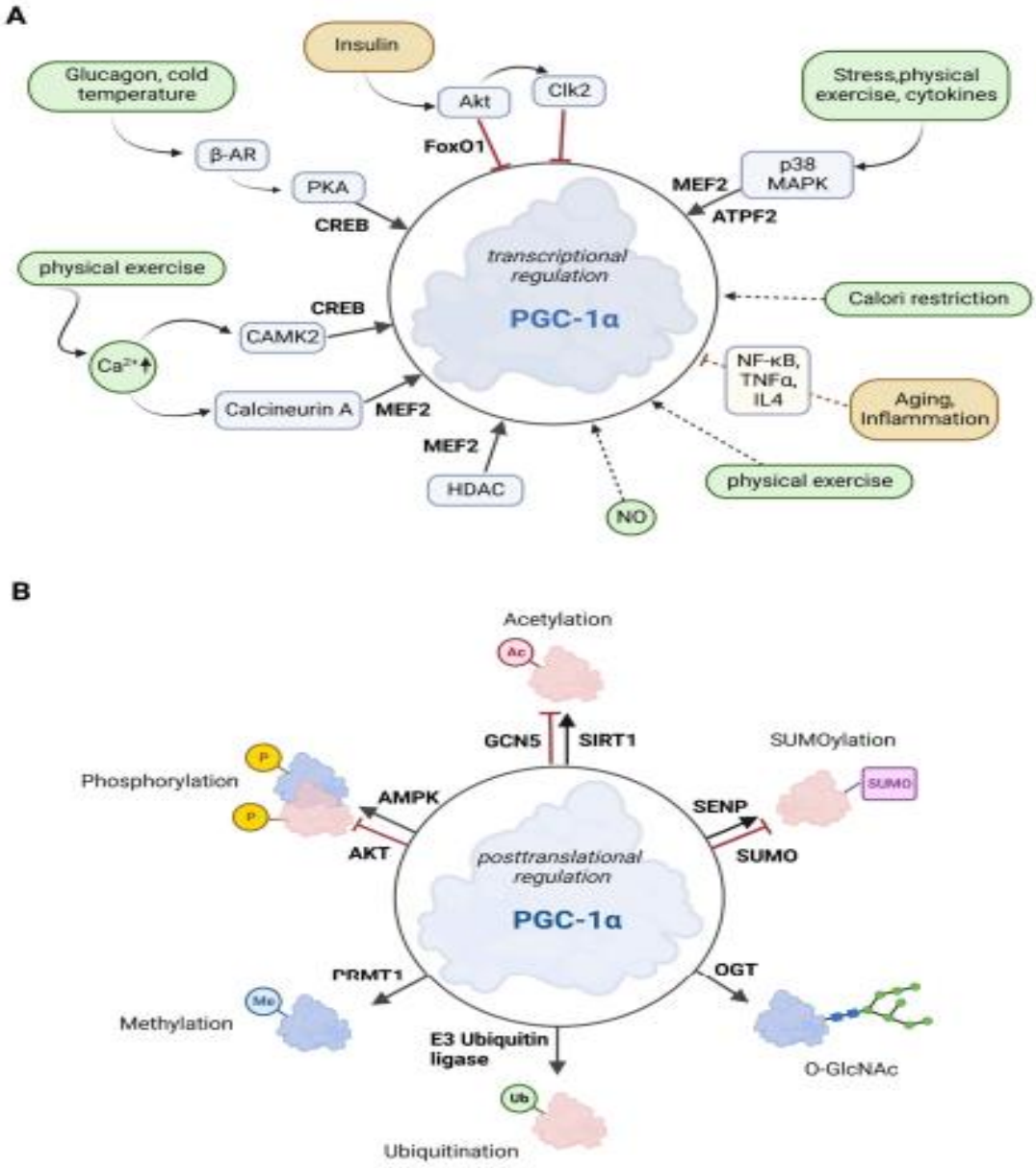

Figure 2.2*: Depiction of summary of PGC1α effectors. (A) PGC1α posttranscriptional regulation. (B) PGC1α posttranslational alterations. For PGC1α, several modifications have been identified, including phosphorylation, acetylation, methylation, ubiquitination, O linked N-acetylglucosylation, and sumoylation. (Fernandez-Marcos and Auwerx 2011)*

Many transcription factors and external cues transcriptionally control the primary pathways for signaling to target via signaling cascades, including the environment, insulin/glucagon levels, Ca2+, and exercise. PGC1α is subject to many changes at the posttranslational level, including acetylation, phosphorylation, methylation, and ubiquitination as shown in the Figure 2.2A (Fernandez-Marcos and Auwerx 2011). PGC1α expression is stimulated by MEF2 and ATF2, which are both regulated by p38 MAPK. Exercise elevates Ca2+ levels, which in turn cause calcineurin A and Ca2+/calmodulin-dependent protein kinase 2 (CAMK2) to activate MEF and CREB factors (Booth et al. 2015). When the ratio of cellular AMP to ATP rises, AMPK is triggered. Thus, it plays a crucial role in maintaining the energy balance of the cells. PGC1α in muscle cells is specifically bound by AMPK, which phosphorylates at Thr177 and Ser538. This PGC1α phosphorylation increases its transcription. These phosphorylations are also necessary for the AMPK-induced regulation of mitochondrial or nuclear genes and PGC1α itself (Parsamanesh et al. 2021). Furthermore, p38 MAPK-induced phosphorylation of PGC1α at Thr262, Ser265, and Thr298 results in enhanced protein stability (Fernandez-Marcos and Auwerx 2011).

The main driver of mitochondrial energy metabolism is the AMPK/PGC1α axis. Persistent overeating can upset this equilibrium by inhibiting PGC1α activity, which causes AMPK expression to shut down and mitochondrial malfunction (Kong, Cai, and Nie 2022). Whereas, it is shown that Akt phosphorylates many C-terminal locations on PGC1α. Akt suppresses fatty acid oxidation (FAO) and gluconeogenesis via phosphorylating PGC1α (Li et al. 2007). Heras et al showed that the phosphate 3 kinase Akt mechanistic target of the rapamycin transduction pathway. It regulates growth, differentiation, metabolism, and cell death along with PGC1α inhibition (Heras-Sandoval et al. 2014). GSK3β controls PGC1α stability in 3T3 cells by directing PGC1α toward intranuclear degradation by proteasomal enzymes (Anderson et al. 2008).

Sirtuin 1 is a member of the histone deacetylase family related to silent information regulators. Nicotinamide adenine dinucleotide (NAD) is necessary for sirtuin proteins to

conduct the deacetylation of target substrates (Cantó et al. 2009). It is suggested that SIRT1 is a sensor that directly connects metabolic disorders to the cellular balance of NAD+ and NADH, which is intimately related to catabolic metabolism. Consequently, SIRT1 engages in a NAD+-dependent deacetylation of PGC1α (Rodgers et al. 2005). Mitochondrial biogenesis and function is then coactivated by elevated PGC1α (Michishita et al. 2005).

About above Figure 2.2B the protein PRMT1, arginine methyltransferase 1, catalyzes methylation, which boosts PGC1α expression and triggers the transcription of genes crucial for mitochondrial biogenesis (Teyssier et al. 2005). Hence, diverse posttranslational changes establish a flexible and effective range for controlling PGC1α levels and intracellular localization, eventually contributing to its crucial function in mitochondrial biogenesis and energy metabolism.

2.3 Mitochondrial biogenesis

The mechanism that controls mitochondrial biogenesis involves PGC1α-NRF1/2-TFAM (Figure 2.2). When brown adipose tissue was first exposed to cold, it was observed that PGC1α was elevated. This, in turn, caused the production of several respiratory chain genes and an increase in the amount of mtDNA (Puigserver et al. 1998). This involvement was substantiated by the gain of function tests in transgenic mice and cultured cells. Eukaryotic cells undergo mitochondrial biogenesis to produce healthy mitochondria and increase the number of mitochondria by dividing the old ones, which are already fully developed and have finished their DNA replication (Uittenbogaard and Chiaramello 2014). John Holloszy was the first to describe it in the 1960s. During his experiment, he found that physical endurance training causes larger mitochondrial content levels, which resulted in better glucose uptake by muscles (Holloszy and Coyle 1984). PGC1α, is a transcription factor and a key regulator of mitochondrial biogenesis (Friedman and Nunnari 2014).

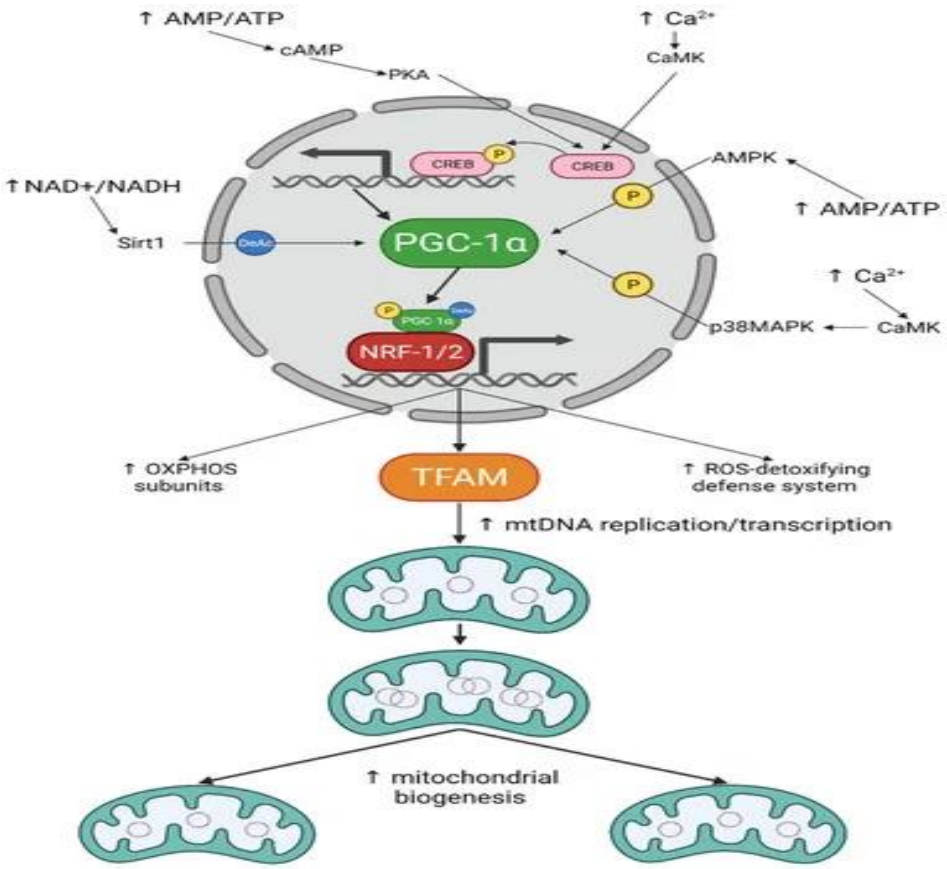

Figure 2.3*: Potential molecular signals involved in the regulation of mitochondrial biogenesis (Cardanho-Ramos and Morais 2021).*

Through the deacetylation of its primary targets, the NAD+-dependent protein deacetylase SIRT1 regulates a variety of biological processes, including inflammation, cell death, and metabolism (Imai et al. 2000). SIRT1 deacetylates several non-histone proteins, such as PGC1α to activate the transcription via SIRT1/PGC1α pathway that plays a role in protecting mitochondrial biogenesis (Zhou et al. 2018). Furthermore, Hu et al have shown that in ischemic heart disease, PGC1α is decreased by SIRT1 suppression (Hu et al. 2016).

Whereas experiments involving decreased function demonstrated that AMPK is involved in the upkeep of mitochondrial biogenesis. Irregularities have been observed in the regulation of mitochondrial biogenesis and function induced by muscle-specific deletion

of AMPK α-subunits. It appears that AMPK regulates the downstream effector molecules such as PGC1α by phosphorylation at two different sites (Jäer et al. 2007). The estrogen-related receptor (ERR) family, NRF1, and NRF2 are the most often observed transcription factors activating promoters of mitochondrial genes (Ivanova et al. 2013). PGC1α's interactions with both NRF1 and NRF2 have been proven. Wu et al have shown that deleting NRF1's N-terminal segment eliminates PGC1α's influence on mitochondrial biogenesis (Z. Wu et al. 1999). In the respiratory complex, cytochrome C oxidase subunit IV (COXIV), cytochrome c, mitochondrial protein import machinery (TOMM34), and transcription of mtDNA transcription factor A mitochondrial (TFAM), transcription factor B1 mitochondrial (TFB1M), transcription factor B2 mitochondrial (TFB2M) are among the many target genes that NRF1 regulates (Ivanova et al. 2013; Satoh, Kawana, and Yamamoto 2013). Multiple tasks are carried out by TFAM for mtDNA, and their interactions play a role in the regulation of mitochondrial biogenesis. Among these, it has been shown that TFAM and TFB2M are necessary for the replication and transcription of the mitochondrial genome.

2.4 Mitochondrial Dynamics: Fusion and Fission

Mitochondria are highly dynamic and constantly alter their shape through fusion and fission events. The size, quantity, distribution, quality control, and transit of mitochondria in cells are all governed by mitochondrial dynamics in addition to mitochondrial morphology (Green, Hossain, and Eckmann 2022). Numerous cellular activities, including the cell cycle, immunology, apoptosis, and mitochondrial quality control, depend on these brief and rapid morphological modifications. Numerous human diseases have been linked to mutations in the basic machinery parts and flaws in mitochondrial dynamics. The joining of two mitochondria into one functional mitochondrion is known as mitochondrial fusion (Figure2.3). Two mitochondria collide end to end in a normal

mitochondrial fusion and the membrane fusion event take place there to create ring-like structures, fusion reactions can also take place inside a single mitochondrion or end-to-side. As mitochondria have two membranes, fusion occurs first at the outer membrane and then at the inner membrane. Outer membrane fusion is ensured by the two large GTPases homologs Mitofusion 1 (MFN1) and Mitofusion 2 (MFN2) (Meeusen, McCaffery, and Nunnari 2004). Inner membrane fusion occurs downstream of outer membrane fusion and is mediated by the large GTPase Optic Atrophy 1 (OPA1) (Ono et al. 2001). OPA1 performs a separate role in preserving cristae structure in addition to fusing the inner membrane.

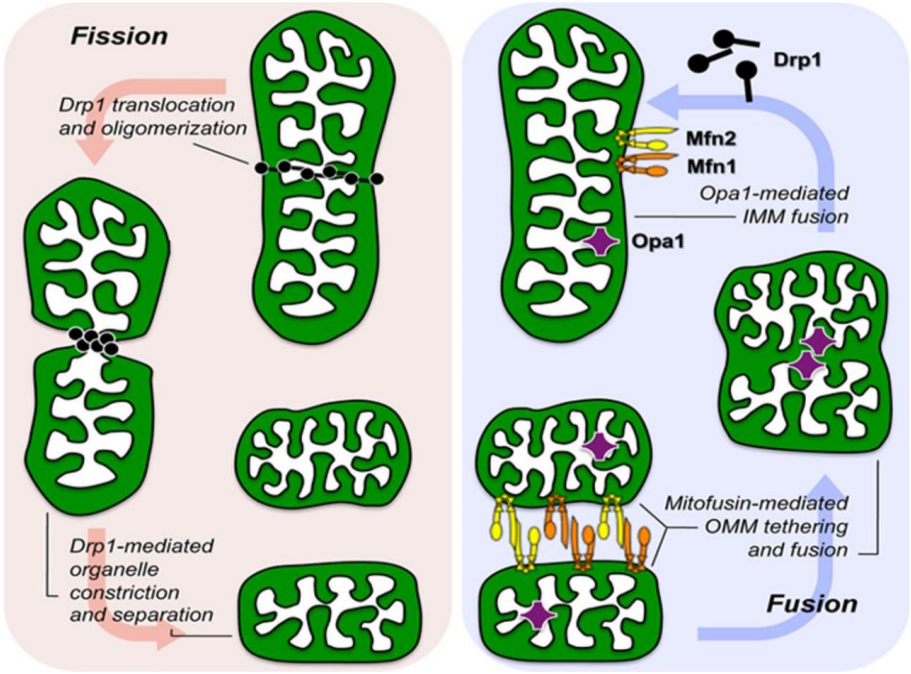

***Figure 2.4**: Representation depicts the dynamic process of mitochondrial fusion and fission (Dorn and Kitsis 2015).*

The respiratory chain super complexes are significantly diminished, and the ultrastructure of the cristae is substantially disturbed when OPA1 is absent (Hsiuchen Chen et al. 2010). Whereas the process in which the mitochondrion divides into two smaller

mitochondria is known as mitochondrial fission (Figure 2.3). Mitochondrial fission is majorly controlled by the dynamin-like protein 1 (DRP1), a GTP-hydrolyzing enzyme (Detmer and Chan 2007). DRP1 is an ortholog of yeast Dnm1p, and the two proteins have a 42% homology (Pitts et al. 1999). One important step in DRP1-mediated fission is the recruitment of cytosolic DRP1 to mitochondria. DRP1 appears to undergo significant structural changes after being recruited to mitochondria, which restricts the mitochondrial tubule and starts the event.

Mitochondrial fission and fusion contribute to the maintenance of the following:

- Mitochondrial integrity,
- Electrical and biochemical connectivity
- Mitochondrial turnover
- Segregation and protection of mitochondrial DNA (mtDNA)

The shape of the mitochondria is dynamic and responsive to changes in metabolism. Increased ATP production is positively correlated with mitochondrial fusion, while its inhibition is linked to reduced OXPHOS, mtDNA depletion, and ROS production. Changes in nutritional supply and metabolic needs can tilt the balance of fission and fusion in either direction, resulting in mitochondrial fragmentation or hypertubularity (Mitsopoulos et al. 2015). In response to different physiological and environmental cues, two opposing processes, fusion, and fission along with mitophagy and mitobiogenesis cooperate to maintain the homeostasis of mitochondria.

2.5 Mitophagy

Lemasters coined the term "mitophagy," which describes a conserved cellular mechanism that permits autophagy to selectively eliminate diseased or superfluous mitochondria. Selective mitochondrial autophagy, or mitophagy, as a targeted defense against oxidative stress, mitochondrial dysfunction, and aging (Lemasters 2005). Most of the time, oxidative stress causes mitophagy, which is a cellular defense process that eliminates damaged mitochondria as a side effect of high ROS generation (Schofield and Schafer

2021). By interacting with the necessary autophagy protein LC3, the mitophagy receptor selectively destroys impaired mitochondria in response to a variety of mitochondrial stresses, including hypoxia, loss of mitochondrial membrane potential, and oxidative stress (Onishi and Okamoto 2021). Unlike those linked to mitobiogenesis, the signaling pathways that trigger mitophagy have not yet been fully investigated. The control of mitophagy has been linked to a number of pathways, however the exact molecular processes behind these pathways are yet unknown (L. Liu et al. 2023). Autosomal recessive parkinsonism (ARP) is caused by mutations in the Parkin gene, which is a cytosolic E3 ubiquitin ligase. Subsequent research also revealed a connection between ARP and a serine/threonine kinase found in mitochondria called PTEN-induced kinase 1 (PINK1). According to preliminary studies, the Parkin/PINK1 pathway supports both the maintenance of mitochondrial function and the regulation of mitophagy (Poole et al. 2008).

It is well acknowledged that optimal mitochondrial quantity and function are necessary for sustaining physiological and biological equilibrium of the cell, and that their lack of regulation is closely related to the development of metabolic disorders like obesity and type 2 diabetes (Kim, Wei, and Sowers 2008). Nutrient overload, like excess free fatty acids or hyperglycemia, promotes the generation of reactive oxygen species (ROS) and decreases mitochondrial biogenesis and oxidative phosphorylation, leading to the malfunction of the mitochondria. Insulin resistance, obesity, diabetes, and cardiovascular disease are caused by enhanced ROS generation, reduced oxidative phosphorylation, and ATP synthesis resulting in mitochondrial dysfunction (Caturano et al. 2023; Cojocaru et al. 2023).

2.6 Mitochondrial dysfunction in metabolic disorders.

The traditional definition of mitochondrial dysfunction is when they are incapable of producing adequate amounts of ATP to cater to the requirements of the cells (Kusminski and Scherer 2012). One crucial node that unifies the cell's need for energy with the availability of nutrients is the mitochondrial network. As a result, identifying the reason

behind mitochondria's inability to perform important functions necessitates combining measurements of the structure and function and the quality control of the organelles (Anello et al. 2005; Glancy et al. 2020). Literature has demonstrated a correlation between obesity and reduced mitochondrial respiration, elevated generation of reactive oxygen species inside the mitochondria, dysregulation of mitochondrial biogenesis, reduced mitophagy signaling, and elevated apoptosis (W. Chen, Zhao, and Li 2023; Rocha et al. 2020). Similarly, in those with type 2 diabetes or obesity, there is a correlation between reduced tissue sensitivity to insulin and mitochondrial dysfunction. Increased ROS generation and oxidative stress are caused by high nutrition concentrations found in these metabolic diseases. Such disorders also activate many signaling pathways that mediate repercussions on the mitochondrial function (Lu et al. 2020; Newsholme et al. 2016). The process of β-oxidation of fatty acid into acetyl-CoA, which provides a basis for the TCA, is interfered with obesity. Reduced β-oxidation results in tri-glycerol production and ectopic lipid accumulation, which impair cellular function. Increased lipid peroxidation byproducts, or lipotoxicity, are caused by increased free fatty acids, which also encourages mitochondrial dysfunction. Raising the NADH/NAD+ ratio in conjunction with a sedentary lifestyle, which reduces energy need, may cause an increase in the production of mitochondrial ROS. It's probable that high fragmentation of mitochondria is a defensive mechanism by lowering OCR (Whitley, Engelhart, and Hoppins 2019). Mitochondrial biogenesis is also a tightly regulated process, taking place in coordination with mitochondrial dynamics through various transcription factors within healthy cells. It should come as no surprise that mitochondria appear to play a significant role in several facets of metabolic disease, including etiology, consequences, therapy, and prevention, given that they are the primary locations for energy disposal (Filippi et al. 2017; Volpe et al. 2018).

Reduced mitochondrial shape and size, quantity, and impaired cristae have been linked with a diminished ability of mitochondrial function in skeletal muscle tissue obtained from obese and type 2 diabetes patients compared to control (Whytock et al. 2023). Approximately forty percent of the mass of the human body is made up of skeletal muscle

tissue, a highly flexible tissue that's vital for sustaining posture of the limbs and movement. Skeletal muscle tissue loss due can raise the morbidity and mortality of many diseases and have a major negative effect on patient's quality of life (Yan et al. 2022). The ability of these mitochondrial homeostatic mechanisms to identify and address mitochondrial malfunction is crucial for the preservation of skeletal muscle mass (Egerman and Glass 2014). Gene expression is promoted by catabolic signaling pathways that become activated by mitochondria's inability and feed back to the nucleus in skeletal muscle of obese and type 2 diabetic patients (Shen et al. 2022)

The morphological analysis of mitochondria has long been considered a crucial adjunct to functional research, as altered morphology of mitochondria is a characteristic of several distinct myopathies known to cause disruptions of the metabolic activity of mitochondria (Vogel 2001). For mitochondrial biosynthesis, energy metabolism, and oxidative stress, the AMP-activated protein kinase (AMPK), silent information regulator Sirutin 1 (SIRT1), PGC1α signaling pathway functions as an energy sensing network (Tian et al. 2019). By collaborating with SIRT1, AMPK regulates the expression of genes related to energy metabolism in mouse skeletal muscle by causing downstream SIRT1 targets, such as PGC1α, to become deacetylated (Cantó et al. 2009). By promoting mitochondrial biogenesis and oxidative phosphorylation through the AMPK/PGC1α pathway, FGF19 may mitigate the effects of mitochondrial dysfunction and oxidative stress in obesity-induced skeletal muscle (Guo, Li, and Xiao 2020). An imbalance in the availability and consumption of nutrients in several tissues, including the liver, adipose tissue, and skeletal muscle, results in Insulin resistance (Petersen and Shulman 2018).

The expression of the electron transport chain complexes governs the mitochondrial capacity for oxidative phosphorylation (OXPHOS). Since some of subunits in these structures have been encoded by mitochondrial DNA, this is a possible explanation for the mitochondrial malfunction. The decrease in mitochondria number in diabetes is probably due to decreased PGC1α expression and activity; the reduced activity will be explained by an increase in reductive stress caused by excess diet. However, the reduced respiration

was linked to lower mitochondrial content, as determined by mitochondrial DNA and citrate synthase efficiency. ETS activity was reduced in diabetic muscle and this decrease was only partially due to a reduction in mitochondria, indicating that mitochondrial content and function are interdependent. Activating PI 4,5bisphosphate to PI 3,4,5-triphosphate, phosphatidylinositol 3-kinase (PI3K) stimulates many downstream serine kinases, such as PI-dependent kinase-1, Akt, and atypical PKC (Heras-Sandoval et al. 2014). Though mitochondrial dysfunction and subsequent lipid buildup are the main candidates, increased activity of phosphatases involved in the negative regulation of the pathway and reduced activation of enzymes like Akt via PGC1α could be equally important (Koliaki and Roden 2016).

Schrauwen et al in the study discuss the challenges and treatment approach of mitochondrial dysfunction, which are boosting mitochondrial biogenesis, removing inactive mitochondria and replacing them with functional ones, supplying or swapping out malfunctioning parts, addressing the fallout from mitochondrial malfunction, and altering the mitochondrial DNA (Y. Chen et al. 2022; Schrauwen et al. 2006). However, to date, almost none of these strategies have yielded satisfactory results. The primary issues are choosing appropriate targets and the absence of a trustworthy technique for focusing on mitochondrial dysfunction.

2.7 MicroRNA, the fine tuners: Biogenesis and Function

A family of endogenous non-coding RNAs known as microRNAs (miRNAs) predominantly acts through post-transcriptional processes to regulate and fine-tune the genome. The majority of miRNA loci are located in the introns of genes that code for proteins, while they can also be embedded in exonic regions or distinct transcriptional units (Winter et al. 2009). During a 1993 study on C. elegans evolution, Victor Ambros and colleagues found lin-4, miRNA. When antisense RNA was injected into C. elegans in 1995, it was seen that the corresponding gene it was injected into was suppressed in terms of expression (Slack et al. 2000; Wightman, Ha, and Ruvkun 1993). This phenomenon was subsequently dubbed RNA interference (RNAi). However, it wasn't until three years

later when Andrew Fire and Craig C. Mello provided previously unheard-of levels of clarity on the RNA interference mechanism was discovered in Drosophila, effectively utilized to mute a gene in Xenopus, and reported in mice (Svoboda et al. 2000; Wianny and Zernicka-Goetz 2000).

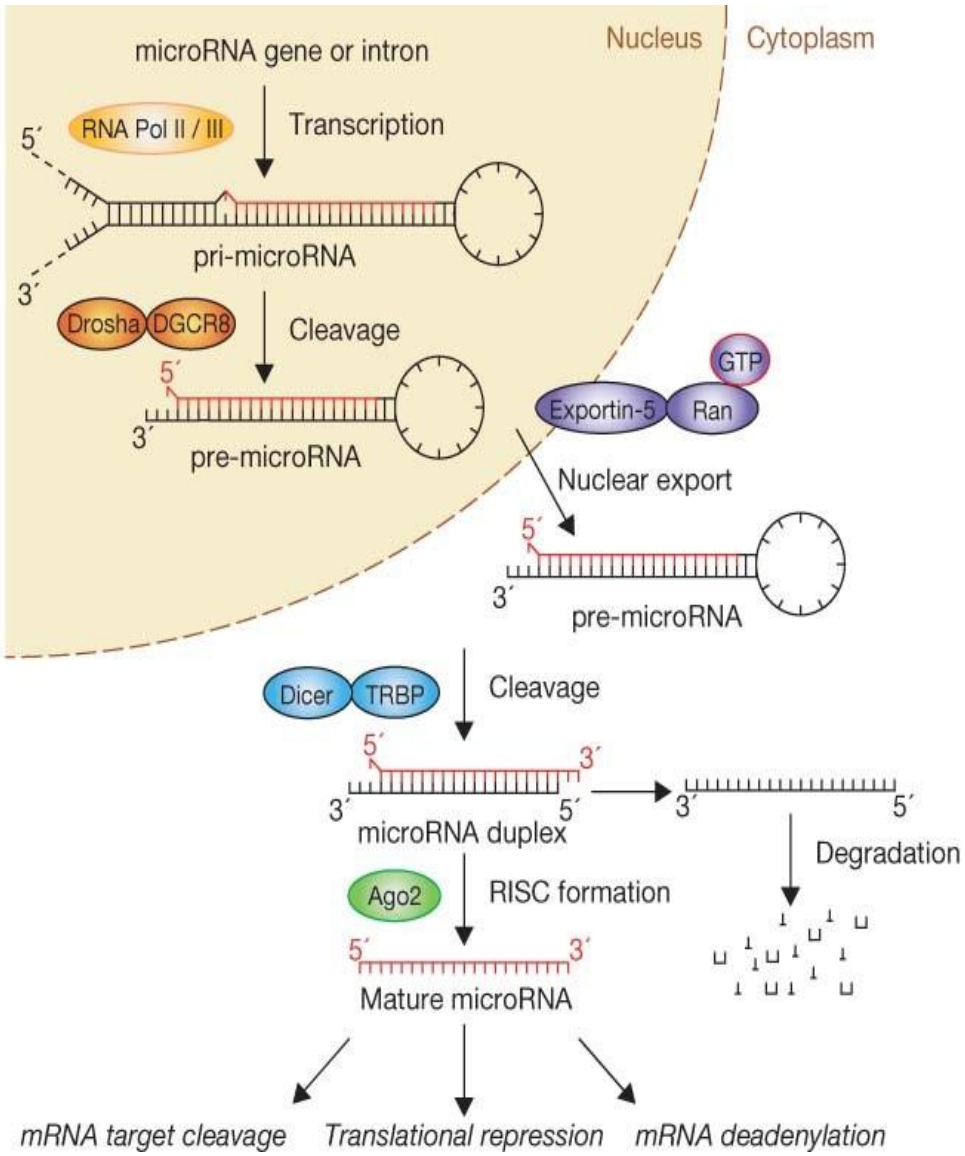

***Figure 2.5**: Overview of the key steps in miRNA biogenesis, their functional role in post-transcriptional gene regulation (Winter et al. 2009).*

The Drosha (RNAse III enzyme) protein complex processes the transcripts of miRNA genes that have been produced by RNA polymerase II (pol II) in the nucleus with the help of DiGeorge syndrome critical region 8 (DGCR8). Long primary miRNAs (Pri-miRNAs) are cut into 70–100 nt precursor miRNAs (Pre-miRNAs) by the Drosha-DGCR8 complex, and exportin-5 (XPO5) ultimately exports the pre-miRNAs outside of the nuclei into the cytoplasm. A protein complex consisting of the human immunodeficiency virus transactivating response RNA-binding protein (TRBP) and enzyme Dicer cleaves the pre-miRNA hairpins to produce double-stranded RNA (ds-RNA), which is ~22 nucleotide bp in the cytoplasm. This dsRNA contains two miRNA strands in both arms of pre-miRNA, which are referred to as miRNA-3p and miRNA-5p. Formerly, it was believed that one strand is a mature miRNA and the other is degradable; however, recent research indicates that, depending on the tissue, either arm may be chosen as a mature miRNA. The RNA-induced silencing complex (RISC) interacts with the mature miRNA, which induces posttranscriptional gene silencing by base-pairing to partly complementary sequence motifs within the 3' untranslated regions (3'UTR) of target mRNAs. The miRNA does not carry out the regulatory role of translational suppression or mRNA degradation on its own.

The complementarity of miRNA sequences to the sequence of their target transcript indicates that miRNAs have recognized their target. The portion of RISC that directly binds the miRNA is a protein that belongs to the Argonaute family (Ago1, Ago2, Ago3, and Ago4). These genes are found in the mammalian genome. It is believed that all four Ago proteins are capable of functioning as RISC components; however, only Ago2 can catalyze RNAi through endo-nucleolytic activity.

Consequently, it is believed that the primary function of Ago proteins in animals is the miRNA-mediated translation inhibition or target mRNA degradation. Both the beginning and elongation phases of translation are inhibited. RISC may obstruct 80S ribosome assembly or the initiation complex. Ribosomes may stall during the elongation step and then drop off the transcript because of RISC (Cai et al. 2009; O'Brien et al. 2018). Additional in-depth details about the molecular process underlying miRNA-

mediated translational repression and mRNA destabilization are provided elsewhere (Bofill-De Ros and Vang Ørom 2024).

2.8 miRNA-mediated regulation of mitochondrial biogenesis and function.

A preclinical study done by Wu et al states that overexpression of the miR-499 enhanced mitochondrial biogenesis and skeletal muscle mass (L. Wu et al. 2019). The intrinsic regulator of mitochondrial dynamics, miR-181a, acts by cooperatively regulating Park2, p62/SQSTM1, and DJ-1 *in vitro*. In elderly mice, increasing the levels of miR-181a reduced the build-up of these autophagy genes, and enhanced muscular function and mitochondrial quality (Goljanek-Whysall et al. 2020). MiR-133a is a skeletal muscle tissue-enriched miRNA that promotes the proliferation of C2C12 myoblast by downregulating PRDM16 and reducing brown fat accumulation in tissue by targeting SRFs (Serum response factors). MiR-133a expression was downregulated in the skeletal muscle of individuals with insulin resistance and type 2 diabetes, comparable. This was accompanied by a reduction in the mRNA expression levels of key factors associated with mitochondrial biosynthesis in the skeletal muscle (Yin et al. 2013).

MiR-149 suppresses PARP-2 expression in healthy skeletal muscle, upregulates the NAD+ levels, and activates SIRT-1, which in turn activates PGC1α and the mitochondrial biogenesis pathway. On the other hand, the high-fat diet-induced skeletal muscle showed a downregulation in the expression level of miR-149 and as well as SIRT1/PGC1α pathway. As a result a downregulation was observed in the levels of the mitochondrial biogenesis markers such as COX1, Cyt C, TFAM, NRF1/2, and UCP1 (Mohamed et al. 2014). Targeting the 3′UTR of PGC1α mRNA and controlling PGC1α protein expression in vitro and in vivo, miR-23a might have some function as a regulator of mitochondrial biogenesis. Aaron et al has indicated in their study that, the expression of miR-23a is upregulated in the skeletal muscle tissue of insulin resistance mice model of type 2 diabetes and an inverse relation is observed with the expression of PGC1α.

The downregulation of COX IV protein expression suggests that miR-23a can adversely influence mitochondrial biogenesis. The enzyme adenosine kinase (ADK) converts adenosine to adenosine monophosphate and then into adenosine diphosphate. Overexpression of miRNA-96-5p inhibits ADK and has been associated with oxidative phosphorylation leading to mitochondrial dysfunction (Russell et al. 2013). Furthermore, it has been demonstrated that obesity causes a decrease in the amount expression of glucagon-like peptide-1 (GLP-1), which can result in metabolic disorders. Since GLP-1 was decreased in expression and miR-194 was enhanced in the plasma and ileum tissue of obese mice, miR-194 has been identified as a regulator of GLP-1. Overexpression of miR-194 and suppression of GLP-1 expression caused worsening of myocardial damage and mitochondrial dysfunction in obese mice. Therefore, miR-194 is a crucial biomarker for GLP-1 expression as well as for the relationship between obesity and its underlying metabolic processes (J. Wang et al. 2021). It appears that miR-221/222 and miR-33 have a significant pro-atherogenic impact on oxidative phosphorylation and mitochondrial biogenesis. Their overexpression lowers PGC1α, which in turn causes endothelial mitochondria to malfunction (Karunakaran et al. 2015; Xue et al. 2015).

In conclusion, many studies collectively indicate that miRNAs play a significant role within the tissue of individuals with metabolic disorders in the regulation of mitochondrial metabolism. However, based on the reviewed literature, it is determined that further study is necessary to fully comprehend the role that miRNA activity plays in the mechanisms that lead to the development of obesity and the potential applications of these small molecules for the treatment of diseases.

2.9 miR-128 and Human Diseases

2.9.1 miR-128 biogenesis

On chromosome 2 (q21.3), hsa-miR-128-1 is in the intronic region of the R3HDM1 gene, whereas on chromosome 3 (p22.3), hsa-miR-128-2 is embedded within the intronic region of the ARPP21 gene. RNA polymerase II/III transcribes the microRNA gene R3HDM1 or

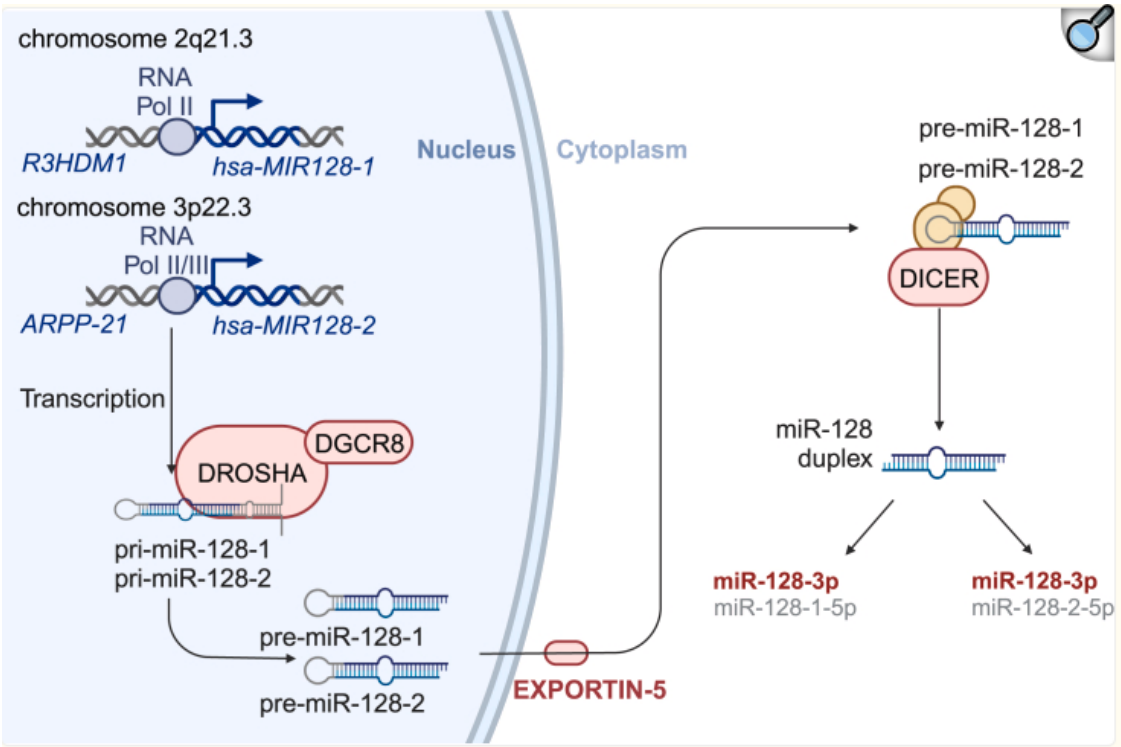

***Figure 2.6**: Figure represents the canonical pathway of miR-128 biogenesis*(Kiel et al. 2024).

ARPP-21, producing the long primary transcript (pri-microRNA) for the biogenesis of the mature miR-128 via the canonical pathway. Regarding the mature transcripts, the seed sequence is most important for target recognition and silencing, miR-128-1-5p (CGGCCCCA) and miR-128-3p (target sequence CACUGUGA). However, independent of the location of origin, miR-128-5p expression is hardly noticeable, whereas miR-128-3p is one of the most abundant in the brain, skeletal muscle, and other tissues.

2.9.2 Role of miR-128 in human diseases.

MiR-128 is a multipurpose molecule that plays several roles in the physiopathology of different human diseases such as cancer, neurodegenerative disorders, metabolic disorders like type 2 diabetes and obesity, cardiovascular disorders, and musculoskeletal diseases as shown in Figure 2.7. Herein, based on the current literature, we provide an overview of miR-128 playing a role in multiple disorders.

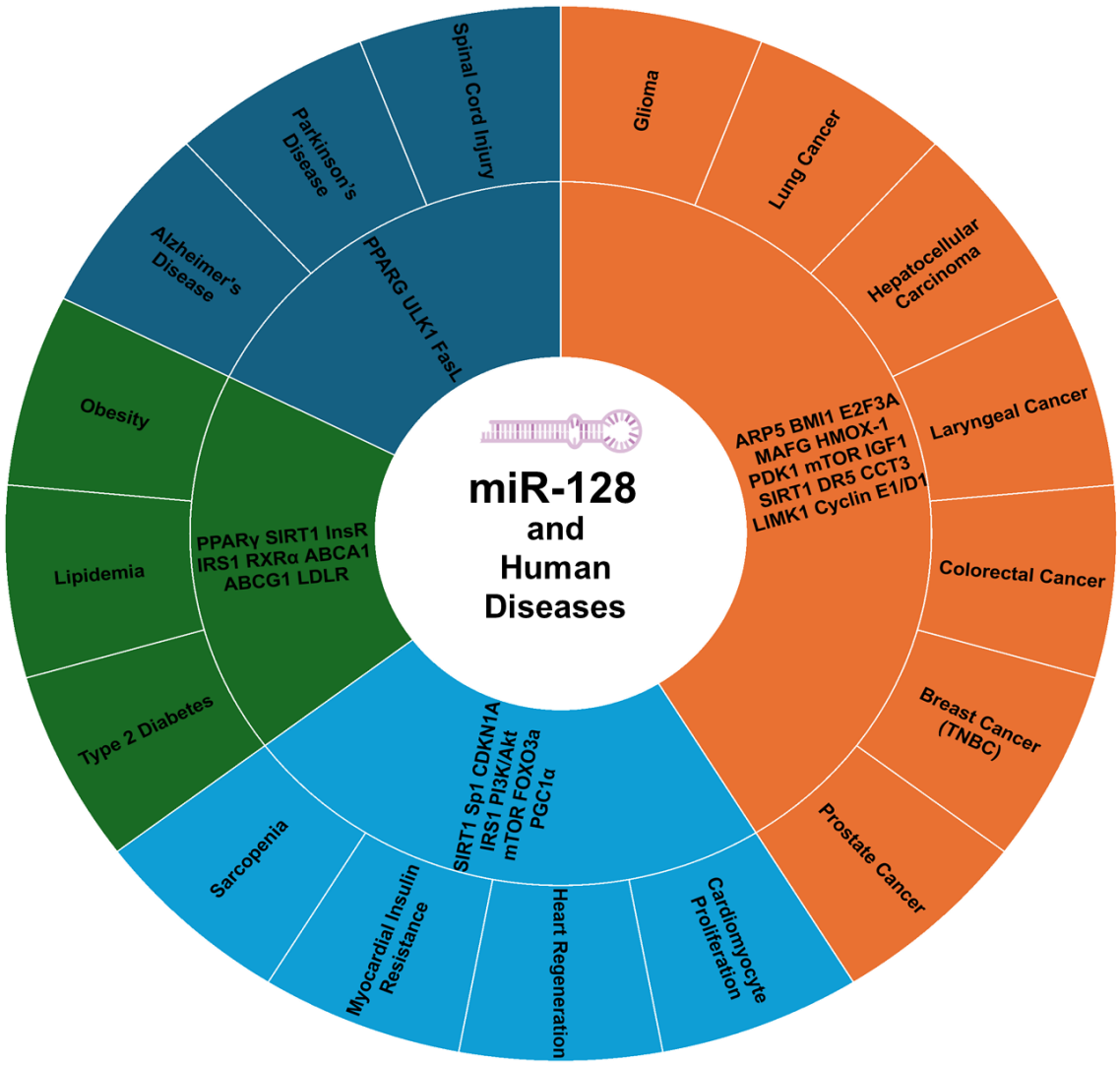

Figure 2.7: *Highlighting the relationship between miR-128, different diseases, and their target genes.*

Role of miR-128 in neurodegenerative diseases

miR-128 is a brain-enriched miRNA involved in modulating various aspects of brain function, including neuronal plasticity. Interestingly, a recent study found that the Mini-Mental State Examination scores positively and strongly correlate with changes in miR-128 levels, which are likewise increased in the sera of Alzheimer's Disease patients (Miners et al. 2009). In the hippocampus of both fetal brains and adult Alzheimer's disease

patients, miR-128 exhibits aberrant accumulation, and its direct target, peroxisome proliferator-activated receptor gamma (PPARG), which is known to reduce amyloid beta levels, is downregulated. Restoring PPARG expression with deletion of miR-128-3p reduces amyloid beta-induced inflammation and cytotoxicity by blocking NF-κB activity in vitro (Geng et al. 2018). When miR-128 is deleted in mice, many mRNAs involved in the mitogen-activated protein kinase (MAPK) pathway are overexpressed, which causes fatal epilepsy (Vidigal and Ventura 2015).

Similarly, increased expression of miR-128-3p has been shown to reduce neuronal apoptosis and inflammation, while also enhancing motor function after spinal cord injury (SCI). This effect is achieved by suppressing serine/threonine-protein kinase ULK1 and upregulating Fas ligand (FasL) (LIU et al. 2021). Elevated levels of miR-128-3p have been shown to markedly decrease the apoptosis of dopaminergic neurons by restoring activity in the Wnt/beta-catenin signaling pathway. This restoration helps safeguard neurons from disorders caused by protein misfolding, in Parkinson's disease (PD) (Lanza et al. 2023).

Role of miR-128 in the pathophysiology of cancer

It has been demonstrated that some malignancies, including lung cancer, glioma, and hepatocellular carcinoma, have differential expression of miR-128 (Weiss et al. 2008; Zhang et al. 2009). Besides miR-128 inhibition assists tumor cells evade stressors. By targeting ARP5, BMI1, and E2F3A, miR-128 functioned as a tumor suppressor molecule, slowing the growth of gliomas (Cui et al. 2010). Similarly, Bmi-1 maintains tumorigenic laryngeal development and aids in the evolution of laryngeal squamous cell carcinoma (LSCC), indicating that miR-128 has a tumor suppressor function in laryngeal cancer (Hui Chen et al. 2011). Additionally, by inhibiting the BMI1 proto-oncogene, Polycomb Ring Finger (Bmi1), miR-128 also increases ROS. In addition, under hypoxia, miR-128 levels reduce, and MAFG and heme oxygenase 1 (HMOX-1) protein levels elevate in both in vitro and in vivo experiments (Caggiano et al. 2017; Venkataraman et al. 2010).

The expression of miR-128-2 is notably higher in individuals with hepatocellular carcinoma (HCC) compared to healthy individuals. Additionally, this increased level of miR-128-2 is closely associated with the levels of alpha-fetoprotein (AFP), a biomarker commonly used in diagnosing and monitoring HCC (Jin and Ren 2024). In the cells treated with TRAIL, the overexpression of miR-128 increased the formation of ROS via suppressing SIRT1 expression. A spike in ROS then caused DR5 expression, which in turn boosted the amount of TRAIL-induced apoptosis in colorectal cancer (Lian et al. 2018). Research suggests that miR-128 regulates oxidative stress-induced damage to cells, antioxidant defense systems, and oxidative ROS generation. The eukaryotic group II chaperone TRiC, sometimes called CCT or C-CPN, is essential for the folding and conformational assembly of cytosolic proteins. This complex guarantees that 15% of proteins fold correctly within the cell. It was discovered that miR-128-mediated CCT3 inhibition reduced the potential of the mitochondrial membrane and was associated with higher ROS levels in CRL-2329 and PC3 cells. The apoptotic pathway and CCT3 inhibition inadvertently interfered, changing the morphology, and speeding up the rate of cell death in prostate cancer (Temiz, Koyuncu, and Sahin 2021).

Changda Qu et al demonstrated that miR-128 suppressed PDK1 expression, which in turn caused most of the pyruvate generated by glycolysis to be transported into the matrix of the mitochondria and enter the citric acid cycle. This induces a significant amount of ROS and aids in the demise of glioma cells by impairing the function of the mitochondria (Qu et al. 2020). The TMZ-repressed mTOR signaling was impacted by the overexpression or inhibition of miR-128 expression, indicating that miR-128-targeted mTOR signaling, by directly targeting mTOR, RICTOR, IGF1, and PIK3R1 transcripts, and regulates TMZ-mediated apoptosis along with mitochondrial dysfunction, ER stress, and autophagy in glioma cells (P. H. Chen et al. 2016).

It has been observed that miR-128-3p can inhibit the proliferation, differentiation, and motility of breast cancer (BC) cells. In all TNBC cell lines, miR-128 overexpression also resulted in decreased mitochondrial DNA content and ATP concentrations. TNBC cell

proliferation, mitochondrial respiration, and glucose utilization were all inhibited by miR-128. These outcomes were in line with the suppression of the insulin receptor and insulin receptor substrate 1 caused by miR-128 targeting (Xiao et al. 2018). Additionally, increased levels of miR-128-3p may influence cell cycle progression by downregulating the expression of CDK2/Cyclin E1 and CDK4/6/Cyclin D1. Moreover, miR-128-3p inhibits the LIM domain kinase 1 (LIMK1) signaling pathway in BC by directly targeting the LIMK1 gene. These insights suggest a potential regulatory role of the miR-128-3p-LIMK1/CFL1 axis in BC, which could pave the way for novel therapeutic strategies (Zhao, Li, and Fang 2019).

Role of miR-128 in metabolic diseases

miR-128-1 seems to directly regulate the expression of several crucial metabolic proteins, including, PPARγ, SIRT1, InsR, and IRS1, which play significant roles in adipose tissue, liver, and skeletal muscle. Yogita et al. established that miR-128 directly targets SIRT1 (Yogita K. Adlakha and Saini 2011). Additionally, miR-128 controlled genes linked to lipid metabolism. Through targeting of key genes that regulated cholesterol metabolism, such as retinoid X receptor α (RXRα), ATP-binding cassette A1 (ABCA1), ATP-binding cassette G1 (ABCG1), and LDL receptor (LDLR), miR-128 was found to be positively correlated with cholesterol levels in previous investigations (Y. K. Adlakha et al. 2013). The studies provide experimental validation that miR-128 is not only a pro-apoptotic molecule.

Remarkably, IGF-1 counteracts the effects of FOXO3a's nuclear translocation by encouraging PI3K/AKT phosphorylation, which in turn causes FOXO3a phosphorylation, which causes FOXO3a to relocate from the nucleus to the cytoplasm and is inhibited. This additionally safeguards the skeletal muscle of diabetic mice's mitochondrial respiratory function and complex activity (PI3K/AKT activation attenuates acute kidney injury following liver transplantation by inducing FoxO3a nuclear export and deacetylation. Insulin-like growth factor-1 (IGF-1) is the direct target of miR-128, and its inhibition increases the expression of IGF-1. Through the activation of PI3K/AKT, IGF-1 may

further boost the phosphorylation of FOXO3a, and alterations in PGC1α may enhance mitochondrial activity (Z. L. Chen et al. 2023). Sarcopenia is a condition that is more common in sedentary individuals than in regular exercisers. It is characterized by a decreased skeletal muscle mass and poor function. As cells age, they express more FOXO3a, and the localization changes from the cytoplasm to the nucleus, causing impairment in the mitochondria function (Zhuan et al. 2022).

The decreased translocation of GLUT4 and inhibition of insulin-stimulated glucose consumption via IRS1, and miR-128 also affected the PI3K/Akt pathway's activity in C2C12 myotubes (Motohashi et al. 2013). Moreover, it has been shown that in the visceral adipose tissue (VAT) of obese individuals, a negative correlation exists between rising body mass index and falling insulin receptor activation. miR-128 reduces insulin receptor mRNA stability in adipocytes, VAT-specific insulin receptor downregulation is an early event in obesity-related adipose cell dysfunction that exacerbates systemic insulin resistance in obese humans and mice (Arcidiacono et al. 2020).

Role of miR-128 and cardiovascular diseases

Literature has several pieces of evidence such as in the cardiac muscle cells, elevation in miR-128 level plays a role in cardiomyocyte proliferation and heart regeneration (Sucharov et al. 2017). Interestingly, a small number of additional research has also discussed the therapeutic potential of miR-128a during myoblast development (Sun et al. 2010). On the other hand, miR-128 inhibiting elevates Sp1 protein levels, which leads to decreased proliferation and myogenic differentiation. Sp1 suppresses cyclin-dependent kinase inhibitor 1A (CDKN1A) and is necessary to activate MyoD which suggests that the miR-128 has an impact on myogenesis (Dai et al. 2016). In a mouse heart model, it was also shown that downregulating miR-128 attenuated Ang II (Angiotensinogen)-induced apoptosis, autophagy, and oxidative stress by directly targeting the SIRT1 and/or via PI3K/Akt target of rapamycin complex 1 (mTOR1) pathways (Zhan et al. 2021). It's interesting to note that while miR-128-3p suppression reduces myocardial insulin resistance, it is overexpressed in the mice model with severe cardiac dysfunction together

with IRS1 degradation and insulin resistance (Ruiz-Velasco et al. 2020). In our previous pilot study, we observed a reduction in miR-128-3p levels in coronary artery disease (CAD) patients compared to healthy individuals. Additionally, we demonstrated that miR-128-3p plays a key role in regulating cholesterol efflux in macrophages, a critical process in the progression of CAD (Choudhury et al. 2024).

MiRNA inhibition frequently has subtle phenotypic effects. However phenotypic consequences might be severe even from moderate overexpression of several target mRNAs, especially if the targets are functionally related.

Understanding the molecular mechanisms that govern mitochondrial function is important for developing targeted therapeutic strategies. However, functional characterization was required to fully understand the biology of miR-128. Herein, skeletal muscle myoblast cells were transfected with miR-128/Antimir-128 to elucidate how it regulates mitochondrial function.

Chapter 3

Functional Characterization of miR-128 in Mitochondrial Biogenesis and Function

3.1 Introduction

Double-membrane organelles called mitochondria regulate the balance of life and death of eukaryotic cells in a pervasive manner. In addition to serving as eukaryotic cell's primary energy transducers, they also actively control several biosynthetic processes, including metabolism, intracellular signaling, and apoptosis. Regular cycles of fusion and fission allow mitochondria to dynamically change their size and form in response to different pathological situations and the metabolic demands of the cell. While dynamin-related protein 1 protein is required for fission, mitofusin 1 and 2 (MFN1 and MFN2, respectively) and OPA1 mitochondrial dynamin-like GTPase (OPA1) proteins are required for mitochondrial fusion. The metabolic dysfunctions of skeletal muscle are closely associated with impaired mitochondrial biogenesis and dysfunction, which is seen in many diseases including diet-induced obesity and type 2 diabetes. The identification of peroxisome proliferator-activated receptor gamma coactivator 1α as the primary regulator led to a significant advancement in our knowledge of mitochondrial biogenesis and function. By controlling mitochondrial transcription factor, A through the co-activation of nuclear respiratory factors 1 and 2 (NRF1 and NRF2, respectively), PGC1α triggers the transcription and replication of mitochondrial DNA. In the current chapter, we aim to elucidate the mechanism behind miR-128's mode of action in controlling mitochondrial biogenesis and function.

3.2 Material and Methods

3.2.1 miR-128 Target Prediction Genes

The miR-128 predicted targets were identified using TargetScan (version 8.0) *(https://www.targetscan.org/vert_80/).*

3.2.2 Cell culture and transfections

Cell lines used for the experiments in the thesis are in Table 3.1.1 and were procured from the National Centre of Cell Sciences, Pune, India. All cell lines were cultured in Dulbecco′s Modified Eagle′s Medium (D7777, Sigma). Additionally, the media was

supplemented with 3.7 g/L sodium bicarbonate, 10% FBS (Gibco, Thermo Fisher Scientific, MA, USA), and 100 IU/mL penicillin-streptomycin (Gibco, Thermo Fisher Scientific, MA, USA). The cells were maintained in a humidified atmosphere at 37°C and 5% CO2 in a separate room designated for cell culture. These cells were seeded and cultured in the 6-well or 12-well plates at 70–80% confluency in subsequent experiments. Transfection with miR-128 plasmid vector previously cloned in pSilencer 4.1 Vector, (Ambion, Thermo Fisher Scientific, MA, USA) in the lab or with antimiR-128 AM17000, assay ID AM11746, Thermo Fisher Scientific, MA, USA) along with their respective controls i.e., pSilencer 4.1 vector (P(Sil)) or antimiR negative control (AMNC) was done in C2C12 myoblast cells. Lipofectamine LTX and Plus™ (Invitrogen, Thermo Fisher Scientific, MA, USA) were used for all transfections at a 1:1 ratio as per instructions.

Table 3.1: Lists of cell lines used as cited below

Type	Cell line
Mouse	C2C12 myoblasts
Human	HEK293

3.2.3 Animal experiments

C57BL/6 mice (Male, 4 weeks old) were purchased from Livon Biolabs (Bengaluru), India. They were kept under an alternating cycle of dark and light for 12 hours long periods at the animal house facility in CSIR-Institute of Genomics and Integrative Biology, New Delhi. According to NIH's "Guide for the Care and Use of Laboratory Animals," every animal was treated humanely. All the experiments and methods were given the nod of approval by the CSIR-IGIB's Animal Ethics Committee. Hypercholesterolemia was induced in the mouse by feeding them a high-fat diet that provides 60% energy from an (HFD; Cat. #D12492, Research Diets. Inc., NJ, USA) for 13 weeks. A second group of mice received the same amount of normal chow (ND), which had 10% fewer calories than fats.

Table 3.2 Formulation and caloric information of the high-fat diet used in the study (D12492; Research Diet Inc., *https://researchdiets.com/formulas/d12492*)

Class description	Ingredients	Grams	Caloric information
Protein	Casein, Lactic, 30 Mesh	200.00 g	20 % Kcal
Protein	Cystine, L	3.00 g	
Carbohydrate	Lodex 10	125.00 g	20 % Kcal
Carbohydrate	Sucrose, Fine Granulated	72.80 g	
Fiber	Solka Floc, FCC200	50.00 g	
Fat	Lard	245.00 g	60 % Kcal
Fat	Soybean Oil, USP	25.00 g	
Mineral	S10026B	50.00 g	
Vitamin	Choline Bitartrate	2.00 g	
Vitamin	V10001C	1.00 g	
Dye	Dye, Blue FD&C #1, Alum. Lake 35-42%	0.05 g	
	Total:	773.85 g	Energy density: 5.21 Kcal/g

The hypercholesterolemic mice were allocated into three groups of five each, randomly. On alternate days, each mouse in two HFD-fed groups received five intraperitoneal injections (5 i.p. injections) of antimiR-128 or vehicle control (HFD control) at a concentration of 5 mg/kg. antimiR-128 is a custom designed hairpin inhibitor of mmu-128-3p from Dharmacon Inc. in the United States (ref #IH-310398- 08). For the in vivo delivery of antimiR-128, we followed the manufacturer's instructions when using the In vivo-jetPEI reagent (Polyplus-36 transfection® SA, Illkirch, France). Following the 12-hour fast, all mice were harvested 48 hours following the previous injection. Skeletal muscles from all the control and treated group were kept at -80 °C until additional analysis was done.

3.2.4 RNA isolation and TaqMan assay

Following the manufacturer's instructions, total RNA was extracted from the skeletal muscle tissues and cell pellets post 24 h transfections using the TRIzol reagent (15596026 Thermo Fisher Scientific). By passing the RNA samples (500 ng) across a 1% agarose gel, the integrity of the samples was assessed. The measurement of the quantity of RNA samples was carried out using a NanoDrop spectrophotometer (ND 1000, NanoDrop Technologies, Inc., USA). Following that, cDNA was created from 500 ng of total RNA with miR-128 specific RT primers (AB Assay ID PN442795, Applied Biosystems, Foster City, CA, USA) and was prepared using the TaqMan™ MicroRNA Reverse Transcription Kit as given in the Table 3.3.1. For normalization, 18S rRNA (AB Assay ID 4333760F) was used. cDNA was prepared using the Revert Aid H Minus first-strand cDNA synthesis kit (K1631, Thermo Fisher Scientific).

Table 3.3 Component used for cDNA Synthesis with miR-128 specific RT Primers/ Random hexamer Primers

Reaction Mix components	10 µl reaction
10X Reaction Buffer	1 µl
100mM DNTP Mix	0.1 µl
RiboLock RNase Inhibitor	0.13µl
RTase	0.67 µl
RNA	500ng
miR-128 specific RT Primers/ Random hexamer Primers	0.5 µl
NF water	to 10 µl

TaqMan probes were used to quantify the expression using TaqMan Assay. This TaqMan-based assay was performed using PowerUp™ SYBR Green Master Mix in an ABI Prism 7500 Sequence Detection System (Applied Biosystems, ThermoFisher Scientific, Waltham, MA, USA). The results of the TaqMan-based assay were analyzed using Pfaffl's method (research and 2001 n.d.).

3.2.5 Quantitative Real-time PCR

This technique was used to detect transcript expression patterns at tissue and cellular levels. cDNA synthesis from 500 ng to 1000 ng of total RNA was synthesized using Revert-Aid H minus first strand cDNA kit as mentioned in Tabe 3.3. Subsequently, qRT-PCR was performed by using 1 µl to 2 µl of cDNA using the specific transcript primers mentioned in Table 3.4 either on ABI Prism 7500 Sequence Detection System (Applied Biosystems, ThermoFisher Scientific, Waltham, MA, USA) or on LightCycler 480 (Roche, Indianapolis, USA) using SYBR green master mix. The results were normalized with the mouse or human 18S rRNA according to the tissue/cells.

Table 3.4: Lists of primers used for qRTPCR

Gene name	Forward Primer 5'-3'	Reverse Primer 5'-3'
DRP1	CGGTTCCCTAAACTTCACGA	GCACCATTTCATTTGTCACG
MFN1	TTGCCACAAGCTGTGTTCGG	TCTAGGGACCTGAAAGATGGGC
MFN2	GGGGCCTACATCCAAGAGAG	GCAGAACTTTGTCCCAGAGC
OPA1	GATGACACGCTCTCCAGTGAAG	CTCGGGGCTAACAGTACAACC
PGC1α	GAACAAGACTATTGAGCGAACC	GAGTGGCTGCCTTGGGTA
NRF1	GTGCCCGTGTCCAATCAG	TGACATAGCCATTCCCAACG
TFAM	CACCCAGATGCAAAACTTTCAG	CTGCTCTTTATACTTGCTCACAG
COX2	ATAACCGAGTCGTTCTGCCAAT	TTTCAGAGCATTGGCCATAGAA
NRF2	CCTGAGAGCTGTAGGCCC	GGAATGGAAAATAGCTCCTGCC
ND1	GTGGCTCATCTACTCCACTGA	TCGAGCGATCCATAACAATAA
NDUFS4	CAGACAACCAGACTCGGGAC	TGCATGTTATTGCGAGCAGG
COX1	ACTATACTACTACTAACAGACCG	GGTTCTTTTTTTCCGGGAGT
Mouse 18S rRNA	AGAAACGGCTACCACATCCA	CCCTCCAATGGATCCTCGTT

3.2.6 Cloning of UTR Constructs used in the study.

Ensembl genome browser *(https://asia.ensembl.org/index.html)* was used to retrieve the 3′ UTR sequence of PGC1α, and NDUFS4 (Ensembl Release 97, July 2019). The 3′ UTR

has the binding site of miR-128 in the region between 3078 and 3084 nucleotides of PGC1α and 27–33 nucleotides of NDUFS4 mRNA transcripts. The site containing the seed sequence was amplified from the mouse genome respectively, using the primers enlisted in **Table 3.5.** The amplified regions were inserted in the pMIR REPORT luciferase vector (Ambion Inc., TX, USA) at cut sites of MluI and SpeI for PGC1α (742 bp), MluI and HindIII for NDUFS4 (518 bp) and. The constructs cloned hereafter are denoted as 3′ UTR PGC1α, and 3′ UTR NDUFS4. Control plasmid was constructed with no miR-128 binding site using a completely unrelated mouse sequence, denoted as unrelated UTR. All plasmids were verified by sequencing.

Table 3.5: Lists of primers used for the construction of UTR clones.

Gene	Forward Primer 5'-3'	Reverse Primer 5'-3'
PGC1α 3' UTR	CTAGACTAGTAAGGACCAGATGCGTTCTCT	CGACGCGTACAGCCATCAAAAAGGGACA
NDUFS4 3' UTR	CGACGCGTGGAGCTGGCTACATCTCTGC	CCCAAGCTTGGGAAGAACGGGCTTAACTT

3.2.7 Luciferase assay

Luciferase assay was performed with C2C12 myoblast cells at 70–80% confluency in 12 well cell culture plates. Cells were then co-transfected with the 200 ng of firefly luciferase reporter construct with 3' UTR site of PGC1α and NDUFS4 in pmiR-Report vector and 50 ng of renilla luciferase containing pRL-CMV plasmid (Promega, WI, USA). At the same time, cells were also transfected with either 2 ug of P(128) or 100 nM of antimiR-128, or their respective negative control. Post 24 h transfection, luciferase activity was measured using a dual luciferase reporter assay system according to the manufacturer's protocol.

3.2.8 Western blotting

For the lysis and protein extraction from tissues or mammalian cells, RIPA buffer (Radioimmunoprecipitation assay buffer) was used. The formulation includes two ionic detergents and one non-ionic detergent (50 mM Tris-HCl, pH 7.4, 150 mM NaCl, 1% NP-40, 0.25% Na-deoxycholate, 1 mM EDTA, pH 7.4). The protease and phosphatase inhibitors (G-Biosciences, MO, USA) were added. As previously mentioned, protein quantification was carried out using the BCA method (Sigma, MO, USA) (Y. K. Adlakha and Saini 2013). SDS-PAGE (10–12%) was used to separate an equal amount of total protein (40 – 60 μg) and then transferred to the PVDF membrane (mdi; Advanced Microdevices, Ambala Cantt., India). 5 % of BSA blocking buffer was used to block the membrane on the rocking platform for 2 h at room temperature. The primary antibody, which may be acquired from Santa Cruz (Santa Cruz Biotechnology, CA, USA), Abcam (Abcam, MA, USA) respectively were used at a dilution of 1:500 to 1:1000 depending on the antibody, were incubated on the membranes for either 2 hours or 16 hours. Followed by the secondary HRP-linked antibody for 1 hr at a dilution of 1:5000. The primary antibodies against PGC1α (sc13067), and NRF1 (sc101102), were procured from Santa Cruz, whereas those against TFAM (ab272885), NRF2 (ab92946), NDUFS4 (ab137064), DRP1 (ab154879), MFN2 (ab56889), and OPA1 (ab42364), were purchased from Abcam. GAPDH (G9545, Sigma Aldrich, Merck KgaA, Darmstadt, Germany) was used as the loading control. The blots were developed using the enhanced chemiluminescence (Thermo Fisher Scientific, CA, USA) method. Integrated density values were obtained and quantified using AlphaImager 3400 (Alpha Inno Tech, CA, USA).

3.2.9 Fluorescent microscopy

C2C12 myoblast cells were grown in chambered culture slides till 60- 70 % confluency and then transfected either with miR-128 or antimir-128 along with their respective controls. Post 24 h transfection to assess the morphology, cellular mitochondria were then fluorescently labeled with a mitochondria-specific cationic dye- MitoTracker Green FM (M7514, Thermo Fisher Scientific). Cells were incubated with 200nM of Mitotracker

Green FM for 30 min at 37◦C according to the manufacturer's instructions. A Leica SP8 confocal laser scanning microscope with 60X magnification was used to capture the images. Using ImageJ software, mitochondrial morphology was measured according to standard parameters as previously stated (Iannetti et al., 2016).

3.2.10 Oxygen consumption rate (OCR)

The Sea Horse (Bioscience, CA, USA), Xfe24 Analyzer was used to measure cellular bioenergetics. After seeding each well with about 30,000 C2C12 myoblasts, the wells were treated with either 400 ng of P(128), 60 nM of anti-miR-128, or their corresponding negative controls. Following a 24-hour transfection, cells were rinsed and then incubated with XF assay medium for 1 h at 37 °C in a CO_2-free atmosphere. OCR was evaluated after the inhibitors—oligomycin (1.5 μM), FCCP (0.5 μM), rotenone (0.5 μM), and antimycin A (0.5 μM)—were successively introduced to each well following the manufacturer's instructions. Total protein was used to normalize the data.

3.3 Results

3.3.1 miR-128 negatively regulates peroxisome proliferator-activated receptor gamma coactivator 1α by binding to its 3'UTR.

Remarkably, in our earlier investigation, we've shown that miR-128 targets the NAD+-dependent protein deacetylase Sirtuin 1 (SIRT1) (Y. K. Adlakha and Saini 2013). Through its regulation of various histone and non-histone proteins, including PGC1α, SIRT1 is widely linked to mitochondrial biogenesis as well as several other biological processes like apoptosis, inflammation, and metabolism (Zhou et al. 2017). In addition, we found that the overexpression of miR-128 in the transcriptome profile of HEK293T cells, PGC1α was shown to be among the downregulated genes (uploaded in the GEO database, accession number GSE31297). We then checked the protein expression of PGC1α in HEK293 cells and found the expression was downregulated at the higher dose of miR-128 and vice versa as shown in Figure 3.1.

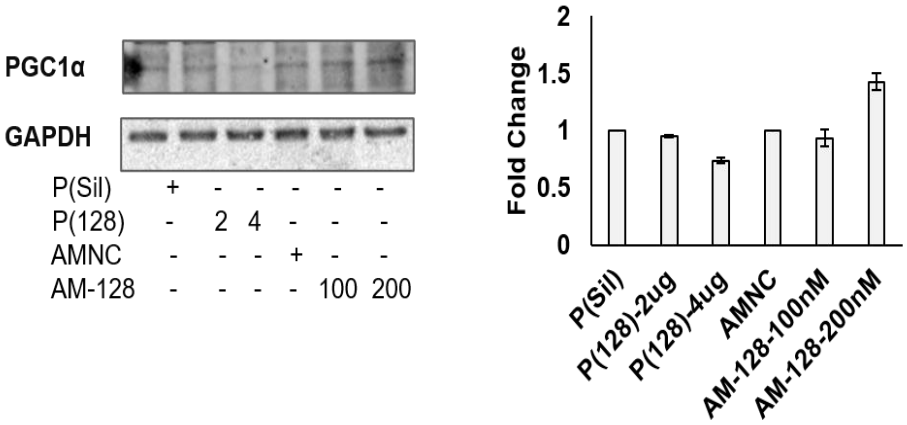

Figure 3.1*: Western blot analysis of PGC1α protein 24h post-treatment in HEK293. GAPDH was used as the loading control. The graph depicts the relative fold change of PGC1α protein levels versus control. AntimiR-128 = AM- 128, AntimiR negative control = AMNC, pSilencer vector = P(Sil), plasmid (128) = P(128),. *p < 0.05, **p < 0.01.*

Since the largest metabolic tissue, skeletal muscle is critically regulated by mitochondrial impairment, we next investigated into the downstream effects of cellular miR-128 level in C2C12 myoblasts and mouse skeletal muscle tissues. The TargetScan database (Release 7.2) indicated that PGC1α mRNA harbors the target sequence (3078–3084 nucleotide) for miR-128 in its 3′ UTR. Remarkably, this region was shown to be broadly conserved in mammals, including humans, chimpanzees, and rhesus monkeys (Figure 3.2).

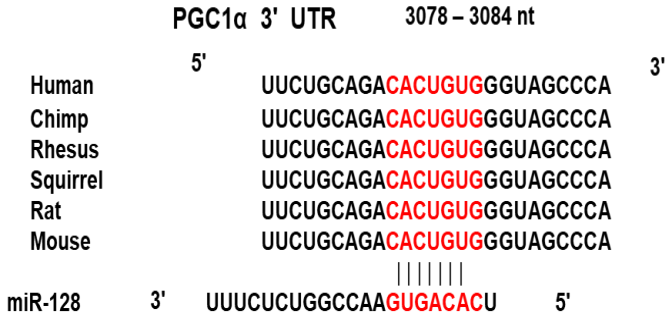

Figure 3.2*: Diagram showing the expected binding locations for miR-128 in the PGC1α 3'UTR (highlighted in red) which shows an evolutionary conservation among mammals. Numbers are the binding positions in the 3'UTR of PGC1α as predicted by TargetScan database*

Next, we first checked whether miR-128 targets PGC1α, the quantification of mature miR-128 levels post 24 h of transfection in C2C12 myoblast was done using TaqMan qRT-PCR assay. After miR-128 was overexpressed, there was a significant increase in miR-128 levels by 13.46 fold ($p = 0.0040$), while treatment with antimiR-128 significantly reduced miR-128 levels by 6.23 fold ($p = 0.0086$) as shown in Figure 3.3A.

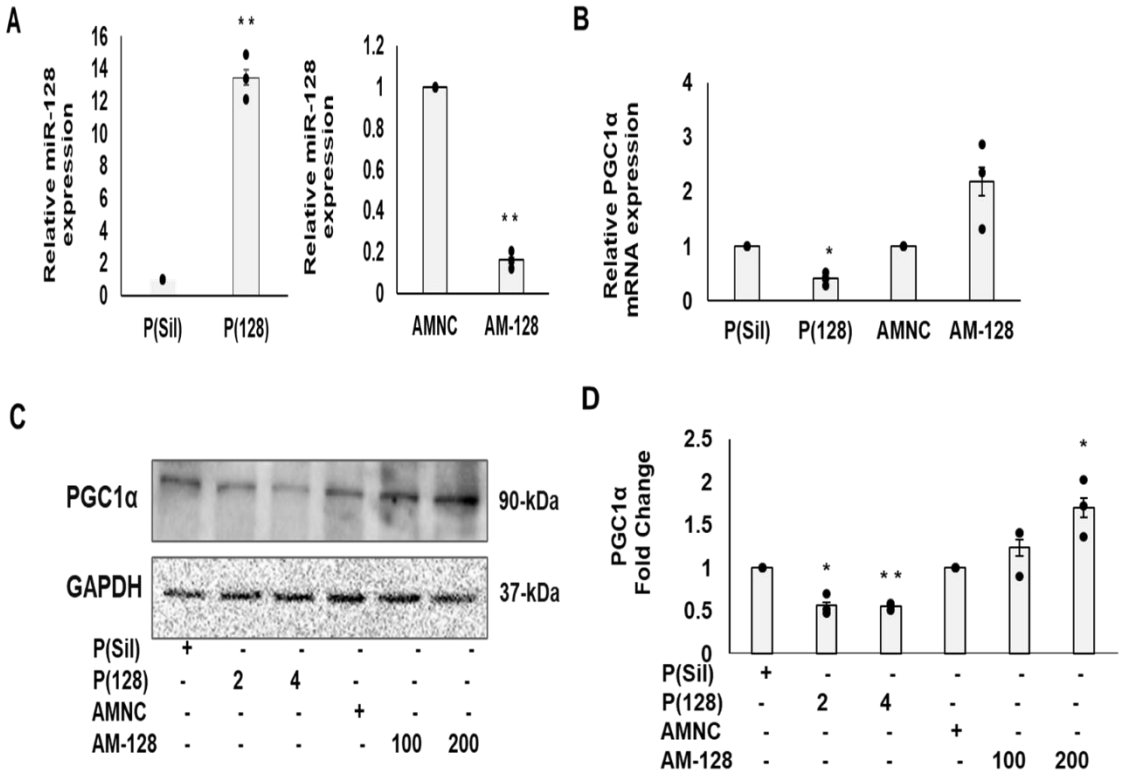

Figure 3.3: *miR-128 directly targets PGC1α (A) MiR-128 overexpression and inhibition was examined using TaqMan qRT-PCR after transfection for 24 hours with P(128), P(Sil), AM-128, or negative control treatment in C2C12 cells. (B) Using qRT-PCR the relative mRNA expression of PGC1α was estimated. (C & D) Western blotting was used to quantify the expression of PGC1α protein. The integrated densitometry results are displayed as a bar graph normalized to GAPDH. AntimiR-128 = AM- 128, AntimiR negative control = AMNC, pSilencer vector = P(Sil), plasmid (128) = P(128). (mean ± S.E.M), n=3. *p < 0.05, **p < 0.01.*

Additionally, we measured the transcriptional levels of PGC1α expression. When miR-128 was overexpressed, PGC1α mRNA levels dramatically dropped by 2.46 fold ($p = 0.0124$) and increased by 2.18 fold ($p = 0.1214$) when antimiR-128 treatment was applied.

In a comparable direction, western blot analysis showed that PGC1α protein levels decreased by miR-128 overexpression in a dose-dependent manner to 1.76 fold ($p = 0.023$) and 1.80 fold ($p = 0.0029$) and increased by 1.23 fold ($p = 0.291$) and 1.70 fold ($p = 0.0655$) upon antimir-128 treatment. Both transcriptional and translational quantification are shown in Figure 3.3B-3.3D. All these results thereby confirm that miR-128 is involved in regulating the mitochondrial biogenesis and function by down-regulation of PGC1α protein.

To further determine whether miR-128 directly targets PGC1α 3'UTR, we cloned the containing seed sequence of miR-128 from the 3′ UTR region of PGC1α mRNA into the PmiR-luciferase reporter vector. PCR amplification using the forward primer and reverse primer specifically designed to amplify the 742 bp region 3'UTR of PGC1α from mouse genomic DNA as mentioned in the material and methods. The amplified product was gel purified, digested, and inserted at cut sites of MluI and SpeI for PGC1α 3'UTR in PmiR report vector and construct was verified using sequencing (Figure 3.4 and Figure 3.5). When miR-128 was overexpressed, the luciferase activity was found to be significantly reduced by 1.41 fold ($p = 0.0482$), however when antimiR-128 was used, it was found to be significantly enhanced by 1.97 fold ($p = 0.0266$) as shown in Figure 3.6. Thus, it can be confirmed that miR-128 directly targets PGC1α.

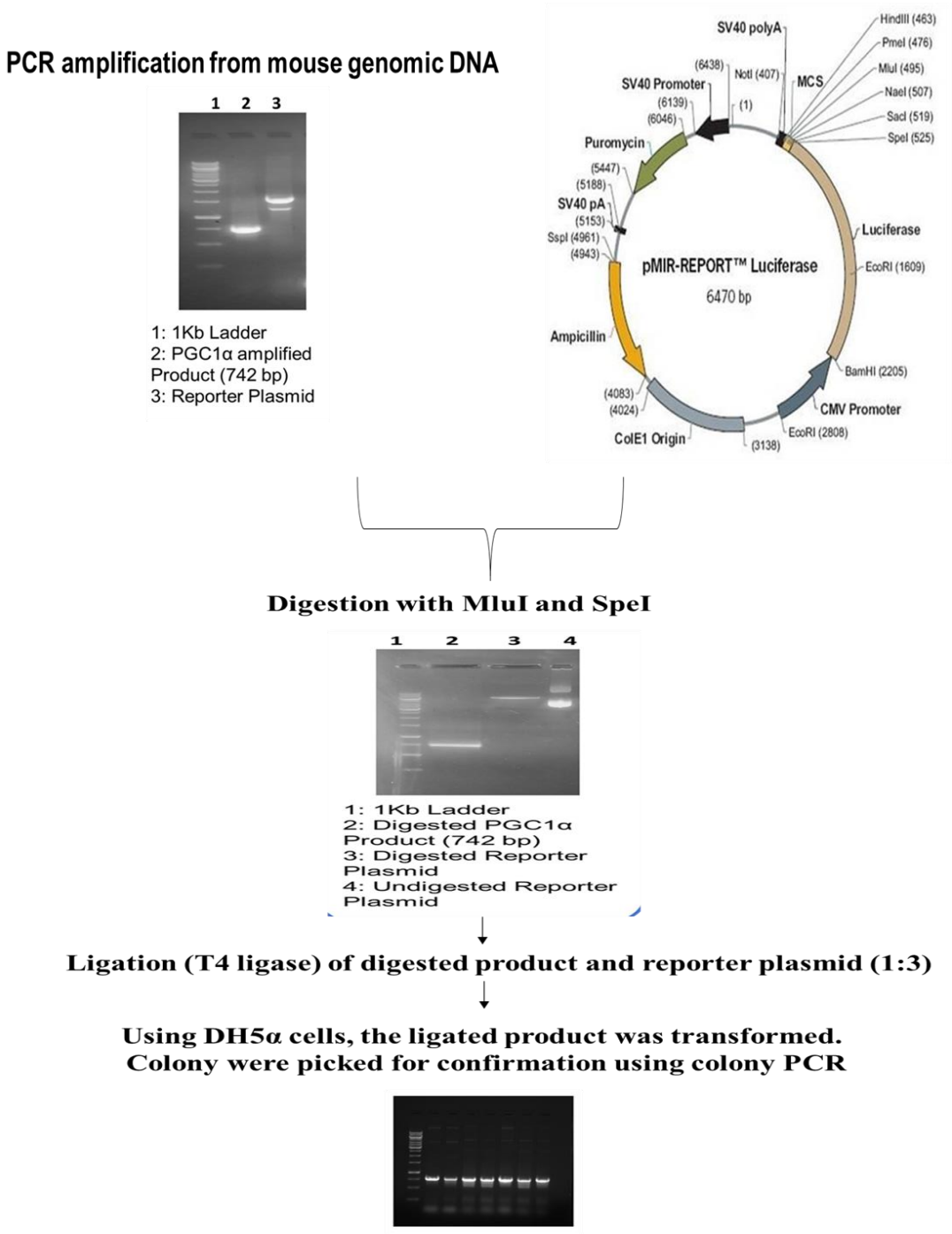

Figure 3.4: (A) *Schematic representation of PGC1α 3'UTR cloning into PmiR luciferase reporter vector.*

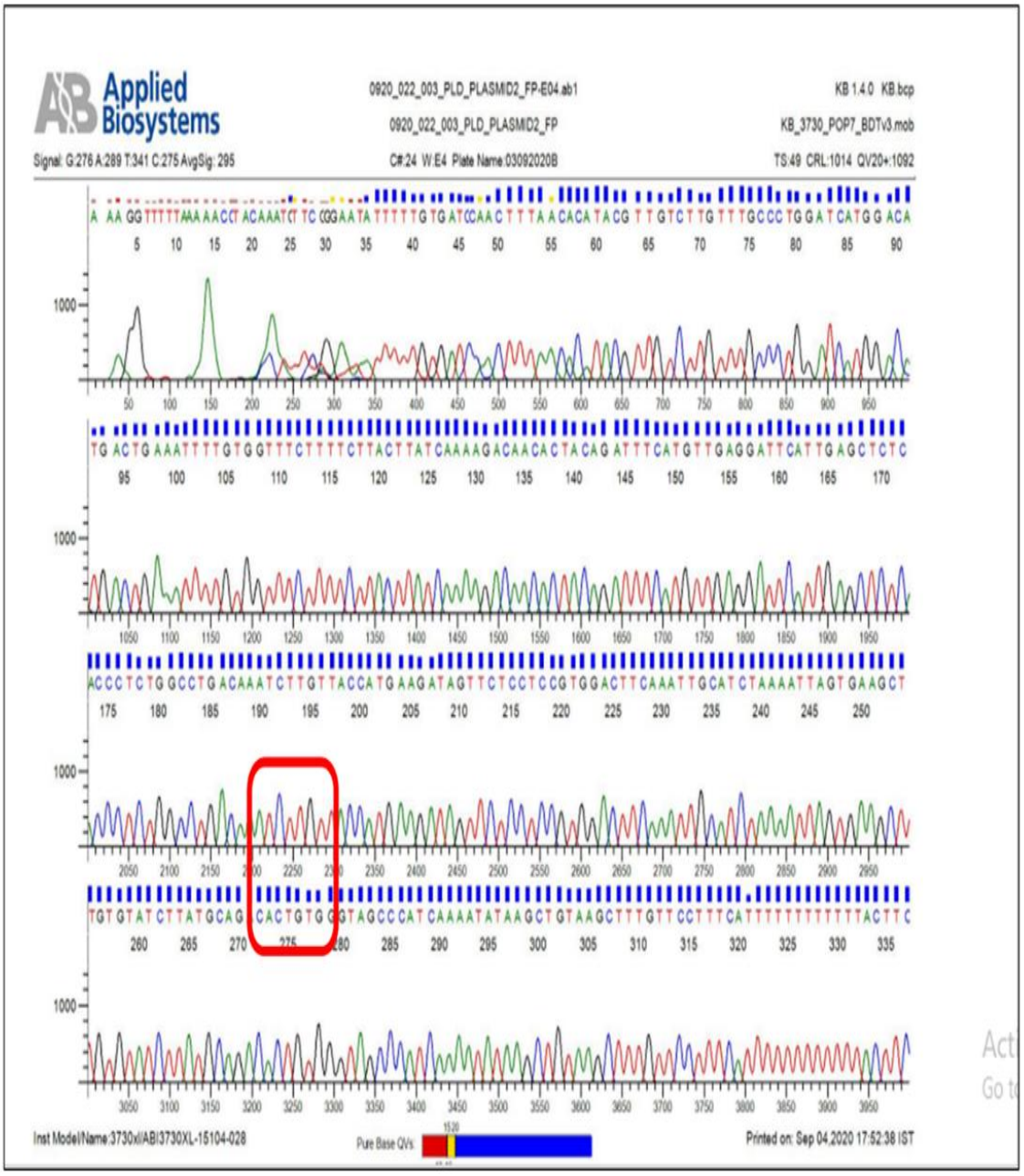

Figure 3.5: *The clone constructed for PGC1α was confirmed by sequencing*

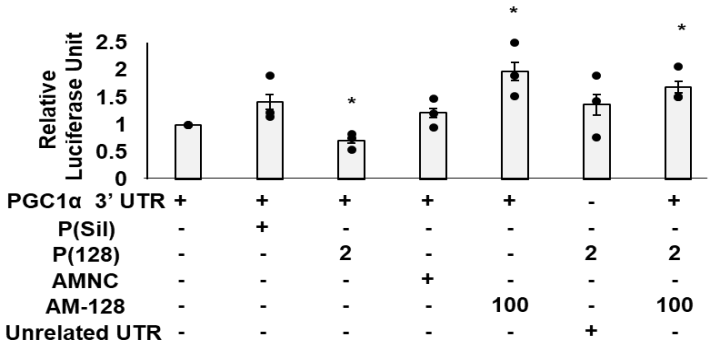

Figure 3.6*:Luciferase assay of PGC1α 3′ UTR. C2C12 cells were transfected with PGC1α 3′ UTR and either P(128), P(Sil), AM-128, or negative control, and luciferase activity was assessed. AntimiR-128 = AM- 128, AntimiR negative control = AMNC, pSilencer vector = P(Sil), plasmid (128) = P(128). (mean ± S.E.M), n=3. *p < 0.05, **p < 0.0*

3.3.2 Mitochondrial biogenesis is inhibited via miR-128-PGC1α/NRF1-2/TFAM pathway.

The effects of miR-128 on the regulatory crosstalk between NRF1, NRF2, and TFAM expression at the transcriptional and translational levels were then investigated. The elevated expression of miR-128 led to a 2.43-fold (p = 0.1138) decrease in NRF1 mRNA levels and a 1.94-fold (p = 0.0235) decrease in NRF2 mRNA levels. Conversely, treatment with antimiR-128 notably raised NRF1 mRNA levels by 1.68-fold (p = 0.0100) and NRF2 mRNA levels by 2.27-fold (p = 0.2432). In a qRT-PCR experiment conducted 24 hours after transfection, we found that overexpression of miR-128 decreased the mRNA levels of TFAM by 2.42-fold (p = 0.0853), whereas anti-miR-128 therapy increased the mRNA levels of TFAM by 1.15-fold (p = 0.404). Figure 3.7A and 3.7B has shown that the downstream pathway was downregulated concomitant with overexpression of miR-128.

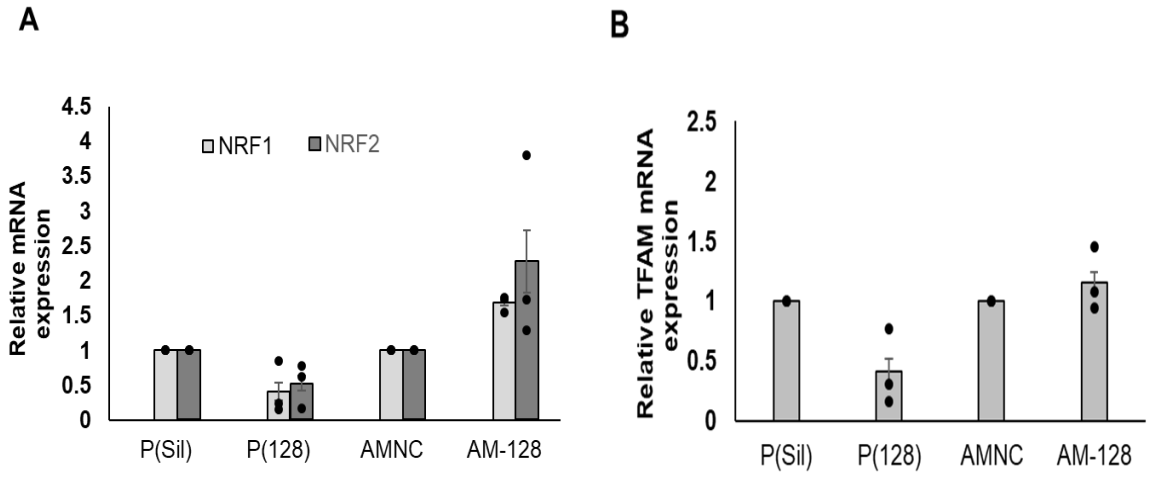

Figure 3.7: *Depicts the relative mRNA expression of (A) NRF1, NRF2 and (B) TFAM was quantified using qRT-PCR. AntimiR-128 = AM- 128, AntimiR negative control = AMNC, pSilencer vector = P(Sil), plasmid (128) = P(128). (mean ± S.E.M), n=3. *p < 0.05, **p < 0.01.*

Simultaneously, the protein levels of both nuclear respiratory factors significantly decreased that is NRF1 (1.12-fold and 1.47-fold) and NRF2 (1.13-fold and 1.34-fold) post overexpression of miR-128 and significantly increased the level of NRF1 (1.31-fold at 200 nM) and NRF2 (1.78-fold and 1. 81-fold) upon antimiR-128 in a dose-dependent manner (Figure 4.5A). The protein that binds to mitochondrial DNA (mtDNA) and is crucial for maintaining genome integrity is called mitochondrial transcription factor A, or TFAM. Following the overexpression of miR-128, TFAM protein levels decreased by 1.54 fold ($p = 0.0131$) and 1.44 fold ($p = 0.0883$), while following the treatment with anti-miR-128, TFAM protein levels significantly rose by 1.35 fold ($p = 0.184$) and 1.63 fold ($p = 0.0473$) as analyzed by western blots in Figure3.8. All these results confirm that the miR-128 inhibits the downstream pathway that regulates mitochondrial biogenesis and function.

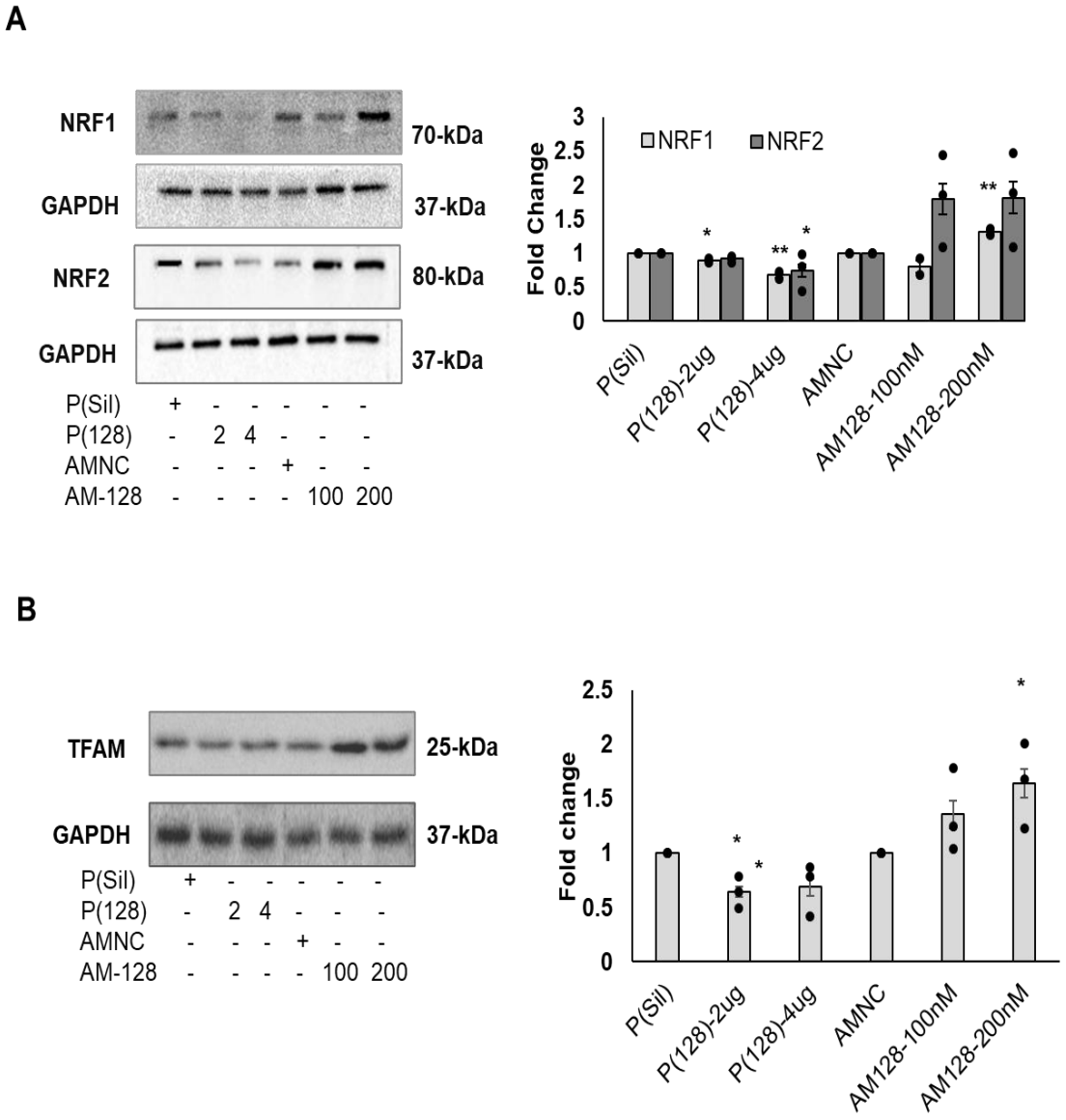

Figure 3.8*: Western blotting was used to quantify the expression of protein (A) NRF1, NRF2 and (B) TFAM 24h post-treatment in C2C12 myoblast cells. The integrated densitometry results are displayed as a bar graph normalized to GAPDH. AntimiR-128 = AM- 128, AntimiR negative control = AMNC, pSilencer vector = P(Sil), plasmid (128) = P(128). (mean ± S.E.M), n=3. *p < 0.05, **p < 0.01.*

High-fat diet (HFD) is a major contributor to mitochondrial dysfunction in metabolic conditions affecting the skeletal muscle (Kazeminasab et al., 2018). It is unknown, though,

how altered mitochondrial biogenesis and function lead to diet-induced abnormalities of skeletal muscle metabolism. Prior research have shown that human skeletal muscle samples from Type 2 diabetic or pre-diabetic patients had higher levels of miR-128 than did those from healthy controls (Prabu et al. 2015). Since downregulating miR-128 in vitro has the potential to enhance PGC1α mediated mitochondrial biogenesis and function, we investigated whether downregulating miR-128 in a model of hypercholesterolemic mice could reverse the effects of HFD-induced mitochondrial dysfunction by increasing PGC1α in the skeletal muscle of these mice. We next checked the expression of NRF2 and TFAM proteins in skeletal muscle tissue. As expected, the protein levels of all three proteins were increased in mice that were treated with the intraperitoneal dose of AntimiR-128 as in Figure 3.9.

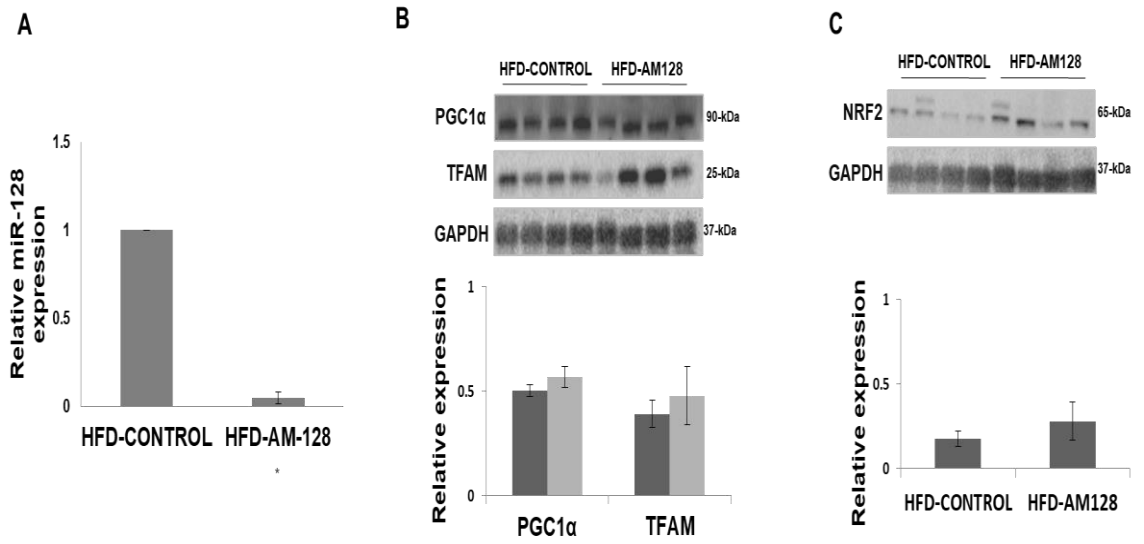

Figure 3.9: *Expression of miR-128 and PGC1α, NRF2, and TFAM protein in the skeletal muscle tissues of high-fat-diet-fed mice. (A) Relative miR-128 expression as quantified by TaqMan assay. (B) Western blot analysis of PGC1α and TFAM protein from the skeletal muscle tissue. (C) Western blot analysis of NRF2 protein from the skeletal muscle tissue. These values were normalized to GAPDH. Mice fed with a high-fat diet and treated with antimiR-128 (5mg/Kg) = HFD-AM128, Mice fed with a high-fat diet and treated with vehicle control =HFD-Control. Data are mean ± SD. n=4, *p < 0.05, **p < 0.01.*

3.3.3 miR-128 inhibited mitochondrial function by targeting oxidative respiration via NDUFS4.

Mitochondrial function have been linked to changes in the amount of mitochondrial DNA (MtDNA), which is commonly evaluated as the ratio of the mitochondrial genome to the nuclear genome using real-time quantitative PCR (https://pubmed.ncbi.nlm.nih.gov/23085537/). Using qRT-PCR analysis, we quantified a subset of electron transport chain transcripts that are exclusively transcribed by the mitochondrial genome: COX1, ND1, and COX2 by overexpressing miR-128 and inhibiting antimiR-128 treatment. As mitochondrial biogenesis is followed by mitochondrial DNA replication, we found that the transcription of mtDNA is reduced when cells are treated with miR-128 and vice versa (Figure 3.10A). Apart from that we also checked the mitochondrial mass by staining the C2C12 myoblast cells post 24 h transfection with non-acridine-orange because of its high affinity for phospholipid exclusive to inner membrane of mitochondria i.e., cardiolipin (CL). After miR-128 overexpression, the mitochondrial mass decreased by 1.23 fold ($p = 0.060$), whereas the mitochondrial mass increased by 1.27 fold ($p = 0.035$) when treated with antimiR-12 (Figure 3.10B)

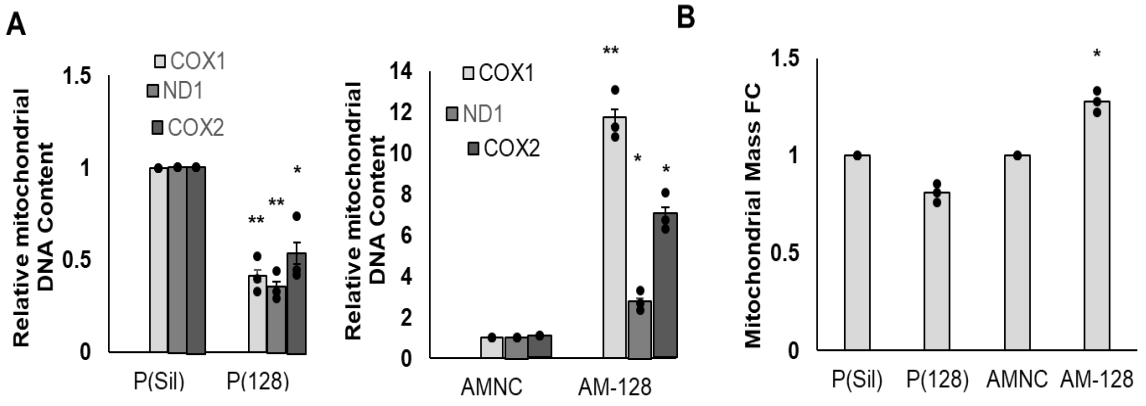

Figure 3.10: *Mitochondrial DNA and mitochondrial mass quantification. (A) qRT-PCR quantification was done to assess the mitochondrial DNA with mRNA levels of COX1, ND1, and COX2 in C2C12 myoblast cells post 24h transfection. (B) Using flow cytometry and nonyl-acridine orange labeling, the mitochondrial mass was examined. AntimiR-128 = AM- 128, AntimiR negative control = AMNC, pSilencer vector = P(Sil), plasmid (128) = P(128). (mean ± S.E.M), n=3. *p < 0.05, **p < 0.01.*

Bioinformatic analysis using TargetScan database revealed that the 3′ UTR of several oxidative phosphorylation (Electron Transport Chain) subunits contain miR-128 binding sites. This might imply that there is a negative relationship between ATP levels and miR-128 (Figure 3.11).

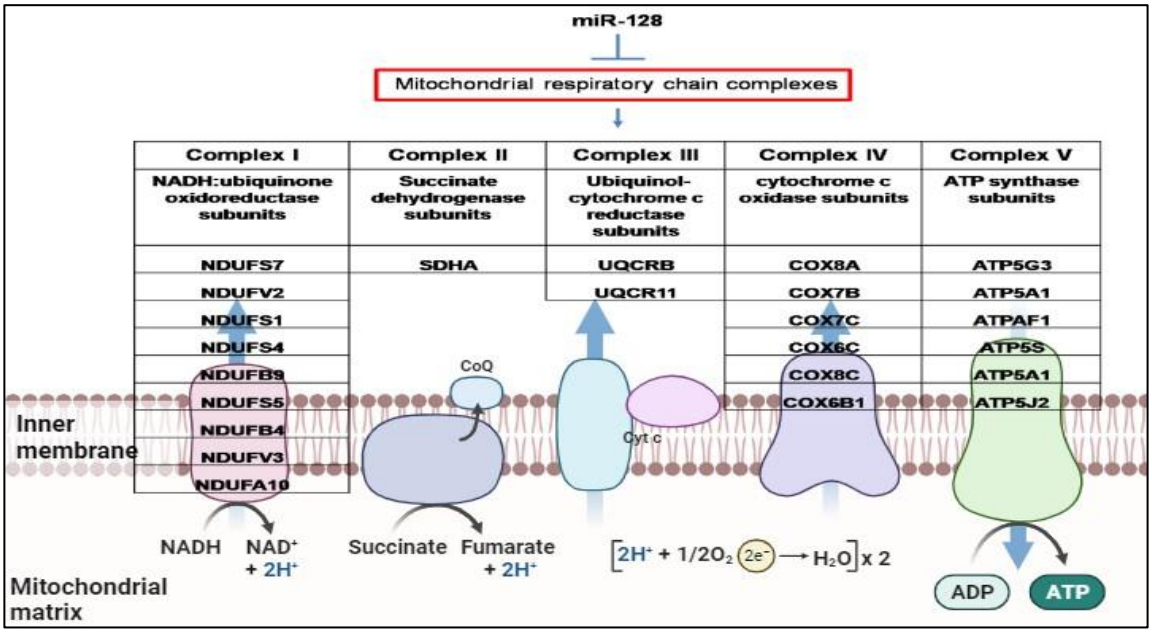

Figure 3.11: *Potential target genes for miR-128, predicted by the TargetScan database that builds different components of the mitochondrial respiratory complexes.*

To further validate that miR-128 targets NDUFS4 gene involved in the formation of the electron transport complex subunit I. According to the predicted binding location of miR-128 is widely conserved in the 3′ UTR of NDUFS4 (TargetScan), we cloned the NDUFS4 3'UTR region containing the miR-128 seed sequence in the luciferase PmiR reporter vector. The predicted binding location of miR-128 is widely conserved in the 3′ UTR of NDUFS4. The steps of cloning were followed as shown in Figure 3.12.

PCR amplification from mouse genomic DNA

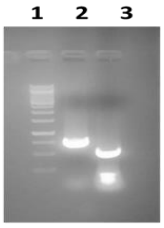

1: 1Kb Ladder
2: Positive Control
3: NDUFS4 amplified Product (518 bp)

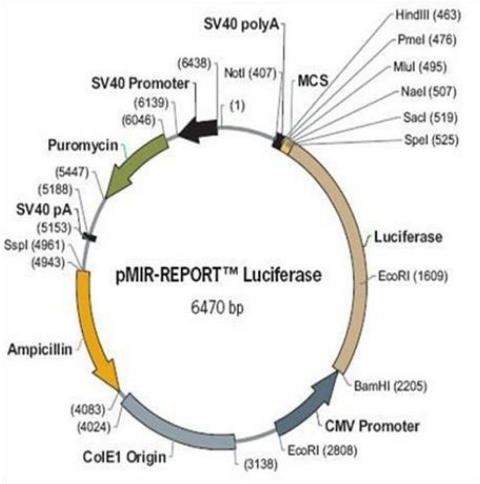

Digestion with MluI and HindIII

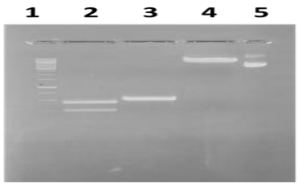

1: 1Kb Ladder
2: Digested PGC1α Product (742 bp)
3: Digested NDUFS4 Product (518 bp)
4: Digested Reporter Plasmid
5: Undigested Reporter Plasmid

Ligation (T4 ligase) of digested product and reporter plasmid (1:3)

Using DH5α cells, the ligated product was transformed. Colony were picked for confirmation using colony PCR

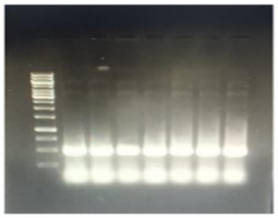

Figure 3.12*: Schematic representation depicts the cloning of NDUFS4 3'UTR region containing the miR-128 seed sequence in the luciferase reporter vector.*

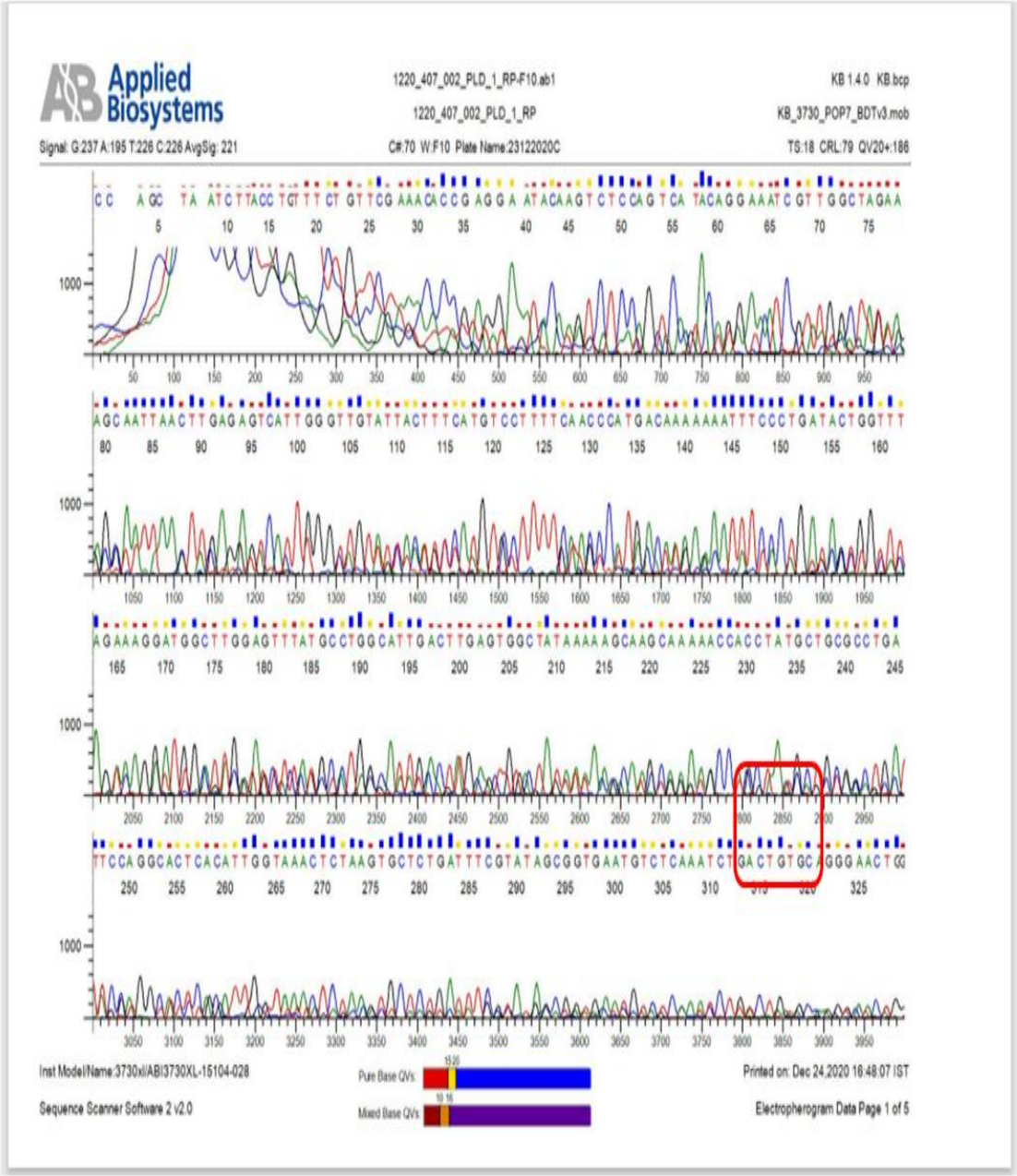

Figure 3.13: *The clone constructed for NDUFS4 was confirmed by sequencing*

Next, we measured the luciferase activity by performing dual luciferase assay on co-transfected cells with NDUFS4 3'UTR reporter vector and/or miR-128 or AntimiR-128 or their respective control. Figure 3.14B demonstrates that the luciferase activity of NDUFS4 3′ UTR reporter construct was significantly reduced relatively by 4.72 fold (p = 0.0044) on treating the cells with miR-128 and significantly increased 1.30 fold (p = 0.0331) upon antimiR-128 treatment in C2C12 myoblast cells.

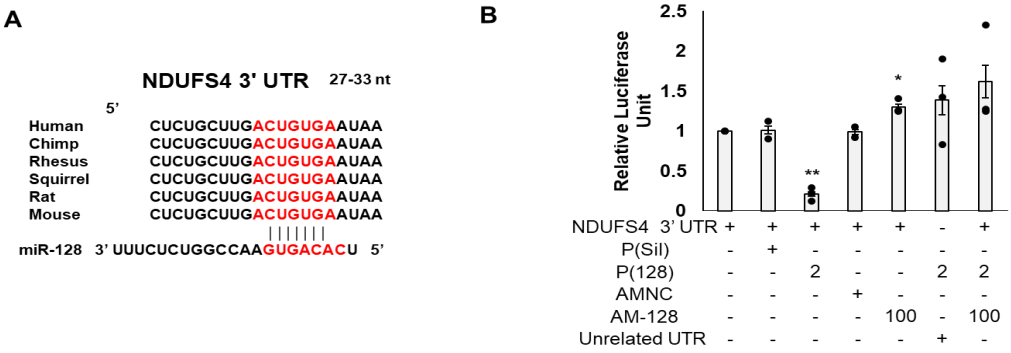

Figure 3.14: *miR-128 directly targets NDUFS4 (A) Diagrams represent the predicted binding site of miR-128 on the 3′ UTR of NDUFS4 gene by TargetScan database. (B) Lufciferase activity was measured post 24 h of co-transfected cells with PGC1α 3′ UTR and either P(128), P(Sil), AM-128, or negative control. AntimiR-128 = AM- 128, AntimiR negative control = AMNC, pSilencer vector = P(Sil), plasmid (128) = P(128). (mean ± S.E.M), n=3. *p < 0.05, **p < 0.01*

We next analyzed the mRNA and protein expression of NDUFS4 gene post 24 h transfection in C2C12 myoblast cells. We found that the mRNA levels of NDUFS4 were not changed upon overexpression or inhibition of miR-128. While the protein expression of the NDUFS4 gene is downregulated by 1.19 fold (p = 0.0123) and 1.47 fold (p = 0.0987) with overexpression of miR-128 treatment, it is found to be increased by 1.43 fold (p = 0.153) and 1.34 fold (p = 0.041) with suppression of miR-128 with antimir-128 treatment

(Figure 3.15). The mRNA level of NDUFS4 in C2C12 myoblasts does not correspond with the protein expression after miR-128 treatment.

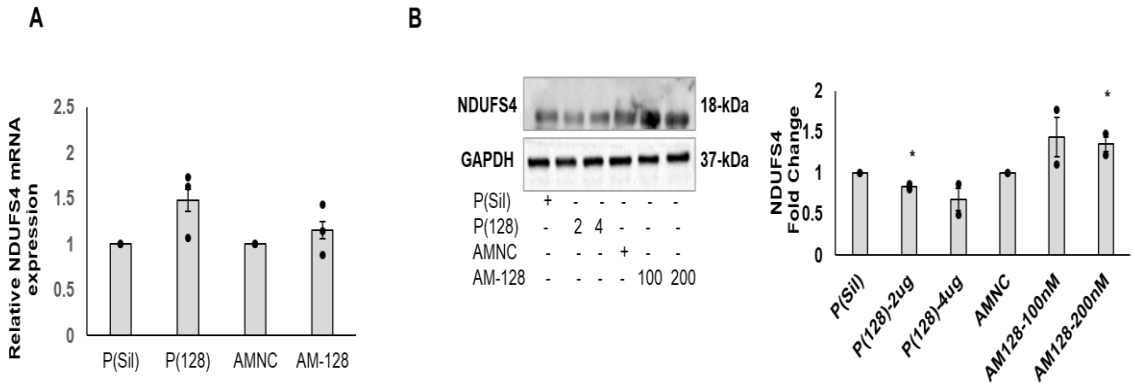

Figure 3.15: *NDUFS4 expression after transfection with miR-128. (A) Using qRT-PCR, the relative mRNA expression of NDUFS4 was quantified. (F) NDUFS4 protein expression were evaluated by western blotting. Bar graph of the western blot represents IDVs normalized to GAPDH. AntimiR-128 = AM- 128, AntimiR negative control = AMNC, pSilencer vector = P(Sil), plasmid (128) = P(128). (mean ± S.E.M), n=3. *p < 0.05, **p < 0.01*

All these results point towards a potential inverse relationship between miR-128 and ATP levels by downregulating the genes of mitochondrial biogenesis as well as genes involved in oxidative phosphorylation. Mitochondrial dysfunction refers to the mitochondria's inability to create and sustain adequate cellular ATP levels, and this dysfunction is related to the size of the mitochondrial pool. To examine the impact induced by miR-128 on ATP synthesis in the myoblast cells, we assessed the mitochondrial oxygen consumption rate (OCR). The upregulation of miR-128 leads to a reduction in the mitochondrial respiration rate, whereas treatment with antimiR-128 results in an increase. Additionally, various respiratory parameters, such as basal respiration, maximal respiration, ATP production, and spare respiratory capacity, exhibit a decline following miR-128 overexpression and an elevation upon miR-128 inhibition (Figure 3.16A-3.16E). Decline in mitochondrial DNA, mitochondrial mass, and ATP level upon miR-128 overexpression suggest that miR-128 inhibits mitochondrial function.

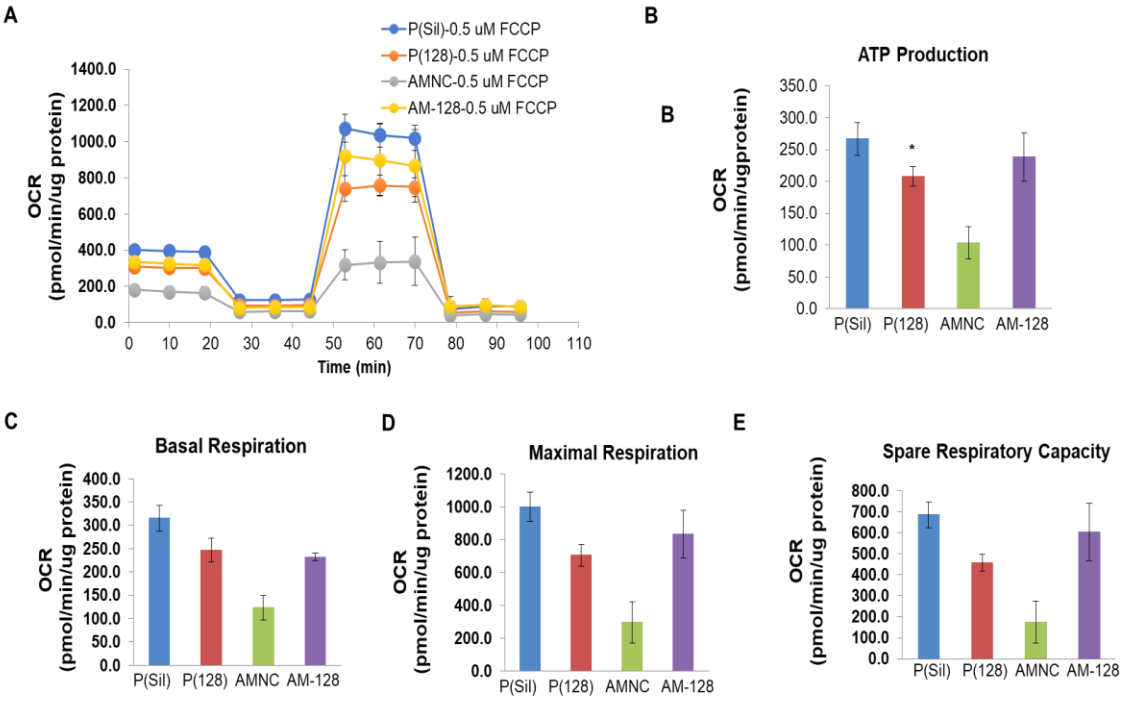

Figure 3.16: *(A) Bioenergetics changes was assessed by measuring the changes in oxygen consumption rates (OCR) with time in response to a mitochondrial respiratory function using sequential applications of oligomycin, carbonyl cyanide-4-trifluoromethoxy phenylhydrazone (FCCP), antimycin, and rotenone post 24 h transfection in C2C12 myoblasts cells. The data analysis of mitochondrial function was calculated from the OCR values (B) ATP production (C) Basal respiration (D) Maximal respiration, and (E) Spare respiratory capacity. Total cellular protein was used for normalization. AntimiR-128 = AM- 128, AntimiR negative control = AMNC, pSilencer vector = P(Sil), plasmid (128) = P(128). (mean ± S.E.M), n=3. *p < 0.05, **p < 0.01*

3.3.4 Mitochondrial dynamics is regulated by miR-128, thereby shaping their morphology.

As previous results reveal, miR-128 has impacted mitochondrial biogenesis and function. The alteration in mitochondrial biogenesis and function majorly correlates with mitochondrial dynamics. We then determined the regulatory role of miR-128 in mitochondrial dynamics, elucidating its impact on mitochondrial morphology. The MFN2

and OPA1 protein expression were significantly downregulated and the DRP1 protein expression was upregulated with miR-128 and vice versa (Figure 3.17A-3.17C).

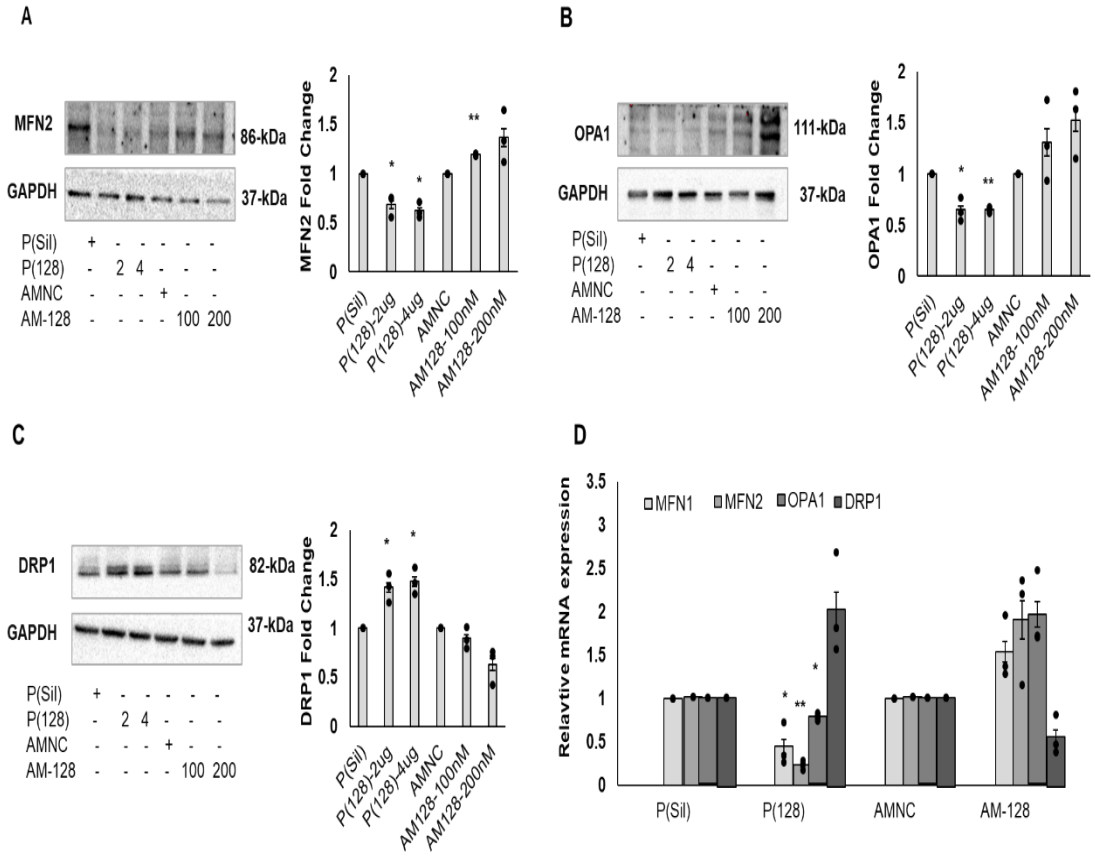

Figure 3.17: *miR-128 inhibits mitochondrial fusion and promotes fission. Protein expression was quantified using a western blot of key fusion such as (A) MFN2, (B) OPA1, and fission (C) DRP1 genes. The bar graphs represent the IDV normalized to GAPDH. (D) Relative transcriptional levels of MFN1, MFN2, OPA1, and DRP1 were quantified using qRT-PCR post 24 h transfection in myoblast cells. AntimiR-128 = AM- 128, AntimiR negative control = AMNC, pSilencer vector = P(Sil), plasmid (128) = P(128). (mean ± S.E.M), n=3. *p < 0.05, **p < 0.01*

Quantification of the genes involved in mitochondrial fusion (MFN1, MFN2, and OPA1) and mitochondrial fusion (DRP1) at the transcriptional level in C2C12 myoblast post 24 h transfections. There was a significant increase in the mRNA expression of mitochondrial fission protein and the expression of mitochondrial fusion proteins were downregulated upon miR-128 overexpression as in Figure 3.17D. On the contrary this trend was inverted with the AntimiR-128 treatment.

Simultaneously, MitoTracker Green FM dye cells were visualized for the mitochondrial morphology post 24 h transfection in C212 myoblasts as mentioned in material and methods. Increased mitochondrial fission was observed by the higher proportion of fragmented mitochondria in poorly linked networks in C2C12 myoblasts overexpressing miR-128 (Figure 3.18A). In contrast, cells treated with antimiR-128 showed clear signs of hyperfused mitochondria. Numerous metrics, including ferret's diameter, form factor, mitochondrial area, and perimeter, were used to assess the mitochondrial morphology. The results showed that the overexpression of miR-128 considerably decreased the area and perimeter of mitochondria by 1.32-fold ($p = 0.0045$) and 1.36-fold ($p = 0.0081$), respectively. When miR-128 was overexpressed, the form factor—which symbolizes the branching feature of mitochondria—was decreased by 1.35-fold ($p = 0.0009$), indicating that miR-128 therapy increased mitochondrial circularity and vice versa. Similar trends were also seen in the ferret's diameter, which reduced to 1.32-fold ($p = 0.0162$) after miR-128 overexpression and increased 1.10-fold ($p = 0.1248$) after receiving antimiR-128 therapy. Together, these findings show that overexpression of miR-128 stimulates mitochondrial fission and is reversed by miR-128 inhibition (Figure 3.18B).

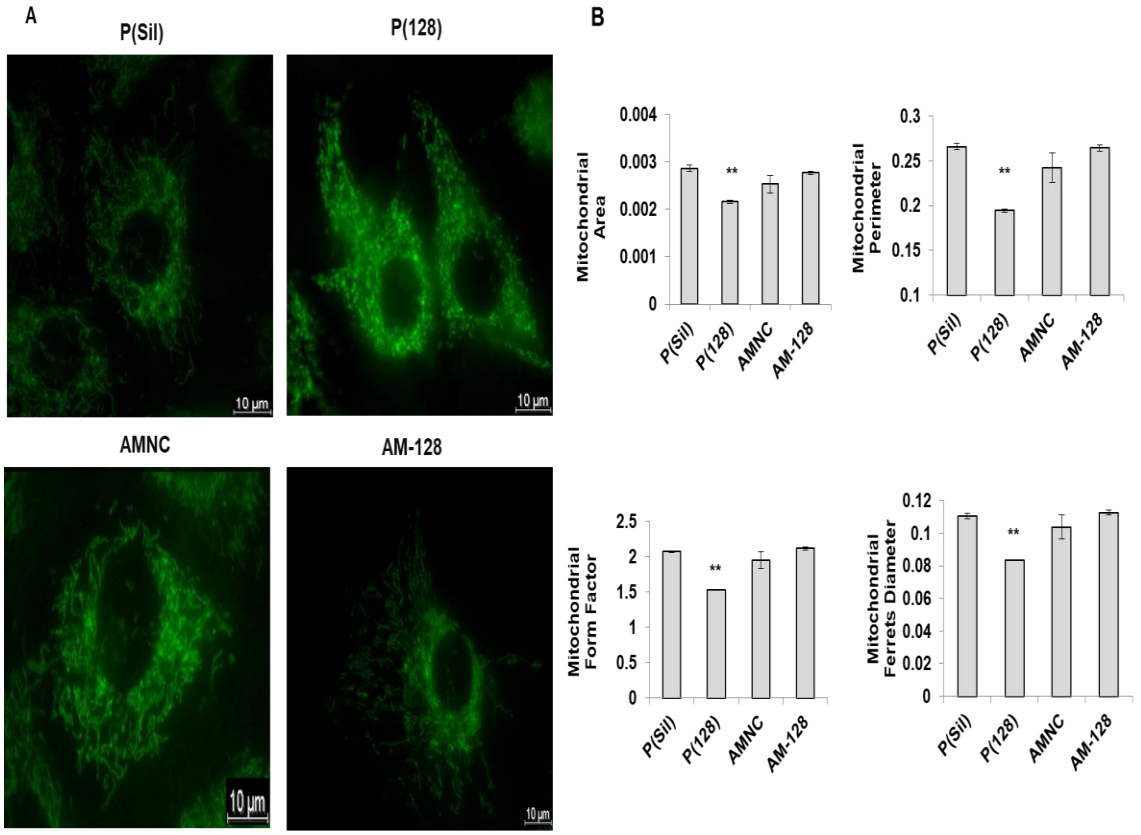

Figure 3.18: *Visualization of mitochondrial morphology. (A) Fluorescence staining (MitoTracker Green FM) was used to visualize the mitochondrial morphology after 24 h of transfection in C2C12 myoblast cells. (B) The volume of mitochondria is represented by the surface area and perimeter; the complexity and branching nature of mitochondria are reflected in the mitochondrial form factor, which is computed as [(perimeter2)/(4π·surface area)]; and the longest stretch of distance across the two points within a particular mitochondrion is indicated by Feret's diameter. . AntimiR-128 = AM- 128, AntimiR negative control = AMNC, pSilencer vector = P(Sil), plasmid (128) = P(128). (mean ± S.E.M), n=3. *p < 0.05, **p < 0.01*

3.4 Key Findings

- MiR-128 targets PGC1α and NDUFS4, two important regulators that directly affect mitochondrial biogenesis and function.
- Inhibition of PGC1α leads to reduced expression of crucial transcription factors (NRF1, NRF2, and TFAM), thereby hindering the transcription and translation of mitochondrial DNA.
- MiR-128 plays a role mitochondrial dynamic, by promoting fission (increased DRP1 expression) and suppressing fusion (decreased MFN1, MFN2, and OPA1 expression) affecting morphology, quantity, and size.
- MiR-128 may emerge as a critical regulator in the intricate network of mitochondrial processes like mitochondrial biogenesis, mitochondrial function and mitochondrial dynamics.

Chapter 4

Determining the network of mitochondrial metabolism by integrating machine learning and explainable artificial intelligence

4.1 Introduction

Understanding the interactions between miRNA and the genes in skeletal muscle responsible for mitochondrial biogenesis and function may help us better understand the molecular processes causing the various diseases, particularly metabolic and muscle-related disorders. Mitochondria, as we know, is the powerhouse of the cell, and their efficient function is essential for energy metabolism, especially in skeletal muscles that require high energy during physical activity (Mengeste, Rustan, and Lund 2021). Understanding these interactions could provide insights into developing targeted therapies, such as miRNA-based treatments, to correct or mitigate these dysfunctions. High-throughput gene expression data has dramatically changed clinical research and patient treatment. By examining the linked biological roles of gene expression, underlying processes implicated in metabolic disorders such as obesity and diabetes, cancer, and drug development can be identified (Edsjö et al. 2024). However, it has proven challenging to interpret enormous volumes of data. Additionally, different platforms and approaches might yield different results. Machine learning is a subfield of computer science that uses data-driven methods to find patterns and predict behavior (Sarker 2021). The present work used the machine learning interpretation method known as "Shapley additive explanation" to highlight significant aspects in gene expression data associated with type 2 diabetes. This approach offered more comprehensiveness and explicability. The "Black box" of machine learning models, which typically yield exceptional results in terms of accuracy and predictive power but don't explain how they arrived at the prediction, is becoming less common as XAI (eXpaintable artificial intelligence) makes these models easier to understand. Disease prevention, risk stratification, and early identification of people at high risk of type 2 diabetes are critical. By utilizing the XGBoost technique to train the machine learning model, we concentrated on the target mitochondrial genes that are particular to skeletal muscle tissue in patients with type 2 diabetes in the current study.

4.2 Material and Methods

4.2.1 Data selection and processing

Studies that are publicly accessible and examine the mRNA and miRNA expression profiles of human Skeletal Muscle tissue, affected by type 2 diabetes were selected using the NCBI's Gene Expression Omnibus (GEO) (https://www.ncbi.nlm.nih.gov/geo/) database. We prioritized the expression profile GSE IDs with many samples by concentrating on the tissue of origin and excluding any treatments or additional conditions. For the above-mentioned conditions, we were able to extract the pre-processed data, and the sample information presented in **Table 4.1** from the GEO datasets.

Table 4.1: Details of the gene expression datasets used in the study.

GEO ID	Disease	Organism	Tissue	Platform	Experimental Design
GSE22309	Type 2 Diabetes	*Homo sapiens*	Skeletal Muscle	Affymetrix Human Genome U95A Array	20 control patients and 15 type 2 diabetes patients
GSE25462	Type 2 Diabetes	*Homo sapiens*	Skeletal Muscle	Affymetrix Human Genome U133 Plus 2.0 Array	40 control patients and 10 type 2 diabetes patients
GSE18732	Type 2 Diabetes	*Homo sapiens*	Skeletal Muscle	Affymetrix GeneChip Human Genome U133 Plus 2.0 Array	47 control patients and 45 type 2 diabetes patients

GSE22309, GSE25462, and GSE18732 were retrieved, and log 2 transformations and quantile normalization were performed after combining the three datasets. The samples in the dataset were classified as control samples (107) and type 2 diabetic samples (70).

4.2.2 Retrieval of genes involved in mitochondrial homeostasis.

MitoCarta3.0 is centered on proteins contributing to mitochondrial homeostasis, encompassing 1,136 human genes sourced directly from the MitoCarta3.0 database (http://www.broadinstitute.org/mitocarta).

4.2.3 Machine earning model and testing.

A machine learning model was trained to uncover consistent patterns to predict features within a new dataset. XGBoost has been a popular option in Kaggle events combining structured data and applied machine learning due to its scalability. Gradient-boosted decision trees (GBM) have been made more effective and efficient using XGBoost. Since its introduction, GBM has routinely outperformed most other ML techniques, and conventional decision trees (boosting). To implement this approach, the dataset was partitioned into two distinct sets — training and testing sets, adhering to an 80:20 ratio. The construction of the model was executed using the Scikit-learn library (Pedregosa et al. 2012). The model's accuracy was assessed and the confusion matrix for the test was evaluated.

4.2.4 Interpreting the machine learning model using eXplainable Artificial Intelligence (XAI).

Machine learning models, on the other hand, make it challenging to comprehend the stages that guide the model's decision-making process (Anguita-Ruiz et al. 2020). Most of the time, artificial intelligence is a "black box," meaning that not even experts can fully understand how it arrived at a given decision (Nelson et al. 2020). XAI is a means of implementing social rights to the explanation (Savage 2022). The SHAP approach which was derived from cooperative game theory helped the classifiers in this case to produce both a global and individualized interpretation of the expected result. The trained XGBoost model was subjected to an XAI analysis using the Python SHAP module. As characteristics, we identified the 20 genes with higher SHAP values. Using GraphPad Prism Software (v.5.01 GraphPad, Inc., CA, USA), we tested the expression of each gene

based on the combined expression data of the control and patient samples. An unpaired t-test was used. A threshold of p-value <0.05 was employed to ascertain the statistical significance of genes.

4.2.5 Protein-protein interaction network analysis

Using String version 11.5 (https://string-db.org/), the role and interaction network of the proteins involved in mitochondrial homeostasis were identified by providing an input list of the 20 genes derived by SHAP values. For the interaction score, a medium confidence of 0.4 and a significance of p <0.05 were used. The network was subjected to k-means clustering to find genes in related complexes with important biological functionality.

4.2.6 Pathway Enrichment Analysis

We used the KEGG database to perform pathway enrichment analysis for the top genes. The study covered the following domains: molecular function, cellular component, and biological process. The genes were mapped against *Homo sapiens* as the reference species. Consideration of significant pathways was carried out employing a p-value < 0.05.

4.2.7 mRNA-miRNA interaction network analysis

Software for network analysis and visualization focusing on miRNAs and their functional insights is MiRNet 2.0 (https://www.mirnet.ca/). It was used to anticipate the possible mRNA-miRNA network. The number of interactions based on degree and betweenness is represented by the size of the shapes. Using the MIENTURNET platform, significant miRNAs with maximum target characteristics and mRNA-miRNA interaction based on strong evidence were found (http://userver.bio.uniroma1.it/apps/mienturnet/). The cut-off value for statistical significance was set at p-value < 0.05. For network visualization, the mRNA-miRNA network based on compelling evidence was loaded into Cytoscape 3.8.0.

4.3 Results

4.3.1 Determining the genes responsible for mitochondrial homeostasis expressed in skeletal muscle of type 2 diabetes patients.

First, the gene expression datasets were searched in the GEO database with the help of keywords 'Diabetes + Skeletal Muscle'. In return for the search, we got thirty-six datasets. GSE22309, GSE25462, and GSE18732 microarray expression data were identified based on that expression consisting of skeletal muscle tissue samples from human control and type 2 diabetes patients. After obtaining pre-processed series matrix files, sample profiles from each of the three datasets were combined to form a single dataset.

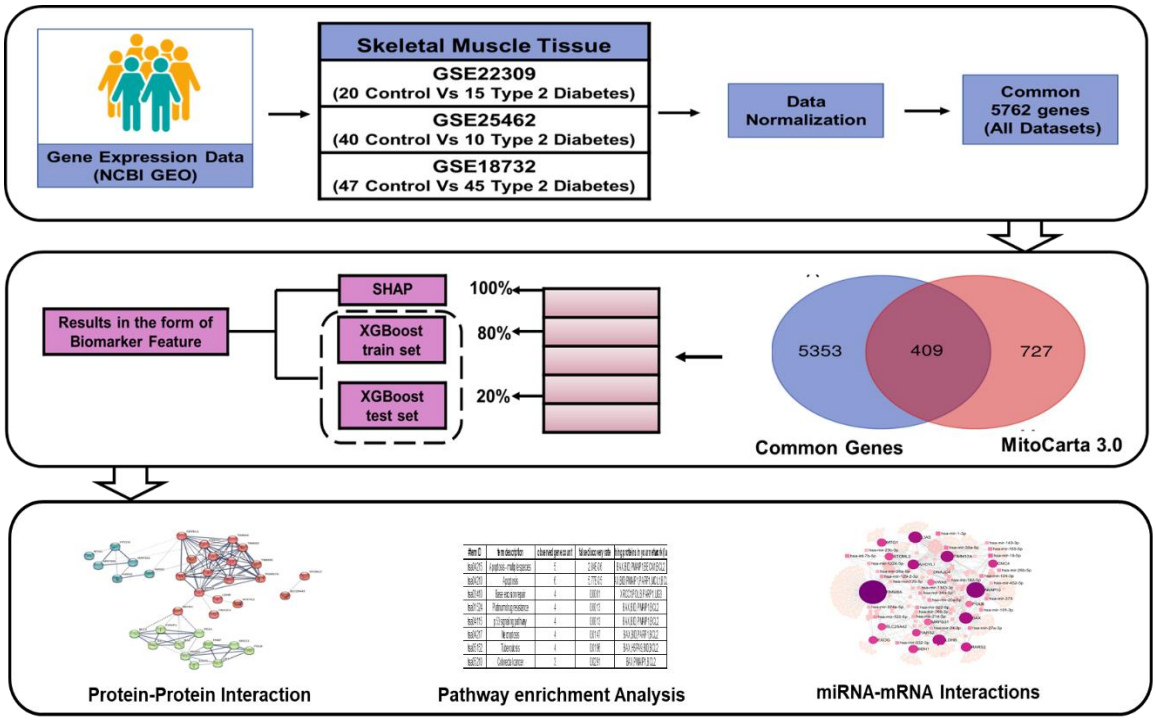

***Figure 4.1**: Depicts the methodology followed for the study. The NCBI GEO database was used to obtain the expression data for GSE22309, GSE25462, and GSE18732. Type 2 diabetes patient samples and control samples were categorized. Shared transcripts were then identified from the three datasets (5762 genes). The Venny tool was used to identify the overlapping genes from mitochondrial gene list from the Mitocarta 3.0 database as well as a list of common genes from the three datasets.The XGboost technique was used to train the model, and SHapley Additive exPlanations were used to analyze the findings. Additionally, pathway enrichment analysis, miRNA-mRNA network analysis, and protein-protein interaction are used to functionally characterize the genes participation.*

We limited our attention to the shared transcripts exclusively because of the differences in transcript coverage between the U133 Plus and U95A platforms. The flow charts in Figure 4.1 represent the schematics of the steps followed for data analysis. There were 5762 genes shared by all three datasets after normalization of the datasets. We employed batch effect correction techniques together with normalization techniques for data harmonization. For a more seamless integration of the datasets and to minimize any biases coming from the use of two separate platforms or experimental variation, Log2 transformation, and Quantile normalization were applied to this single file to normalize the expression data (Figure 4.2A and 4.2B).

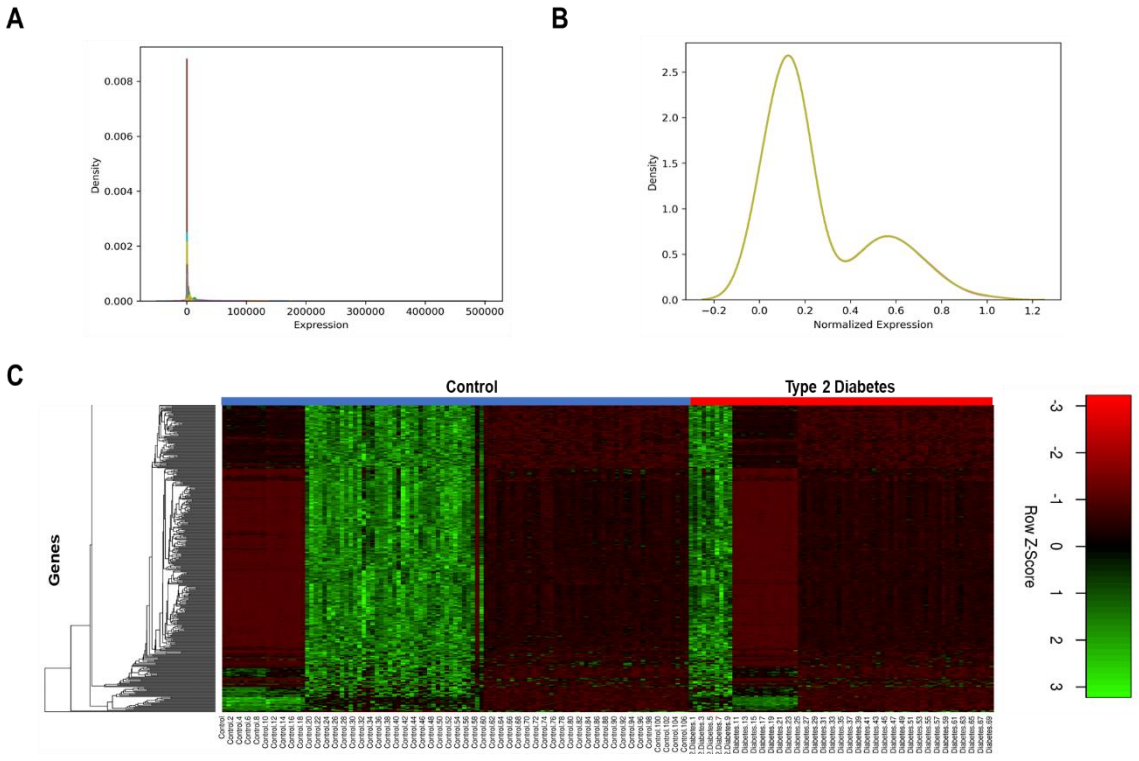

Figure 4.2: *Data Normalization. (A & B) Expression data before and after log 2 transformation and quantile normalization respectively. (C) Heatmap displaying of the mitochondrial genes found from a single pooled dataset (all three GEO expression profiles) normalized using Z-score scaling. Z<0 (Red); Z>0 (Green); Z=0 (Black).*

The list of 409 genes expressed for mitochondrial homeostasis in skeletal muscle of type 2 diabetes patients was then obtained using the Venny 2.1.0 tool by giving an input list of

shared genes from three datasets (5762 genes) and 1136 genes from the Mitocarta 3.0 database. Figure 4.2C shows the heatmap of the genes identified based on the Z- score.

4.3.2 Utilizing the XGboost algorithm technique to train the ML model.

To achieve the goal of predicting the genes altered in type 2 diabetes patient's skeletal muscle tissue samples compared to that of control patients, XGboost machine learning algorithms were used for a better understanding of the mitochondrial etiology in the disease. We then trained the model on sample profile data containing the expression of 409 mitochondrial genes in an 80% to 20% ratio. Hence, 80% of the data was supplied to the training set, while the remaining 20% was used for the test set. The model was trained by utilizing the Scikit-learn package.

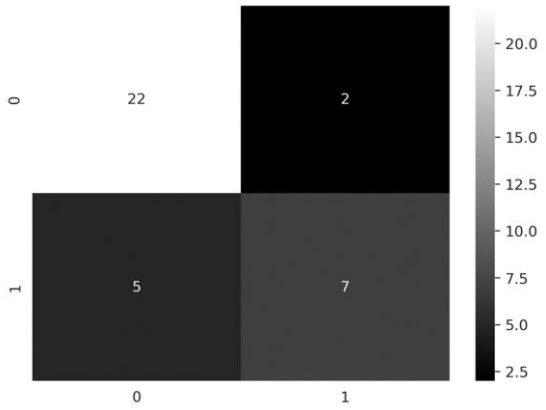

Figure 4.3*: The machine learning model was assessed by using a confusion matrix from the test data. The grey squares of the matrix represent the true positive (TP), black squares represent the false positive (FP) and false negative (FN), and white squares represent the proportion of the True Negative (TN).*

The test set, or remaining data, was then used to evaluate the model. The test set was evaluated, and the machine learning model's precision and accuracy were computed using the confusion matrix for the test set shown in Figure 4.3. The contingency table created a

confusion matrix with four distinct sets of expected and actual values. For this test dataset, the precision is 77.7% and the accuracy is 80.55% percent. In machine learning, good accuracy is a subjective concept. However, anything above 70% to be excellent model performance. It is actually feasible to go for an accuracy measure of between 70% and 90%. Additionally, this complies with industry norms.

4.3.3 Explainable AI predicts genes responsible for mitochondrial health and function.

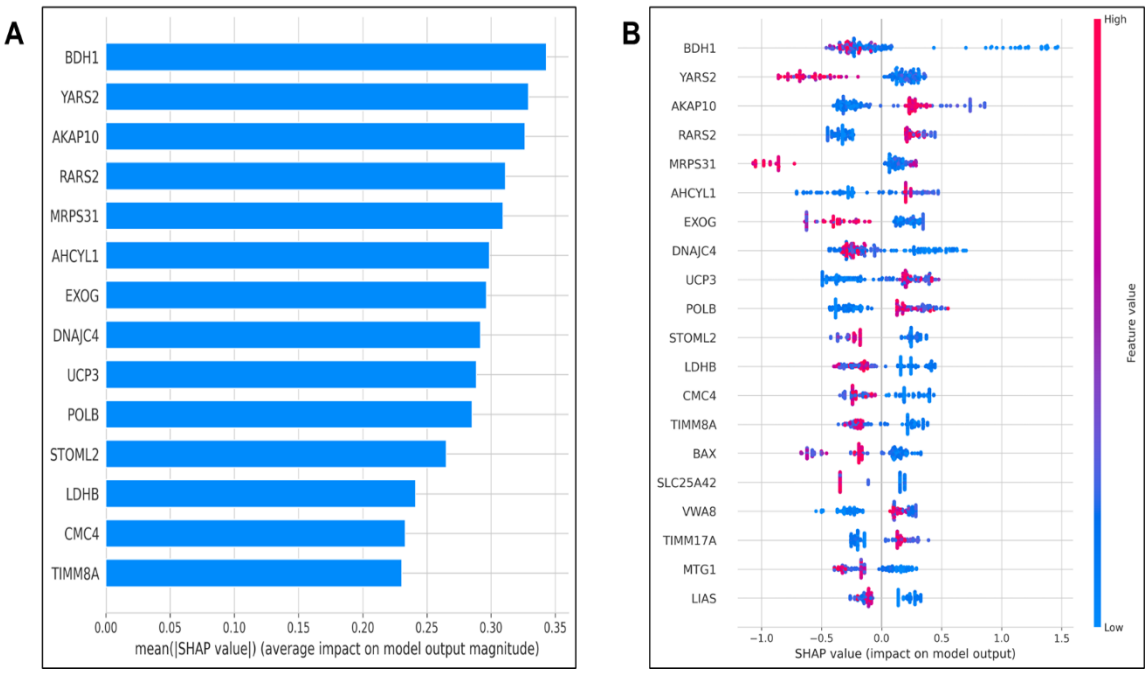

***Figure 4.4**: Output of the Model. (A) The absolute average impact of the most important genes and their effects on Type 2 diabetes patients compared to Control patients are depicted in the bar plot. (B) A summary diagram illustrating the SHAP values. The sorted genes are arranged in decreasing order of feature importance on the y-axis. The x-axis displays the relationship between a gene's expression and a greater or lower prediction, indicating the gene's impact on the model's output. A minimum impact is shown in blue, and pink indicates a high impact of the gene.*

The Python SHAP module aids in determining attributes that significantly affect the model's prediction confidence score. A machine learning model that makes decisions is the foundation of this study. Next, we plotted the global features, which is shown as a bar plot in Figure 4.4A, as the average of the SHAP values for each feature by gene of relevance arranged in decreasing order. To see how the feature affected the value and target prediction, we also created a SHAP summary graph (Figure 4.4B). Regardless of whether the genes are upregulated or downregulated, genes with high significance scores are thought to have a greater influence on the disease.

The 20 genes based on the feature's importance score were selected. These genes could be good candidates for further investigation or as possible targets for therapy. Apart from that, we did a literature search and found there was a significant degree of consistency with previous reports (Table 4.2). RARS2, CMC4 (C-X9-C Motif Containing 4), TIMM17A (Translocase of Inner Mitochondrial Membrane 17A), MTG1 (Mitochondrial Ribosome Associated GTPase 1), and VWA8 (Von Willebrand Factor A Domain Containing 8) were investigated in several diseases besides type 2 diabetes.

Table 4.2: Gene expression of the identified genes in type 2 diabetes.

S. No.	Gene	Expression in type 2 diabetes	Reference
1	**BDH1**	Low	(Thai et al. 2021)
2	**YARS2**	Low	(López-Soldado et al. 2023)
3	**AKAP**	Low	(Ando et al. 2018)
4	**RARS2**	Low	(López-Soldado et al. 2023)
5	**MRPS31**	Low	(Arden et al. 1996)
6	**EXOG**	Low	(Pardo et al. 2016)
7	**HSP40/DNAJ**	Low	(Gupte, Bomhoff, and Geiger 2008) (Abu-Farha et al. 2015) (Abubaker et al. 2013)
8	**UCP3**	Low	(Schrauwen et al. 2006) (J. Liu et al. 2013)
9	**POLB**	Low	(Grindel et al. 2016)
10	**STOML2**	Low	(Mitsopoulos et al. 2015)
11	**LDHB**	Low	(Palsgaard et al. 2009)
12	**TIMM8A**	Low	(Dubé et al. 2020)
13	**BAX**	Low	(S. Wang et al. 2023)
14	**SLC25A42**	Low	(Khin, Lee, and Jun 2023)
15	**LIAS**	Low	(Padmalayam et al. 2009)

In addition, we used GraphPad Prism 8 to calculate the overall relative expression and p-value from the combined single dataset created after normalization from three GEO expression profiles to characterize the significance and importance of the genes that emerged as the features, as given in Table 4.3. We surprisingly discovered that each gene had decreased significant expression supporting mitochondrial homeostasis. UCP3 and BAX also decreased but was not significant. In this investigation, we did identify upregulated genes, however they were not in the list of twenty genes based on the SHAP values.

Table 4.3: Statistical Analysis Results for Each Identified Gene from the Combined Dataset.

Control vs Type 2 diabetes		
Genes	**Regulation**	**p-value**
BDH1	Downregulated	0.0001
YARS2	Downregulated	0.0017
AKAP10	Downregulated	0.0082
RARS2	Downregulated	0.0031
MRPS31	Downregulated	0.0002
AHCYL1	Downregulated	0.0306
EXOG	Downregulated	0.0003
DNAJC4	Downregulated	0.0001
UCP3	Downregulated	Ns
POLB	Downregulated	0.0120
STOML2	Downregulated	0.0001
LDHB	Downregulated	0.0001
CMC4	Downregulated	0.0008
TIMM8A	Downregulated	0.0003
BAX	Downregulated	Ns
SLC25A42	Downregulated	0.0010
VWA8	Downregulated	0.0010
TIMM17A	Downregulated	0.0007
MTG1	Downregulated	0.0007
LIAS	Downregulated	0.0002

4.3.4 Pathways linked to the identified genes through Gene Set Analysis.

Functional enrichment analysis is a widely used technique for finding commonalities in large biological datasets. The area of biomedicine uses functional enrichment analysis of gene expression data to identify the disease's pathophysiology. The protein-protein network of genes that were extracted based on SHAP values was examined using the String version 11.5 database to determine their function in the course of the disease. We used k-means clustering for this network, and as shown in Figure 4.5, the network was separated into three clusters: 23 genes in red-colored cluster 1, 11 genes in green-colored cluster 2, and 6 genes in blue-colored cluster 3.

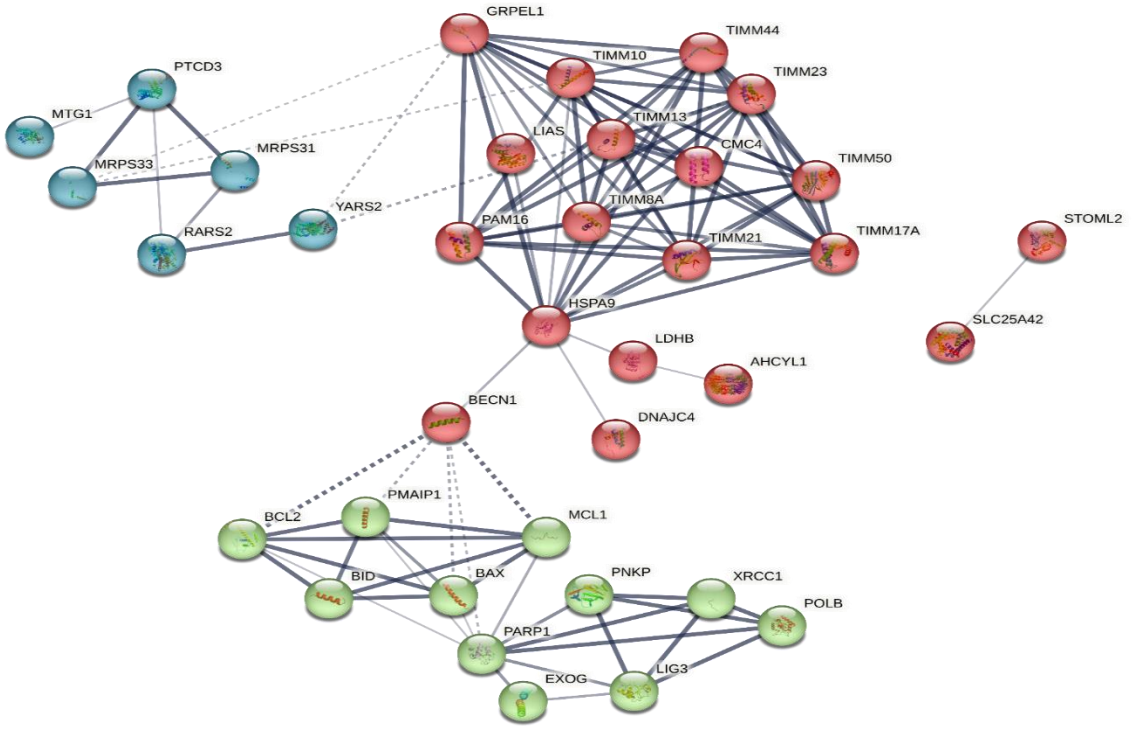

Figure 4.5: *The identified mitochondrial genes are used as SHAP characteristics in constructing the protein-protein interactions (PPIs) network utilizing the String database.*

Moreover, this network's analysis revealed that the greatest number of genes play a major role in biological processes such as base-excision repair, DNA ligation, apoptosis signaling factor release, mitochondrial membrane potential maintenance, and protein transport (import/export) as shown in Table 4.4. Collectively, the data point to the regulation of many nuclear and mitochondrial import, export, and assembly routes by nuclear genes in these pathways, which results in the necessity of multimeric proteins for mitochondrial biogenesis. Membrane potential collapse brought on by impaired glucose metabolism and mitochondrial malfunction might affect ATP generation and may contribute to insulin resistance. Mitochondria are the main players in apoptosis, or programmed cell death. Dysregulation of apoptosis might be linked to the death of pancreatic beta cells in type 2 diabetes. It may begin with the release of apoptotic signaling components from damaged mitochondria, which would then impact on insulin secretion. These dysfunctions simultaneously lower insulin secretion and contribute to insulin resistance. Research on understanding and treating these mitochondrial-related issues is ongoing in the context of managing and preventing diabetes. Four key molecular functions—protein transmembrane transporter activity, chaperone binding, BH3 domain binding, and P-P-bond-hydrolysis-driven protein transmembrane transporter activity—were the predominant areas of enrichment in the PPI network. In type 2 diabetes, BH3 protein binding to BAD and BCL lowers the threshold for apoptosis to occur and prevents anti-apoptotic proteins from acting.

Table 4.4: Enrichment analysis of identified genes based on SHAP values.

Biological Processes			
#term ID	**term description**	**p-value**	**matching proteins in the network (labels)**
GO:0072655	Establishment of protein localization to mitochondrion	1.48E-15	TIMM21, TIMM13, TIMM10, GRPEL1, TIMM44, BAX, PAM16, BID, PMAIP1, T IMM17A, TIMM50, TIMM23
GO:0006839	Mitochondrial transport	2.00E-15	TIMM21, TIMM13, TIMM10, GRPEL1, TIMM44, BAX, PAM16,

			BID, UCP3, PMAIP1, STOML2, TIMM17A, BCL2, TIMM50, TIMM23
GO:0007005	Mitochondrion organization	2.00E-15	TIMM21, TIMM13, TIMM10, GRPEL1, TIMM44, BAX, HSPA9, PAM16, BID, PMAIP1, STOML2, BECN1, PARP1, TIMM17A, LIG3, BCL2, TIMM50, TIMM23
GO:0006626	Protein targeting to mitochondrion	1.84E-13	TIMM21, TIMM13, TIMM10, GRPEL1, TIMM44, PAM16, BID, TIMM17A, TIMM50, TIMM23
GO:0030150	Protein import into mitochondrial matrix	1.16E-10	TIMM21, GRPEL1, TIMM44, PAM16, TIMM17A, TIMM50, TIMM23
GO:1990542	Mitochondrial transmembrane transport	1.02E-09	TIMM21, GRPEL1, TIMM44, PAM16, UCP3, STOML2, TIMM17A, TIMM50, TIMM23
GO:0071806	Protein transmembrane transport	1.55E-09	TIMM21, GRPEL1, TIMM44, PAM16, TIMM17A, MCL1, TIMM50, TIMM23
GO:0007006	Mitochondrial membrane organization	4.97E-07	TIMM13, TIMM10, BAX, HSPA9, BID, PMAIP1, BCL2, TIMM50
GO:0001836	Release of cytochrome c from mitochondria	2.11E-06	BAX, BID, PMAIP1, BCL2, TIMM50
GO:2001244	Positive regulation of intrinsic apoptotic signaling pathway	3.47E-06	BAX, BID, PMAIP1, BECN1, MCL1, BCL2
GO:0006886	Intracellular protein transport	4.67E-06	TIMM21, TIMM13, TIMM10, GRPEL1, TIMM44, BAX, HSPA9, PAM16, BID, PMAIP1, TIMM17A, AHCYL1, TIMM50, TIMM23
GO:0015031	Protein transport	1.05E-05	TIMM21, TIMM13, TIMM10, GRPEL1, TIMM44, BAX, HSPA9, PAM16, BID, PMAIP1, TIMM17A, MCL1, AHCYL1, TIMM8A, TIMM50, TIMM23
GO:0051881	Regulation of mitochondrial membrane potential	1.05E-05	BAX, BID, PMAIP1, STOML2, PARP1, BCL2
GO:0046907	Intracellular transport	1.27E-05	TIMM21, TIMM13, TIMM10, GRPEL1, TIMM44, BAX, HSPA9, PAM16, BID, PMAIP1, STOML2, BECN1, TIMM17A, AHCYL1, TIMM50, TIMM23
GO:0071705	Nitrogen compound transport	1.76E-05	TIMM21, TIMM13, TIMM10, GRPEL1, TIMM44, BAX, HSPA9,

			PAM16, BID, PMAIP1, SLC25A42, TIMM17A, MCL1, AHCYL1, TIMM8A, TIMM50, TIMM23
GO:2001242	Regulation of intrinsic apoptotic signaling pathway	2.45E-05	BAX, BID, PMAIP1, BECN1, PARP1, MCL1, BCL2
GO:0006288	Base-excision repair, DNA ligation	7.46E-05	XRCC1, POLB, LIG3
GO:0051204	Protein insertion into mitochondrial membrane	8.07E-05	TIMM13, TIMM10, BAX, PMAIP1
GO:0008104	Protein localization	0.00015	TIMM21, TIMM13, AKAP10, TIMM10, GRPEL1, TIMM44, BAX, HSPA9, PAM16, BID, PMAIP1, TIMM17A, MCL1, AHCYL1, TIMM8A, TIMM50, TIMM23
GO:2001020	Regulation of response to DNA damage stimulus	0.00016	XRCC1, BID, PNKP, PMAIP1, PARP1, MCL1, BCL2
GO:0071702	Organic substance transport	0.00017	TIMM21, TIMM13, TIMM10, GRPEL1, TIMM44, BAX, HSPA9, PAM16, BID, PMAIP1, SLC25A42, TIMM17A, MCL1, AHCYL1, TIMM8A, TIMM50, TIMM23
GO:0033036	Macromolecule localization	0.00019	TIMM21, TIMM13, AKAP10, TIMM10, GRPEL1, TIMM44, BAX, HSPA9, PAM16, BID, PMAIP1, STOML2, TIMM17A, MCL1, AHCYL1, TIMM8A, TIMM50, TIMM23
GO:0055085	Transmembrane transport	0.00046	TIMM21, GRPEL1, TIMM44, BAX, PAM16, UCP3, SLC25A42, STOML2, TIMM17A, MCL1, BCL2, TIMM50, TIMM23
GO:1901030	Positive regulation of mitochondrial outer membrane permeabilization involved in apoptotic signaling pathway	0.00051	BAX, BID, PMAIP1, BCL2
GO:2001233	Regulation of apoptotic signaling pathway	0.00058	BAX, PAM16, BID, PMAIP1, BECN1, PARP1, MCL1, BCL2
GO:0097190	Apoptotic signaling pathway	0.00061	POLB, BAX, BID, PMAIP1, MCL1, BCL2, TIMM50
GO:0072321	Chaperone-mediated protein transport	0.00082	TIMM13, TIMM10, TIMM8A
GO:0051402	Neuron apoptotic process	0.00091	POLB, BAX, BID, BCL2

GO:0006974	Cellular response to DNA damage stimulus	0.00097	XRCC1, POLB, BAX, BID, PNKP, PMAIP1, PARP1, MCL1, LIG3, BCL2
GO:0032543	Mitochondrial translation	0.0011	PTCD3, MRPS31, YARS2, RARS2, MRPS33
GO:0090199	Regulation of release of cytochrome c from mitochondria	0.0011	BAX, PAM16, BID, PMAIP1
GO:0097345	Mitochondrial outer membrane permeabilization	0.0016	BAX, BID, PMAIP1
GO:0010332	Response to gamma radiation	0.0018	POLB, BAX, PARP1, BCL2
GO:0006915	Apoptotic process	0.0028	POLB, EXOG, BAX, BID, PMAIP1, BECN1, PARP1, MCL1, BCL2, TIMM50
GO:0006996	Organelle organization	0.0031	TIMM21, TIMM13, TIMM10, XRCC1, GRPEL1, TIMM44, BAX, HSPA9, PAM16, BID, PMAIP1, STOML2, BECN1, PARP1, TIMM17A, LIG3, BCL2, TIMM50, TIMM23
GO:0008630	Intrinsic apoptotic signaling pathway in response to DNA damage	0.0034	POLB, BAX, MCL1, BCL2
GO:0097193	Intrinsic apoptotic signaling pathway	0.0034	POLB, BAX, PMAIP1, MCL1, BCL2
GO:0033554	Cellular response to stress	0.0047	XRCC1, POLB, BAX, HSPA9, BID, PNKP, PMAIP1, STOML2, BECN1, PARP1, MCL1, LIG3, BCL2
GO:1903518	Positive regulation of single strand break repair	0.0047	XRCC1, PARP1
GO:0006810	Transport	0.0055	TIMM21, TIMM13, TIMM10, GRPEL1, TIMM44, BAX, HSPA9, PAM16, BID, UCP3, PMAIP1, SLC25A42, STOML2, BECN1, TIMM17A, MCL1, AHCYL1, TIMM8A, BCL2, TIMM50, TIMM23
GO:1900740	Positive regulation of protein insertion into mitochondrial membrane involved in apoptotic signaling pathway	0.0057	BID, PMAIP1, BCL2
GO:0090200	Positive regulation of release of cytochrome c from mitochondria	0.0061	BAX, BID, PMAIP1

GO:0006808	Regulation of nitrogen utilization	0.0071	BAX, BCL2
GO:0010836	Negative regulation of protein ADP-ribosylation	0.0071	XRCC1, PNKP
GO:0090296	Regulation of mitochondrial DNA replication	0.0071	STOML2, LIG3
GO:0010821	Regulation of mitochondrion organization	0.0086	BAX, PAM16, BID, PMAIP1, BCL2
GO:0043029	T cell homeostasis	0.0092	BAX, PMAIP1, BCL2
GO:0097191	Extrinsic apoptotic signaling pathway	0.0092	BAX, BID, MCL1, BCL2
GO:0008625	Extrinsic apoptotic signaling pathway via death domain receptors	0.0098	BAX, BID, BCL2
GO:0048872	Homeostasis of number of cells	0.0098	POLB, BAX, HSPA9, PMAIP1, BCL2
GO:0097192	Extrinsic apoptotic signaling pathway in absence of ligand	0.0098	BAX, MCL1, BCL2
GO:2001022	Positive regulation of response to DNA damage stimulus	0.0108	XRCC1, PNKP, PMAIP1, PARP1
GO:0016043	Cellular component organization	0.0118	TIMM21, TIMM13, PTCD3, TIMM10, XRCC1, GRPEL1, TIMM44, EXOG, BAX, HSPA9, MRPS31, PAM16, BID, PMAIP1, STOML2, BECN1, PARP1, TIMM17A, LIG3, MRPS33, BCL2, TIMM50, TIMM23
GO:0006289	Nucleotide-excision repair	0.0126	XRCC1, PNKP, PARP1, LIG3
GO:0042149	Cellular response to glucose starvation	0.0149	PMAIP1, BECN1, BCL2
GO:0043504	Mitochondrial DNA repair	0.0156	PARP1, LIG3
GO:0080135	Regulation of cellular response to stress	0.0156	XRCC1, BAX, BID, PNKP, PMAIP1, PARP1, MCL1, BCL2
GO:2001234	Negative regulation of apoptotic signaling pathway	0.0158	BAX, PAM16, BID, MCL1, BCL2
GO:0001844	Protein insertion into mitochondrial membrane	0.019	BAX, PMAIP1

	involved in apoptotic signaling pathway		
GO:0006979	Response to oxidative stress	0.019	LIAS, XRCC1, PNKP, UCP3, PARP1, BCL2
GO:0007007	Inner mitochondrial membrane organization	0.0197	TIMM13, TIMM10, HSPA9
GO:0044271	Cellular nitrogen compound biosynthetic process	0.0227	PTCD3, POLB, BAX, MRPS31, YARS2, PNKP, STOML2, PARP1, RARS2, LIG3, MRPS33
GO:0045039	Protein insertion into mitochondrial inner membrane	0.0228	TIMM13, TIMM10
GO:1903376	Regulation of oxidative stress-induced neuron intrinsic apoptotic signaling pathway	0.0228	PARP1, MCL1
GO:0048087	Positive regulation of developmental pigmentation	0.0266	BAX, BCL2
GO:0090150	Establishment of protein localization to membrane	0.0266	TIMM13, TIMM10, BAX, BID, PMAIP1
GO:0006950	Response to stress	0.029	AKAP10, LIAS, XRCC1, POLB, BAX, HSPA9, BID, PNKP, UCP3, PMAIP1, STOML2, BECN1, PARP1, MCL1, LIG3, BCL2, DNAJC4
GO:0010918	Positive regulation of mitochondrial membrane potential	0.0352	BID, STOML2
GO:2001236	Regulation of extrinsic apoptotic signaling pathway	0.039	BID, PMAIP1, MCL1, BCL2
GO:1902510	Regulation of apoptotic DNA fragmentation	0.0403	BAX, PAM16
GO:0010917	Negative regulation of mitochondrial membrane potential	0.0456	BAX, PMAIP1
GO:0051179	Localization	0.0456	TIMM21, TIMM13, AKAP10, TIMM10, GRPEL1, TIMM44, BAX, HSPA9, PAM16, BID, UCP3, PMAIP1, SLC25A42, STOML2, BECN1, TIMM17A, MCL1, AHCYL1, TIMM8A, BCL2, TIMM50, TIMM23
GO:0045739	Positive regulation of DNA repair	0.0494	XRCC1, PNKP, PARP1

Molecular Processes			
#term ID	**term description**	**p-value**	**matching proteins in network (labels)**
GO:0051434	BH3 domain binding	0.0021	BAX, MCL1, BCL2
GO:0008320	Protein transmembrane transporter activity	0.0095	TIMM17A, MCL1, TIMM23
GO:0051087	Chaperone binding	0.0286	TIMM10, GRPEL1, TIMM44, BAX
GO:0015450	P-P-bond-hydrolysis-driven protein transmembrane transporter activity	0.0406	TIMM17A, TIMM23
Cellular Components			
#term ID	**term description**	**p-value**	**matching proteins in network (labels)**
GO:0005739	Mitochondrion	1.16E-29	TIMM21, TIMM13, AKAP10, PTCD3, TIMM10, LIAS, GRPEL1, TIMM44, EXOG, BAX, HSPA9, MRPS31, PAM16, BID, YARS2, MTG1, PNKP, UCP3, PMAIP1, SLC25A42, STOML2, BECN1, PARP1, TIMM17A, MCL1, CMC4, RARS2, TIMM8A, LIG3, VWA8, BDH1, MRPS33, BCL2, TIMM50, TIMM23
GO:0005740	Mitochondrial envelope	9.81E-26	TIMM21, TIMM13, PTCD3, TIMM10, GRPEL1, TIMM44, EXOG, BAX, HSPA9, MRPS31, PAM16, BID, MTG1, UCP3, PMAIP1, SLC25A42, STOML2, BECN1, TIMM17A, MCL1, CMC4, TIMM8A, BDH1, MRPS33, BCL2, TIMM50, TIMM23
GO:0031966	Mitochondrial membrane	6.83E-25	TIMM21, TIMM13, PTCD3, TIMM10, GRPEL1, TIMM44, EXOG, BAX, HSPA9, MRPS31, PAM16, BID, MTG1, UCP3, PMAIP1, SLC25A42, STOML2, BECN1, TIMM17A, MCL1, TIMM8A, BDH1, MRPS33, BCL2, TIMM50, TIMM23
GO:0031967	Organelle envelope	2.33E-22	TIMM21, TIMM13, PTCD3, TIMM10, GRPEL1, TIMM44, EXOG, BAX, HSPA9, MRPS31, PAM16, BID, MTG1, UCP3, PMAIP1, SLC25A42, STOML2, BECN1, PARP1, TIMM17A, MCL1, CMC4, TIMM8A,

			BDH1, MRPS33, BCL2, TIMM50, TIMM23
GO:0005743	Mitochondrial inner membrane	8.26E-18	TIMM21, TIMM13, PTCD3, TIMM10, GRPEL1, TIMM44, EXOG, MRPS31, PAM16, MTG1, UCP3, SLC25A42, STOML2, TIMM17A, TIMM8A, BDH1, MRPS33, TIMM50, TIMM23
GO:0005744	TIM23 mitochondrial import inner membrane translocase complex	2.04E-12	TIMM21, TIMM10, GRPEL1, PAM16, TIMM17A, TIMM50, TIMM23
GO:0098798	Mitochondrial protein complex	3.25E-11	TIMM21, TIMM13, TIMM10, GRPEL1, BAX, HSPA9, MRPS31, PAM16, TIMM17A, MRPS33, TIMM50, TIMM23
GO:0031090	Organelle membrane	1.73E-09	TIMM21, TIMM13, PTCD3, TIMM10, GRPEL1, TIMM44, EXOG, BAX, HSPA9, MRPS31, PAM16, BID, MTG1, UCP3, PMAIP1, SLC25A42, STOML2, BECN1, TIMM17A, MCL1, AHCYL1, TIMM8A, BDH1, MRPS33, BCL2, TIMM50, TIMM23
GO:0005759	Mitochondrial matrix	3.94E-07	LIAS, GRPEL1, TIMM44, HSPA9, MRPS31, PAM16, YARS2, MTG1, RARS2, BDH1, MRPS33
GO:0005758	Mitochondrial intermembrane space	2.85E-06	TIMM13, TIMM10, STOML2, CMC4, TIMM8A, TIMM23
GO:0005737	Cytoplasm	2.25E-05	TIMM21, TIMM13, AKAP10, PTCD3, TIMM10, LIAS, GRPEL1, POLB, TIMM44, EXOG, BAX, HSPA9, MRPS31, PAM16, BID, YARS2, MTG1, PNKP, UCP3, PMAIP1, SLC25A42, STOML2, BECN1, PARP1, TIMM17A, MCL1, CMC4, RARS2, AHCYL1, TIMM8A, LIG3, VWA8, BDH1, MRPS33, LDHB, BCL2, TIMM50, TIMM23
GO:0043231	Intracellular membrane-bounded organelle	2.67E-05	TIMM21, TIMM13, AKAP10, PTCD3, TIMM10, LIAS, XRCC1, GRPEL1, POLB, TIMM44, EXOG, BAX, HSPA9, MRPS31, PAM16, BID, YARS2, MTG1, PNKP, UCP3, PMAIP1, SLC25A42, STOML2, BECN1, PARP1, TIMM17A, MCL1, CMC4, RARS2, TIMM8A, LIG3,

			VWA8, BDH1, MRPS33, BCL2, TIMM50, TIMM23
GO:0043227	Membrane-bounded organelle	3.19E-05	TIMM21, TIMM13, AKAP10, PTCD3, TIMM10, LIAS, XRCC1, GRPEL1, POLB, TIMM44, EXOG, BAX, HSPA9, MRPS31, PAM16, BID, YARS2, MTG1, PNKP, UCP3, PMAIP1, SLC25A42, STOML2, BECN1, PARP1, TIMM17A, MCL1, CMC4, RARS2, AHCYL1, TIMM8A, LIG3, VWA8, BDH1, MRPS33, LDHB, BCL2, TIMM50, TIMM23
GO:0070013	Intracellular organelle lumen	0.0001	TIMM13, PTCD3, TIMM10, LIAS, XRCC1, GRPEL1, POLB, TIMM44, HSPA9, MRPS31, PAM16, YARS2, MTG1, PNKP, STOML2, PARP1, TIMM17A, MCL1, CMC4, RARS2, TIMM8A, LIG3, BDH1, MRPS33, BCL2, TIMM50, TIMM23
GO:0005741	Mitochondrial outer membrane	0.00024	BAX, HSPA9, BID, PMAIP1, MCL1, BCL2
GO:0098796	Membrane protein complex	0.00089	TIMM21, TIMM10, GRPEL1, BAX, HSPA9, PAM16, BECN1, TIMM17A, BCL2, TIMM50, TIMM23
GO:0016020	Membrane	0.00092	TIMM21, TIMM13, AKAP10, PTCD3, TIMM10, GRPEL1, TIMM44, EXOG, BAX, HSPA9, MRPS31, PAM16, BID, MTG1, PNKP, UCP3, PMAIP1, SLC25A42, STOML2, BECN1, PARP1, TIMM17A, MCL1, AHCYL1, TIMM8A, BDH1, MRPS33, LDHB, BCL2, DNAJC4, TIMM50, TIMM23
GO:0005622	Intracellular	0.0033	TIMM21, TIMM13, AKAP10, PTCD3, TIMM10, LIAS, XRCC1, GRPEL1, POLB, TIMM44, EXOG, BAX, HSPA9, MRPS31, PAM16, BID, YARS2, MTG1, PNKP, UCP3, PMAIP1, SLC25A42, STOML2, BECN1, PARP1, TIMM17A, MCL1, CMC4, RARS2, AHCYL1, TIMM8A, LIG3, VWA8, BDH1, MRPS33, LDHB, BCL2, TIMM50, TIMM23

4.3.5 Integrated mRNA-miRNA Networks in Skeletal Muscle of Type 2 Diabetes

Comprehending the factors that impact changes in gene expression is crucial for determining the exact molecular pathophysiology of intricate diseases such as type 2 diabetes. Numerous research has indicated that type 2 diabetes is associated with altered miRNA and target expressions. As a result, we used the miRNET 2.0 database for constructing the possible miRNA network of the top 20 SHAP characteristics. We mapped all 20 of the genes to the human reference database. As seen in Figure 4.6, the network has 463 miRNA nodes and 19 gene nodes with a total of 717 edges (interactions). In the network, TIMM8A, AKAP10, TIMM17A, BAX, and LIAS have the most interactions.

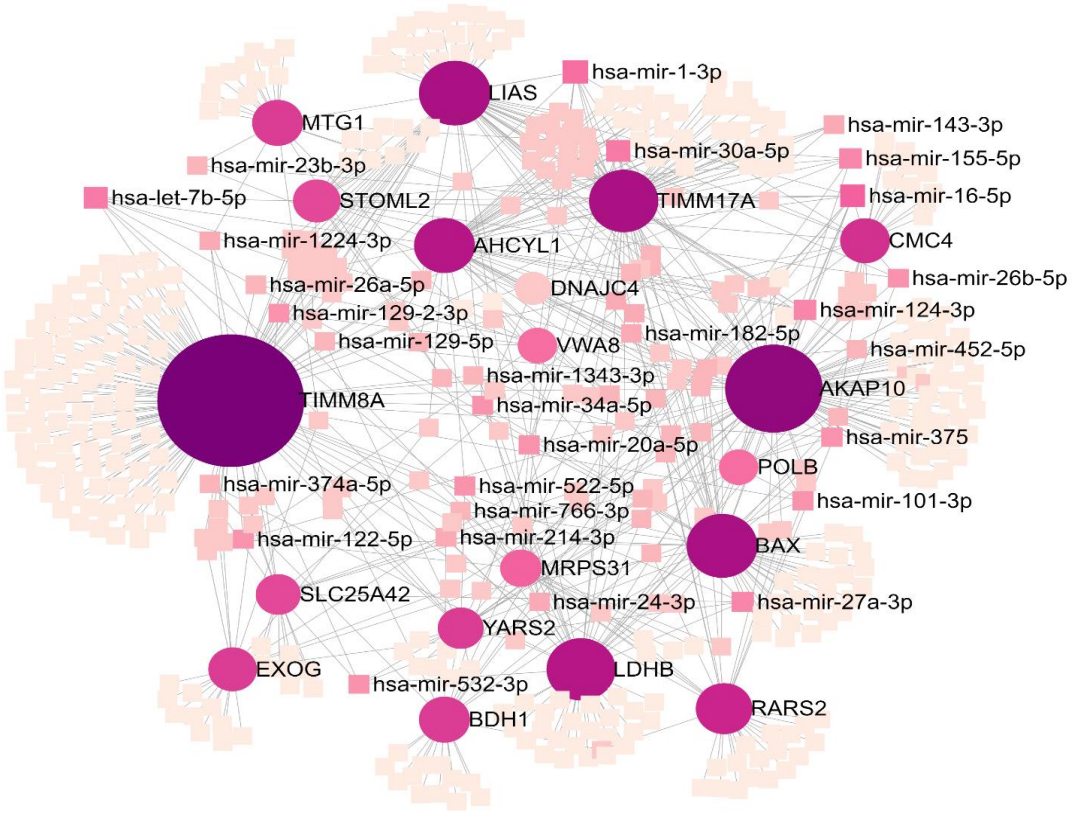

Figure 4.6*: The illustration depicts the miRNA-mRNA network of the identified genes from the machine learning model.*

Figure 4.7A shows miR-375, miR-30a-5p, miR-16-5p, miR-129-5p, miR-1229-3p, and miR-1224-3p have the most significant interactions. Mienturnet database was used for the further studying the characteristics of the miRNAs based on compelling literature evidence, which revealed that miR-375, miR-766-3p, miR-298, and miR-24-3p had a large number of interactions (Figure 4.7B). miRNA-mRNA network previously developed bears similarities to miR-375, miR-298, and numerous additional miRNAs. A number of miRNAs also target BAX, which controls the mitochondrial apoptotic signaling, as illustrated by Figure 4.8B. In HEK cells, miR-128 is an endogenous regulator of the apoptotic signaling cascade via BAX, as we have earlier investigated. In addition, we have previously demonstrated that miR-128 inhibits mitochondrial biogenesis and function in skeletal muscle model cells.

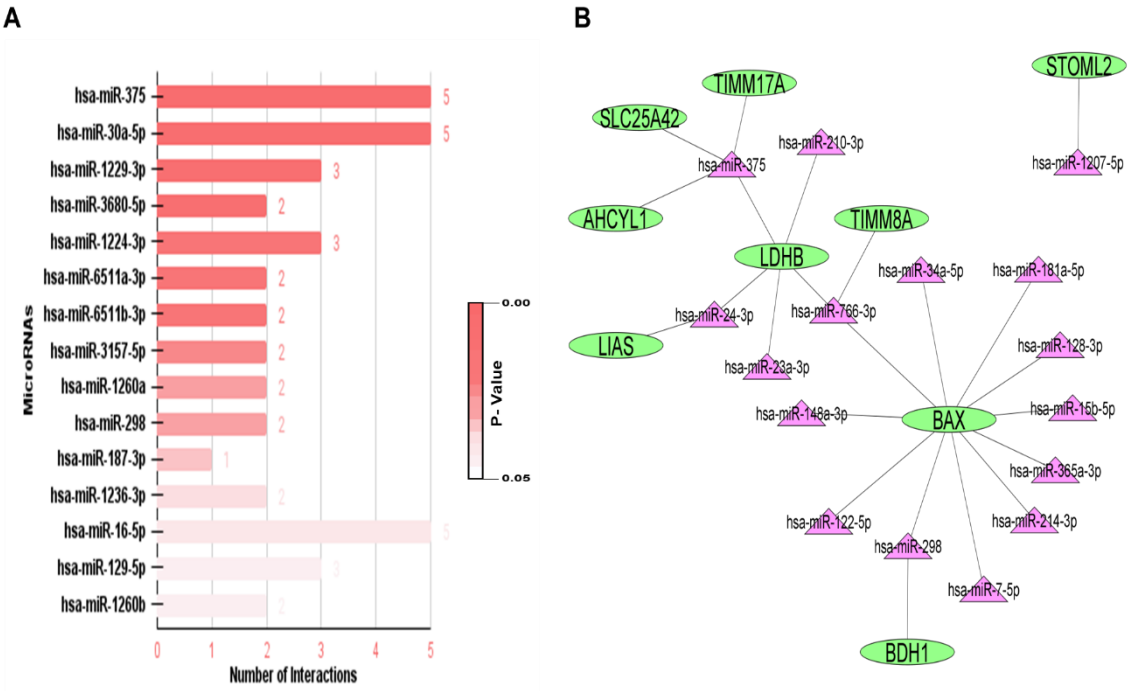

Figure 4.7: *(A) Following enrichment analysis, significant miRNAs are shown as a bar plot with targeted mRNAs. (B) Cytoscape was used to visualize the interaction network based on compelling literature evidence.*

4.4 Key Findings

- We have predicted gene regulation in type 2 diabetic skeletal muscle using machine learning as a systems biology method.
- The study employed the XGBoost algorithm and SHAP interpretations to identify the mitochondrial target genes associated with type 2 diabetes.
- The study of the mRNA-miRNA interaction network was used to discover non-coding biomarkers.

Chapter 5

A bioinformatics analysis reveals miR-128 mediated mitochondrial dysfunction in major metabolic organs via Bicaudal D Homolog 1 gene

5.1 Introduction

The disruptions in cellular homeostasis, primarily in the liver, fat, skeletal muscle, and pancreas mainly impact the pathophysiology of metabolic diseases, including type 2 diabetes and obesity. In multicellular animals, these metabolic organs have developed concurrently to preserve energy balance and meet the organism's metabolic requirements. Genes involved in transcription regulatory networks of these metabolic organs may be viable targets for therapy from a pathophysiological standpoint. As demonstrated earlier, miR-128 directly targets and adversely controls the production of the NAD+-dependent protein deacetylase known as SIRT1 (Sirutin 1). Furthermore, we have demonstrated that miR-128 also targets PGC1α (Peroxisome Proliferator Activated Receptor Gamma, Coactivator 1α), which is an essential regulator of oxidative phosphorylation and mitochondrial biogenesis. This limits the activity of mitochondria in skeletal muscle. miR-128 came out to be a significant player in several metabolic pathways, as it regulates key molecules. Future therapeutics may benefit from our comprehension of its regulation mechanism. Thus, we postulated that miR-128 may be involved in a major way in controlling the gene regulatory network that links the many organs in human metabolism.

5.2 Material and Methods

5.2.1 miRNA target prediction and Functional enrichment analysis

TargetScan (version 8.0) (https://www.targetscan.org/vert 80/) (Agarwal et al., 2015), was used to determine miR-128 predicted targets. We performed enrichment analysis for the predicted target genes of miR-128 using the DAVID database (Version 6.8) (https://david.ncifcrf.gov/tools.jsp) (D. W. Huang et al., 2007), and the analysis encompassed disease classification. For statistical significance for the disease classification analysis, a cutoff of p-value < 0.05 was used.

5.2.3 Study selection and data extraction

Expression data from Gene Expression Omnibus (GEO) (https://www.ncbi.nlm.nih.gov/geo/), including miRNA and mRNA microarray

expression profiling were downloaded (Edgar, Domrachev, and Lash 2002). PubMed provided the literature. GEO datasets used, and their sample information is presented in Table 1. Datasets used are of serum/tissue and are free of any therapies or other ailments that were retrieved.

Table 5.1: Details of GEO expression profiles from serum and tissues used in the study.

GEO Accession	Platform	Sample Profile Selected	Serum/Tissue	Organism	PMID
GSE169290	Affymetrix Multispecies miRNA-4 Array	Unique samples from 20 middle-aged obese individuals were included: 10 MHO (metabolically healthy obese) and 10 MUO (metabolically unhealthy obese).	Serum	Homo sapiens	33801145 (Rovira-Llopis et al. 2021)
GSE148961	NanoString nCounter miRNA Expression Panel	12 Control and 18 Diabetes Patients	Serum	Homo sapiens	32664305 (Sidorkiewicz et al. 2020)
GSE185845	NanoString nCounter miRNA Expression Panel	20 serum samples of T2DM without IHD were collected. The control group consisted of 16 patients without T2DM and IHD.	Serum	Homo sapiens	35663309 (Bielska et al. 2022)
GSE83452	Affymetrix Human Gene 2.0 ST Array	44 Control samples Vs 54 Obese samples	Liver	Homo sapiens	28679947 (Lefebvre et al. 2017)
GSE12643	Affymetrix Human Genome U95 Version 2 Array	10 Control samples Vs 10 T2DM samples	Skeletal Muscle	Homo sapiens	18719883 (Frederiksen et al. 2008)
GSE76894	Affymetrix Human Genome U133 Plus 2.0 Array	84 Control samples Vs 19 T2DM/Obese samples	Pancreas	Homo sapiens	30956117 (Khamis et al. 2019)
GSE27951	Affymetrix Human Genome U133 Plus 2.0 Array	12 Control sample Vs 11 T2DM/Obese sample	Adipose Tissue	Homo sapiens	21426570 (Keller et al. 2011)

5.2.3 Data Processing

GEO2R (http://www.ncbi.nlm.nih.gov/geo/geo2r) was used to perform differential expression analysis between samples from the control/diseased group, and Benjamini & Hochberg (False discovery rate) was applied to obtain a corrected p-value. An auto-detect function that evaluates the values of chosen samples and does a log2 transformation on any values that are not in the log space was selected. Limma and quantile normalization were selected for each dataset to obtain DEGs, and a significance level cut-off at $p < 0.05$ was chosen for the DEG's.

5.2.4 Cell culture and transfections

HepG2 cells were procured from the National Centre of Cell Sciences, Pune, India. All cell lines were cultured in Dulbecco′s Modified Eagle′s Medium (D7777, Sigma). Additionally, the media was supplemented with 3.7 g/L sodium bicarbonate, 10% FBS (Gibco, Thermo Fisher Scientific, MA, USA), and 100 IU/mL penicillin-streptomycin (Gibco, Thermo Fisher Scientific, MA, USA). The cells were maintained at 37°C and 5% CO_2 humidified chamber. The cells were seeded and cultured in the 6-well at 70–80% confluency in subsequent experiments. Transfection with miR-128 plasmid vector previously cloned in pSilencer 4.1 Vector, (Ambion, Thermo Fisher Scientific, MA, USA) in the lab or with antimiR-128 AM17000, assay ID AM11746, Thermo Fisher Scientific, MA, USA) along with their respective controls i.e., pSilencer 4.1 vector (P(Sil)) or antimiR negative control (AMNC). Lipofectamine LTX and Plus TM (Invitrogen, Thermo Fisher Scientific, MA, USA) were used for transfection as per instructions.

5.2.5 RNA isolation and qRT-PCR

RNA was isolated from the transfected cell pellets using TRIzol reagent (15596026 Thermo Fisher Scientific) as per the manufacturer's instructions. The integrity of the RNA was checked on 1% agarose gel, it was quantified using NanoDrop spectrophotometer (ND 1000, NanoDrop Technologies, Inc., USA). 500ng of total RNA was used to synthesize the cDNA as mentioned using the Revert Aid H Minus first-strand cDNA

synthesis kit (K1631, Thermo Fisher Scientific) as given in Table 3.3.3. Following this, qRT-PCR technique was used to detect transcript expression post-transfection. Subsequently, qRT-PCR was performed by using 1 µl to 2 µl of cDNA using the specific transcript primers mentioned in Table 5.1 on LightCycler 480 (Roche, Indianapolis, USA) using SYBR green master mix. The results were normalized with the human 18S rRNA according to the tissue/cells.

Table 5.2: List of primers and their sequences used in the study for qRT-PCR.

Primer name	Primer Sequence 5'- 3'
Hsa-miR-128 Stem Loop Primer	CTCAACTGGTGTCGTGGAGTCGGCAATTCAGTTGAGAAAGAGAC
miR-128 Forward Primer	ACACTCCAGCTGGGTCACAGTGAACCGGT
miR-128 Reverse Primer	GTGTCGTGGAGTCGGCAATTC
Sno Stem Loop Primer	CTCAACTGGTGTCGTGGAGTCGGCAATTCAGTTGAG
Sno Forward Primer	GGCTTTTGGAACTGAATCTAAGT
Sno Reverse Primer	GAGGTATTCGCACCAGAGGA
BICD1 Forward Primer	TCCATCCACCGGAAGGTTG
BICD1 Reverse Primer	GGCTCTGTTTCAGCTCGTTC
Human 18s rRNA Forward Primer	GAGGATGAGGTGGAACGTGT
Human 18s rRNA Reverse Primer	GGACCTGGCTGTATTTTCCA

5.2.6 Plasmid reporter Construct of BICD1 3'UTR

Human genomic DNA was used to amplify the 3'UTR region of BICD1 mRNA harboring the seed sequence of miR-128 (2682-2688) using PCR. The primers (5' to 3') used to amplify the template of 511 bp in length were Forward Primer: CCGCTCGAGCCCACAAAACATTTCTTCCA and Reverse Primer: ATAAGAATGCGGCCGCAATCTTTGCTCACTCTGTTTGC. The amplified template was then inserted into the XhoI and NotI sites in psiCHECK-2 reporter plasmid (Promega, USA), yielding the BICD1 3' UTR reporter construct. The reporter construct was verified by sequencing.

5.2.7 Luciferase Assay

HepG2 cells were seeded with the density of ~30000 cells/well in a 24-well plate. 100 ng of BICD1 3' UTR reporter plasmid along with either 1 μg of miR-128 plasmid or 40 nM of AM-128, or their corresponding negative controls were co-transfected using Lipofectamine™ 3000 (Invitrogen, Thermo Fisher Scientific, MA, USA). Luciferase and Renilla reporter activity were measured post 24 h after co-transfection, using a dual-luciferase reporter assay kit (Promega, USA). Luciferase activity was normalized against the Renilla activity as directed by the manufacturer.

5.2.8 Western blotting

BICD1 (NBP1-85843, Novus Biologicals, USA) and HIF1α (MAB1536-SP, R&D Systems, USA) were used for the primary antibody incubation done overnight. B-Actin (ab8226, Abcam, USA) was used as loading control. Thermo Fisher Scientific's HRP-linked anti-rabbit (cat. #31460) or anti-mouse (cat. #31430) secondary antibody was incubated for 1 h at room temperature. Enhanced chemiluminescence (Bio-Rad Laboratories, Inc., CA, USA) was used to detect the bands. Quantitative analysis was done using AlphaImager 3400 (Alpha InnoTech, CA, USA).

5.3 Results

5.3.1 miR-128, a possible blood biomarker for metabolic disorders including type 2 diabetes and obesity.

We obtained the miRNA-128 predicted target gene lists from TargetScan version 8.0 (5655 genes) in order to further functionally characterize miR-128. To further understand the significance of miR-128-associated disorders, these genes were then examined disease classification (DAVID software), as seen in Figure 5.1. As seen by the dot plot, the metabolic abnormality was determined to be statistically significant and to have a substantial number of miR-128 target genes (1633 genes, $p<0.05$).

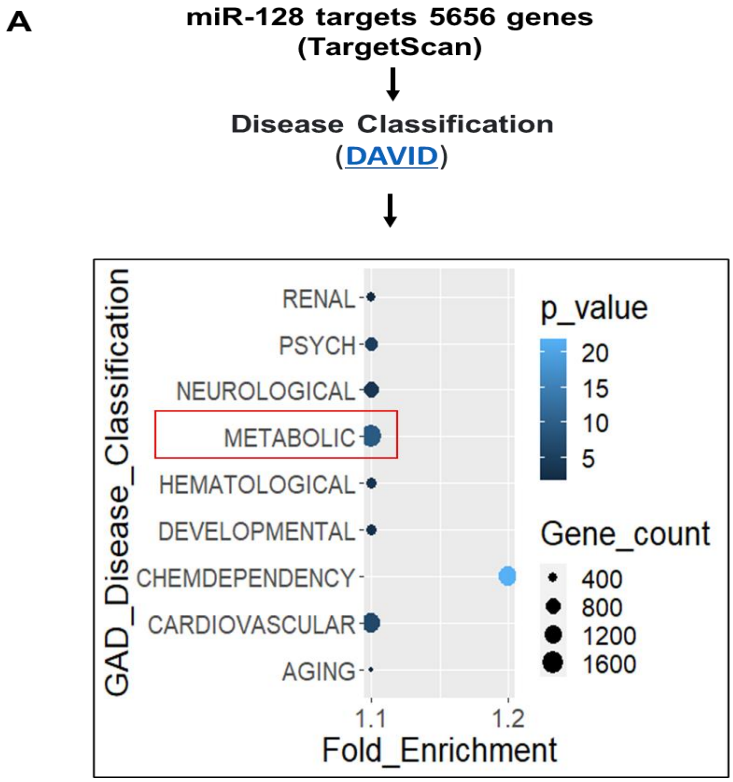

Figure 5.1: *DAVID analysis tool revealed miR-128 linked diseases represented as a bubble plot. The size of the bubbles indicates the number of genes, and the color gradation indicates the negative log10 p-value.*

5.3.2 MiR-128, a putative circulating indicator for type 2 diabetes and obesity

Literature has shown pieces of evidence that circulatory miRNAs are so persistent in serum and plasma, they are involved in a wide range of pathophysiological activities (Errafii et al. 2022). An analysis of three different miRNA profiling of blood samples from type 2 diabetic and obese patients compared to control was done to investigate the expression of miR-128. For the differentially expressed miRNA

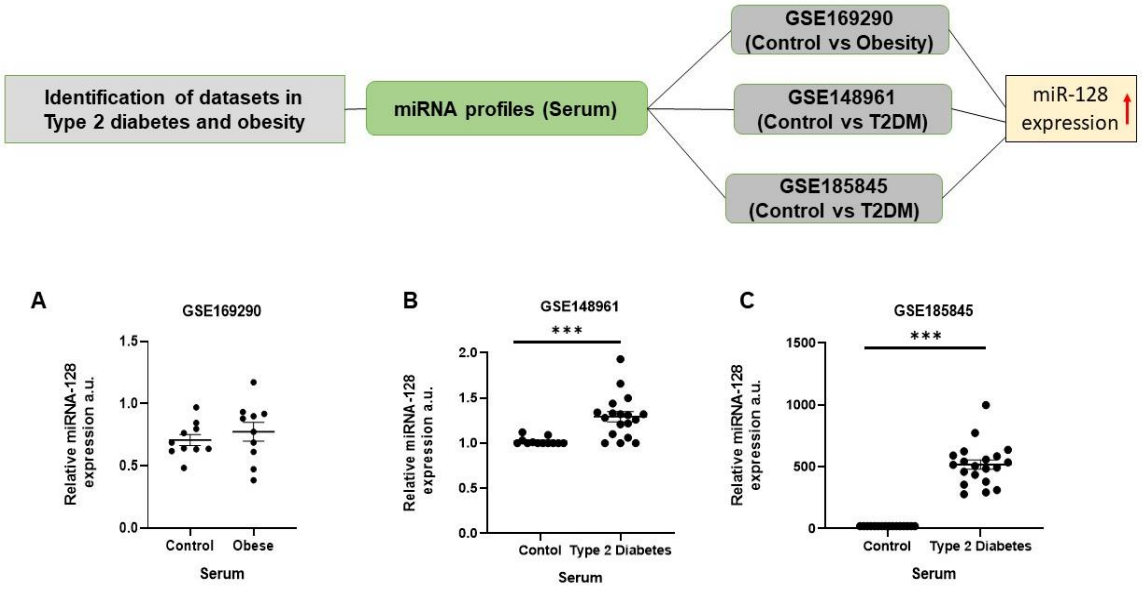

***Figure 5.2**: miR-128 expression in blood serum samples (A) GSE169290 (Control vs obese) (B & C) GSE148961 and GSE185845 (Control vs. Type 2 diabetes)*

profiles, GSE169290 (Control vs. Obese), GSE148961 (Control vs. Type 2 diabetes), and GSE185845 (Control vs. Type 2 diabetes) were utilized. When compared to control serum, we discovered that obese individuals had higher expression of miR-128 (Figure 5.2A). Similarly, in Figures 5.2B and 5.2C, the expression of circulating miR-128 was significantly greater in T2DM patients. It was also one of the miRNAs that were differently expressed in both datasets (GSE148961 and GSE185845, $p<0.001$). Elevated

levels of miR-128 in obese, and type 2 diabetic individuals, may dysregulate the expression of target genes that are implicated in important metabolic processes. According to two distinct investigations conducted in the Asian Indian community, individuals with obesity, pre-diabetes, and type 2 diabetes had considerably higher levels of miR-128 than healthy control patients. While these results offer insightful information, more investigation is required to confirm miR-128's potential as a therapeutic target and to clarify the specific pathways by which it leads to metabolic dysfunction. These results suggest that miR-128 may be a novel circulatory miRNA marker in obese and type 2 diabetes patients as it has never been reported in previous studies or other population groups.

5.3.3 Determining the miR-128 associated differentially expressed genes from the Liver, Pancreas, Skeletal Muscle, and Adipose Tissue.

To comprehend the physiological processes behind energy consumption and storage in obesity and type 2 diabetes. The mRNA expression patterns of metabolically active organs, including the liver, skeletal muscle, pancreas, and adipose tissue, were examined to determine the multidirectional association between miR-128 and the majorly affected metabolic organs. Accordingly, the steps of analysis are represented in the flow chart of Figure 3. The liver (GSE83452), skeletal muscle (GSE12643), adipose tissue (GDS3961), and pancreas (GSE76894) were analyzed using the GEO2R tool as mentioned in the material and method section. We found differentially expressed genes in the liver, skeletal muscle, pancreas, and adipose tissue were 2885, 464, 8553 and 2104 genes respectively. Using the list of projected target genes for miR-128 and the DEG lists from the liver, skeletal muscle, pancreas, and adipose tissue, the Venn tool was used to find shared genes. Bicaudal D Homolog 1 (BICD1) was the only link between the liver, pancreas, skeletal muscle, and adipose tissue as a target of miR-128 (Figure 5.3). By interacting with the motor complex (dynein-dynactin) and GTPase RAB6 between the

golgi apparatus and endoplasmic reticulum, mammalian BICD1 is known to aid in the movement of cargo.

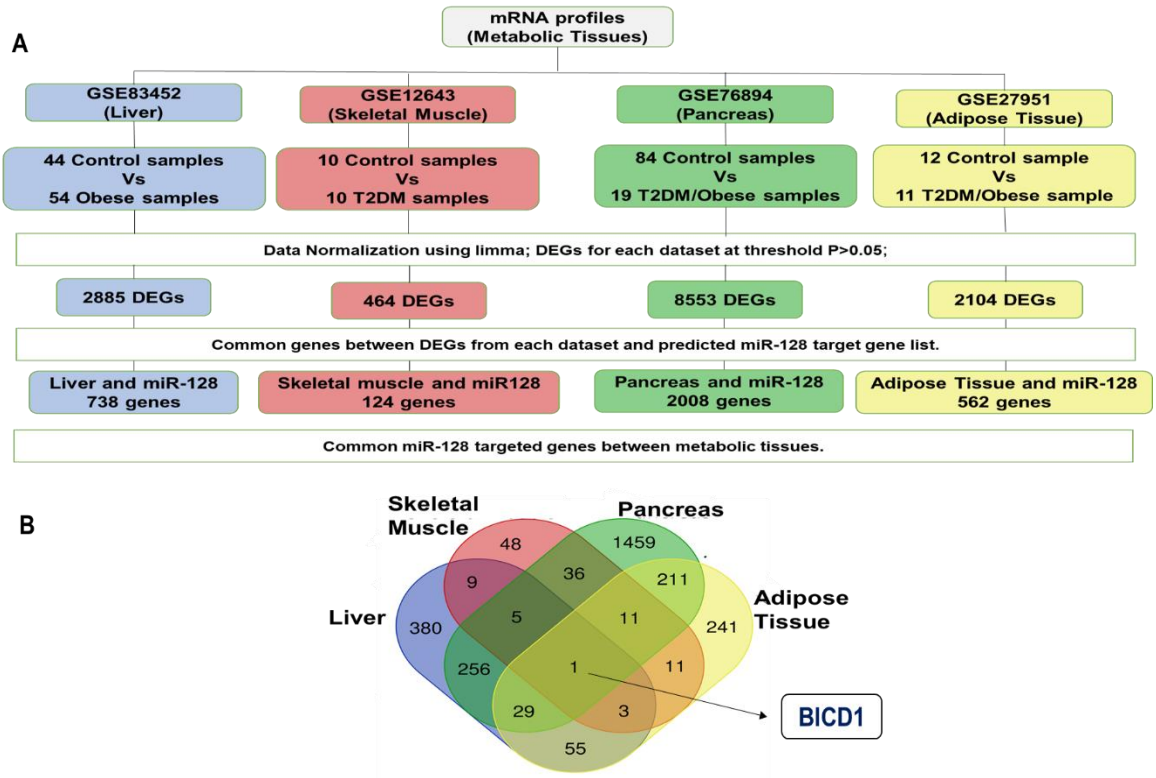

Figure 5.3: *(A) This flowchart illustrates the bioinformatic workflow that was utilized to find shared genes between miR-128 predicted targets and the differentially expressed genes from the liver, skeletal muscle, pancreas, and adipose tissue. (B) Venn diagrams illustrating shared miR-128 predicted target genes among the four metabolic organs.*

5.3.4 Bicaudal D Homolog 1 gene is a direct target of miR-128.

Many biological processes, including G protein signaling and internalization, RNA binding, translational repression, Golgi-endoplasmic reticulum transport, neurotrophin receptor signaling, and RNA binding, utilize BICD1. Also, R Depping et al suggested that HIF1α nuclear translocation is regulated by BICD1 gene. It interacts with HIF1α and forms the protein complex which then further regulates their transcription factors (Depping et al. 2008). We have examined the downstream impact of miR-128 on HepG2

cells in the present work. The liver is a vital metabolic organ that regulates the body's energy metabolism, which is why HepG2 cells were selected. It acts as the primary metabolic hub for the pancreas, skeletal muscle, and adipose tissue, among other organs. Remarkably, the miR-128 seed sequence of 7mer at position 2682-2688, which is conserved in humans, chimpanzees, and rhesus monkeys, is present in BICD1 3' UTR. First, the goal was to clone the 3' UTR of BICD1 mRNA to investigate whether it is a potential target for miR-128 binding. Figure depicts the steps followed to clone the reporter construct.

As shown in Figure 5.4, we next quantified the expression of the mature miR-128 expression in post-24 h of transfection in HepG2 cells. The miR-128 expression was elevated 5.73-fold ($p=0.0481$) on transfecting the cells with miR-128 plasmid. After receiving AM-128 treatment, cells showed a downregulation for miR-128 levels to 2.47-fold ($p=0.0134$) significantly. We then checked the luciferase activity of the BICD1 3'UTR reporter construct by co-transfecting it with miR-128 plasmid and/or AM-128 with their respective controls as mentioned in materials and methods.

We also examined the effect of miR-128 on both the transcriptional and translational levels of the BICD1 gene using qRT-PCR and western blotting, respectively after its overexpression and inhibition. In both the presence and absence of miR-128, we discovered that the mRNA level of BICD1 did not vary significantly. It's interesting to note that miR-128 overexpression dramatically reduced the BICD1 protein expression to 1.56-fold ($p=0.015$) and an increase was observed in cells treated with AM-128. As a downstream effector, HIF1α modifies gene expression by regulating many transcriptional regulators linked to mitochondrial glycolysis and respiration.

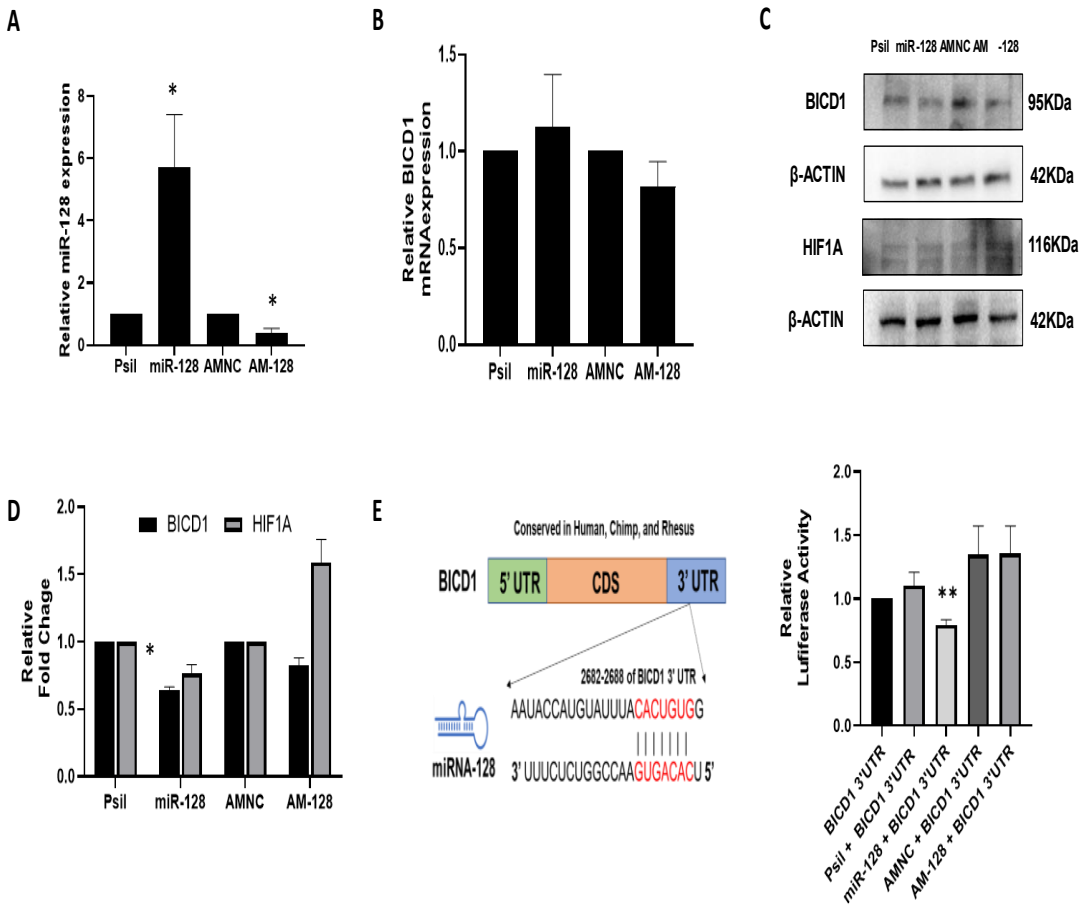

Figure 5.4: *miR-128 directly targets BICD1 (A) qRT-PCR was used to determine the expression of miR-128 in Hep G2 cells following transfection with either 4 µg of the miR-128 vector or 200 nM of AM-128, along with the corresponding negative controls. (B) mRNA expression of BICD1 gene was quantified using qRT-PCR. (C & D) Using western blotting, the expression of BICD1 and HIF1α proteins was measured. Bar graphs utilizing densitometric analysis reflect relative fold change, with β-actin serving as the loading control. (E) TargetScan data bae predicts that BICD1 gene contains the seed region of miR-128 in its 3'UTR. Relative luciferase activity 24 hours after co-transfection of BICD1 3'UTR reporter construct with either 1 µg of miR-128 plasmid or 40 nM of Am-128 together with their corresponding controls. Data are mean ± SEM, n=3, *p < 0.05, **p < 0.01*

Therefore, following the overexpression of miR-128 in HepG2 cells, we examined the translational expression of HIF1α. The protein expression of HIF1α showed a similar

trend to that of BICD1 but was not significant as in Figure. These findings suggest that BICD1 is a direct target of miR-128 and is negatively regulated when miR-128 is overexpressed in HepG2 cells.

5.4 Key Findings

- miR-128 is upregulated in the serum of type 2 diabetes and obese patients and could be a potential biomarker.
- Inhibition of miR-128 mediates mitochondrial dysfunction via BICD1-HIF1α axis.
- miR-128 silencing might have potential therapeutic implications in type 2 diabetes and obesity.

Chapter 6

Conclusion

6.1 Conclusion

- MiR-128 directly targets PGC1α and downregulates mitochondrial biogenesis.
- MiR-128 inhibits mitochondrial fusion and induces fission.
- MiR-128 promotes impairment in cellular ATP production by targeting NDUFS4.
- Inhibition of miR-128 reverses the HFD-induced mitochondrial dysfunction.
- Machine learning as a systems biology approach helped with the discovery of fresh therapeutic targets and the prospect of new disease biomarkers
- miR-128 targets BICD1 gene expression and could be responsible for mitochondrial dysfunction via HIF1α.

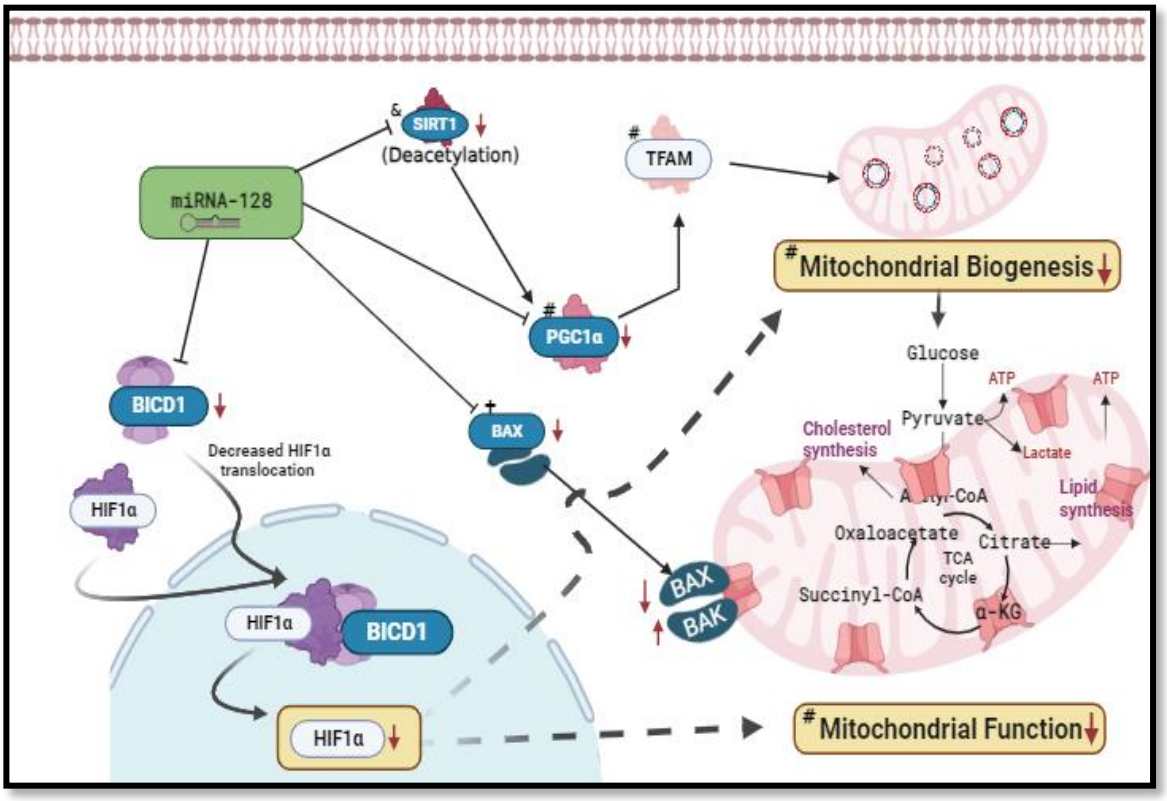

***Figure 7.1**: Proposed model for miR-128 mediated regulation of mitochondrial biogenesis and function*

Chapter 7

Discussion

7.1 Discussion

Metabolic disorders such as type 2 diabetes and obesity are currently serious public health issues. They have become worldwide epidemic in the last 20 years that threatened people's lives by impacting nearly every organ system (Glovaci, Fan, and Wong 2019; Whytock et al. 2023). Increased prevalence of such metabolic disorders and other related comorbidities shows that there is an urgent need to understand the molecular mechanisms and to find effective therapeutic interventions to prevent this rise. Innovative treatment approaches can be thought of because of the recent developments in miRNAs that can modulate the expression and functions of the mRNAs using miRNA mimics or antimiRs (Diener, Keller, and Meese 2022).

Previous evidence from our laboratory has shown that miR-128 directly targets SIRT1, a deacetylase that is reliant on nicotinamide adenosine dinucleotide (NAD) (Y. K. Adlakha and Saini 2013). It eliminates acetyl groups from a vast range of proteins including PGC1α (Yap et al. 2020), that enhances the biosynthesis of mitochondria and oxidative phosphorylation by acting upstream (Abu Shelbayeh et al. 2023). We showed that miR-128 directly targets PGC1α and the region is conserved at the miR-128 binding in its 3′ UTR. We next examined the expression of important downstream proteins and RNAs involved in the pathway. Our findings revealed an increase in the total mitochondrial mass and mitochondrial DNA content in C2C12 myoblasts after miR-128 inhibition. Simultaneously, there was an increase in the expression of NRF1 and NRF2, two important nuclear respiratory transcription factors that support the TFAM-mediated replication of mitochondrial DNA necessary for mitochondrial biogenesis and function. We also showed that miR-128 decreases the protein levels of MFN1, MFN2, and OPA1, three genes involved in the fusion of mitochondria. Furthermore, after miR-128 overexpression, the expression of DRP1, which causes fission was increased. Together all these results validate the fragmented shape of mitochondria that became apparent after overexpression of miR-128 in C2C12 myoblasts and corroborate the notion that overexpression of miR-128 causes smaller, fragmented mitochondria with compromised

functioning. Similar to our findings, Li et al. demonstrated that miR-30-induced DRP1 inhibition lowers fragmentation of the mitochondria and triggers apoptosis (Mao et al. 2014). Further, Wang et al showed upregulation in miR-140 and miR-195 levels inhibited mitochondrial fusion, and the cells are unable to preserve mitochondrial homogeneity and functional stability in congenital heart defects (G. Wang et al. 2024).

There are five multi-subunit complexes arranged in the electron transport chain that are involved in ATP generation during mitochondrial respiration (Vedel et al. 1999). Interestingly we found 24 genes in the electron transfer chain to be predicted targets of miR-128 according to the TargetScan database including NDUFS4. In this study, we experimentally proved that miR-128 directly targets NDUFS4 by binding to its 3' UTR. According to Zhu et al when kidney transplants from cadaver donors are used, miR-147 expressed after Cold Storage-Associated Transplantation (CST) injury represses NDUFS4, resulting in mitochondrial damage and renal tubular cell death (Zhu et al. 2023).

Interestingly an increase in PGC1α mediated NRF2 expression in HFD-fed mice was also observed because of anti-miR-128 therapy in the skeletal muscle tissue. Our findings support that inhibiting endogenous miR-128 levels could repair the decrease in mitochondrial biogenesis and skeletal muscle dysfunction brought on by a high-fat diet. Concurrently, Wang et al. demonstrated genetic deletion of miR-128 in mice models, which greatly improves glucose tolerance, increases consumption of energy and reduces obesity caused by high-fat diets (L. Wang et al. 2020).

Using another approach to understand the mitochondrial network via machine learning and explainable artificial intelligence in skeletal muscle of metabolic disorders like type 2 diabetes can forecast novel patterns more accurately than previous strategies (Nazarov et al. 2017). In this study, we identified genes responsible for mitochondrial homeostasis from skeletal muscle transcript data of 70 patients with type 2 diabetes and 107 control subjects using the recognized mitochondrial database MitoCarta 3.0 for the first time. Using the pooled expression dataset, we came across 409 mitochondrial genes in total. Applying the SHAP values to the genes after quantifying the machine learning predictions

allowed us to eventually identify 20 genes. The SHAP values were applied, and the results were compared before and after. Since the accuracy was comparable in both situations, it can be concluded that each of the genes that were discovered using feature values are reliable predictors of important information.

We have cross-referenced our findings with previously published literature to verify the validity of the conclusions drawn from our investigation, even with the different platforms and gene expressions as shown in Table 4.2. We discovered that the data that had been previously reported showed a notable level of consistency. These genes are important for a wide range of biological processes, including transport, structure, membrane potential regulation, and intrinsic apoptotic signaling in the mitochondria. Impairment in any of the pathways, it may be possible that they are contributing significantly to the initiation and progression of the metabolic disorder.

The significance of miRNAs, such as miR-375, miR-30a-5p, miR-16-5p, miR-129-5p, and miR1229-3p, in regulating mitochondrial metabolism in type 2 diabetic patients is further highlighted by our research. The disease-related mitochondrial functions may be changed by these dysregulated miRNAs, and these processes may be crucial in controlling gene expression. Furthermore, using the Mienturnet database based on significant literary evidence, we observed that one of the top features, i.e., BAX is a direct target of miR-128. Research from our laboratory has demonstrated that miR-128 can affect apoptosis in a variety of cell types by targeting BAX mRNA (Yogita K. Adlakha and Saini 2011). This interaction draws attention to the complex regulatory networks that control biological processes like apoptosis and emphasizes how crucial it is to comprehend the functions of miR-128 and BAX in metabolic disorders like type 2 diabetes and obesity.

Using several miRNA profiling experiments, we found that miR-128 is considerably elevated in the serum of patients with metabolic disorders as a circulatory miRNA. There is the possibility of miR-128 to influence homeostasis and intercellular communication in the liver, pancreas, adipose tissue, and skeletal muscle in such metabolic disorders. Herein,

we used clinical sample data and did a computational analysis to find out if BICD1 has significant differential expressions in all tissues and is a target of miR-128.

The human equivalent of the Drosophila Bicaudal-D gene, or BICD1, is in charge of the intracellular cargo transport cofactor that regulates the loading of cargo onto the dynein motor complex through microtubules (Swift et al. 2010). Through direct targeting in the 3' UTR region of the BICD1 transcript, we have experimentally shown that the overexpression of miR-128 negatively influences the expression of the protein. It's interesting to note that BICD1 protein, the microtubule-associated factors have recently been connected to the nuclear translocation of hypoxia-inducible factor 1 α (HIF1α) (Lee et al. 2018). HIF1α expression in cells is decreased by overexpression of miR-128, and vice versa. We think that one possible cause of aberrant mitochondrial metabolism could be reduced HIF1α signaling but further research in this area is warranted.

Altogether, it has previously been shown that miR-128 is essential for initiating apoptosis via pathways that include the release of cytochrome c and the activation of caspases, which ultimately lead to the insufficiency of mitochondrial function. Also shown before that miR-128 targets the NAD+-dependent protein deacetylase Sirtuin 1 (SIRT1). As a metabolic sensor, SIRT1 has a major role in the biogenesis of mitochondria via PGC1α/TFAM axis (Tang 2016). Herein, our research findings have demonstrated that miR-128 directly targets important regulators including PGC1α and NDUFS4 in myoblast cells, suppressing both the synthesis and function of mitochondria. The overexpression of miR-128 upregulates mitochondrial fission via DRP1 and downregulates the genes involved in the fusion of the mitochondria. Growing evidence suggests that DRP1 participates in several biological processes by interacting with p53, including mitophagy, oxidative stress, and cell death (Duan et al. 2020; D. B. Wang et al. 2014). These results imply that miR-128 modulates the homeostasis of mitochondria and impacts the tissue's overall health. The suppression of miR-128 using antimiR treatment may provide a foundation for diagnostic and therapeutic approaches for metabolic disorders linked to mitochondrial dysfunction.

References

Abu-Farha, Mohamed et al. 2015. “DNAJB3/HSP-40 Cochaperone Improves Insulin Signaling and Enhances Glucose Uptake in Vitro through JNK Repression.” *Scientific Reports 2015 5:1* 5(1): 1–12. https://www.nature.com/articles/srep14448 (September 25, 2023).

Abu Shelbayeh, Othman, Tasnim Arroum, Silke Morris, and Karin B. Busch. 2023. “PGC-1α Is a Master Regulator of Mitochondrial Lifecycle and ROS Stress Response.” *Antioxidants* 12(5). /pmc/articles/PMC10215733/ (April 17, 2024).

Abubaker, Jehad et al. 2013. “DNAJB3/HSP-40 Cochaperone Is Downregulated in Obese Humans and Is Restored by Physical Exercise.” *PLOS ONE* 8(7): e69217. https://journals.plos.org/plosone/article?id=10.1371/journal.pone.0069217 (September 25, 2023).

Adlakha, Y. K. et al. 2013. “Pro-Apoptotic MiRNA-128-2 Modulates ABCA1, ABCG1 and RXRα Expression and Cholesterol Homeostasis.” *Cell Death & Disease 2013 4:8* 4(8): e780–e780. https://www.nature.com/articles/cddis2013301 (April 15, 2024).

Adlakha, Y. K., and N. Saini. 2013. “MiR-128 Exerts pro-Apoptotic Effect in a P53 Transcription-Dependent and -Independent Manner via PUMA-Bak Axis.” *Cell Death & Disease 2013 4:3* 4(3): e542–e542. https://www.nature.com/articles/cddis201346 (January 24, 2024).

Adlakha, Yogita K., and Neeru Saini. 2011. “MicroRNA-128 Downregulates Bax and Induces Apoptosis in Human Embryonic Kidney Cells.” *Cellular and molecular life sciences : CMLS* 68(8): 1415–28. https://pubmed.ncbi.nlm.nih.gov/20924637/ (June 7, 2023).

Al Amir Dache, Zahra, and Alain R. Thierry. 2023. “Mitochondria-Derived Cell-to-Cell Communication.” *Cell reports* 42(7). https://pubmed.ncbi.nlm.nih.gov/37440408/ (December 20, 2023).

Anderson, Rozalyn M. et al. 2008. “Dynamic Regulation of PGC-1alpha Localization and

Turnover Implicates Mitochondrial Adaptation in Calorie Restriction and the Stress Response." *Aging cell* 7(1): 101–11. https://pubmed.ncbi.nlm.nih.gov/18031569/ (September 9, 2024).

Ando, Fumiaki et al. 2018. "AKAPs-PKA Disruptors Increase AQP2 Activity Independently of Vasopressin in a Model of Nephrogenic Diabetes Insipidus." *Nature Communications 2018 9:1* 9(1): 1–11. https://www.nature.com/articles/s41467-018-03771-2 (September 25, 2023).

Anello, M. et al. 2005. "Functional and Morphological Alterations of Mitochondria in Pancreatic Beta Cells from Type 2 Diabetic Patients." *Diabetologia* 48(2): 282–89.

Anguita-Ruiz, Augusto et al. 2020. "EXplainable Artificial Intelligence (XAI) for the Identification of Biologically Relevant Gene Expression Patterns in Longitudinal Human Studies, Insights from Obesity Research." *PLOS Computational Biology* 16(4): e1007792. https://journals.plos.org/ploscompbiol/article?id=10.1371/journal.pcbi.1007792 (May 31, 2023).

Arcidiacono, Biagio et al. 2020. "Obesity-Related Hypoxia via MiR-128 Decreases Insulin-Receptor Expression in Human and Mouse Adipose Tissue Promoting Systemic Insulin Resistance." *EBioMedicine* 59: 102912. /pmc/articles/PMC7502675/ (December 14, 2022).

Arden, Susan D. et al. 1996. "Imogen 38: A Novel 38-KD Islet Mitochondrial Autoantigen Recognized by T Cells from a Newly Diagnosed Type 1 Diabetic Patient." *The Journal of clinical investigation* 97(2): 551–61. https://pubmed.ncbi.nlm.nih.gov/8567980/ (September 25, 2023).

Bielska, Agnieszka et al. 2022. "Serum MiRNA Profile in Diabetic Patients With Ischemic Heart Disease as a Promising Non-Invasive Biomarker." *Frontiers in endocrinology* 13: 888948. http://www.ncbi.nlm.nih.gov/pubmed/35663309 (January 30, 2023).

Bofill-De Ros, Xavier, and Ulf Andersson Vang Ørom. 2024. “Recent Progress in MiRNA Biogenesis and Decay.” *RNA Biology* 21(1): 1–8. https://www.tandfonline.com/doi/abs/10.1080/15476286.2023.2288741 (May 6, 2024).

Booth, Frank W., Gregory N. Ruegsegger, Ryan G. Toedebusch, and Zhen Yan. 2015. “Endurance Exercise and the Regulation of Skeletal Muscle Metabolism.” *Progress in molecular biology and translational science* 135: 129–51. https://pubmed.ncbi.nlm.nih.gov/26477913/ (September 9, 2024).

Bost, Frederic, and Lisa Kaminski. 2019. “The Metabolic Modulator PGC-1α in Cancer.” *American Journal of Cancer Research* 9(2): 198. /pmc/articles/PMC6405967/ (September 9, 2024).

Brand, M. D., A. L. Orr, I. V. Perevoshchikova, and C. L. Quinlan. 2013. “The Role of Mitochondrial Function and Cellular Bioenergetics in Ageing and Disease.” *The British journal of dermatology* 169(0 2): 1. /pmc/articles/PMC4321783/ (December 20, 2023).

Caggiano, Rocco et al. 2017. “MiR-128 Is Implicated in Stress Responses by Targeting MAFG in Skeletal Muscle Cells.” *Oxidative Medicine and Cellular Longevity* 2017.

Cai, Yimei, Xiaomin Yu, Songnian Hu, and Jun Yu. 2009. “A Brief Review on the Mechanisms of MiRNA Regulation.” *Genomics, proteomics & bioinformatics* 7(4): 147–54. https://pubmed.ncbi.nlm.nih.gov/20172487/ (May 6, 2024).

Cantó, Carles et al. 2009. “AMPK Regulates Energy Expenditure by Modulating NAD+ Metabolism and SIRT1 Activity.” *Nature 2009 458:7241* 458(7241): 1056–60. https://www.nature.com/articles/nature07813 (April 15, 2024).

Cardanho-Ramos, Carlos, and Vanessa Alexandra Morais. 2021. “Mitochondrial Biogenesis in Neurons: How and Where.” *International journal of molecular sciences* 22(23). https://pubmed.ncbi.nlm.nih.gov/34884861/ (April 15, 2024).

Caturano, Alfredo et al. 2023. “Oxidative Stress in Type 2 Diabetes: Impacts from Pathogenesis to Lifestyle Modifications.” *Current Issues in Molecular Biology 2023, Vol.*

45, Pages 6651-6666 45(8): 6651–66. https://www.mdpi.com/1467-3045/45/8/420/htm (March 19, 2024).

Chen, Hsiuchen et al. 2010. "Mitochondrial Fusion Is Required for MtDNA Stability in Skeletal Muscle and Tolerance of MtDNA Mutations." *Cell* 141(2): 280–89. https://pubmed.ncbi.nlm.nih.gov/20403324/ (March 19, 2024).

Chen, Hui et al. 2011. "BMI1'S Maintenance of the Proliferative Capacity of Laryngeal Cancer Stem Cells." *Head & neck* 33(8): 1115–25. https://pubmed.ncbi.nlm.nih.gov/21755556/ (October 16, 2024).

Chen, Peng Hsu et al. 2016. "The Inhibition of MicroRNA-128 on IGF-1-Activating MTOR Signaling Involves in Temozolomide-Induced Glioma Cell Apoptotic Death." *PLOS ONE* 11(11): e0167096. https://journals.plos.org/plosone/article?id=10.1371/journal.pone.0167096 (April 15, 2024).

Chen, Wen, Huakan Zhao, and Yongsheng Li. 2023. "Mitochondrial Dynamics in Health and Disease: Mechanisms and Potential Targets." *Signal Transduction and Targeted Therapy 2023 8:1* 8(1): 1–25. https://www.nature.com/articles/s41392-023-01547-9 (December 20, 2023).

Chen, Yifei et al. 2022. "Mitochondrial Transplantation: Opportunities and Challenges in the Treatment of Obesity, Diabetes, and Nonalcoholic Fatty Liver Disease." *Journal of Translational Medicine 2022 20:1* 20(1): 1–16. https://translational-medicine.biomedcentral.com/articles/10.1186/s12967-022-03693-0 (April 15, 2024).

Chen, Zhang Lin et al. 2023. "Aerobic Exercise Enhances Mitochondrial Homeostasis to Counteract D-Galactose-Induced Sarcopenia in Zebrafish." *Experimental Gerontology* 180: 112265.

Choudhury, Raj Rajeshwar et al. 2024. "Role of MiR-128-3p and MiR-195-5p as Biomarkers of Coronary Artery Disease in Indians: A Pilot Study." *Scientific Reports*

2024 14:1 14(1): 1–11. https://www.nature.com/articles/s41598-024-61077-4 (October 19, 2024).

Cojocaru, Karina Alexandra et al. 2023. "Mitochondrial Dysfunction, Oxidative Stress, and Therapeutic Strategies in Diabetes, Obesity, and Cardiovascular Disease." *Antioxidants 2023, Vol. 12, Page 658* 12(3): 658. https://www.mdpi.com/2076-3921/12/3/658/htm (March 20, 2024).

Cui, J. G. et al. 2010. "Micro-RNA-128 (MiRNA-128) down-Regulation in Glioblastoma Targets ARP5 (ANGPTL6), Bmi-1 and E2F-3a, Key Regulators of Brain Cell Proliferation." *Journal of neuro-oncology* 98(3): 297–304. https://pubmed.ncbi.nlm.nih.gov/19941032/ (April 15, 2024).

Dai, Yang et al. 2016. "MicroRNA-128 Regulates the Proliferation and Differentiation of Bovine Skeletal Muscle Satellite Cells by Repressing Sp1." *Molecular and cellular biochemistry* 414(1–2): 37–46. https://pubmed.ncbi.nlm.nih.gov/26833195/ (April 15, 2024).

Das, Manasi, Consuelo Sauceda, and Nicholas J.G. Webster. 2021. "Mitochondrial Dysfunction in Obesity and Reproduction." *Endocrinology* 162(1): 1–13. https://dx.doi.org/10.1210/endocr/bqaa158 (December 20, 2023).

Depping, Reinhard et al. 2008. "Nuclear Translocation of Hypoxia-Inducible Factors (HIFs): Involvement of the Classical Importin Alpha/Beta Pathway." *Biochimica et biophysica acta* 1783(3): 394–404. https://pubmed.ncbi.nlm.nih.gov/18187047/ (May 6, 2024).

Detmer, Scott A., and David C. Chan. 2007. "Functions and Dysfunctions of Mitochondrial Dynamics." *Nature reviews. Molecular cell biology* 8(11): 870–79. https://pubmed.ncbi.nlm.nih.gov/17928812/ (March 19, 2024).

Diener, Caroline, Andreas Keller, and Eckart Meese. 2022. "Emerging Concepts of MiRNA Therapeutics: From Cells to Clinic." *Trends in Genetics* 38(6): 613–26.

http://www.cell.com/article/S016895252200018X/fulltext (October 13, 2024).

Do, Yura et al. 2020. “The Accessory Subunit of Human DNA Polymerase γ Is Required for Mitochondrial DNA Maintenance and Is Able to Stabilize the Catalytic Subunit.” *Mitochondrion* 53: 133–39.

Dorn, Gerald W., and Richard N. Kitsis. 2015. “The Mitochondrial Dynamism-Mitophagy-Cell Death Interactome.” *Circulation Research* 116(1): 167–82. https://www.ahajournals.org/doi/abs/10.1161/circresaha.116.303554 (April 15, 2024).

Duan, Chenyang et al. 2020. “Drp1 Regulates Mitochondrial Dysfunction and Dysregulated Metabolism in Ischemic Injury via Clec16a-, BAX-, and GSH- Pathways.” *Cell Death and Disease* 11(4).

Dubé, John J. et al. 2020. “Decreased Mitochondrial Dynamics Is Associated with Insulin Resistance, Metabolic Rate, and Fitness in African Americans.” *The Journal of Clinical Endocrinology & Metabolism* 105(4): 1210–20. https://dx.doi.org/10.1210/clinem/dgz272 (September 30, 2023).

Edgar, Ron, Michael Domrachev, and Alex E. Lash. 2002. “Gene Expression Omnibus: NCBI Gene Expression and Hybridization Array Data Repository.” *Nucleic Acids Research* 30(1): 207–10. https://dx.doi.org/10.1093/nar/30.1.207 (July 17, 2023).

Edsjö, Anders et al. 2024. “High-Throughput Molecular Assays for Inclusion in Personalised Oncology Trials – State-of-the-Art and Beyond.” *Journal of Internal Medicine* 295(6): 785–803. https://onlinelibrary.wiley.com/doi/full/10.1111/joim.13785 (September 20, 2024).

Egerman, Marc A., and David J. Glass. 2014. “Signaling Pathways Controlling Skeletal Muscle Mass.” *Critical Reviews in Biochemistry and Molecular Biology* 49(1): 59. /pmc/articles/PMC3913083/ (March 20, 2024).

Ekstrand, Mats I. et al. 2004. “Mitochondrial Transcription Factor A Regulates MtDNA Copy Number in Mammals.” *Human molecular genetics* 13(9): 935–44.

https://pubmed.ncbi.nlm.nih.gov/15016765/ (March 19, 2024).

El-Hattab, Ayman W., William J. Craigen, and Fernando Scaglia. 2017. "Mitochondrial DNA Maintenance Defects." *Biochimica et biophysica acta. Molecular basis of disease* 1863(6): 1539–55. https://pubmed.ncbi.nlm.nih.gov/28215579/ (December 20, 2023).

Errafii, Khaoula et al. 2022. "Comprehensive Analysis of Circulating MiRNA Expression Profiles in Insulin Resistance and Type 2 Diabetes in Qatari Population." *All Life* 15(1): 191–202. https://www.tandfonline.com/doi/abs/10.1080/26895293.2022.2033853 (December 14, 2022).

Fernandez-Marcos, Pablo J., and Johan Auwerx. 2011. "Regulation of PGC-1α, a Nodal Regulator of Mitochondrial Biogenesis." *The American journal of clinical nutrition* 93(4). https://pubmed.ncbi.nlm.nih.gov/21289221/ (September 9, 2024).

Filippi, Beatrice M. et al. 2017. "Dynamin-Related Protein 1-Dependent Mitochondrial Fission Changes in the Dorsal Vagal Complex Regulate Insulin Action." *Cell reports* 18(10): 2301–9. https://pubmed.ncbi.nlm.nih.gov/28273447/ (March 20, 2024).

Frederiksen, C. M. et al. 2008. "Transcriptional Profiling of Myotubes from Patients with Type 2 Diabetes: No Evidence for a Primary Defect in Oxidative Phosphorylation Genes." *Diabetologia* 51(11): 2068–77. https://pubmed.ncbi.nlm.nih.gov/18719883/ (July 19, 2023).

Friedman, Jonathan R., and Jodi Nunnari. 2014. "Mitochondrial Form and Function." *Nature* 505(7483): 335–43. https://pubmed.ncbi.nlm.nih.gov/24429632/ (December 27, 2023).

Geng, Lijiao, Tao Zhang, Wei Liu, and Yong Chen. 2018. "Inhibition of MiR-128 Abates Aβ-Mediated Cytotoxicity by Targeting PPAR-γ via NF-KB Inactivation in Primary Mouse Cortical Neurons and Neuro2a Cells." *Yonsei medical journal* 59(9): 1096–1106. https://pubmed.ncbi.nlm.nih.gov/30328325/ (October 16, 2024).

Glancy, Brian, Yuho Kim, Prasanna Katti, and T. Bradley Willingham. 2020. "The

Functional Impact of Mitochondrial Structure Across Subcellular Scales." *Frontiers in Physiology* 11. /pmc/articles/PMC7686514/ (December 20, 2023).

Glovaci, Diana, Wenjun Fan, and Nathan D. Wong. 2019. "Epidemiology of Diabetes Mellitus and Cardiovascular Disease." *Current Cardiology Reports* 21(4): 21–21. https://europepmc.org/article/med/30828746 (May 31, 2023).

Goljanek-Whysall, Katarzyna et al. 2020. "MiR-181a Regulates P62/SQSTM1, Parkin, and Protein DJ-1 Promoting Mitochondrial Dynamics in Skeletal Muscle Aging." *Aging Cell* 19(4): e13140. https://onlinelibrary.wiley.com/doi/full/10.1111/acel.13140 (March 23, 2024).

Green, Adam, Tanvir Hossain, and David M. Eckmann. 2022. "Mitochondrial Dynamics Involves Molecular and Mechanical Events in Motility, Fusion and Fission." *Frontiers in Cell and Developmental Biology* 10. /pmc/articles/PMC9626967/ (December 27, 2023).

Grindel, Annemarie et al. 2016. "Oxidative Stress, DNA Damage and DNA Repair in Female Patients with Diabetes Mellitus Type 2." *PLOS ONE* 11(9): e0162082. https://journals.plos.org/plosone/article?id=10.1371/journal.pone.0162082 (September 25, 2023).

Guo, Ai, Kai Li, and Qian Xiao. 2020. "Fibroblast Growth Factor 19 Alleviates Palmitic Acid-Induced Mitochondrial Dysfunction and Oxidative Stress via the AMPK/PGC-1α Pathway in Skeletal Muscle." *Biochemical and biophysical research communications* 526(4): 1069–76. https://pubmed.ncbi.nlm.nih.gov/32305136/ (March 23, 2024).

Gupte, Anisha A., Gregory L. Bomhoff, and Paige C. Geiger. 2008. "Age-Related Differences in Skeletal Muscle Insulin Signaling: The Role of Stress Kinases and Heat Shock Proteins." *Journal of Applied Physiology* 105(3): 839–48. https://journals.physiology.org/doi/10.1152/japplphysiol.00148.2008 (September 25, 2023).

Heras-Sandoval, David, Jazmin M. Pérez-Rojas, Jacqueline Hernández-Damián, and José

Pedraza-Chaverri. 2014. “The Role of PI3K/AKT/MTOR Pathway in the Modulation of Autophagy and the Clearance of Protein Aggregates in Neurodegeneration.” *Cellular signalling* 26(12): 2694–2701. https://pubmed.ncbi.nlm.nih.gov/25173700/ (September 9, 2024).

Hill, Geoffrey E. 2020. “Mitonuclear Compensatory Coevolution.” *Trends in genetics : TIG* 36(6): 403–14. https://pubmed.ncbi.nlm.nih.gov/32396834/ (December 20, 2023).

Holloszy, J. O., and E. F. Coyle. 1984. “Adaptations of Skeletal Muscle to Endurance Exercise and Their Metabolic Consequences.” *Journal of applied physiology: respiratory, environmental and exercise physiology* 56(4): 831–38. https://pubmed.ncbi.nlm.nih.gov/6373687/ (December 27, 2023).

Hu, Ming Zhu et al. 2016. “Exogenous Hydrogen Sulfide Postconditioning Protects Isolated Rat Hearts From Ischemia/Reperfusion Injury Through Sirt1/PGC-1α Signaling Pathway.” *International heart journal* 57(4): 477–82. https://pubmed.ncbi.nlm.nih.gov/27357440/ (March 19, 2024).

Huang, Shiyuan, Chunhua Xiang, and Yi Song. 2022. “Identification of the Shared Gene Signatures and Pathways between Sarcopenia and Type 2 Diabetes Mellitus.” *PLOS ONE* 17(3): e0265221. https://journals.plos.org/plosone/article?id=10.1371/journal.pone.0265221 (May 31, 2023).

Imai, Shin Ichiro, Christopher M. Armstrong, Matt Kaeberlein, and Leonard Guarente. 2000. “Transcriptional Silencing and Longevity Protein Sir2 Is an NAD-Dependent Histone Deacetylase.” *Nature 2000 403:6771* 403(6771): 795–800. https://www.nature.com/articles/35001622 (March 19, 2024).

Ivanova, Margarita M. et al. 2013. “Estradiol and Tamoxifen Regulate NRF-1 and Mitochondrial Function in Mouse Mammary Gland and Uterus.” *Journal of Molecular Endocrinology* 51(2): 233–46. https://jme.bioscientifica.com/view/journals/jme/51/2/233.xml (December 27, 2023).

Jäer, Sibylle, Christoph Handschin, Julie St-Pierre, and Bruce M. Spiegelman. 2007. "AMP-Activated Protein Kinase (AMPK) Action in Skeletal Muscle via Direct Phosphorylation of PGC-1alpha." *Proceedings of the National Academy of Sciences of the United States of America* 104(29): 12017–22. https://pubmed.ncbi.nlm.nih.gov/17609368/ (March 19, 2024).

Jin, Jingzhe, and Mingcheng Ren. 2024. "The Biological Function of MiR-128-2 in Hepatocellular Carcinoma and Its Molecular Mechanism Functioning." *Pathology - Research and Practice* 254: 155178.

Jomova, Klaudia et al. 2023. "Reactive Oxygen Species, Toxicity, Oxidative Stress, and Antioxidants: Chronic Diseases and Aging." *Archives of Toxicology 2023 97:10* 97(10): 2499–2574. https://link.springer.com/article/10.1007/s00204-023-03562-9 (December 27, 2023).

Karunakaran, Denuja et al. 2015. "Macrophage Mitochondrial Energy Status Regulates Cholesterol Efflux and Is Enhanced by Anti-MiR33 in Atherosclerosis." *Circulation research* 117(3): 266. /pmc/articles/PMC4578799/ (March 23, 2024).

Keller, Pernille et al. 2011. "Gene-Chip Studies of Adipogenesis-Regulated MicroRNAs in Mouse Primary Adipocytes and Human Obesity." *BMC endocrine disorders* 11. https://pubmed.ncbi.nlm.nih.gov/21426570/ (July 19, 2023).

Khamis, Amna et al. 2019. "Laser Capture Microdissection of Human Pancreatic Islets Reveals Novel EQTLs Associated with Type 2 Diabetes." *Molecular metabolism* 24: 98–107. https://pubmed.ncbi.nlm.nih.gov/30956117/ (July 19, 2023).

Khin, Phyu Phyu, Jong Han Lee, and Hee Sook Jun. 2023. "Pancreatic Beta-Cell Dysfunction in Type 2 Diabetes." *European Journal of Inflammation* 21. https://journals.sagepub.com/doi/full/10.1177/1721727X231154152 (September 30, 2023).

Kiel, Klaudia, Sylwia Katarzyna Król, Agnieszka Bronisz, and Jakub Godlewski. 2024.

"MiR-128-3p - a Gray Eminence of the Human Central Nervous System." *Molecular therapy. Nucleic acids* 35(1). https://pubmed.ncbi.nlm.nih.gov/38419943/ (November 4, 2024).

Kim, Jeong A., Yongzhong Wei, and James R. Sowers. 2008. "Role of Mitochondrial Dysfunction in Insulin Resistance." *Circulation research* 102(4): 401. /pmc/articles/PMC2963150/ (March 19, 2024).

Koliaki, Chrysi, and Michael Roden. 2016. "Alterations of Mitochondrial Function and Insulin Sensitivity in Human Obesity and Diabetes Mellitus." *Annual review of nutrition* 36: 337–67. https://pubmed.ncbi.nlm.nih.gov/27146012/ (March 23, 2024).

Kong, Shaofen, Bolin Cai, and Qinghua Nie. 2022. "PGC-1α Affects Skeletal Muscle and Adipose Tissue Development by Regulating Mitochondrial Biogenesis." *Molecular genetics and genomics : MGG* 297(3): 621–33. https://pubmed.ncbi.nlm.nih.gov/35290519/ (September 9, 2024).

Kusminski, Christine M., and Philipp E. Scherer. 2012. "Mitochondrial Dysfunction in White Adipose Tissue." *Trends in endocrinology and metabolism: TEM* 23(9): 435. /pmc/articles/PMC3430798/ (December 20, 2023).

Lanza, Marika et al. 2023. "The Role of MiR-128 in Neurodegenerative Diseases." *International Journal of Molecular Sciences* 24(7): 6024. https://pmc.ncbi.nlm.nih.gov/articles/PMC10093830/ (October 18, 2024).

Lee, Hyun Jik et al. 2018. "BICD1 Mediates HIF1α Nuclear Trans1. Lee HJ, Jung YH, Oh JY, et Al. BICD1 Mediates HIF1α Nuclear Translocation in Mesenchymal Stem Cells during Hypoxia Adaptation. Cell Death Differ 2018 269. 2018;26(9):1716-1734. Doi:10.1038/S41418-018-0241-1location In ." *Cell Death & Differentiation 2018 26:9* 26(9): 1716–34. https://www.nature.com/articles/s41418-018-0241-1 (February 8, 2023).

Lefebvre, Philippe et al. 2017. "Interspecies NASH Disease Activity Whole-Genome Profiling Identifies a Fibrogenic Role of PPARα-Regulated Dermatopontin." *JCI insight*

2(13). https://pubmed.ncbi.nlm.nih.gov/28679947/ (July 19, 2023).

Lemasters, John J. 2005. "Selective Mitochondrial Autophagy, or Mitophagy, as a Targeted Defense against Oxidative Stress, Mitochondrial Dysfunction, and Aging." *Rejuvenation research* 8(1): 3–5. https://pubmed.ncbi.nlm.nih.gov/15798367/ (March 19, 2024).

Li, Xinghai, Bobby Monks, Qingyuan Ge, and Morris J. Birnbaum. 2007. "Akt/PKB Regulates Hepatic Metabolism by Directly Inhibiting PGC-1alpha Transcription Coactivator." *Nature* 447(7147): 1012–16. https://pubmed.ncbi.nlm.nih.gov/17554339/ (September 9, 2024).

Lian, Bo et al. 2018. "MiR-128 Targets the SIRT1/ROS/DR5 Pathway to Sensitize Colorectal Cancer to TRAIL-Induced Apoptosis." *Cellular Physiology and Biochemistry* 49(6): 2151–62. https://dx.doi.org/10.1159/000493818 (April 15, 2024).

Liesa, Marc, Manuel Palacín, and Antonio Zorzano. 2009. "Mitochondrial Dynamics in Mammalian Health and Disease." *Physiological reviews* 89(3): 799–845. https://pubmed.ncbi.nlm.nih.gov/19584314/ (December 27, 2023).

Liu, Jing, Ji Li, Wen Jian Li, and Chun Ming Wang. 2013. "The Role of Uncoupling Proteins in Diabetes Mellitus." *Journal of Diabetes Research* 2013.

Liu, Lei, Yanjun Li, Guo Chen, and Quan Chen. 2023. "Crosstalk between Mitochondrial Biogenesis and Mitophagy to Maintain Mitochondrial Homeostasis." *Journal of biomedical science* 30(1). https://pubmed.ncbi.nlm.nih.gov/37821940/ (March 19, 2024).

LIU, RUIXUAN et al. 2021. "Upregulation of MiR-128 Inhibits Neuronal Cell Apoptosis Following Spinal Cord Injury via FasL Downregulation by Repressing ULK1." *Molecular Medicine Reports* 24(3): 667. https://pmc.ncbi.nlm.nih.gov/articles/PMC8335739/ (October 16, 2024).

López-Soldado, Iliana et al. 2023. "Decreased Expression of Mitochondrial Aminoacyl-TRNA Synthetases Causes Downregulation of OXPHOS Subunits in Type 2 Diabetic

Muscle." *Redox Biology* 61: 102630.

Lu, Shan et al. 2020. "Hyperglycemia Acutely Increases Cytosolic Reactive Oxygen Species Via-Linked GlcNAcylation and CaMKII Activation in Mouse Myocytes." *Circulation research* 126(10): e80. /pmc/articles/PMC7210078/ (March 20, 2024).

Mao, Cuiping et al. 2014. "MiRNA-30a Inhibits AECs-II Apoptosis by Blocking Mitochondrial Fission Dependent on Drp-1." *Journal of Cellular and Molecular Medicine* 18(12): 2404. /pmc/articles/PMC4302646/ (April 17, 2024).

Meeusen, Shelly, J. Michael McCaffery, and Jodi Nunnari. 2004. "Mitochondrial Fusion Intermediates Revealed in Vitro." *Science (New York, N.Y.)* 305(5691): 1747–52. https://pubmed.ncbi.nlm.nih.gov/15297626/ (December 27, 2023).

Mengeste, Abel M., Arild C. Rustan, and Jenny Lund. 2021. "Skeletal Muscle Energy Metabolism in Obesity." *Obesity* 29(10): 1582–95. https://onlinelibrary.wiley.com/doi/full/10.1002/oby.23227 (December 14, 2022).

Michishita, Eriko et al. 2005. "Evolutionarily Conserved and Nonconserved Cellular Localizations and Functions of Human SIRT Proteins." *Molecular biology of the cell* 16(10): 4623–35. https://pubmed.ncbi.nlm.nih.gov/16079181/ (September 9, 2024).

Miners, James Scott et al. 2009. "Angiotensin-Converting Enzyme Levels and Activity in Alzheimer's Disease: Differences in Brain and CSF ACE and Association with ACE1 Genotypes." *American Journal of Translational Research* 1(2): 163. https://pmc.ncbi.nlm.nih.gov/articles/PMC2776311/ (October 16, 2024).

Mitsopoulos, Panagiotis et al. 2015. "Stomatin-like Protein 2 Is Required for in Vivo Mitochondrial Respiratory Chain Supercomplex Formation and Optimal Cell Function." *Molecular and cellular biology* 35(10): 1838–47. https://pubmed.ncbi.nlm.nih.gov/25776552/ (September 30, 2023).

Mohamed, Junaith S., Ameena Hajira, Patricia S. Pardo, and Aladin M. Boriek. 2014. "MicroRNA-149 Inhibits PARP-2 and Promotes Mitochondrial Biogenesis via SIRT-

1/PGC-1α Network in Skeletal Muscle." *Diabetes* 63(5): 1546–59. https://dx.doi.org/10.2337/db13-1364 (March 23, 2024).

Motohashi, Norio et al. 2013. "Regulation of IRS1/Akt Insulin Signaling by MicroRNA-128a during Myogenesis." *Journal of Cell Science* 126(12): 2678–91. /pmc/articles/PMC3687700/ (April 15, 2024).

Nazarov, Petr V. et al. 2017. "RNA Sequencing and Transcriptome Arrays Analyses Show Opposing Results for Alternative Splicing in Patient Derived Samples." *BMC Genomics* 18(1): 1–18. https://bmcgenomics.biomedcentral.com/articles/10.1186/s12864-017-3819-y (April 17, 2024).

Nelson, Caroline A. et al. 2020. "Patient Perspectives on the Use of Artificial Intelligence for Skin Cancer Screening: A Qualitative Study." *JAMA Dermatology* 156(5): 501–12. https://jamanetwork.com/journals/jamadermatology/fullarticle/2762711 (May 31, 2023).

Newsholme, Philip et al. 2016. "Molecular Mechanisms of ROS Production and Oxidative Stress in Diabetes." *The Biochemical journal* 473(24): 4527–50. https://pubmed.ncbi.nlm.nih.gov/27941030/ (March 20, 2024).

O'Brien, Jacob, Heyam Hayder, Yara Zayed, and Chun Peng. 2018. "Overview of MicroRNA Biogenesis, Mechanisms of Actions, and Circulation." *Frontiers in Endocrinology* 9(AUG): 402. /pmc/articles/PMC6085463/ (May 6, 2024).

Onishi, Mashun, and Koji Okamoto. 2021. "Mitochondrial Clearance: Mechanisms and Roles in Cellular Fitness." *FEBS letters* 595(8): 1239–63. https://pubmed.ncbi.nlm.nih.gov/33615465/ (March 19, 2024).

Ono, Tomoko, Kotoyo Isobe, Kazuto Nakada, and Jun Ichi Hayashi. 2001. "Human Cells Are Protected from Mitochondrial Dysfunction by Complementation of DNA Products in Fused Mitochondria." *Nature genetics* 28(3): 272–75. https://pubmed.ncbi.nlm.nih.gov/11431699/ (December 27, 2023).

Padmalayam, Indira, Sumera Hasham, Uday Saxena, and Sivaram Pillarisetti. 2009.

"Lipoic Acid Synthase (LASY)A Novel Role in Inflammation, Mitochondrial Function, and Insulin Resistance." *Diabetes* 58(3): 600–608. https://dx.doi.org/10.2337/db08-0473 (September 30, 2023).

Palsgaard, Jane et al. 2009. "Gene Expression in Skeletal Muscle Biopsies from People with Type 2 Diabetes and Relatives: Differential Regulation of Insulin Signaling Pathways." *PLOS ONE* 4(8): e6575. https://journals.plos.org/plosone/article?id=10.1371/journal.pone.0006575 (September 30, 2023).

Pardo, Rosario et al. 2016. "EndoG Knockout Mice Show Increased Brown Adipocyte Recruitment in White Adipose Tissue and Improved Glucose Homeostasis." *Endocrinology* 157(10): 3873–87. https://dx.doi.org/10.1210/en.2015-1334 (September 25, 2023).

Parsamanesh, Negin et al. 2021. "Resveratrol and Endothelial Function: A Literature Review." *Pharmacological research* 170. https://pubmed.ncbi.nlm.nih.gov/34119624/ (September 9, 2024).

Pedregosa, Fabian et al. 2012. "Scikit-Learn: Machine Learning in Python." *Journal of Machine Learning Research* 12: 2825–30. https://arxiv.org/abs/1201.0490v4 (June 5, 2023).

Peng, Jinghua et al. 2022. "Development and Functions of Mitochondria in Early Life." *Newborn (Clarksville, Md.)* 1(1): 131. /pmc/articles/PMC10193534/ (December 20, 2023).

Petersen, Max C., and Gerald I. Shulman. 2018. "Mechanisms of Insulin Action and Insulin Resistance." *Physiological reviews* 98(4): 2133–2223. https://pubmed.ncbi.nlm.nih.gov/30067154/ (March 23, 2024).Picard, Martin, Douglas C. Wallace, and Yan Burelle. 2016. "The Rise of Mitochondria in Medicine." *Mitochondrion* 30: 105–16. https://pubmed.ncbi.nlm.nih.gov/27423788/ (December 20, 2023).

Pitts, K. R., Y. Yoon, E. W. Krueger, and M. A. McNiven. 1999. “The Dynamin-like Protein DLP1 Is Essential for Normal Distribution and Morphology of the Endoplasmic Reticulum and Mitochondria in Mammalian Cells.” *Molecular biology of the cell* 10(12): 4403–17. https://pubmed.ncbi.nlm.nih.gov/10588666/ (March 19, 2024).

Poole, Angela C. et al. 2008. “The PINK1/Parkin Pathway Regulates Mitochondrial Morphology.” *Proceedings of the National Academy of Sciences of the United States of America* 105(5): 1638–43. https://pubmed.ncbi.nlm.nih.gov/18230723/ (March 19, 2024).

Prabu, Paramasivam et al. 2015. “Circulating MiRNAs of ‘Asian Indian Phenotype’ Identified in Subjects with Impaired Glucose Tolerance and Patients with Type 2 Diabetes.” *PloS one* 10(5). https://pubmed.ncbi.nlm.nih.gov/26020947/ (December 14, 2022).

Prasun, Pankaj. 2020. “Role of Mitochondria in Pathogenesis of Type 2 Diabetes Mellitus.” *Journal of Diabetes and Metabolic Disorders* 19(2): 2017–22. https://link.springer.com/article/10.1007/s40200-020-00679-x (September 30, 2023).

Puigserver, Pere et al. 1998. “A Cold-Inducible Coactivator of Nuclear Receptors Linked to Adaptive Thermogenesis.” *Cell* 92(6): 829–39.

Qu, Changda et al. 2020. “MiR-128-3p Contributes to Mitochondrial Dysfunction and Induces Apoptosis in Glioma Cells via Targeting Pyruvate Dehydrogenase Kinase 1.” *IUBMB Life* 72(3): 465–75. https://onlinelibrary.wiley.com/doi/full/10.1002/iub.2212 (April 15, 2024).

Ramachandran, Aparna et al. 2017. “Human Mitochondrial Transcription Factors TFAM and TFB2M Work Synergistically in Promoter Melting during Transcription Initiation.” *Nucleic Acids Research* 45(2): 861. /pmc/articles/PMC5314767/ (December 20, 2023).

research, MW Pfaffl - Nucleic acids, and undefined 2001. “A New Mathematical Model for Relative Quantification in Real-Time RT–PCR.” *academic.oup.com*. https://academic.oup.com/nar/article-abstract/29/9/e45/2384081 (January 30, 2023).

Rocha, Milagros et al. 2020. “Mitochondria and T2D: Role of Autophagy, ER Stress, and Inflammasome.” *Trends in endocrinology and metabolism: TEM* 31(10): 725–41. https://pubmed.ncbi.nlm.nih.gov/32265079/ (December 20, 2023).

Rodgers, Joseph T. et al. 2005. “Nutrient Control of Glucose Homeostasis through a Complex of PGC-1α and SIRT1.” *Nature 2005 434:7029* 434(7029): 113–18. https://www.nature.com/articles/nature03354 (September 9, 2024).

Rovira-Llopis, Susana et al. 2021. “Characterization of Differentially Expressed Circulating MiRNAs in Metabolically Healthy versus Unhealthy Obesity.” *Biomedicines* 9(3). http://www.ncbi.nlm.nih.gov/pubmed/33801145 (January 30, 2023).

Ruiz-Velasco, Andrea et al. 2020. “Targeting Mir128-3p Alleviates Myocardial Insulin Resistance and Prevents Ischemia-Induced Heart Failure.” *eLife* 9. https://pubmed.ncbi.nlm.nih.gov/32223896/ (April 15, 2024).

Russell, Aaron P. et al. 2013. “Disruption of Skeletal Muscle Mitochondrial Network Genes and MiRNAs in Amyotrophic Lateral Sclerosis.” *Neurobiology of Disease* 49(1): 107–17.

Sarker, Iqbal H. 2021. “Machine Learning: Algorithms, Real-World Applications and Research Directions.” *SN Computer Science* 2(3): 1–21. https://link.springer.com/article/10.1007/s42979-021-00592-x (September 20, 2024).

Satoh, Jun Ichi, Natsuki Kawana, and Yoji Yamamoto. 2013. “Pathway Analysis of ChIP-Seq-Based NRF1 Target Genes Suggests a Logical Hypothesis of Their Involvement in the Pathogenesis of Neurodegenerative Diseases.” *Gene regulation and systems biology* 7(7): 139–52. https://pubmed.ncbi.nlm.nih.gov/24250222/ (December 27, 2023).

Schofield, James H., and Zachary T. Schafer. 2021. “Mitochondrial Reactive Oxygen Species and Mitophagy: A Complex and Nuanced Relationship.” *Antioxidants & redox signaling* 34(7): 517–30. https://pubmed.ncbi.nlm.nih.gov/32079408/ (March 19, 2024).

Schrauwen, Patrick et al. 2006. “Reduced Skeletal Muscle Uncoupling Protein-3 Content

in Prediabetic Subjects and Type 2 Diabetic Patients: Restoration by Rosiglitazone Treatment." *The Journal of Clinical Endocrinology & Metabolism* 91(4): 1520–25. https://dx.doi.org/10.1210/jc.2005-1572 (September 25, 2023).

Shen, Yuntian et al. 2022. "Diabetic Muscular Atrophy: Molecular Mechanisms and Promising Therapies." *Frontiers in endocrinology* 13(1). https://pubmed.ncbi.nlm.nih.gov/35846289/ (March 20, 2024).

Sidorkiewicz, Iwona et al. 2020. "Circulating MiRNAs as a Predictive Biomarker of the Progression from Prediabetes to Diabetes: Outcomes of a 5-Year Prospective Observational Study." *Journal of clinical medicine* 9(7). http://www.ncbi.nlm.nih.gov/pubmed/32664305 (January 30, 2023).

Slack, Frank J. et al. 2000. "The Lin-41 RBCC Gene Acts in the C. Elegans Heterochronic Pathway between the Let-7 Regulatory RNA and the LIN-29 Transcription Factor." *Molecular cell* 5(4): 659–69. https://pubmed.ncbi.nlm.nih.gov/10882102/ (May 6, 2024).

Spinelli, Jessica B., and Marcia C. Haigis. 2018. "The Multifaceted Contributions of Mitochondria to Cellular Metabolism." *Nature cell biology* 20(7): 745. /pmc/articles/PMC6541229/ (December 20, 2023).

Sucharov, Carmen C. et al. 2017. "Myocardial MicroRNAs Associated with Reverse Remodeling in Human Heart Failure." *JCI Insight* 2(2): 89169.

Sun, Yuting et al. 2010. "Mammalian Target of Rapamycin Regulates MiRNA-1 and Follistatin in Skeletal Myogenesis." *The Journal of cell biology* 189(7): 1157–69. https://pubmed.ncbi.nlm.nih.gov/20566686/ (April 15, 2024).

Svoboda, P., P. Stein, H. Hayashi, and R. M. Schultz. 2000. "Selective Reduction of Dormant Maternal MRNAs in Mouse Oocytes by RNA Interference." *Development (Cambridge, England)* 127(19): 4147–56. https://pubmed.ncbi.nlm.nih.gov/10976047/ (May 6, 2024).

Swift, Steven et al. 2010. "A Novel Protease-Activated Receptor-1 Interactor, Bicaudal

D1, Regulates G Protein Signaling and Internalization." *Journal of Biological Chemistry* 285(15): 11402–10.

Tang, Bor Luen. 2016. "Sirt1 and the Mitochondria." *Molecules and Cells* 39(2): 87. /pmc/articles/PMC4757807/ (April 17, 2024).

Temiz, Ebru, İsmail Koyuncu, and Emel Sahin. 2021. "CCT3 Suppression Prompts Apoptotic Machinery through Oxidative Stress and Energy Deprivation in Breast and Prostate Cancers." *Free Radical Biology and Medicine* 165: 88–99.

Teyssier, Catherine et al. 2005. "Activation of Nuclear Receptor Coactivator PGC-1α by Arginine Methylation." *Genes & Development* 19(12): 1466. /pmc/articles/PMC1151663/ (September 9, 2024).

Thai, Phung N. et al. 2021. "Ketone Ester D-β-Hydroxybutyrate-(R)-1,3 Butanediol Prevents Decline in Cardiac Function in Type 2 Diabetic Mice." *Journal of the American Heart Association* 10(19). https://www.ahajournals.org/doi/abs/10.1161/JAHA.120.020729 (May 31, 2023).

Tian, Li et al. 2019. "Pretreatment with Tilianin Improves Mitochondrial Energy Metabolism and Oxidative Stress in Rats with Myocardial Ischemia/Reperfusion Injury via AMPK/SIRT1/PGC-1 Alpha Signaling Pathway." *Journal of pharmacological sciences* 139(4): 352–60. https://pubmed.ncbi.nlm.nih.gov/30910451/ (April 15, 2024).

Uittenbogaard, Martine, and Anne Chiaramello. 2014. "Mitochondrial Biogenesis: A Therapeutic Target for Neurodevelopmental Disorders and Neurodegenerative Diseases." *Current pharmaceutical design* 20(35): 5574. /pmc/articles/PMC4823001/ (December 27, 2023).

Vedel, Fernand et al. 1999. "The Mitochondrial Respiratory Chain and ATP Synthase Complexes: Composition, Structure and Mutational Studies." *Plant Physiology and Biochemistry* 37(9): 629–43.

Venkataraman, Sujatha et al. 2010. "MicroRNA 128a Increases Intracellular ROS Level

by Targeting Bmi-1 and Inhibits Medulloblastoma Cancer Cell Growth by Promoting Senescence." *PLoS ONE* 5(6). /pmc/articles/PMC2888574/ (April 15, 2024).

Vidigal, Joana A., and Andrea Ventura. 2015. "The Biological Functions of MiRNAs: Lessons from in Vivo Studies." *Trends in cell biology* 25(3): 137–47. https://pubmed.ncbi.nlm.nih.gov/25484347/ (April 15, 2024).

Vogel, Hannes. 2001. "Mitochondrial Myopathies and the Role of the Pathologist in the Molecular Era." *Journal of neuropathology and experimental neurology* 60(3): 217–27. https://pubmed.ncbi.nlm.nih.gov/11245207/ (April 15, 2024).

Volpe, Caroline Maria Oliveira, Pedro Henrique Villar-Delfino, Paula Martins Ferreira Dos Anjos, and José Augusto Nogueira-Machado. 2018. "Cellular Death, Reactive Oxygen Species (ROS) and Diabetic Complications." *Cell death & disease* 9(2). https://pubmed.ncbi.nlm.nih.gov/29371661/ (March 20, 2024).

Wallace, Douglas C. 2018. "Mitochondrial Genetic Medicine." *Nature genetics* 50(12): 1642–49. https://pubmed.ncbi.nlm.nih.gov/30374071/ (December 20, 2023).

Wang, David B., Chizuru Kinoshita, Yoshito Kinoshita, and Richard S. Morrison. 2014. "P53 and Mitochondrial Function in Neurons." *Biochimica et Biophysica Acta (BBA) - Molecular Basis of Disease* 1842(8): 1186–97.

Wang, Guanglei et al. 2024. "Small Molecule Activators of Mitochondrial Fusion Prevent Congenital Heart Defects Induced by Maternal Diabetes." *JACC: Basic to Translational Science*.

Wang, Jiao et al. 2021. "MicroRNA-194: A Novel Regulator of Glucagon-like Peptide-1 Synthesis in Intestinal L Cells." *Cell Death & Disease 2021 12:1* 12(1): 1–14. https://www.nature.com/articles/s41419-020-03366-0 (March 23, 2024).

Wang, Lifeng et al. 2020. "A MicroRNA Linking Human Positive Selection and Metabolic Disorders." *Cell* 183(3): 684-701.e14.

Wang, Shengnan et al. 2023. "New Therapeutic Directions in Type II Diabetes and Its

Complications: Mitochondrial Dynamics." *Frontiers in Endocrinology* 14: 1230168.

Weiss, G. J. et al. 2008. "EGFR Regulation by MicroRNA in Lung Cancer: Correlation with Clinical Response and Survival to Gefitinib and EGFR Expression in Cell Lines." *Annals of oncology : official journal of the European Society for Medical Oncology* 19(6): 1053–59. https://pubmed.ncbi.nlm.nih.gov/18304967/ (October 16, 2024).

Whitley, B. N., E. A. Engelhart, and S. Hoppins. 2019. "Mitochondrial Dynamics and Their Potential as a Therapeutic Target." *Mitochondrion* 49: 269. /pmc/articles/PMC6885535/ (March 20, 2024).

Whytock, Katie L. et al. 2023. "Comprehensive Interrogation of Human Skeletal Muscle Reveals a Dissociation between Insulin Resistance and Mitochondrial Capacity." *American journal of physiology. Endocrinology and metabolism* 325(4): E291–302. https://pubmed.ncbi.nlm.nih.gov/37584609/ (March 20, 2024).

Wianny, F., and M. Zernicka-Goetz. 2000. "Specific Interference with Gene Function by Double-Stranded RNA in Early Mouse Development." *Nature cell biology* 2(2): 70–75. https://pubmed.ncbi.nlm.nih.gov/10655585/ (May 6, 2024).

Wightman, Bruce, Ilho Ha, and Gary Ruvkun. 1993. "Posttranscriptional Regulation of the Heterochronic Gene Lin-14 by Lin-4 Mediates Temporal Pattern Formation in C. Elegans." *Cell* 75(5): 855–62. https://pubmed.ncbi.nlm.nih.gov/8252622/ (May 6, 2024).

Winter, Julia et al. 2009. "Many Roads to Maturity: MicroRNA Biogenesis Pathways and Their Regulation." *Nature cell biology* 11(3): 228–34. https://pubmed.ncbi.nlm.nih.gov/19255566/ (May 6, 2024).

Wu, Luting et al. 2019. "Myricetin Improves Endurance Capacity by Inducing Muscle Fiber Type Conversion via MiR-499." *Nutrition and Metabolism* 16(1): 1–13. https://nutritionandmetabolism.biomedcentral.com/articles/10.1186/s12986-019-0353-8 (March 23, 2024).

Wu, Zhidan et al. 1999. "Mechanisms Controlling Mitochondrial Biogenesis and

Respiration through the Thermogenic Coactivator PGC-1." *Cell* 98(1): 115–24. https://pubmed.ncbi.nlm.nih.gov/10412986/ (December 27, 2023).

Xiao, M. et al. 2018. "MiR-128 Regulation of Glucose Metabolism and Cell Proliferation in Triple-Negative Breast Cancer." *The British journal of surgery* 105(1): 75–85. https://pubmed.ncbi.nlm.nih.gov/29116653/ (April 15, 2024).

Xue, Yunxing et al. 2015. "MicroRNA-19b/221/222 Induces Endothelial Cell Dysfunction via Suppression of PGC-1α in the Progression of Atherosclerosis." *Atherosclerosis* 241(2): 671–81. https://pubmed.ncbi.nlm.nih.gov/26117405/ (March 23, 2024).

Yan, Yan et al. 2022. "Adenosine Monophosphate Activated Protein Kinase Contributes to Skeletal Muscle Health through the Control of Mitochondrial Function." *Frontiers in Pharmacology* 13. /pmc/articles/PMC9632297/ (March 20, 2024).

Yap, Kah Heng et al. 2020. "Catalpol Ameliorates Insulin Sensitivity and Mitochondrial Respiration in Skeletal Muscle of Type-2 Diabetic Mice Through Insulin Signaling Pathway and AMPK/SIRT1/PGC-1α/PPAR-γ Activation." *Biomolecules 2020, Vol. 10, Page 1360* 10(10): 1360. https://www.mdpi.com/2218-273X/10/10/1360/htm (June 1, 2023).

Yin, Hang et al. 2013. "MicroRNA-133 Controls Brown Adipose Determination in Skeletal Muscle Satellite Cells by Targeting Prdm16." *Cell metabolism* 17(2): 210–24. https://pubmed.ncbi.nlm.nih.gov/23395168/ (March 23, 2024).

Zhan, Heqin et al. 2021. "Downregulation of MiR-128 Ameliorates Ang II-Induced Cardiac Remodeling via SIRT1/PIK3R1 Multiple Targets." *Oxidative medicine and cellular longevity* 2021. https://pubmed.ncbi.nlm.nih.gov/34646427/ (April 15, 2024).

Zhang, Yu et al. 2009. "MicroRNA-128 Inhibits Glioma Cells Proliferation by Targeting Transcription Factor E2F3a." *Journal of molecular medicine (Berlin, Germany)* 87(1): 43–51. https://pubmed.ncbi.nlm.nih.gov/18810376/ (October 16, 2024).

Zhao, Junyong, Dengfeng Li, and Lin Fang. 2019. “MiR-128-3p Suppresses Breast Cancer Cellular Progression via Targeting LIMK1.” *Biomedicine & Pharmacotherapy* 115: 108947.

Zhou, Yang et al. 2017. “SIRT1/PGC-1α Signaling Promotes Mitochondrial Functional Recovery and Reduces Apoptosis after Intracerebral Hemorrhage in Rats.” *Frontiers in Molecular Neuroscience* 10. /pmc/articles/PMC5767311/ (March 19, 2024).

Zhu, Jiefu et al. 2023. “MiR-147 Represses NDUFA4, Inducing Mitochondrial Dysfunction and Tubular Damage in Cold Storage Kidney Transplantation.” *Journal of the American Society of Nephrology* 34(8): 1381–97. https://journals.lww.com/jasn/fulltext/2023/08000/mir_147_represses_ndufa4,_inducing_mitochondrial.10.aspx (March 23, 2024).

Zhuan, Qingrui et al. 2022. “Nampt Affects Mitochondrial Function in Aged Oocytes by Mediating the Downstream Effector FoxO3a.” *Journal of Cellular Physiology* 237(1): 647–59. https://onlinelibrary.wiley.com/doi/full/10.1002/jcp.30532 (April 15, 2024).

ANNEXURE I

Solution Preparation

DMEM Complete Media (1 L)

- DMEM powder
-HEPES:3.7 g
- Sodium biocarbonate: 3.9g
- Antibiotic-Antimycotic solution: 10 ml
- Fetal Calf Serum (FCS): 100 ml

Dissolve all the contents in 890 ml of autoclaved Milli-Q water and adjust the pH to 7.2 with 1N NaOH. Add 10 ml of Antibiotic-Antimycotic solution and 100 ml fetal calf serum and filter it through a 0.22µ membrane filter. Store the media at 4 °C until use.

0.50%Trypsin -EDTA solution (100 ml)

- Trypsin: 500 mg
- EDTA: 200 mg
- PBS: 100 ml

First, dissolve EDTA in PBS (Less than 60 ml) and set the pH to 7. Add trypsin to this clear solution and after trypsin, add PBS to make the solution up to 100ml. Filter the solution through a 0.22µ membrane filter, stored at 4 °C.

10X Phosphate Buffer Saline (100 ml)

- Na_2HPO_4: 1.44 g
- KH_2PO_4: 0.24 g
- KCl: 0.20 g
- NaCl: 8.00 g

Dissolve in 80 ml of Milli-Q water and adjust the pH to 7.4 with 1N HCl. Make up the volume to 100 ml, Filter the solution through a 0.22µ membrane filter, autoclave, and store at 4 °C.

Freezing Solution (10 ml)

- Fetal Calf Serum (FCS): 9 ml
- DMSO: 1 ml

Dissolve and Filter the solution through a 0.22 µ membrane filter and store it at 4 °C.

RIPA Buffer for Cell Lysis (100 ml)

- Tris base: 790 mg
- NaCl: 900 mg
- NP-40: 1 ml
- Na-deoxycholate: 2.5 g

Dissolve Tris base and NaCl in 80 ml of Milli-Q water and adjust the pH to 7.4 with 1N HCl. Then add 1ml of NP-40 and 2.5 g of Na-deoxycholate to the solution. Mix the contents and make up the volume to 100 ml with Milli-Q water. Store the buffer at 4°C.

30%: Acrylamide: Bis-acrylamide Solution (100 ml)

- Acrylamide: 29 g
- Bis-acrylamide: 1 g

Dissolve in Milli-Q water and make the volume up to 100 ml. Filter sterilize and store in a dark bottle at 4°C.

1 M Tris, pH 6.8 (100 ml)

- Tris base: 12.11 g

Dissolve in Milli-Q water and adjust the pH to 6.8 using concentrated HCl. Make the volume up to 100 ml. Autoclave and store at 4°C.

1.5 M Tris, pH 8.8 (100 ml)

- Tris base: 18.16 g

Dissolve in Milli-Q water and adjust the pH to 8.8 using concentrated HCl. Make the volume up to 100 ml. Autoclave and store at 4°C.

10% SDS (100 ml)

- SDS: 10 g

Dissolve in Milli-Q water and make the volume up to 100 ml and store at room temperature.

10% APS (10 ml)

- APS: 1 g

Dissolve in Milli-Q water and make the volume up to 10 ml. Make aliquots of 1 ml and store them at -20°C.

12% Resolving Gel for SDS-PAGE (10 ml)

- Distilled water: 3.3 ml
- 30% Acrylamide mix: 4.0 ml
- 1.5 M Tris-HCl (pH 8.8): 2.5 ml
- 10% SDS: 100 µL
- 10% APS: 100 µL
- TEMED: 4 µL

5% Stacking Gel for SDS-PAGE (4 ml)

- Distilled water: 2.7 ml
- 30% Acrylamide mix: 0.67 ml
- 1.5 M Tris-HCl (pH 8.8): 0.5 ml
- 10% SDS: 40 µL
- 10% APS: 40 µL
- TEMED: 4 µL

5X SDS-PAGE Running Buffer (1 L)

- Tris: 15.1 g
- Glycine: 72 g
- SDS: 5 g

Dissolve in Milli-Q water up to 900 ml and adjust the pH of the buffer to 8.3 with 1N HCl. Make up the volume to 1 liter after adjusting the pH and store at room temperature.

Transfer Buffer (1 L)

- Tris base: 1.452 g
- Glycine: 7.2 g
- Methanol: 200 ml

Dissolve in Elix water, make up the volume to 800 ml, and then add 200 ml of methanol. Store the buffer at 4^{o}C.

5X SDS-PAGE Loading Dye (10 ml)

- 1 M Tris-HCl (pH 6.8): 2.5 ml
- SDS: 1 g
- Bromophenol blue: 50 mg
- Glycerol: 5 ml
- DTT: 0.771 g

Dissolve in Milli-Q water and make up the volume to 10 ml. Make aliquots and store at room temperature.

10X TBS (500 ml)

- Tris base: 12.1 g
- NaCl: 40 g

Dissolve in 900 ml of Milli-Q water and adjust the pH to 7.6 with 1N HCl. Make up the volume to 1 liter and store at room temperature. For making TBST add 0.01% Tween20 in 1x TBS.

Mitochondrion 60 (2021) 160–169

Contents lists available at ScienceDirect

Mitochondrion

journal homepage: www.elsevier.com/locate/mito

MicroRNA-128 inhibits mitochondrial biogenesis and function via targeting PGC1α and NDUFS4

Kritika Sharma [a,b,1], Amit Chandra [a,c,1], Yasha Hasija [b], Neeru Saini [a,c,*]

[a] CSIR-Institute of Genomics and Integrative Biology, Mall Road, New Delhi 110007, India
[b] Delhi Technological University, Delhi, India
[c] Academy of Scientific & Innovative Research (AcSIR), Ghaziabad 201002, India

ARTICLE INFO

Keywords:
MiR-128
PGC1α
NDUFS4
Mitochondrial biogenesis
Mitochondrial dysfunction

ABSTRACT

The size and morphology of mitochondria are very heterogeneous and correlates well with their healthy functioning. In many pathological conditions, mitochondrial morphology is altered due to impaired mitochondrial dynamics (a collective term for mitochondrial fusion and fission) and dysfunction. The current study aimed at identifying the role of microRNA-128 (miR-128) in regulating mitochondrial biogenesis. Previously, peroxisome proliferator activator receptor γ coactivator 1α (PGC1α) has been shown to co-activate key intermediates of mitochondrial biogenesis, function, and dynamics; however, the upstream regulatory network remains largely unknown. We, herein using in silico analysis followed by in vitro experiments in C2C12 myoblasts, showed that miR-128 reduces mitochondrial biogenesis by directly targeting PGC1α. The expression of downstream genes, nuclear respiratory factors 1 and 2 (NRF1 and NRF2, respectively), and mitochondrial transcription factor A (TFAM) were decreased in C2C12 myoblasts upon overexpression of miR-128. Also, miR-128 is shown to promote mitochondrial dysfunction by directly targeting NADH Dehydrogenase (Ubiquinone) Fe-S Protein 4 (NDUFS4). The mitochondrial dynamics and morphology were impaired post miR-128 overexpression, as revealed by downregulation of fusion proteins (mitofusin1 and 2, i.e., MFN1 and MFN2, respectively) and upregulation of fission protein (dynamin-related protein 1, i.e., DRP1). Conversely, inhibition of miR-128 expression improved mitochondrial biogenesis, function, and dynamics, as evidenced by increased mitochondrial mass and ATP production after antimiR-128 treatment. Our findings reveal that inhibition of miR-128 can be a new potential target for reversing the effects of metabolic disorders of skeletal muscle as observed during many pathophysiological conditions such as obesity and type II diabetes.

1. Introduction

Mitochondria are double-membrane organelles that play a permissive role in establishing the life and death of eukaryotic cells. Besides being the central energy transducer of eukaryotic cells, they actively regulate several biosynthetic processes such as apoptosis, intracellular signaling, metabolism (Anderson et al., 2019). Regular cycles of fusion and fission can dynamically regulate the size and shape of mitochondria as an adaptation to metabolic needs of cells and under various pathological conditions. Mitochondrial fusion requires mitofusin 1 and 2 (MFN1 and MFN2 respectively), and OPA1 mitochondrial dynamin like GTPase (OPA1) proteins, whereas fission requires dynamin-related protein 1 (DRP1) protein. Impaired mitochondrial biogenesis and dysfunction is critically linked with the metabolic dysfunctions of skeletal muscle and is observed in various disorders such as diet-induced obesity and type II diabetes (Mohamed et al., 2014).

A major breakthrough in understanding mitochondrial biogenesis and function came with the discovery of peroxisome proliferator activated receptor gamma coactivator 1α (PGC1α) as the key regulator (Handschin and Spiegelman, 2006). PGC1α induces the transcription and replication of mitochondrial DNA by regulating mitochondrial transcription factor A (TFAM) via co-activation of nuclear respiratory factors 1 and 2 (NRF1 and NRF2, respectively) (Kelly and Scarpulla, 2004; Scarpulla, 2008; Taherzadeh-Fard et al., 2011). PGC1α is also

Abbreviations: COX1, Cytochrome *c* oxidase subunit 1; COX2, Cytochrome *c* oxidase subunit 2; ND1, NADH Dehydrogenase Subunit 1; UTR, Untranslated region.

* Corresponding author at: Functional Genomics Unit, CSIR-Institute of Genomics and Integrative Biology, Mall Road, New Delhi 110007, India.
E-mail address: nkhanna@igib.res.in (N. Saini).

[1] Kritika Sharma and Amit Chandra should be considered joint first author.

https://doi.org/10.1016/j.mito.2021.08.008
Received 13 January 2021; Received in revised form 28 July 2021; Accepted 5 August 2021
Available online 9 August 2021

known to regulate mitochondrial fusion and fission, thereby coordinating mitochondrial biogenesis and function (Cannavino et al., 2015; Picard et al., 2016). Thus, regulating cellular PGC1α levels could provide a way for therapeutic interventions in several metabolic disorders. However, the upstream signaling mechanism is poorly understood.

Non-coding RNAs, especially microRNAs (~22 nucleotides), are known to regulate post- transcriptional gene expression. Previously, miR-494-3p, miR-133 and miR-149 have been found to play a role in coordinating mitochondrial homeostasis in skeletal muscle during metabolic disorders (Mohamed et al., 2014; Lemecha et al., 2018; Nie et al., 2016). In the current study, we found that miR-128 directly targets PGC1α and NADH Dehydrogenase (Ubiquinone) Fe-S Protein 4 (NDUFS4) by binding to their 3′ UTR. In addition, the overexpression of miR-128 downregulated the expression of NRF1, NRF2, and TFAM, and in turn, inhibited mitochondrial biogenesis leading to mitochondrial dysfunction. On the contrary, inhibition of miR-128 expression by antimiR-128 induced mitochondrial biogenesis and reversed mitochondrial dysfunction in C2C12 myoblasts. In conclusion, our current study helps to understand the mechanism behind the mode of action of miR-128 in regulating mitochondrial biogenesis and function.

2. Materials and methods

2.1. Cell culture

Mouse myoblast cell line, C2C12, was purchased from National Centre for Cell Science, Pune, India, and cultured in DMEM supplemented with 10% FBS (Gibco, Thermo Fisher Scientific, MA, USA) and 100 IU/mL penicillin-streptomycin (Gibco, Thermo Fisher Scientific, MA, USA) at 37°C in a humidified atmosphere with 5% CO2. Cells were seeded in either 6-well or 24-well plates for subsequent growth and treatments. Transient transfections were done at 70–80% confluency with either precursor-microRNA-128 plasmid, designated hereafter as P (128), or antimiR-128, designated hereafter as AM- 128 (AM17000, assay ID AM11746, Thermo Fisher Scientific, MA, USA), using Lipofectamine LTX and Plus reagent (Invitrogen, CA, USA) at 1:1 ratio according to manufacturer's protocol (Adlakha and Saini, 2011). The results from P(128) or AM-128 transfected cells were compared against cells transfected with their respective negative controls i.e., pSilencer 4.1 vector or antimiR negative control designated as P(Sil) and AMNC as previously reported (Adlakha et al., 2013). Cells were trypsinized and harvested after 24 h of transfection and stored in −80 °C until further use.

2.2. Total RNA isolation, TaqMan microRNA assay, and quantitative Real-time PCR

Total RNA was extracted from C2C12 myoblasts transfected with either 4 ug of P(128) or 200 nM of AM-128 or their respective negative controls and from the skeletal muscle tissues using TRIzol reagent (Invitrogen, Paris, France) according to the manufacturer's protocol. RNA quantification was done on a NanoDrop spectrophotometer (ND 1000, NanoDrop Technologies, Inc., Wilmington, USA). A TaqMan based qRT-PCR assay was used to quantify the expression of miR-128 using specific RT primers and TaqMan probes (AB Assay ID PN442795, Applied Biosystems, Foster City, CA, USA) as described by the manufacturer. For normalization, 18S rRNA (AB Assay ID 4333760F) was used. For qRT- PCR, cDNA synthesis was done using RevertAid H Minus first strand cDNA synthesis kit (Fermentas, MD, USA). The qRT-PCR was performed using SYBR Green PCR master mix in an ABI Prism 7500 Sequence Detection System (Applied Biosystems, ThermoFisher Scientific, Waltham, MA, USA). The results were normalized with 18S rRNA. Results of TaqMan assay and qRT-PCR were analyzed using Pfaffl's method (Pfaffl, 2001). The sequence of primers used for detecting the expression levels of PGC1α, TFAM, NRF1, NRF2, MFN1, MFN2, OPA1, DRP1, and 18S rRNA are enlisted in Table 1.

Table 1
List of Primers sequences used for experiments in the study.

Gene	Forward Primer 5′-3′	Reverse Primer 5′-3′
DRP1	CGGTTCCCTAAACTTCACGA	GCACCATTTCATTTGTCACG
MFN1	TTGCCACAAGCTGTGTTCGG	TCTAGGGACCTGAAAGATGGGC
MFN2	GGGGCCTACATCCAAGAGAG	GCAGAACTTTGTCCCAGAGC
OPA1	GATGACACGCTCTCCAGTGAAG	CTCGGGGCTAACAGTACAACC
PGC1α	GAACAAGACTATTGAGCGAACC	GAGTGGCTGCCTTGGGTA
NRF1	GTGCCCGTGTCCAATCAG	TGACATAGCCATTCCCAACG
TFAM	CACCCAGATGCAAAACTTTCAG	CTGCTCTTTATACTTGCTCACAG
COX2	ATAACCGAGTCGTTCTGCCAAT	TTTCAGAGCATTGGCCATAGAA
NRF2	CCTGAGAGCTGTAGGCCC	GGAATGGAAAATAGCTCCTGCC
ND1	GTGGCTCATCTACTCCACTGA	TCGAGCGATCCATAACAATAA
NDUFS4	CAGACAACCAGACTCGGGAC	TGCATGTTATTGCGAGCAGG
COX1	ACTATACTACTACTAACAGACCG	GGTTCTTTTTTTCCGGGAGT
18S rRNA	AGAAACGGCTACCACATCCA	CCCTCCAATGGATCCTCGTT
PGC1α 3′ UTR	CTAGACTAGTAAGGACCAGATGC GTTCTCT	CGACGCGTACAGCCATCAAAAAG GGACA
NDUFS4 3′ UTR	CGACGCGTGGAGCTGGCTACAT CTCTGC	CCCAAGCTTGGGAAGAACGGGCT TAACTT

2.3. Cloning of luciferase reporter constructs

The 3′ UTR sequence of PGC1α and NDUFS4 transcripts were retrieved from the Ensembl genome browser (Ensembl Release 97, July 2019). The region of 3′ UTR (between 3078 and 3084 nucleotides of PGC1α, and 27–33 nucleotides of NDUFS4) containing the target site of miR-128 was amplified from the mouse genome, using primers enlisted in Table 1. The amplified region was inserted between cut sites of MluI and SpeI for PGC1α (742 bp) and MluI and HindIII for NDUFS4 (518 bp) for generating the pMIR REPORT luciferase vector (Ambion Inc., TX, USA). Hereafter, the constructs are represented as 3′ UTR PGC1α and 3′ UTR NDUFS4. A completely unrelated mouse sequence with no miR-128 binding site was cloned and used as the control plasmid, designated hereafter as unrelated UTR. All plasmids were verified by sequencing.

2.4. Luciferase reporter assay

For the luciferase assay, C2C12 myoblasts were seeded at 70–80% confluency in 12-well plates. After 24 h, the cells were co-transfected with 200 ng of firefly luciferase reporter construct and 50 ng of renilla luciferase containing pRL-CMV plasmid (Promega, WI, USA). Simultaneously, C2C12 myoblasts were treated with 2 ug of P(128) or 100 nM of antimiR-128, or their respective negative control. Luciferase activity was measured post 24 h of transfection using the dual-luciferase reporter assay system according to the manufacturer's protocol.

2.5. Western blot analysis

Total protein was extracted from C2C12 myoblasts transfected with either 2 ug or 4 ug of P(128) or 100 nM or 200 nM AM-128, or their respective negative control using RIPA lysis buffer (50 mM Tris-HCl, pH 7.4, 150 mM NaCl, 1% NP-40, 0.25% Na-deoxycholate, 1 mM EDTA, pH 7.4) containing protease and phosphatase inhibitors (G-Biosciences, MO, USA). Protein quantification was done by BCA method (Sigma, MO, USA) as described earlier (Adlakha et al., 2013). Equal amount of total protein (60 μg) was separated by SDS-PAGE (10–12%) and transferred to a PVDF membrane (mdi; Advanced Microdevices, Ambala Cantt., India). Blocking of the membrane was done in 5% BSA for 2 h at room temperature. Incubation of membranes in primary antibody was done for 2 h or 16 h, depending on the antibody at 1:500 to 1:1000 dilution, whether purchased from Santa Cruz (Santa Cruz Biotechnology, CA, USA) or Abcam (Abcam, MA, USA) respectively. This was followed by incubation in their respective HRP-linked secondary antibody for 1 h at room temperature at a dilution of 1 :5000. The primary antibodies against PGC1α (sc13067), and NRF1 (sc101102), were procured from Santa Cruz, whereas those against TFAM (ab272885), NRF2 (ab92946),

NDUFS4 (ab137064), DRP1 (ab154879), MFN2 (ab56889), and OPA1 (ab42364), were purchased from Abcam. GAPDH (G9545), Sigma Alderich, Merck KGaA, Darmstadt, Germany) was used as the loading control. The blots were developed using enhanced chemiluminiscence (Thermo Fisher Scientific, CA, USA) method. Integrated density values were obtained and quantified using AlphaImager 3400 (Alpha Inno-Tech, CA, USA).

2.6. Mitochondrial mass and mitochondrial DNA quantification

Mitochondrial mass was assessed from C2C12 myoblasts, after transfections with P(128) or antimiR-128, in DMEM supplemented with 10 nM of 10-N-nonyl acridine Orange (NAO) dye (A1372; Thermo Fisher Scientific, CA, USA), and incubated at 37°C in an atmosphere containing 5% CO2 for 15 min in the dark. Fluorescence was measured for each sample counted to 5000 events each using GUAVA EasyCyte (Guava Technologies, CA, USA). Relative mitochondrial DNA content was determined using qRT- PCR assay by quantifying the expression of ND1, COX1, and COX2 genes. The Ct values were normalized with 18S rRNA. The sequences of primers are enlisted in Table 1. The results were analyzed using Pfaffl's method (Pfaffl, 2001).

2.7. Fluorescent microscopy

A mitochondria-specific cationic dye, MitoTracker Green FM (M7514, Thermo Fisher Scientific) was used to fluorescently label cellular mitochondria. In brief, C2C12 myoblasts were grown on two chambered culture slides. After 24 h of transfection, cells were incubated with 200 nM of Mitotracker Green FM for 30 min at 37°C according to the manufacturer's instructions. Images were acquired using a Leica SP8 confocal laser scanning microscope (60X magnification). Mitochondrial morphology was quantified using standard parameters as previously described using ImageJ software (Iannetti et al., 2016).

2.8. Oxygen consumption rate (OCR)

Cellular bioenergetics was measured using XFe24 Analyzer (Seahorse Bioscience, CA, USA). C2C12 myoblasts (~30,000) were seeded in each well and then treated with either 400 ng of P(128) or 60 nM of antimiR-128, or their respective negative controls. Post 24 h of transfections, cells were washed and incubated for 1 h at 37 °C in a CO2-free environment with XF assay media. The inhibitors, namely, oligomycin (1.5 μM), FCCP (0.5 μM), rotenone (0.5 μM), and antimycin A (0.5 μM), were sequentially added to each well as per the manufacturer's instructions, and OCR was measured. The data were normalized to total protein.

2.9. Animal studies

Four-week-old male C57BL/6 mice were purchased from Livon Biolabs, Bengaluru, and housed in cages under 12 h of alternating dark and light periods. All animal experiments and procedures were approved by the Institutional Animal Ethics Committee (IAEC) of CSIR-Institute of Genomics and Integrative Biology, New Delhi, India. Mice were fed *ad libitum* with a high-fat diet (HFD) that provides 60% energy from fat (Research Diet, New Brunswick, NJ 08,901 USA) for 13 weeks. Anti-miR-128 (Custom miRIDIAN Hairpin inhibitor, mmu-128-3p, ref#IH-310398–08, in vivo) was purchased from Dharmacon Inc. (CO, USA). In vivo-jetPEI reagent (Polyplus-transfection® SA, Illkirch, France) was used as per the manufacturer's instructions for delivering antimiR-128 in mice. Each mouse received five intraperitoneal injections of either vehicle control (HFD- Control) or antimiR-128 (HFD-AM-128) on alternate days at a dose of 5 mg/kg body weight. Mice were sacrificed after 48 h of the last treatment following a 12 h fasting period. Skeletal muscle tissues were collected and snap-frozen until further use.

2.10. Statistical analysis

All results are presented as mean ± SEM. Student's two-tailed *t*-test was used to compare the differences between the two groups. Values of $p < 0.05$ were considered statistically significant.

3. Results

3.1. MiR-128 directly targets peroxisome proliferator activated receptor gamma coactivator 1α.

We have demonstrated previously that miR-128 targets Sirtuin 1 (SIRT1), an NAD^+ dependent protein deacetylase. SIRT1 is extensively implicated in mitochondrial biogenesis and multiple other biological processes such as apoptosis, inflammation, and metabolism by regulating several histone and non-histone proteins, including PGC1α. Interestingly, in our previous study, PGC1α came out to be one of the downregulated genes in the transcriptome profile of HEK293T cells after overexpression of miR-128 (submitted in the GEO database, accession number GSE31297) (Adlakha et al., 2013). Herein, we investigated the downstream effects of cellular miR-128 level in C2C12 myoblasts and mouse skeletal muscle tissues, as the dysfunction of skeletal muscle (largest metabolic tissue) is critically regulated by mitochondrial impairment.

We first quantified the levels of matured miR-128 by a TaqMan based qRT-PCR assay post 24 h of transfections in C2C12 myoblasts, as described in Materials and Methods. As shown in Fig. 1A, there was a significant increase in the miR-128 levels by 13.46 fold ($p = 0.0040$) after overexpression of miR-128, whereas antimiR-128 treatment significantly decreased miR-128 levels by 6.23 fold ($p = 0.0086$). Interestingly, PGC1α mRNA was found to harbor target sequence (3078–3084 nucleotide) for miR-128 in its 3′ UTR, as predicted by the TargetScan database (Release 7.2), and this sequence was found to be broadly conserved in mammals including human, chimpanzee, and rhesus monkey (Fig. 1B) (Agarwal et al., 2015). To check whether PGC1α is a direct target of miR-128, we herein made luciferase reporter construct containing the binding sequence of miR-128 from the 3′ UTR region of PGC1α mRNA and performed dual luciferase reporter assay. The luciferase activity was found to be significantly decreased by 1.41 fold ($p = 0.0482$) upon miR-128 overexpression, while it was significantly increased by 1.97 fold ($p = 0.0266$) upon antimiR-128 treatment (Fig. 1C). Thereby, confirming PGC1α is a direct target of miR-128.

We also quantified the expression of PGC1α at transcriptional as well as translational level post transfections. The level of PGC1α mRNA was significantly decreased by 2.46 fold ($p = 0.0124$) upon overexpression of miR-128 and increased by 2.18 fold ($p = 0.1214$) after antimiR-128 treatment (Fig. 1D). Similarly, western blot analysis revealed that PGC1α protein levels decreased by 1.76 fold ($p = 0.023$) and 1.80 fold ($p = 0.0029$) upon overexpression of miR-128 and increased by 1.23 fold ($p = 0.291$) and 1.70 fold ($p = 0.0655$) after antimiR-128 treatment, in a dose-dependent manner (Fig. 1E and 1F).

A central cause of mitochondrial dysfunction in skeletal muscle metabolic disorders is the intake of a high-fat diet (HFD) (Kazeminasab et al., 2018). However, the mechanism underlying diet-induced disorders of skeletal muscle metabolism via altered mitochondrial function and biogenesis is unknown. Previously, Latouche et al. (2016) have reported upregulation of miR-128 in the human skeletal muscle samples from pre-diabetic or Type II diabetic patients as compared to the healthy controls (Latouche et al., 2016). Since in vitro downregulation of miR-128 could improve the PGC1α mediated mitochondrial biogenesis and function; therefore, we checked if the downregulation of miR-128 in hypercholesterolemic mice model can rescue the HFD induced mitochondrial dysfunction by upregulating PGC1α in the skeletal muscle of HFD fed mice (Chandra et al., 2021). As expected, the downregulation of miR-128 leads to higher PGC1α expression in the HFD-AM-128 compared to the HFD-Control but change was statistically insignificant

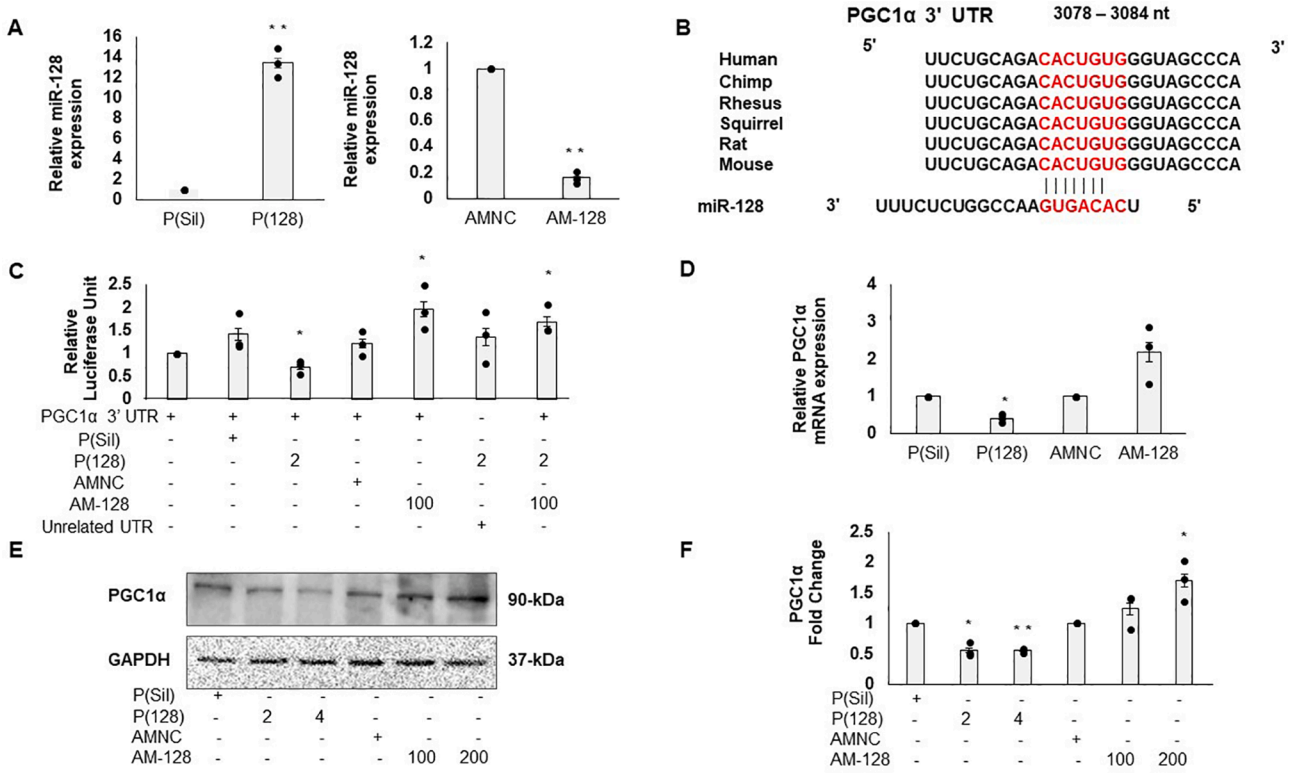

Fig. 1. miR-128 directly targets PGC1α in C2C12 myoblasts. (A) TaqMan qRT-PCR analysis of miR-128 overexpression post 24 h of transfection upon P(128), or P (Sil), or AM-128, or negative control treatment. (B) Predicted binding region of miR-128 seed sequence in the 3′ UTR of PGC1α mRNA. (C) Luciferase activity measured in C2C12 myoblasts transfected with PGC1α 3′ UTR and either P(128), or P(Sil), or AM-128, or negative control (D) Relative mRNA expression of PGC1α was estimated by qRT-PCR. (E & F) PGC1α protein expression were evaluated by western blotting. Bar graph represent the integrated densitometry values normalized to GAPDH AntimiR-128 = AM- 128, AntimiR negative control = AMNC, pSilencer vector = P(Sil), plasmid (128) = P(128). Data are mean ± SEM for three independent experiments, *p < 0.05, **p < 0.01. (2-column fitting).

(Supplementary Fig. 1). Together, our data suggest that miR-128 directly targets PGC1α.

3.2. MiR-128 inhibits mitochondrial biogenesis by downregulating TFAM via NRF transcription factors in C2C12 myoblasts

PGC1α, together with SIRT1, is known to regulate mitochondrial biogenesis through TFAM via nuclear respiratory factors (Tang, 2016). So, we next explored the effects of miR-128 on the expression of NRF1, NRF2, and TFAM at both transcriptional and translational levels. Overexpression of miR-128 decreased NRF1 mRNA levels by 2.43 fold ($p = 0.1138$) and NRF2 mRNA levels by 1.94 fold ($p = 0.0235$), whereas antimiR-128 treatment significantly increased NRF1 mRNA levels by 1.68 fold ($p = 0.0100$) and NRF2 mRNA levels by 2.27 fold ($p = 0.2432$) (Fig. 2A). Further, there was also a dose-dependent significant decrease in NRF1 (1.12 fold and 1.47 fold) and NRF2 (1.13 fold and 1.34 fold) protein levels after overexpression of miR-128 and a significant increase in NRF1 (1.31 fold at 200 nM) and NRF2 (1.78 fold and 1. 81 fold) protein levels after antimiR-128 treatment (Fig. 2B and 2C).

Simultaneously, we observed that overexpression of miR-128 reduced the mRNA levels of TFAM by 2.42 fold ($p = 0.0853$), whereas antimiR-128 treatment increased the mRNA levels of TFAM as revealed by 1.15 fold ($p = 0.404$) in qRT-PCR experiment post 24 h of transfection (Fig. 2D). As shown in Fig. 2E-2F, western blot analysis revealed that the TFAM protein levels decreased by 1.54 fold ($p = 0.0131$) and 1.44 fold ($p = 0.0883$) after the overexpression of miR-128, whereas upon the antimiR-128 treatment, TFAM protein levels significantly increased by 1.35 fold ($p = 0.184$) and 1.63 fold ($p = 0.0473$) in a dose-dependent manner. We also quantified NRF2 and TFAM protein levels in skeletal muscle and found that it was higher in HFD-AM-128 when compared with HFD-Control, although the changes were not statistically significant (Supplementary Fig. 1).

3.3. Overexpression of miR-128 decreased mitochondrial respiration by targeting energy metabolism gene NDUFS4 in C2C12 myoblasts

To explore the changes in mitochondrial DNA content in response to miR-128 levels, we checked a subset of electron transport chain transcripts, namely COX1, ND1, and COX2, which are encoded exclusively by the mitochondrial genome, using qRT-PCR analysis. As shown in Fig. 3A, we found that overexpression of miR-128 reduced transcripts of mitochondrial DNA while antimiR-128 treatment increased the transcripts post 24 h of transfections. It has been reported that the replication of mitochondrial DNA precedes mitochondrial biogenesis, which is inherent to the cellular energy homeostasis and corresponds well with the mitochondrial mass (Li et al., 2012). Hence, we next quantified the mitochondrial mass following NAO treatment, which specifically stains cardiolipin of the inner mitochondrial membrane. The mitochondrial mass reduced following miR-128 overexpression by 1.23 fold ($p = 0.060$), while antimiR-128 treatment increased the mitochondrial mass by 1.27 fold ($p = 0.035$) (Fig. 3B).

The 3′ UTR of NDUFS4 has a broadly conserved predicted binding site of miR-128 (Fig. 3C). We validated that NDUFS4 (Mitochondrial Energy Metabolism Gene) is directly targeted by miR-128 using dual luciferase assay. Fig. 3D shows that overexpression of miR-128 significantly reduced the luciferase activity of NDUFS4 3′ UTR reporter construct by 4.72 fold ($p = 0.0044$) and significantly increased the luciferase activity of NDUFS4 3′ UTR reporter construct by 1.30 fold ($p = 0.0331$) upon antimiR-128 treatment post 24 h of transfection. The mRNA level of NDUFS4 does not correlate with miR-128 treatment in

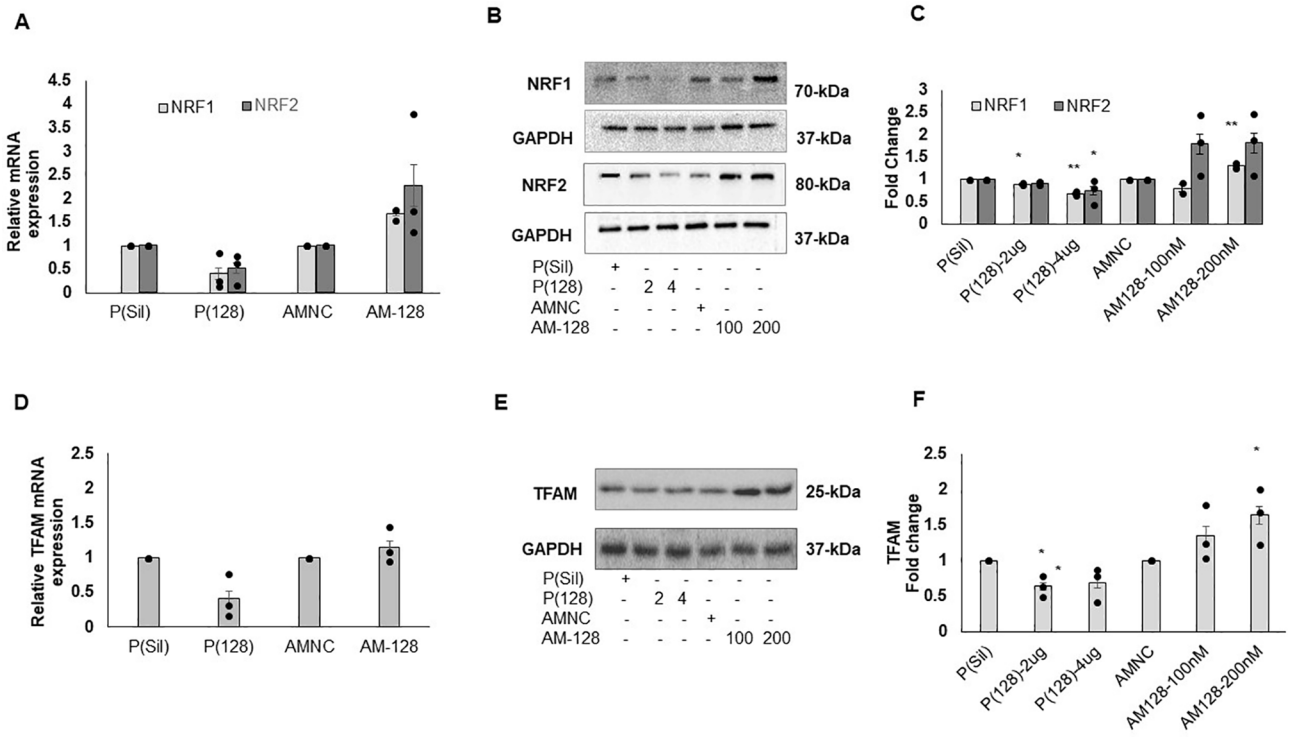

Fig. 2. MiR-128 inhibits key genes of mitochondrial biogenesis in C2C12 myoblasts. Relative mRNA expression of (A) NRF1, NRF2, and (D) TFAM were quantified using qRT-PCR post 24 h of transfection with P(128), or P(Sil), or AM-128, or negative control. Western blotting was done to quantify the protein levels of (B, C) NRF1, NRF2, and (E, F) TFAM and Bar graph represent the integrated densitometry values normalized to GAPDH. AntimiR-128 = AM-128, AntimiR negative control = AMNC, pSilencer vector = P(Sil), plasmid (128) = P(128). Data are mean ± SEM for three independent experiments, *p < 0.05, **p < 0.01. (2-column fitting).

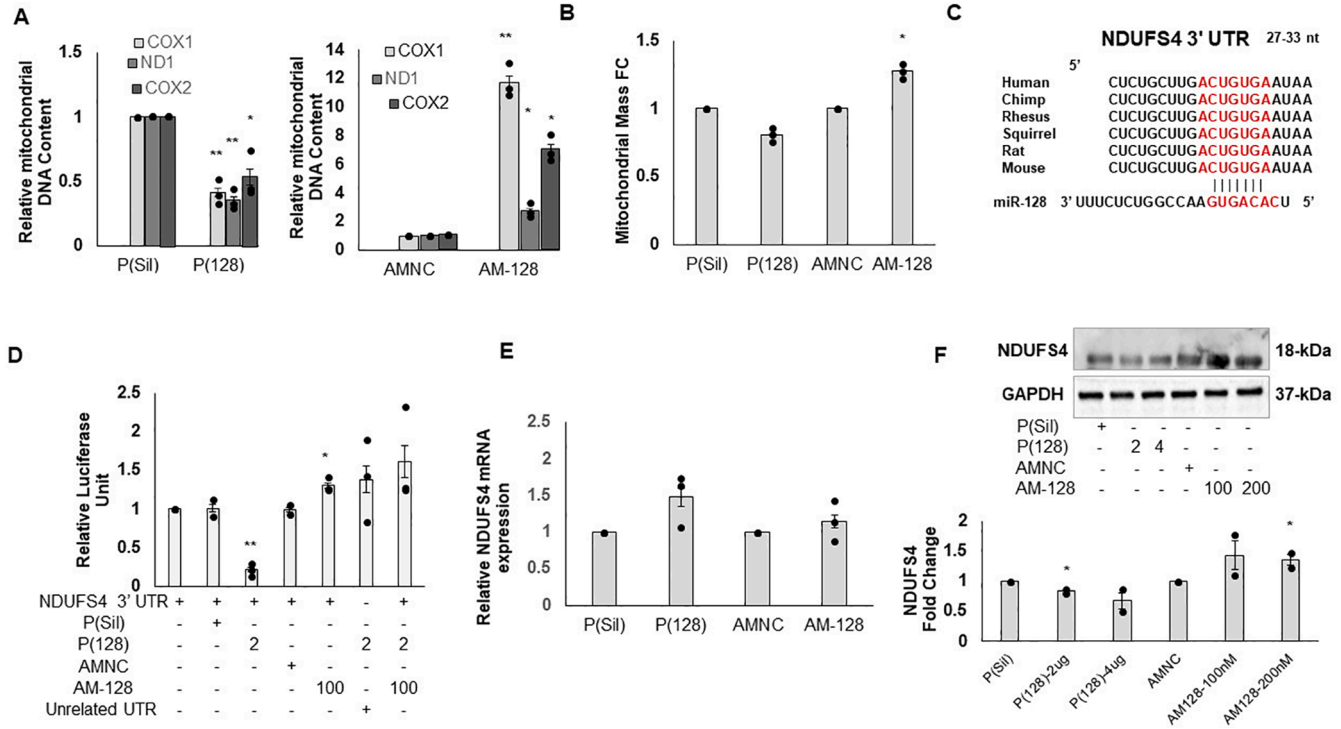

Fig. 3. Downregulation of miR-128 reverses mitochondrial dysfunction in C2C12. myoblasts. (A) Mitochondrial DNA content was measured by quantifying the mRNA levels of COX1, ND1, and COX2 using qRT-PCR. (B) Mitochondrial mass was analyzed by NonylacridineOrange staining using flow cytometry. (C) Predicted binding region of miR-128 seed sequence in the 3′ UTR of NDUFS4 mRNA. (D) Luciferase activity measured in cells transfected with NDUFS4 3′ UTR and either P (128), or P(Sil), or AM-128, or negative control (E) Relative mRNA expression of NDUFS4 was estimated by qRT-PCR. (F) NDUFS4 protein expression were evaluated by western blotting. Bar graph represent the integrated densitometry values normalized to GAPDH. AntimiR-128 = AM-128, AntimiR negative control = AMNC, pSilencer vector = P(Sil), plasmid (128) = P(128). Data are mean ± SEM for three independent experiments, *p < 0.05, **p < 0.01. (2-column fitting).

C2C12 myoblasts whereas the protein expression of the NDUFS4 gene is downregulated by 1.19 fold ($p = 0.0123$) and 1.47 fold ($p = 0.0987$) with overexpression of miR-128 treatment and is found to be increased by 1.43 fold ($p = 0.153$) and 1.34 fold ($p = 0.041$) with inhibition of miR-128 with antimir-128 treatment (Fig. 3E and 3F). Interestingly, we found that several subunits of the electron transport chain (ETC) have miR-128 binding sites in their 3′ UTR (Fig. 4). This could possibly suggest a negative correlation between miR-128 and ATP levels.

Mitochondrial dysfunction is the inability of the mitochondrial pool to generate and sustain sufficient cellular ATP levels and is correlated with the size of the mitochondrial pool. To ascertain the influence of mitochondrial dysfunction (in response to miR-128 levels) on cellular ATP production, we next assessed the mitochondrial oxygen consumption rate (OCR) as described in the Materials and Methods. As shown in Fig. 5A, overexpression of miR-128 decreases, whereas antimiR-128 treatment increases the mitochondrial respiration rate. In addition, other respiratory parameters, such as basal respiration, maximal respiration, ATP production, and spare respiratory capacity, decreased after miR-128 overexpression and increased upon miR-128 inhibition (Fig. 5C–F).

3.4. *MiR-128 regulates mitochondrial dynamics and affects mitochondrial morphology*

Accumulating evidence indicate that the alterations in mitochondrial biogenesis and function correlate with the changes in mitochondrial dynamics (Chen et al., 2021; Medala et al., 2021). Since the data till now suggested that miR-128 altered mitochondrial biogenesis and function, we further hypothesized that miR-128 would also be regulating mitochondrial dynamics.

We quantified the expression of MFN1, MFN2, OPA1, and DRP1 at both transcriptional and translational levels post 24 h of transfection. Overexpression of miR-128 significantly decreased the levels of mitochondrial fusion promoting proteins (MFN2 and OPA1) and significantly increased the level of fission protein (DRP1). On the contrary, the trend was reversed following antimiR-128 treatment (Fig. 6A, B and C). Similar findings were also observed at the mRNA levels as quantified by the qRT-PCR assay (Fig. 6D).

Simultaneously, visualization of mitochondrial morphology was done using MitoTracker Green FM dye using confocal microscopy. As shown in Fig. 7A, C2C12 myoblasts overexpressing miR-128 showed more fraction of fragmented mitochondria in poorly connected networks, suggesting increased mitochondrial fission. In contrast, hyperfused mitochondria were evident in cells treated with antimiR-128. The mitochondrial morphology was quantified using various parameters, namely, mitochondrial area, perimeter, form factor, and ferret's diameter. We found that miR-128 overexpression significantly reduced mitochondrial area and perimeter by 1.32 fold ($p = 0.0045$) and 1.36 fold ($p = 0.0081$), respectively. The form factor, which represents the branching aspect of mitochondria, was reduced upon miR-128 overexpression by 1.35 fold ($p = 0.0009$), thus suggesting more mitochondrial circularity with miR-128 treatment and vice versa. The ferret's diameter also showed a similar trend; it was decreased by 1.32 fold ($p = 0.0162$) post miR-128 overexpression and increased by 1.10 fold ($p = 0.1248$) upon antimiR-128 treatment. All this data together indicates that miR-128 overexpression promotes mitochondrial fission, and this effect is counteracted upon miR-128 inhibition (Fig. 7B).

Taken together, these results demonstrate that miR-128 inhibits mitochondrial biogenesis and function by directly inhibiting PGC1α and NDUFS4 (Fig. 8).

4. Discussion

To date, studies have demonstrated that miR-128 has a role of skeletal muscle related miRNA but it is not yet fully characterized that how miR-128 regulate skeletal muscle health and regeneration. MiR-128 regulate proliferation and differentiation of myoblast via insulin signaling pathway by targeting insulin receptor (IR), insulin receptor substrate 1 (IRS-1), and phosphatidylinositol 3-kinases receptor 1 (PI3K-R1). Another study by Motohashi et al shows negative regulation of miR-128 and its Tumor necrosis factor α (TNF-α) which is involved in regulating skeletal muscle hypertrophy. In addition, miR-128 is also known to regulates its target myostatin inturn inhibiting myoblast proliferation and differentiation (Motohashi et al., 2013). Cellular energy levels are directly correlating with skeletal muscle regeneration (Ryten et al., 2002). This correlations of miRNA with its target mRNAs, and cellular energy levels for skeletal muscle health and regeneration is yet undetermined. Furthermore, miR-128 has shown to target myostatin, inhibiting C2C12 myoblast proliferation and promoting its differentiation into myotubes in a study by Shi et al. (2015).

The experiments performed in the current study were to understand the effects of miR-128 on mitochondrial regulators of biogenesis and function in C2C12 myoblasts apart from response of myogenic factors controlling mitochondrial activity in C2C12 myotubes. Hence, a study in differentiated myotube could possibly extend the physiological relevance. The present study identifies a central role of miR-128 in

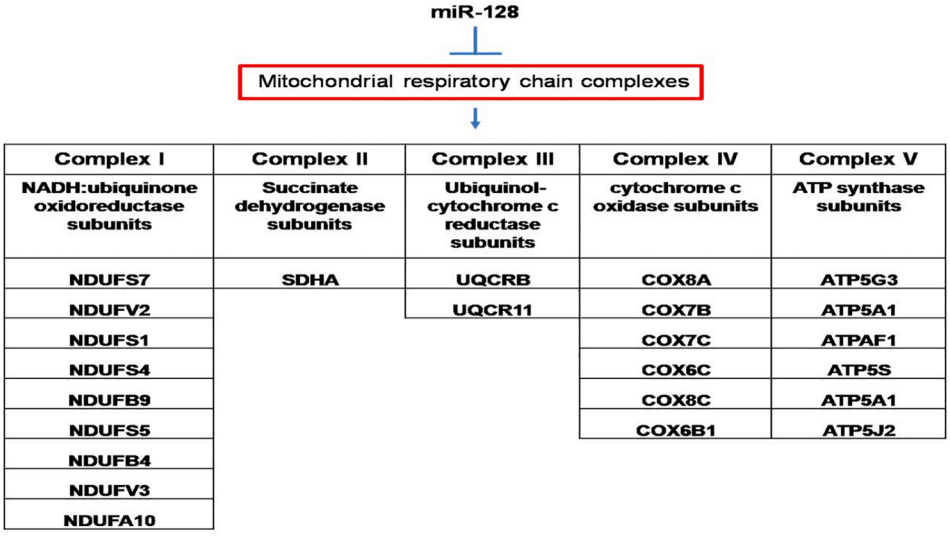

Complex I	Complex II	Complex III	Complex IV	Complex V
NADH:ubiquinone oxidoreductase subunits	Succinate dehydrogenase subunits	Ubiquinol-cytochrome c reductase subunits	cytochrome c oxidase subunits	ATP synthase subunits
NDUFS7	SDHA	UQCRB	COX8A	ATP5G3
NDUFV2		UQCR11	COX7B	ATP5A1
NDUFS1			COX7C	ATPAF1
NDUFS4			COX6C	ATP5S
NDUFB9			COX8C	ATP5A1
NDUFS5			COX6B1	ATP5J2
NDUFB4				
NDUFV3				
NDUFA10				

Fig. 4. Putative target genes of miR-128 which forms various subunits of the mitochondrial respiratory complexes, as predicted by the TargetScan database.

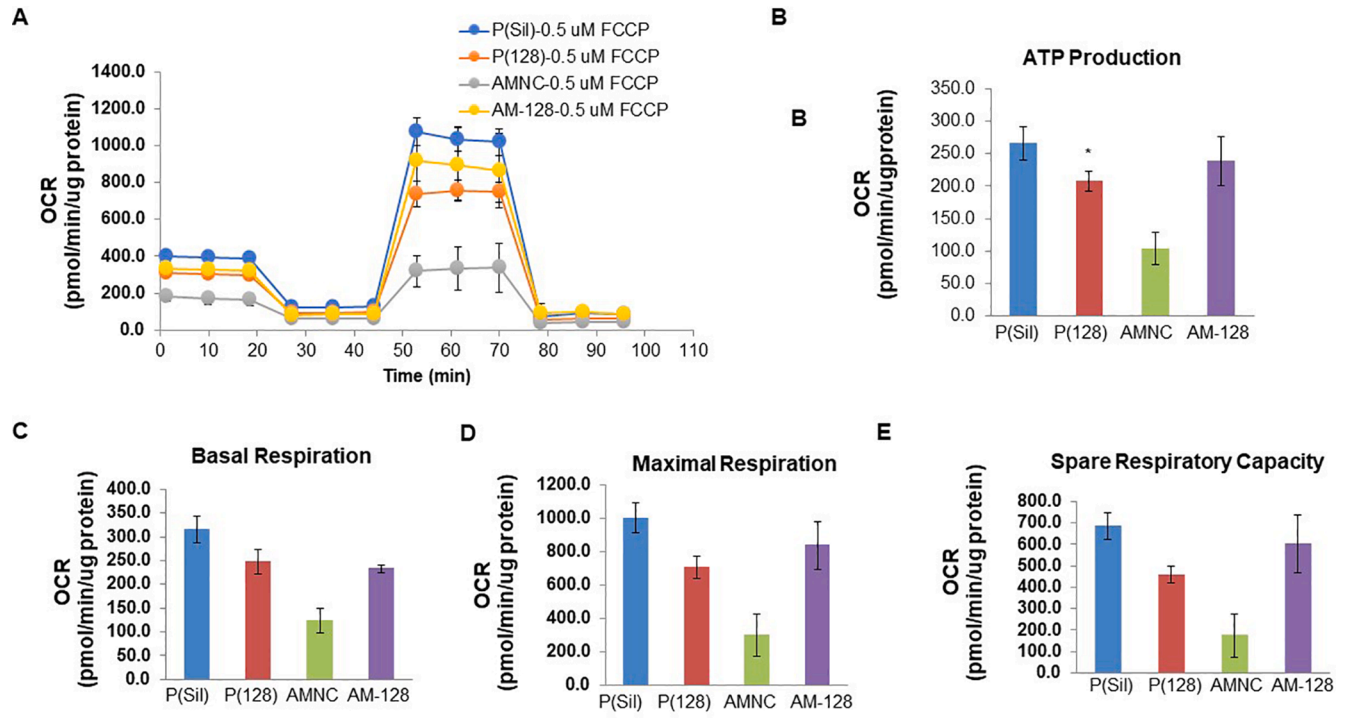

Fig. 5. MiR-128 impairs bioenergetics profiles in C2C12 myoblasts. (A) Mitochondrial OCR was assessed post 24 h of transfection with P(128), or P(Sil), or AM- 128, or negative control Parameters of mitochondrial function were calculated from the OCR values (B) ATP production (C) Basal respiration (D) Maximal respiration, and (E) Spare respiratory capacity,. The OCR values were normalized by total cellular protein. AntimiR-128 = AM-128, AntimiR negative control = AMNC, pSilencer vector = P(Sil), plasmid (128) = P(128). Data are mean ± SE for three independent experiments, *p < 0.05, **p < 0.01. (2-column fitting).

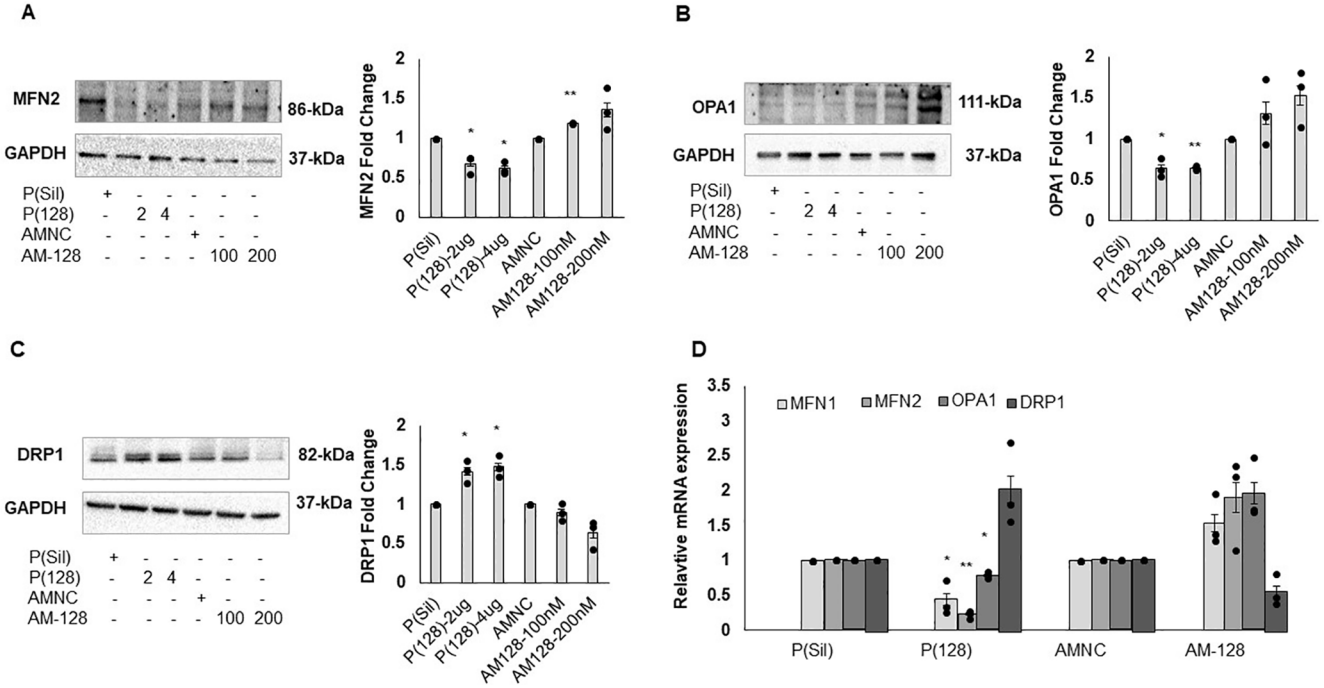

Fig. 6. MiR-128 regulates key fusion and fission genes in C2C12 myoblasts. Western blot analysis of (A) MFN2, (B) OPA1, and (C) DRP1 proteins. Bar graph represent the integrated densitometry values normalized to GAPDH (D) Relative mRNA levels of MFN1, MFN2, OPA1, and DRP1 were quantified using qRT-PCR. AntimiR-128 = AM-128, AntimiR negative control = AMNC, pSilencer vector = P(Sil), plasmid (128) = P(128). Data are mean ± SEM for three independent experiments, *p < 0.05, **p < 0.01. (2- column fitting).

promoting impairment of mitochondrial biogenesis and function by targeting the upstream transcriptional activator PGC1α. Several important observations have been made in this study. First, we validated that the 3′ UTR of PGC1α is a direct target of miR-128. Second, miR-128 inhibits mitochondrial biogenesis and promotes mitochondrial dysfunction. Third, miR-128 inhibits fusion and induces fission of

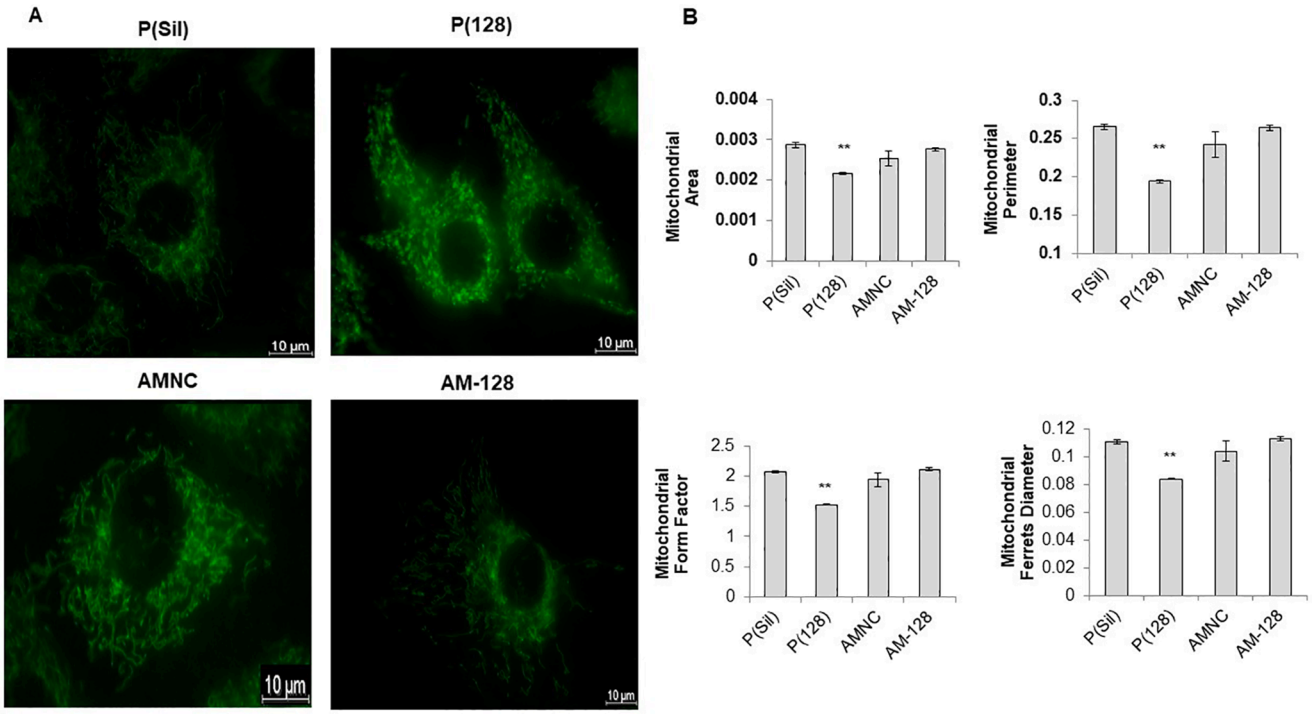

Fig. 7. MiR-128 regulates mitochondrial morphology and dynamics in C2C12 myoblasts (A) Mitochondrial morphology as visualized by fluorescence staining (MitoTracker Green FM) following transfection with P(128), or P(Sil), or AM-128, or negative control. (B) Surface area and perimeter together represents mitochondrial volume; mitochondrial form factor is calculated as [(perimeter^2)/(4π·surface area)] reflects the complexity and branching aspect of mitochondria; and Feret's diameter represents the longest distance between any two points within a given mitochondrion. AntimiR-128 = AM-128, AntimiR negative control = AMNC, pSilencer vector = P(Sil), plasmid (128) = P(128). Data are mean ± SEM for three independent experiments, *p < 0.05, **p < 0.01. (2-column fitting). (For interpretation of the references to colour in this figure legend, the reader is referred to the web version of this article.)

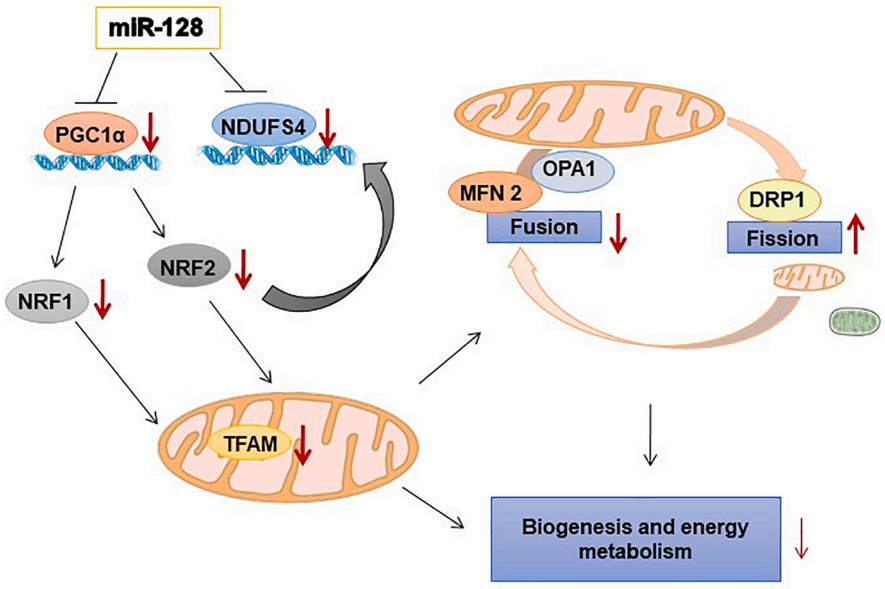

Fig. 8. Schematic of the mechanism by which miR-128 inhibits mitochondrial biogenesis and function. MiR-128 directly targets key regulators of mitochondrial biogenesis and function, PGC1α and NDUFS4, by binding to their respective 3′ UTR. Inhibition of PGC1α further reduces the expression of downstream transcription factors, namely NRF1, NRF2, and TFAM, thus inhibiting the transcription and translation of mitochondrial DNA. As shown, miR-128 regulates the balance of mitochondrial dynamics (morphology, quantity, and size) by upregulating fission (increased DRP1 expression) and downregulating fusion (decreased MFN1, MFN2, and OPA1 expression). Altogether, inhibition of miR-128 may have potential therapeutic implications in improving mitochondrial biogenesis and function via PGC1α and NDUFS4. (2-column fitting).

mitochondria. Lastly, we observed that the inhibition of endogenous miR-128 could reverse high-fat diet induced mitochondrial dysfunction in skeletal muscle. Collectively, for the first time, our study demonstrates the role of miR- 128 in maintaining an optimum pool size of functional mitochondria in C2C12 myoblasts.

We observed that the binding site of miR-128 to the 3′ UTR of PGC1α is broadly conserved. miR-128 restrains its target gene expression with the assistance of a guiding RNA complex to bind the seed sequence with the 3′ UTR of the target and this complex is known as RNA induced silencing complex (RISC). These events could lead to translational repression or even translational degradation of the target mRNAs. As PGC1α acts upstream in the pathway of mitochondrial biogenesis and improves its functions, we further tested the expression of key transcripts and proteins involved in mitochondrial processes (LeBleu et al., 2014). We observed that miR-128 inhibits the expression of genes involved in mitochondrial fusion, namely, MFN1, MFN2, and OPA1.

Also, the expression of DRP1, which induces mitochondrial fission, was increased following overexpression of miR-128 (Fig. 6). These findings support the observed fragmented mitochondrial morphology following miR-128 overexpression in C2C12 myoblasts and strengthen the hypothesis that miR-128 overexpression leads to smaller and fragmented mitochondria with impaired functions (Fig. 7). Similar to our study, Wang et al. (2020) have observed an increased mitochondrial fragmentation after miR-153-3p overexpression in cardiac hypertrophy (Wang et al., 2020). In a separate study, Li et al. (2010) have shown that the inhibition of DRP1 by miR-30 reduces mitochondrial fission and induces apoptosis (Li et al., 2010). The DRP1 induced fission could also trigger the mitopaghic effector molecules within a cell for maintaining the homeostatic function of mitochondria (Woo et al., 2021).

In the current study, we also observed an increase in the mitochondrial DNA content and total mitochondrial mass following upregulation of mitochondrial fusion after miR-128 inhibition in C2C12 myoblasts. NRF1, and NRF2, the key transcription factors that promote the TFAM mediated replication of mitochondrial DNA essential for mitochondrial biogenesis, were increased after miR-128 inhibition (Roe and Qi, 2018).

Furthermore, the oxygen consumption rate was found to be decreased after miR-128 overexpression, thereby suggesting the inhibitory role of miR-128 in mitochondrial respiration. The ATP production in mitochondrial respiration involves five multi-subunit complexes arranged in the ETC (Johnson et al., 2013; Melcher et al., 2017). Interestingly, we found that the binding site of miR- 128 is present in the 3′ UTR of 24 mRNAs coding for various subsets in complex I-V of the ETC, including NDUFS4. In the current study, we validated NDUFS4 to be a direct target of miR-128.

We also examined the effects of in vivo downregulation of miR-128 in HFD fed hypercholesterolemic mice. Fat rich diet is known to promote mitochondrial dysfunction by inhibiting the expression of PGC1α (Kazeminasab et al., 2018; Barroso et al., 2018). To date, only a few microRNAs, such as miR- 133, and miR-696, have been reported to directly target PGC1α mRNA in skeletal muscle (Aoi et al., 2010). Herein, we observed that the downregulation of miR-128 in HFD fed mice positively induces the expression of PGC1α, NRF2, and TFAM in the skeletal muscle, although the observed changes were not statistically significant (Supplementary Fig. 1).

HFD promotes skeletal muscle atrophy by inducing oxidative stress, which leads to mitochondrial dysfunction in metabolic disorders such as type II diabetes (Mohamed et al., 2014). The observed increase in PGC1α mediated NRF2 expression in HFD fed mice due to antimiR-128 treatment can promote the expression of antioxidant genes (Cheng et al., 2013). These results suggest that HFD induced impairment in mitochondrial biogenesis and dysfunction of skeletal muscle can be reversed by silencing endogenous miR-128 levels, although further studies in this area are warranted.

In conclusion, we found that miR-128 directly targets PGC1α and NDUFS4, which is a key regulator of mitochondrial biogenesis and function. In parallel response, a reduced expression of the nuclear-encoded NRF1 and NRF2 has been observed. Endogenous miR-128 is shown to regulate the balance between mitochondrial dynamics (morphology, quantity, and size) by upregulating fission (increased DRP1 expression) and downregulating fusion (decreased MFN1, MFN2, and OPA1 expression) of mitochondria. Further, miR-128 is shown to reduce the transcription and translation of mitochondrial DNA (decreased expression of TFAM). Upregulation of mitochondrial biogenesis and dynamics have great implications in maintaining a healthy mitochondrial pool that can be crucial in preventing age-related muscle loss (Hood et al., 2019). Fig. 8 shows the proposed mechanism of action of miR-128 inhibition in C2C12 myoblasts. AntimiR-128 based drugs may have potential therapeutic implications in reversing mitochondrial biogenesis and function.

Funding

This study was funded under the budget project "In vivo studies on the mechanism of action of miRNA-128" (GAP000110), and the grant number BT/PR16472/BlD/7/629/2016, by the Department of Biotechnology, New Delhi, India.

Declaration of Competing Interest

The authors declare that they have no known competing financial interests or personal relationships that could have appeared to influence the work reported in this paper.

Acknowledgment

The authors are thankful to Dr. Naveen Bhatraju for helping with the measurement of OCR and image quantification. Kritika Sharma is grateful to the Indian Council of Medical Research, Ansari Nagar, New Delhi 110029, India, for the ICMR-SRF fellowship.

Data availability

The data that support the findings of this study are available from the corresponding author upon reasonable request.

Appendix A. Supplementary data

Supplementary data to this article can be found online at https://doi.org/10.1016/j.mito.2021.08.008.

References

Anderson, A.J., Jackson, T.D., Stroud, D.A., Stojanovski, D., 2019. Mitochondria-hubs for regulating cellular biochemistry: emerging concepts and networks. Open Biol. 9 (8), 190126. https://doi.org/10.1098/rsob.190126.

Mohamed, J.S., Hajira, A., Pardo, P.S., Boriek, A.M., 2014. MicroRNA-149 inhibits PARP-2 and promotes mitochondrial biogenesis via SIRT-1/PGC-1α network in skeletal muscle. Diabetes 63 (5), 1546–1559.

Handschin, C., Spiegelman, B.M., 2006. Peroxisome proliferator-activated receptor gamma coactivator 1 coactivators, energy homeostasis, and metabolism. Endocr. Rev. 27 (7), 728–735.

Kelly, D.P., Scarpulla, R.C., 2004. Transcriptional regulatory circuits controlling mitochondrial biogenesis and function. Genes Dev. 18 (4), 357–368.

Scarpulla, R.C., 2008. Nuclear control of respiratory chain expression by nuclear Respiratory factors and PGC-1-related coactivator. Ann. N. Y. Acad. Sci. 1147, 321–334.

Taherzadeh-Fard, E., Saft, C., Akkad, D.A., Wieczorek, S., Haghikia, A., Chan, A., Epplen, J.T., Arning, L., 2011. PGC-1alpha downstream transcription factors NRF-1 and TFAM are genetic modifiers of Huntington disease. Mol. Neurodegener. 6 (1).

Cannavino, J., Brocca, L., Sandri, M., Grassi, B., Bottinelli, R., Pellegrino, M.A., 2015. The role of alterations in mitochondrial dynamics and PGC-1α over-expression in fast muscle atrophy following hindlimb unloading. J. Physiol. 593, 1981–1995.

Picard, M., Wallace, D.C., Burelle, Y., 2016. The rise of mitochondria in medicine. Mitochondrion 30, 105–116.

Lemecha, M., Morino, K., Imamura, T., Iwasaki, H., Ohashi, N., Ida, S., Sato, D., Sekine, O., Ugi, S., Maegawa, H., 2018. MiR-494-3p regulates mitochondrial biogenesis and thermogenesis through PGC1-α signalling in beige adipocytes. Sci. Rep. 8 (1), 15096.

Nie, Y., Sato, Y., Wang, C., Yue, F., Kuang, S., Gavin, T.P., 2016. Impaired exercise tolerance, mitochondrial biogenesis, and muscle fiber maintenance in miR-133a-deficient mice. FASEB J. 30 (11), 3745–3758.

Adlakha, Y.K., Saini, N., 2011. MicroRNA-128 downregulates Bax and induces apoptosis in human embryonic kidney cells. Cell. Mol. Life Sci. 68 (8), 1415–1428.

Adlakha, Y.K., Khanna, S., Singh, R., Singh, V.P., Agrawal, A., Saini, N., 2013. Pro-apoptotic miRNA-128-2 modulates ABCA1, ABCG1 and RXRα expression and cholesterol homeostasis. Cell Death Dis. 4 (8).

Pfaffl, M.W., 2001. A new mathematical model for relative quantification in real-time RT- PCR. Nucleic Acids Res. 29 (9), e45.

Iannetti, E.F., Smeitink, J.A.M., Beyrath, J., Willems, P.H.G.M., Koopman, W.J.H., 2016. Multiplexed high- content analysis of mitochondrial morphofunction using live-cell microscopy. Nat. Protoc. 11 (9), 1693–1710.

Agarwal, V., Bell, G.W., Nam, J.W., Bartel, D.P., 2015. Predicting effective microRNA target sites in mammalian mRNAs. Elife 4.

Kazeminasab, F., Marandi, S.M., Ghaedi, K., Safaeinejad, Z., Esfarjani, F., Nasr-Esfahani, M.H., 2018. A comparative study on the effects of high-fat diet and

endurance training on the PGC-1α-FNDC5/irisin pathway in obese and nonobese male C57BL/6 mice. Appl. Physiol. Nutr. Metab. 43 (7), 651–662.
Latouche, C., Natoli, A., Reddy-Luthmoodoo, M., Heywood, S.E., Armitage, J.A., Kingwell, B.A., Philp, A., 2016. MicroRNA-194 modulates glucose metabolism and its skeletal muscle expression is reduced in diabetes. PLoS ONE 11.
Chandra, A., Sharma, K., Pratap, K., Singh, V., Saini, N., 2021. Inhibition of microRNA-128-3p attenuates hypercholesterolemia in mouse model. Life Sci. 264, 118633. https://doi.org/10.1016/j.lfs.2020.118633.
Tang, B.L., 2016. Sirt1 and the mitochondria. Mol. Cells 39 (2), 87–95.
Li, P., Jiao, J., Gao, G., Prabhakar, B.S., 2012. Control of mitochondrial activity by miRNAs. J. Cell. Biochem. 113 (4), 1104–1110.
Chen, C.-Y., Lee, D.S., Choong, O.K., Chang, S.-K., Hsu, T., Nicholson, M.W., Liu, L.-W., Lin, P.-J., Ruan, S.-C., Lin, S.-W., Hu, C.-Y., Hsieh, P.C.H., 2021. Cardiac-specific microRNA-125b deficiency induces perinatal death and cardiac hypertrophy. Sci. Rep. 11, 2377.
Medala, V.K., Gollapelli, B., Dewanjee, S., Ogunmokun, G., Kandimalla, R., Vallamkondu, J., 2021. Mitochondrial dysfunction, mitophagy, and role of dynamin-related protein 1 in Alzheimer's disease. J. Neurosci. Res. 99 (4), 1120–1135.
Motohashi, N., Alexander, M.S., Shimizu-Motohashi, Y., Myers, J.A., Kawahara, G., Kunkel, L.M., 2013 Jun 15. Regulation of IRS1/Akt insulin signaling by microRNA-128a during myogenesis. J. Cell Sci. 126 (Pt 12), 2678–2691.
Ryten, M., Dunn, P.M., Neary, J.T., Burnstock, G., 2002. ATP regulates the differentiation of mammalian skeletal muscle by activation of a P2X5 receptor on satellite cells. J. Cell Biol. 158 (2), 345–355.
Shi, L., Zhou, B.o., Li, P., Schinckel, A.P., Liang, T., Wang, H., Li, H., Fu, L., Chu, Q., Huang, R., 2015. MicroRNA-128 targets myostatin at coding domain sequence to regulate myoblasts in skeletal muscle development. Cell. Signal. 27 (9), 1895–1904.
LeBleu, V.S., O'Connell, J.T., Gonzalez Herrera, K.N., et al. PGC-1α mediates mitochondrial biogenesis and oxidative phosphorylation in cancer cells to promote metastasis [published correction appears in Nat Cell Biol. 2014 Nov;16(11):1125]. Nat Cell Biol. 2014;16(10):992–1015.
Wang, T., Zhai, M., Xu, S., Ponnusamy, M., Huang, Y., Liu, C.-Y., Wang, M., Shan, C., Shan, P.-P., Gao, X.-Q., Wang, K., Chen, X.-Z., Liu, J., Xie, J.-Y., Zhang, D.-Y., Zhou, L.-y., Wang, K., 2020. NFATc3-dependent expression of miR-153-3p promotes mitochondrial fragmentation in cardiac hypertrophy by impairing mitofusin-1 expression. Theranostics 10 (2), 553–566.
Li, J., Donath, S., Li, Y., Qin, D., Prabhakar, B.S., Li, P., 2010. miR-30 regulates mitochondrial fission through targeting p53 and the dynamin-related protein-1 pathway. PLoS Genet. 6.
Woo, H.-N., Park, S., Kim, H.L., Jung, M.-K., Pack, C.-G., Park, J., Cho, Y., Jo, D.-G., Kim, D.K., Mook-Jung, I., Kim, S.W., Lee, H., 2021. miR-351-5p/Miro2 axis contributes to hippocampal neural progenitor cell death via unbalanced mitochondrial fission. Mol. Ther. – Nucleic Acids 23, 643–656.
Roe, A.J., Qi, X., 2018. Drp1 phosphorylation by MAPK1 causes mitochondrial dysfunction in cell culture model of Huntington's disease. Biochem. Biophys. Res. Commun. 496 (2), 706–711.
Johnson, S.C., Yanos, M.E., Kayser, E.-B., Quintana, A., Sangesland, M., Castanza, A., Uhde, L., Hui, J., Wall, V.Z., Gagnidze, A., Oh, K., Wasko, B.M., Ramos, F.J., Palmiter, R.D., Rabinovitch, P.S., Morgan, P.G., Sedensky, M.M., Kaeberlein, M., 2013. mTOR inhibition alleviates mitochondrial disease in a mouse model of Leigh syndrome. Science 342 (6165), 1524–1528.
Melcher, M., Danhauser, K., Seibt, A., Degistirici, Ö., Baertling, F., Kondadi, A.K., Reichert, A.S., Koopman, W.J.H., Willems, P.H.G.M., Rodenburg, R.J., Mayatepek, E., Meisel, R., Distelmaier, F., 2017. Modulation of oxidative phosphorylation and redox homeostasis in mitochondrial NDUFS4 deficiency via mesenchymal stem cells. Stem Cell Res. Ther. 8.
Barroso, W.A., Victorino, V.J., Jeremias, I.C., Petroni, R.C., Ariga, S.K.K., Salles, T.A., Barbeiro, D.F., de Lima, T.M., de Souza, H.P., 2018. High-fat diet inhibits PGC-1α suppressive effect on NFκB signaling in hepatocytes. Eur. J. Nutr. 57, 1891–1900.
Aoi, W., Naito, Y., Mizushima, K., Takanami, Y., Kawai, Y., Ichikawa, H., Yoshikawa, T., 2010. The microRNA miR-696 regulates PGC-1α in mouse skeletal muscle in response to physical activity. Am. J. Physiol. – Endocrinol. Metab. 298 (4), E799–E806.
Cheng, X., Ku, C.-H., Siow, R.C.M., 2013. Regulation of the Nrf2 antioxidant pathway by microRNAs: New players in micromanaging redox homeostasis. Free Radic. Biol. Med. 64, 4–11.
Hood, D.A., Memme, J.M., Oliveira, A.N., Triolo, M., 2019. Maintenance of skeletal muscle mitochondria in health, exercise, and aging. Annu. Rev. Physiol. 81 (1), 19–41.

Mitochondrion 74 (2024) 101821

Contents lists available at ScienceDirect

Mitochondrion

journal homepage: www.elsevier.com/locate/mito

Identifying the mitochondrial metabolism network by integration of machine learning and explainable artificial intelligence in skeletal muscle in type 2 diabetes

Kritika Sharma [a,b], Neeru Saini [a,c], Yasha Hasija [b,*]

[a] CSIR-Institute of Genomics and Integrative Biology, Mall Road, New Delhi 110007, India
[b] Department of Biotechnology, Delhi Technological University, Delhi 110042, India
[c] Academy of Scientific & Innovative Research (AcSIR), Ghaziabad 201002, India

ARTICLE INFO

Keywords:
Explanable Artificial Intelligence
SHAP
XGBoost
Type 2 Diabetes
miRNA

ABSTRACT

Imbalance in glucose metabolism and insulin resistance are two primary features of type 2 diabetes/diabetes mellitus. Its etiology is linked to mitochondrial dysfunction in skeletal muscle tissue. The mitochondria are vital organelles involved in ATP synthesis and metabolism. The underlying biological pathways leading to mitochondrial dysfunction in type 2 diabetes can help us understand the pathophysiology of the disease. In this study, the mitochondrial gene expression dataset were retrieved from the GSE22309, GSE25462, and GSE18732 using Mitocarta 3.0, focusing specifically on genes that are associated with mitochondrial function in type 2 disease. Feature selection on the expression dataset of skeletal muscle tissue from 107 control patients and 70 type 2 diabetes patients using the XGBoost algorithm having the highest accuracy. For interpretation and analysis of results linked to the disease by examining the feature importance deduced from the model was done using SHAP (SHapley Additive exPlanations). Next, to comprehend the biological connections, study of protein-protien and mRNA-miRNA networks was conducted using String and Mienturnet respectively. The analysis revealed BDH1, YARS2, AKAP10, RARS2, MRPS31, were potential mitochondrial target genes among the other twenty genes. These genes are mainly involved in the transport and organization of mitochondria, regulation of its membrane potential, and intrinsic apoptotic signaling etc. mRNA-miRNA interaction network revealed a significant role of miR-375; miR-30a-5p; miR-16-5p; miR-129-5p; miR-1229-3p; and miR-1224-3p; in the regulation of mitochondrial function exhibited strong associations with type 2 diabetes. These results might aid in the creation of novel targets for therapy and type 2 diabetes biomarkers.

1. Introduction

Type 2 diabetes is described as a chronic metabolic disorder by world health organization (WHO) marked with high levels of blood glucose that, over time, causes substantial harm to several organs of the body such as pancreas, heart, eyes, blood vessels, kidneys, skeletal muscle (Stumvoll et al., 2005). Obesity, physical inactivity, improper nutrition, and genetic predisposition are all strongly linked to type 2 diabetes. An estimation done in 2019 by the international diabetes federation (IDF) states ~ 470 million individuals were predicted to have this disorder. This figure is expected to increase to 700 million approximately by the year 2045, highlighting the urgent need for preventative measures and efficient management techniques (Glovaci et al., 2019). In healthy people, the largest metabolic organ, and the primary site for the absorption of glucose is skeletal muscle. Therefore, skeletal muscle health is crucial for maintaining the body's homeostasis of glucose. Insulin stimulated absorption and uptake of glucose is associated with insulin signaling in the skeletal muscle are considerably hampered in insulin-resistant conditions (Abdul-Ghani et al., 2006). Skeletal muscle mass is lost due to an imbalance between the protein production rate and its degradation rate. Muscle loss and inactivity combined with catabolic conditions can lower quality of life, limit the ability to do everyday tasks, and ultimately increase mortality. Degradation of proteins in a cell is caused by several pathways like proteasome via ubiquitin, autophagy, and caspases mediated proteolytic pathway, which contribute to the wasting of muscles (Lecker et al., 2006). To control insulin signaling in

* Corresponding author at: Department of Biotechnology, Delhi Technological University, Delhi 110042, India.
E-mail address: yashahasija@dtu.ac.in (Y. Hasija).

https://doi.org/10.1016/j.mito.2023.11.004
Received 26 June 2023; Received in revised form 4 October 2023; Accepted 26 November 2023
Available online 29 November 2023

skeletal muscle cells, mitochondria play an essential role. First, the translocation of glucose by GLUT4 is done by supplying ATP and other metabolic intermediates to the plasma membrane where mitochondria supports the insulin stimulated uptake of glucose (Yap et al., 2020). In type 2 diabetes, impaired glucose absorption and utilization can be caused by impaired mitochondrial function, which can result in decreased ATP generation. Second, secondary messengers produced in the form of reactive oxygen species (ROS) and nitric oxide (NO) by mitochondria contribute to the facilitation of insulin-mediated absorption of glucose. Additionally, Diacylglycerols (DAGs) and ceramides accumulate as a result of the decreased ability of mitochondria to oxidize fatty acids under type 2 diabetic conditions. Alterations in mitochondrial dynamics, such as fission and fusion events, can result from mitochondrial dysfunction in skeletal muscle (Leenders et al., 2013; Cea et al., 2023).

Increasing literature evidence points towards the involvement of non-coding microRNAs, in regulating the process of protein anabolism as well as catabolism pathways in skeletal muscle by targeting the regions either in the 3′ UTR; 5′ UTR; or CDS of the mRNA (Kotagama and McJunkin, 2024). Dysregulated miRNA expression can be a factor in the mitochondrial dysfunction seen in the skeletal muscle of patients with type 2 diabetes. Numerous miRNAs have been found to be important regulators of protein involved in oxidative stress and mitochondrial activity in skeletal muscle (Zhu et al., 2023). The molecular mechanisms underlying the disease can be better understood by understanding the crosstalk between miRNA and genes responsible for mitochondrial biogenesis and function in the skeletal muscle. Clinical research and patient care have been completely transformed by high-throughput gene expression data. The identification of underlying mechanisms involved in cancer, metabolic disorders like obesity and diabetes, or in drug development is done by analyzing the gene expression to examine the associated biological functions. With the development of new technologies like RNA-seq and transcriptome arrays provided by various platforms for example agilent and affymetrix, analysts now have a wide range of options for studying distinct gene expression (Painter et al., 2013). However, it has been difficult to analyze humongous amounts of data. Also, according to Vescovo et al., varied platforms and methodologies can produce varied outcomes (Del Vescovo et al., 2013). A branch of computer science known as machine learning (ML) uses data-driven techniques to identify patterns and anticipate behaviors (Nelson et al., 2020). The identification of hidden patterns in type 2 diabetes risk variables are possible use for prediction on the basis of machine learning algorithm (Moon et al., 2021). For the prediction of underlying biological processes or biomarkers, a variety of ML models have been used, including logistic regression, random forests, artificial neural networks, k-nearest neighbors, support vector, decision trees, and extreme gradient boosting (XGBoost) (Hong et al., 2020). A common method used for determining the gene expression and whether the regulation is connected to that particular disease is differential expression analysis. It identifies quantifiable shifts in expression levels of the experimental group compared to the control group using a statistical method but in disciplines including data analysis of omics and sequencing where they have demonstrated exceptional execution, deep machine learning have seen a rise in popularity in recent years (Hong et al., 2020).

This paper proposes the use of application of machine learning interpretation method “Shapley additive explanation” with more comprehensiveness and explicability to highlight the importance features in gene expression data related to type 2 diabetes. The majority of machine learning models produce outstanding results in regards of its accuracy and prediction power without any explanations that how they reached to the prediction generally known as “Black box” of the model, and now these models are more interpretable and can be explained with the use of XAI (eXpainable Artificial Intelligence) (Anguita-Ruiz et al., 2020). A few of the XAI frameworks that try to access this decision making of the ML which is a black box and explain their working are Local Interpretable Model-agnostic Explanation also known as LIME, SHAP, AIX360, Skaters, and ELI5. SHAP and LIME are the most used and consistent with any machine learning model. Early detection of patients with high-risk of type 2 diabetes, disease prevention, and risk stratification is essential. In the current study, we are focusing on the skeletal muscle tissue specifically targeting the genes responsible for mitochondrial homeostasis by applying XGBoost algorithm to train the ML model in type 2 diabetes. These models can process a large amount of data and can predict new patterns compared to techniques used previously. In Addition, the mRNA-miRNA interaction network analysis is done to identify the non-coding biomarkers. These complex gene regulation networks implicated in type 2 diabetes can also be fully understood by deciphering the protein–protein interactions linked to these genes, opening new research directions and possibly paving the way for new therapeutic strategies.

2. Material and methods

2.1. Data retrieval and processing

Publicly available studies exploring mRNA expression profiles of the human skeletal muscle tissue suffering from type 2 diabetes were identified from the GEO database, NCBI (Barrett et al., 2013). Excluding any treatments or other conditions, a large sample size served as a guide for choosing the gene expression datasets. To include a significant number of datapoints in the analysis including both control and type 2 diabetes patient samples, preference was given to these top three expression profile GSE IDs in Table 1. For the conditions, we were able to extract pre-processed data with accession IDs GSE22309 (20 control patients and 15 type 2 diabetes patients) (Wu et al., 2007); GSE25462 (40 control patients and 10 type 2 diabetes patients) (Jin et al., 2011), and GSE18732 (47 control patients and 45 type 2 diabetes patients) (Gallagher et al., 2010). We have performed log 2 transformation and quantile normalization after combining these three datasets. The samples in the dataset were classified as control samples (107) and type 2 diabetic samples (70). Common genes (5762 genes) across the three datasets were identified. MitoCarta3.0 focuses on proteins involved in mitochondrial homeostasis and this database contains 1136 human genes. This list of genes was retrieved from MitoCarta3.0 (http://www.broadinstitute.org/mitocarta) (Rath et al., 2021). Using the Venny 2.1.0 tool, common mitochondrial genes were identified between the datasets with all samples and MitoCarta3.0 (Fig. 1).

2.2. ML model and testing

A ML model train to unravel similar patterns in a dataset using different algorithm, and this supervised model is then used to predict features in a new dataset (Cordova et al., 2023). XGBoost, because of its scalability, is leading the Kaggle competition for structured data and applied machine learning. The performance and speed of gradient-boosted decision trees (GBM) is increased and were extended using XGBoost. It has consistently performed better than most other ML techniques since its introduction, surpassing traditional decision trees (boosting) and other models (Meena and Hasija, 2022; Kumar and Das, 2023). Samples were divided into two different sets, that is training and testing sets randomly in an 80:20 percent ratio. The training set comprising of 80 % random expression data was used to train the XGBoost model. The Scikit-learn library was used to build the model (Pedregosa et al., 2012). The performance of the model was assessed using the remaining data as a test set. This test set was used to assess the model’s accuracy and the confusion matrix was evaluated.

2.3. Interpreting the ML model using XAI

In contrast, with ML models it is difficult to understand the steps directing the decision process of the model. It is generally a “black box,” where even the analysts are unable to explain how an artificial

Table 1
Details of the studies taken from the GEO database.

GEO ID	Disease	Organism	Tissue	Platform	Experimental Design	Data Preprocessing
GSE22309	Type 2 Diabetes	*Homo sapiens*	Skeletal Muscle	Affymetrix Human Genome U95A Array	20 control patients and 15 type 2 diabetes patients	Quantile normalization and RMA or MAS5.0 (Microarray Suite version 5.0) implemented.
GSE25462	Type 2 Diabetes	*Homo sapiens*	Skeletal Muscle	Affymetrix Human Genome U133 Plus 2.0 Array	40 control patients and 10 type 2 diabetes patients	MAS5.0 algorithm was implemented
GSE18732	Type 2 Diabetes	*Homo sapiens*	Skeletal Muscle	Affymetrix GeneChip Human Genome U133 Plus 2.0 Array	47 control patients and 45 type 2 diabetes patients	Normalized using RMA and MAS 5.0

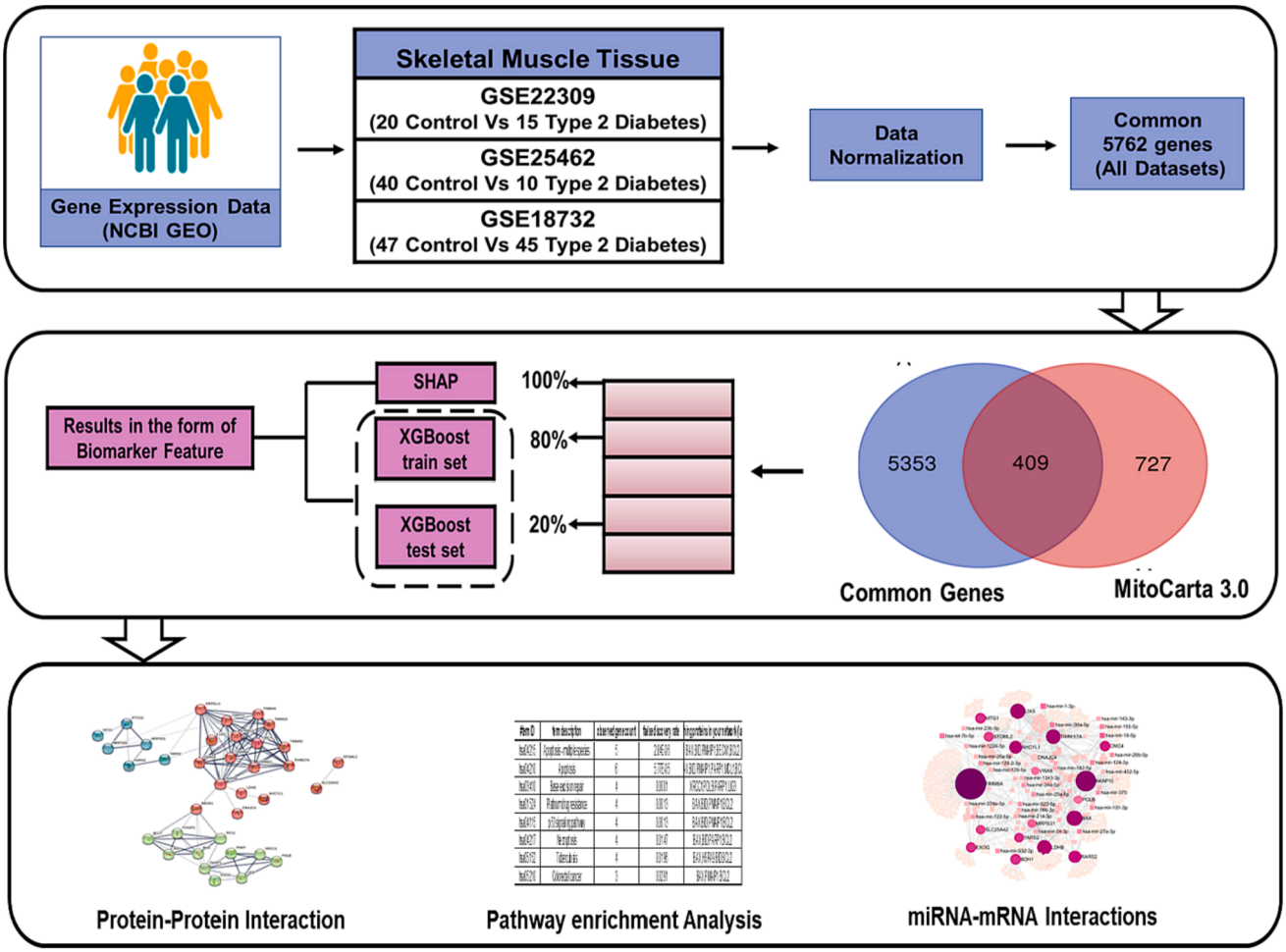

Fig. 1. Schematics representing the proposed method of training data combined with explainable AI. GSE22309, GSE25462, and GSE18732 expression data were retrieved from NCBI GEO database. Samples were classified as Control and Type 2 Diabetes. Common genes (5762) shared by the three datasets were determined. 409 overlapping genes from the input list of 1136 mitochondrial genes from the Mitocarta 3.0 database and a list of common genes from the three datasets were identified using venny tool. Model training was done using XGboost algorithm and results are interpreted by SHapley Additive exPlanations. Further, functional characterization of involvement of the genes is done by protein-protien interaction, pathway enrichment analysis, and miRNA-mRNA network analysis.

intelligence came to a particular choice. XAI is a way to put social right to the explanation into practice (Savage, 2022). Here, the classifiers were able to generate both a global and personal interpretation of the anticipated outcome thanks to the SHAP approach, which was developed from cooperative game theory (Model development and validation) (Li et al., 2021). The Python SHAP library was used to conduct the XAI analysis on the trained XGBoost model. We determined the top 20 genes with high SHAP values as features. We then cross-validated and assessed the performance of these genes on the newly trained model and compared them to the performance of the previous training set. Additionally, we also examined the expression of each gene based on the combined expression data of control and patient samples and an unpaired *t*-test was applied using GraphPad Prism Software (v.5.01 GraphPad, Inc., CA, USA). A cutoff of p value < 0.05, which was used to determine whether genes were statistically significant.

2.4. Protein-protein network analysis

Protein interaction network by giving an input list of the top 20 genes obtained by SHAP values to identify the role and interaction network of the proteins involved in mitochondrial homeostasis was done using String version 11.5 (https://string-db.org/) (Szklarczyk et al., 2021). Medium confidence of 0.4 was selected for the interaction score and a significance of $p < 0.05$. The k-means clustering was applied to the network for identifying the genes in similar complexes with significant biological functionality.

2.5. Pathway enrichment analysis

Pathway enrichment analysis for the top genes was performed using the GO ontology database and KEGG database. The genes were mapped against *Homo Sapiens* as reference species and the analysis encompassed the following domain: biological process; cellular component; and molecular function. Significant pathways were taken into consideration by applying a limit of p value < 0.05.

2.6. mRNA-miRNA interaction network analysis

miRNet is a miRNA-centric network visualization and analytical software to gather functional insights. The potential mRNA-miRNA network was predicted by using miRNet 2.0 (https://www.mirnet.ca/) (Chang and Xia, 2023). The size of the shapes depicts the number of interactions based on degree and betweenness. Significant miRNAs with maximum target features and mRNA-miRNA interaction based on strong evidence were identified using the MIENTURNET platform (http://userver.bio.uniroma1.it/apps/mienturnet/) (Licursi et al., 2019). For statistical significance, a cut-off of p value < 0.05 was used. The mRNA-miRNA network based on strong evidence was imported into Cytoscape 3.8.0 software for visualization of the network (Shannon et al., 2003).

3. Results

3.1. Identification of genes responsible for mitochondrial function expressed in the skeletal muscle tissue of control and type 2 diabetic patients

In total, thirty-six datasets were retrieved from the NCBI GEO by giving the input keywords 'Diabetes + Skeletal Muscle', Three different microarray datasets were identified based on that the dataset consists of clinical samples of skeletal muscle tissue from human patients. Preprocessed series matrix files of GSE22309, GSE25462, and GSE18732 were retrieved, and the sample profiles from all three datasets were then integrated to create a single dataset. Samples were classified as Control and Type 2 Diabetes. Compared to the U133 Plus platform, the U95A platform covers a far fewer number of genes. Due to the variations in transcript coverage between the U133 Plus and U95A platforms, we've restricted our focus to the shared transcripts only. We ensured a fair comparison of gene expression patterns across all datasets by concentrating on the subset of genes that are covered by both platforms. All three datasets had 5762 common genes. We used data harmonization approaches that included normalization and batch effect correction procedures to promote more seamless integration of the datasets to reduce potential biases resulting from the use of two different platforms or experimental variation. Log2 transformation and Quantile normalization were performed on this single file to normalize the expression data. Fig. 2A and 2B show the preprocessed data received and data after normalization. Next, the genes expressed for healthy mitochondrial function were retrieved by giving an input list of common genes from three datasets and 1136 genes from Mitocarta 3.0 database into the Venny 2.1.0 tool. We found 409 genes responsible for mitochondrial function were expressed in the skeletal muscle as depicted in the heat map of Fig. 2C of control and type 2 diabetic patients.

3.2. Training of the machine learning model using XGboost algorithm

The gene expression studies from the skeletal muscle tissue of control patients to that of type 2 diabetic patients to predict the genes altered to understand the mitochondrial pathophysiology of the disease using XGboost machine learning algorithms was the main goal of this study.

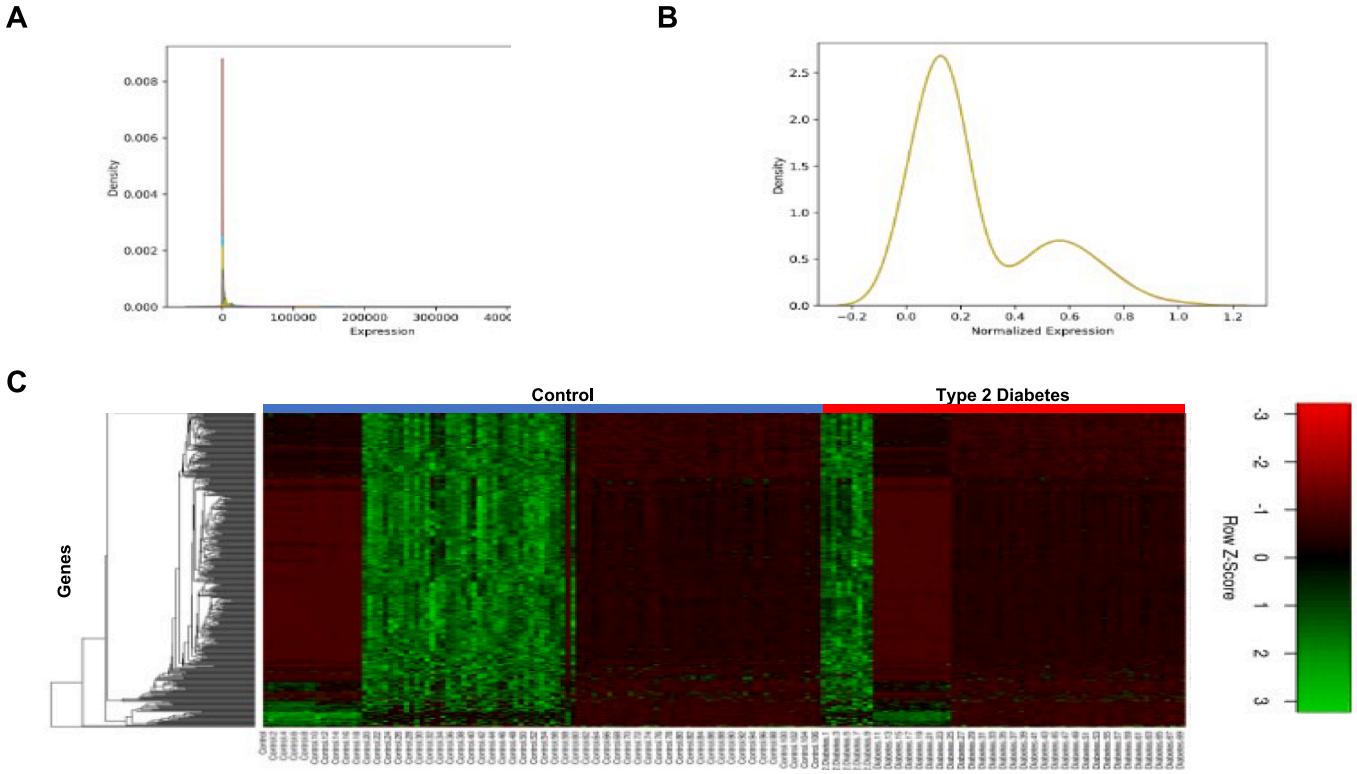

Fig. 2. (A) Expression data before normalization was performed, (B) Expression data after Log2 transformation and Quantile normalization was performed, and (C) Heatmap of the mitochondrial genes identified after normalization from a single combined dataset (All three GEO expression profile) based on the Z-score scaling. The genes with Z-score < 0 have lower expression (Red) and genes with $Z > 0$ have higher expression (Green). It was derived from all the samples (control patients as well as patients suffering from type 2 diabetes). Genes without any significant expression are black with a Z-score of 0. (For interpretation of the references to color in this figure legend, the reader is referred to the web version of this article.)

The sample profiles containing the expression data of 409 mitochondrial genes were randomly divided into a ratio of 80:20. To train the model, the training set was given 80 % of data and the remaining comprises the test set that is of 20 %. Herein, the training set was used to train the model through the implementation of the Scikit-learn library. The model was then assessed by using the remaining data which is the test set. The confusion matrix in Fig. 3A was used to assess the test set and calculate the precision and accuracy of the machine learning model. The confusion matrix constructed by the contingency table contains four separate sets of actual and anticipated values. The matrix's grey squares depict the proportion of true positives represented as TP, black squares depict the proportion of false negatives and false positives represented as FN and FP respectively, whereas white squares depict the proportion of true negatives represent as TN. Precision is equal to the number of TP divided by the total of TP and FP. The accuracy is calculated is done by dividing the total of TP and TN to the total of TP, TN, FP, and FN. The Precision is 77.7 % and the Accuracy is 80.55 % for our combined dataset of skeletal muscle tissue of control vs type 2 diabetic patients.

3.3. Prediction of the mitochondrial genes using explainable AI

SHAP package in Python helps in identifying characteristics that have a significant impact on the confidence score of model's prediction. This analysis is based on a decision-making machine learning model. Thus, we next identified the genes with a significant impact on mitochondrial health in skeletal muscle tissue in type 2 diabetes. The global feature plot is an average of the SHAP values per feature by gene of importance in decreasing order and is represented as a bar plot in Fig. 4A. First, 3-Hydroxybutyrate Dehydrogenase 1 (BDH1) is required for optimal enzymatic activity, to form a homotetrameric lipid of the mitochondrial membrane enzyme regulating ketosis, worsens the heart condition in db/db mice (Thai et al., 2021). Second, tyrosyl-tRNA synthetase 2 (YARS2) catalyzes tyrosine attachment to tRNA (Tyr) in mitochondria. In vivo, studies show that ablation of YARS2 is known to destabilize the ETC complexes and their activity in the oxidative phosphorylation process in type 2 diabetic skeletal muscle (López-Soldado et al., 2023). A-kinase anchoring proteins (AKAPs) are scaffold proteins that bind to the PKA subunits and other signaling enzymes in close proximity to their target substrates. They are significantly responsible for controlling the intracellular distribution and substrate selectivity of PKA (Ando et al., 2018). Mitochondrial aminoacyl-tRNA synthetases is known to decrease in type 2 diabetic muscle by downregulating the OXPHOS subunits whereas RARS2 is not much explored (López-Soldado et al., 2023). The ribosomal protein Imogen 38, is a potential target for autoimmune assault in type 1 diabetes, is found to be encoded by MRPS31 (Arden et al., 1996). Literature evidence is present for the association of MRPS31 with type 2 diabetes but is based on bioinformatics/computational analysis (Savas et al., 2011). In white adipose tissue (WAT), decrease of EXOG is correlated with an increase in the expression of uncoupling protein-1 (UCP1) and peroxisome proliferator-activated receptor-coactivator-1 alpha (PGC1α), which corresponds with the emergence of brown adipocyte-like cells scattered throughout white adipocytes and also, linked to improved glucose tolerance and decreased fat mass (Pardo et al., 2016).

Aged rats with diabetes and adipose tissue from obese and T2D patients, have decreased expression of HSP40/DNAJ, a small class of heat shock protein (Gupte et al., 2008; Abu-Farha et al., 2015; Abubaker et al., 2013). UCP3 is known to mediate energy consumption by uncoupling, particularly in metabolism of fatty acids, and try to rescue the mitochondria from oxidative stress carried on by lipids. Patients with type 2 diabetes and prediabetic people both have lower levels of UCP3 protein (Schrauwen et al., 2006; Liu et al., 2013). To insert the proper complementary base, DNA polymerase beta (POLB) bridges the gap and forms a complex with DNA ligase 3 (LIG3) and X-ray repair cross-complementing protein 1 (XRCC1). While DNA damage and oxidative stress parameters increase in T2DM, it has been observed that the DNA repair system is downregulated (Grindel et al., 2016). STOML2 is a cristae regulatory protein, generally interacts with NDUFS4 (subunit of Respiratory complex 1). In diabetic kidney tissue, the decreased levels of STOML2 and NDUFS4 leads to inappropriate cristae formation, respiratory super complexes assembly, and decreased mitochondrial respiration and dynamics (Mitsopoulos et al., 2015). LDHB, lactate dehydrogenase is essential for appropriate energy homeostasis as it catalyzes the anaerobic glycolytic process that turns pyruvate into lactate and is downregulated in type 2 diabetic muscle tissue compared to control patients (Palsgaard et al., 2009). TIMM8A is associated with inner membrane translocation to contribute in mitochondrial function and is downregulated in type 2 diabetes (Dubé et al., 2020). Drp1 is co-expressed with pro-apoptotic proteins (like Bax) from the Bcl-2 family members near the fission site where Cyt c is released, a crucial first step in caspase 3 activation that ultimately leads to the induction of apoptosis in diabetes (Wang et al., 2023). The downregulation of SLC25A42 (a Coenzyme A importer) in islets isolated from βV59M diabetic mice, in which glycolysis was reduced and mitochondrial metabolism was significantly impaired, was discovered through extensive transcriptomic and proteomic profiling in conjunction with mitochondrial function analysis (Khin et al., 2023). Relative to age- and sex-matched controls, expression of LIAS (Lipoic acid synthase) is considerably lower in tissues from animal models of diabetes and obesity (Padmalayam et al., 2009). While RARS2, CMC4 (C-X9-C Motif Containing 4), TIMM17A (Translocase of Inner Mitochondrial Membrane 17A), MTG1(Mitochondrial Ribosome Associated GTPase 1), and VWA8 (Von Willebrand Factor A

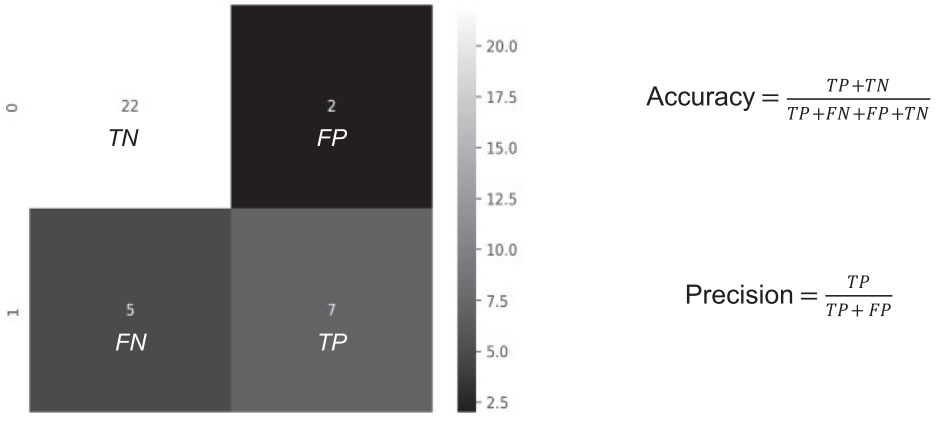

Fig. 3. Confusion matrix from the test set used to assess the ML model. The matrix's grey squares represent the proportion of TP, black squares represent the proportion of FP and FN, and white squares represent the proportion of TN. TP: True Positive; TN: True Negative; FN: False Negative; and FP: False Positive.

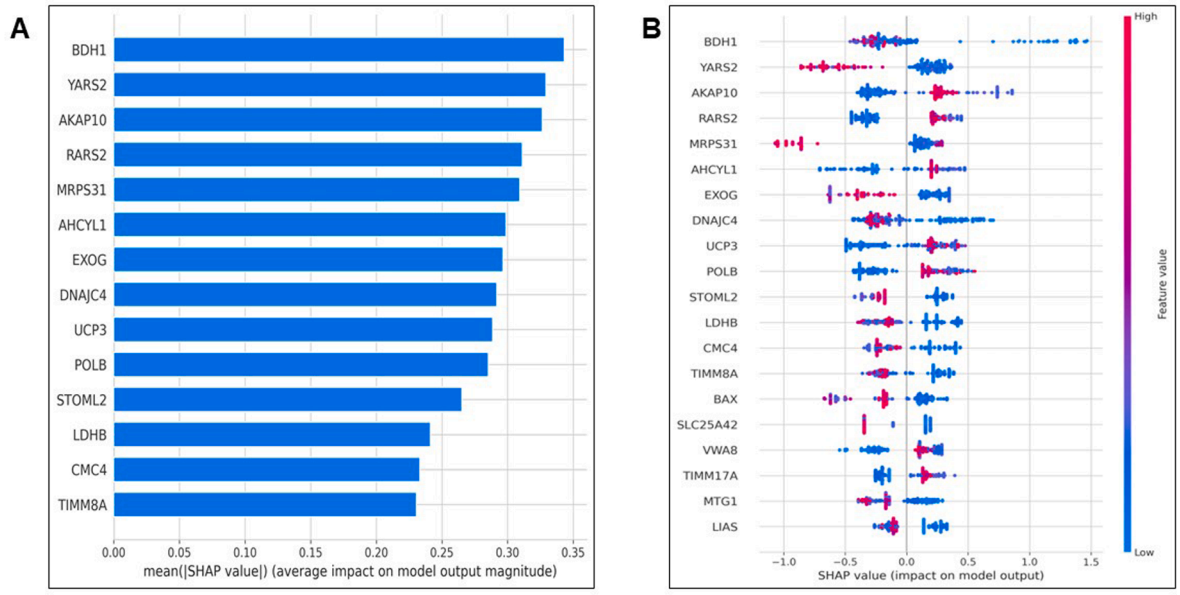

Fig. 4. The SHAP Summary plot depicts the top significant genes and their effects on Type 2 diabetes patients vs Control. (A) The bar plot represents the absolute average impact of the genes. (B) Summary plot representing the SHAP values and impact of the genes. On the y-axis, identified genes are ordered in decreasing order of feature relevance. It is shown on the x-axis whether a gene's expression is linked to higher or lower prediction, illustrating the gene's influence on the output of the model. The color that designates whether an individual gene's impact on an observation is statistically significant is in pink and minimal gene's impact is depicted in blue. (For interpretation of the references to color in this figure legend, the reader is referred to the web version of this article.)

Domain Containing 8) are explored in various disease other than type 2 diabetes and further research in this area is warranted.

Furthermore, we also plotted the SHAP summarization plot to visualize the impact of the feature in relation to the value and target prediction. As shown in Fig. 4B, the SHAP summarization plot depicts the 'BDH1 gene' has a negative impact as shown on the x-axis.

Genes with high importance scores are considered more impactful in the context of the disease, irrespective of whether they are upregulated or downregulated. Based on this feature's importance scores, the top 20 genes that have a significant impact on the disease. These genes could be candidates for further study or as potential therapeutic targets. Additionally, to characterize the significance and importance of the genes that came out as the features, we calculated the overall relative expression and p value as shown in Table 2 from the combined single dataset created after normalization from three GEO expression profiles using GraphPad Prism 8. Surprisingly, we found that all top genes contributing toward mitochondrial homeostasis were significantly downregulated except for UCP3 and BAX as shown in Fig. 5. We did find upregulated genes in the current study, but they were not among the top 20 SHAP values. On the contrary, several genes were upregulated/downregulated in the T2D muscle samples in their respective studies but were not identified while analyzing the combined dataset with the applied model.

Table 2
Results of each identified gene's statistical analysis from the combined dataset.

Control vs Type 2 diabetes		
Genes	**Regulation**	**p-value**
BDH1	Downregulated	0.0001
YARS2	Downregulated	0.0017
AKAP10	Downregulated	0.0082
RARS2	Downregulated	0.0031
MRPS31	Downregulated	0.0002
AHCYL1	Downregulated	0.0306
EXOG	Downregulated	0.0003
DNAJC4	Downregulated	0.0001
UCP3	Downregulated	ns
POLB	Downregulated	0.0120
STOML2	Downregulated	0.0001
LDHB	Downregulated	0.0001
CMC4	Downregulated	0.0008
TIMM8A	Downregulated	0.0003
BAX	Downregulated	ns
SLC25A42	Downregulated	0.0010
VWA8	Downregulated	0.0010
TIMM17A	Downregulated	0.0007
MTG1	Downregulated	0.0007
LIAS	Downregulated	0.0002

3.4. *Gene set analysis and associated pathways of the identified key genes*

The method of functional enrichment analysis is frequently used to recognize similarities within huge biological datasets. Functional enrichment analysis of gene expression data is used in the field of biomedicine to discover the mechanism of the disease. To group regulated gene expression profiles into clear functional categories, numerous techniques have been created. The selection of these functional categories from material found in the literature often reflects signaling or metabolic pathways. String version 11.5 database was used for the protein–protein network of the genes retrieved based on SHAP values to understand their role in the disease. To this network, we applied k-means clustering and the network was divided into three clusters; 23 genes in cluster 1 which is red in color; 11 genes in cluster 2 which is green in color; and 6 genes in cluster 3 which is blue in color as depicted in Fig. 6. Furthermore, analysis of this network suggested that the maximum number of genes are involved significantly in biological processes like mitochondrial protein transport (import/export), membrane organization, maintaining mitochondrial membrane potential, the release of apoptosis signaling factors, and base-excision repair, DNA ligation as shown in Table 3. Nuclear genes in these pathways regulates several nuclear and mitochondrial import, export, and assembly pathways resulting in multimeric proteins requirement for the mitochondrial biogenesis (Jornayvaz and Shulman, 2010). Impaired glucose metabolism and mitochondrial dysfunction can cause membrane potential to collapse, which has an impact on ATP synthesis and might be a factor in insulin resistance (Montgomery and Turner, 2015). The key participants in apoptosis (programmed cell death) are mitochondria. The loss of pancreatic beta cells in T2D may be related to dysregulation of

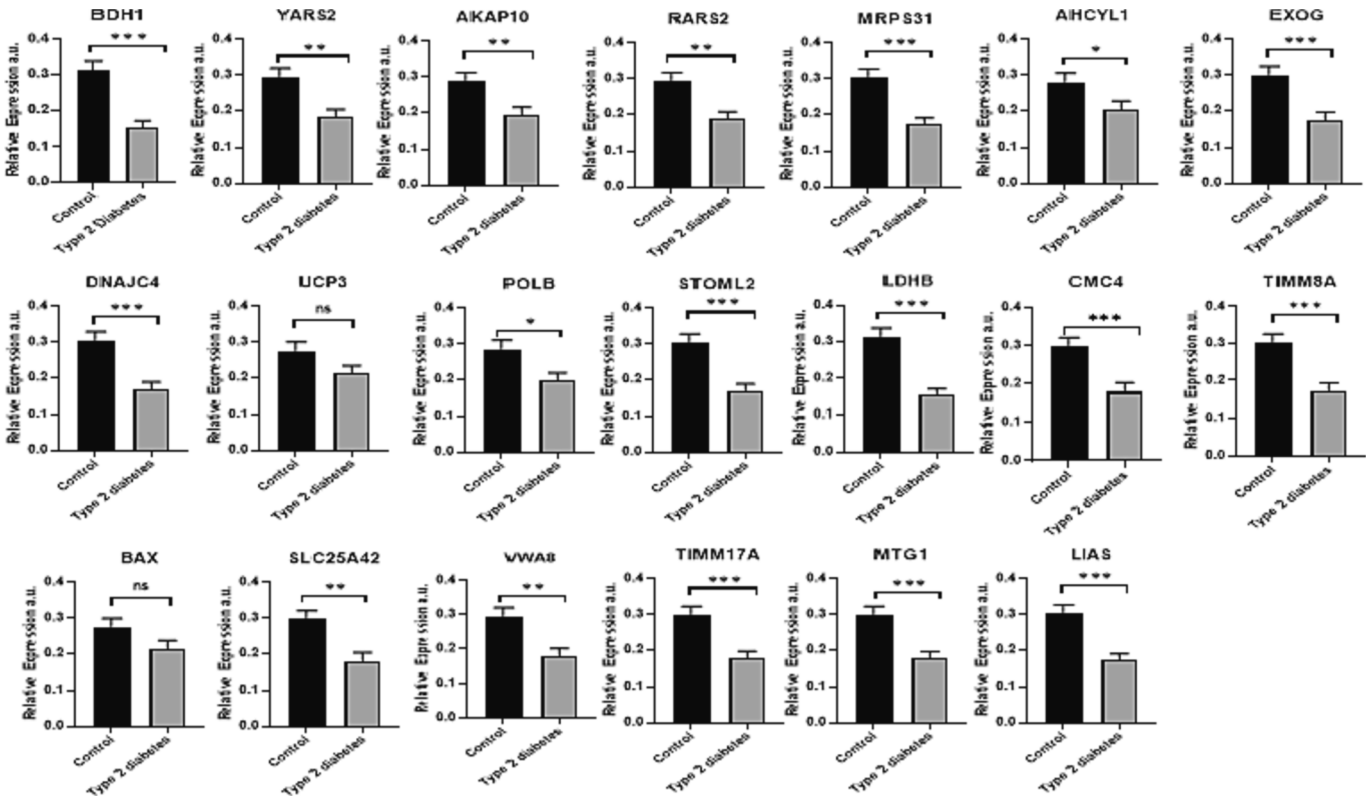

Fig. 5. Each bar graph represents the expression of the identified mitochondrial gene after applying the machine learning framework from the combined dataset. SEM (standard error mean) has been plotted for each gene. For statistical significanc, a cut-off level of 0.05 was set for the p value. p value < 0.05: *; p value < 0.01: **; p value < 0.001: ***; and n.s.: not significant.

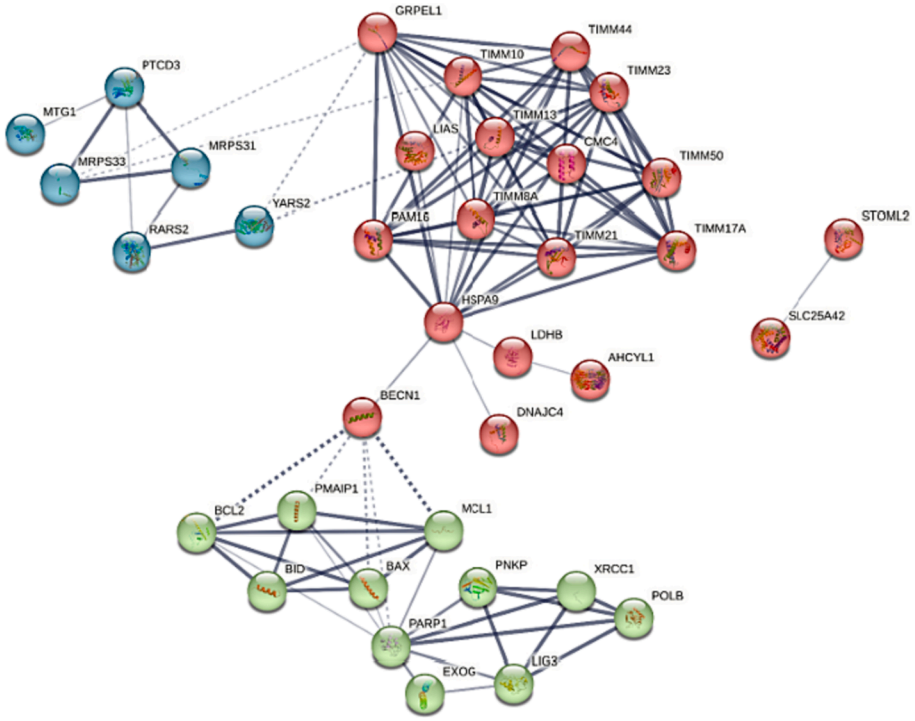

Fig. 6. The protein–protein interactions (PPIs) network is built using String database with the identified mitochondrial genes as SHAP features. Three clusters were identified within this network by applying k-means clustering: red cluster, green cluster, and blue cluster. (For interpretation of the references to color in this figure legend, the reader is referred to the web version of this article.)

Table 3
Functional enrichment analysis of the identified key genes from SHAP values (GO ontology).

Biological Processes			
#term ID	**term description**	**p-value**	**matching proteins in network (labels)**
GO:0072655	Establishment of protein localization to mitochondrion	1.48E-15	TIMM21,TIMM13, TIMM10,GRPEL1, TIMM44,BAX,PAM16, BID,PMAIP1, TIMM17A,TIMM50, TIMM23
GO:0006839	Mitochondrial transport	2.00E-15	TIMM21,TIMM13, TIMM10,GRPEL1, TIMM44,BAX,PAM16, BID,UCP3,PMAIP1, STOML2,TIMM17A, BCL2,TIMM50, TIMM23
GO:0007005	Mitochondrion organization	2.00E-15	TIMM21,TIMM13, TIMM10,GRPEL1, TIMM44,BAX,HSPA9, PAM16,BID,PMAIP1, STOML2,BECN1, PARP1,TIMM17A, LIG3,BCL2,TIMM50, TIMM23
GO:0006626	Protein targeting to mitochondrion	1.84E-13	TIMM21,TIMM13, TIMM10,GRPEL1, TIMM44,PAM16,BID, TIMM17A,TIMM50, TIMM23
GO:0030150	Protein import into mitochondrial matrix	1.16E-10	TIMM21,GRPEL1, TIMM44,PAM16, TIMM17A,TIMM50, TIMM23
GO:1990542	Mitochondrial transmembrane transport	1.02E-09	TIMM21,GRPEL1, TIMM44,PAM16, UCP3,STOML2, TIMM17A,TIMM50, TIMM23
GO:0071806	Protein transmembrane transport	1.55E-09	TIMM21,GRPEL1, TIMM44,PAM16, TIMM17A,MCL1, TIMM50,TIMM23
GO:0007006	Mitochondrial membrane organization	4.97E-07	TIMM13,TIMM10, BAX,HSPA9,BID, PMAIP1,BCL2, TIMM50
GO:0001836	Release of cytochrome *c* from mitochondria	2.11E-06	BAX,BID,PMAIP1, BCL2,TIMM50
GO:2001244	Positive regulation of intrinsic apoptotic signaling pathway	3.47E-06	BAX,BID,PMAIP1, BECN1,MCL1,BCL2
GO:0006886	Intracellular protein transport	4.67E-06	TIMM21,TIMM13, TIMM10,GRPEL1, TIMM44,BAX,HSPA9, PAM16,BID,PMAIP1, TIMM17A,AHCYL1, TIMM50,TIMM23
GO:0015031	Protein transport	1.05E-05	TIMM21,TIMM13, TIMM10,GRPEL1, TIMM44,BAX,HSPA9, PAM16,BID,PMAIP1, TIMM17A,MCL1, AHCYL1,TIMM8A, TIMM50,TIMM23
GO:0051881	Regulation of mitochondrial membrane potential	1.05E-05	BAX,BID,PMAIP1, STOML2,PARP1,BCL2
GO:0046907	Intracellular transport	1.27E-05	TIMM21,TIMM13, TIMM10,GRPEL1, TIMM44,BAX,HSPA9, PAM16,BID,PMAIP1, STOML2,BECN1, TIMM17A,AHCYL1, TIMM50,TIMM23
GO:0071705	Nitrogen compound transport	1.76E-05	TIMM21,TIMM13, TIMM10,GRPEL1, TIMM44,BAX,HSPA9, PAM16,BID,PMAIP1, SLC25A42,TIMM17A, MCL1,AHCYL1, TIMM8A,TIMM50, TIMM23
GO:2001242	Regulation of intrinsic apoptotic signaling pathway	2.45E-05	BAX,BID,PMAIP1, BECN1,PARP1,MCL1, BCL2
GO:0006288	Base-excision repair, DNA ligation	7.46E-05	XRCC1,POLB,LIG3
GO:0051204	Protein insertion into mitochondrial membrane	8.07E-05	TIMM13,TIMM10, BAX,PMAIP1
GO:0008104	Protein localization	0.00015	TIMM21,TIMM13, AKAP10,TIMM10, GRPEL1,TIMM44,BAX, HSPA9,PAM16,BID, PMAIP1,TIMM17A, MCL1,AHCYL1, TIMM8A,TIMM50, TIMM23
GO:2001020	Regulation of response to DNA damage stimulus	0.00016	XRCC1,BID,PNKP, PMAIP1,PARP1,MCL1, BCL2
GO:0071702	Organic substance transport	0.00017	TIMM21,TIMM13, TIMM10,GRPEL1, TIMM44,BAX,HSPA9, PAM16,BID,PMAIP1, SLC25A42,TIMM17A, MCL1,AHCYL1, TIMM8A,TIMM50, TIMM23
GO:0033036	Macromolecule localization	0.00019	TIMM21,TIMM13, AKAP10,TIMM10, GRPEL1,TIMM44,BAX, HSPA9,PAM16,BID, PMAIP1,STOML2, TIMM17A,MCL1, AHCYL1,TIMM8A, TIMM50,TIMM23
GO:0055085	Transmembrane transport	0.00046	TIMM21,GRPEL1, TIMM44,BAX,PAM16, UCP3,SLC25A42, STOML2,TIMM17A, MCL1,BCL2,TIMM50, TIMM23
GO:1901030	Positive regulation of mitochondrial outer membrane permeabilization involved in apoptotic signaling pathway	0.00051	BAX,BID,PMAIP1, BCL2
GO:2001233	Regulation of apoptotic signaling pathway	0.00058	BAX,PAM16,BID, PMAIP1,BECN1, PARP1,MCL1,BCL2
GO:0097190	Apoptotic signaling pathway	0.00061	POLB,BAX,BID, PMAIP1,MCL1,BCL2, TIMM50
GO:0072321	Chaperone-mediated protein transport	0.00082	TIMM13,TIMM10, TIMM8A
GO:0051402	Neuron apoptotic process	0.00091	POLB,BAX,BID,BCL2
GO:0006974	Cellular response to DNA damage stimulus	0.00097	XRCC1,POLB,BAX, BID,PNKP,PMAIP1, PARP1,MCL1,LIG3, BCL2
GO:0032543	Mitochondrial translation	0.0011	PTCD3,MRPS31, YARS2,RARS2, MRPS33
GO:0090199	Regulation of release of cytochrome *c* from mitochondria	0.0011	BAX,PAM16,BID, PMAIP1

(*continued on next page*)

Table 3 (*continued*)

Biological Processes			
#term ID	**term description**	**p-value**	**matching proteins in network (labels)**
GO:0097345	Mitochondrial outer membrane permeabilization	0.0016	BAX,BID,PMAIP1
GO:0010332	Response to gamma radiation	0.0018	POLB,BAX,PARP1, BCL2
GO:0006915	Apoptotic process	0.0028	POLB,EXOG,BAX,BID, PMAIP1,BECN1, PARP1,MCL1,BCL2, TIMM50
GO:0006996	Organelle organization	0.0031	TIMM21,TIMM13, TIMM10,XRCC1, GRPEL1,TIMM44,BAX, HSPA9,PAM16,BID, PMAIP1,STOML2, BECN1,PARP1, TIMM17A,LIG3,BCL2, TIMM50,TIMM23
GO:0008630	Intrinsic apoptotic signaling pathway in response to DNA damage	0.0034	POLB,BAX,MCL1,BCL2
GO:0097193	Intrinsic apoptotic signaling pathway	0.0034	POLB,BAX,PMAIP1, MCL1,BCL2
GO:0033554	Cellular response to stress	0.0047	XRCC1,POLB,BAX, HSPA9,BID,PNKP, PMAIP1,STOML2, BECN1,PARP1,MCL1, LIG3,BCL2
GO:1903518	Positive regulation of single strand break repair	0.0047	XRCC1,PARP1
GO:0006810	Transport	0.0055	TIMM21,TIMM13, TIMM10,GRPEL1, TIMM44,BAX,HSPA9, PAM16,BID,UCP3, PMAIP1,SLC25A42, STOML2,BECN1, TIMM17A,MCL1, AHCYL1,TIMM8A, BCL2,TIMM50, TIMM23
GO:1900740	Positive regulation of protein insertion into mitochondrial membrane involved in apoptotic signaling pathway	0.0057	BID,PMAIP1,BCL2
GO:0090200	Positive regulation of release of cytochrome *c* from mitochondria	0.0061	BAX,BID,PMAIP1
GO:0006808	Regulation of nitrogen utilization	0.0071	BAX,BCL2
GO:0010836	Negative regulation of protein ADP-ribosylation	0.0071	XRCC1,PNKP
GO:0090296	Regulation of mitochondrial DNA replication	0.0071	STOML2,LIG3
GO:0010821	Regulation of mitochondrion organization	0.0086	BAX,PAM16,BID, PMAIP1,BCL2
GO:0043029	T cell homeostasis	0.0092	BAX,PMAIP1,BCL2
GO:0097191	Extrinsic apoptotic signaling pathway	0.0092	BAX,BID,MCL1,BCL2
GO:0008625	Extrinsic apoptotic signaling pathway via death domain receptors	0.0098	BAX,BID,BCL2
GO:0048872	Homeostasis of number of cells	0.0098	POLB,BAX,HSPA9, PMAIP1,BCL2
GO:0097192	Extrinsic apoptotic signaling pathway in absence of ligand	0.0098	BAX,MCL1,BCL2
GO:2001022	Positive regulation of response to DNA damage stimulus	0.0108	XRCC1,PNKP,PMAIP1, PARP1
GO:0016043	Cellular component organization	0.0118	TIMM21,TIMM13, PTCD3,TIMM10, XRCC1,GRPEL1, TIMM44,EXOG,BAX, HSPA9,MRPS31, PAM16,BID,PMAIP1, STOML2,BECN1, PARP1,TIMM17A, LIG3,MRPS33,BCL2, TIMM50,TIMM23
GO:0006289	Nucleotide-excision repair	0.0126	XRCC1,PNKP,PARP1, LIG3
GO:0042149	Cellular response to glucose starvation	0.0149	PMAIP1,BECN1,BCL2
GO:0043504	Mitochondrial DNA repair	0.0156	PARP1,LIG3
GO:0080135	Regulation of cellular response to stress	0.0156	XRCC1,BAX,BID, PNKP,PMAIP1,PARP1, MCL1,BCL2
GO:2001234	Negative regulation of apoptotic signaling pathway	0.0158	BAX,PAM16,BID, MCL1,BCL2
GO:0001844	Protein insertion into mitochondrial membrane involved in apoptotic signaling pathway	0.019	BAX,PMAIP1
GO:0006979	Response to oxidative stress	0.019	LIAS,XRCC1,PNKP, UCP3,PARP1,BCL2
GO:0007007	Inner mitochondrial membrane organization	0.0197	TIMM13,TIMM10, HSPA9
GO:0044271	Cellular nitrogen compound biosynthetic process	0.0227	PTCD3,POLB,BAX, MRPS31,YARS2,PNKP, STOML2,PARP1, RARS2,LIG3,MRPS33
GO:0045039	Protein insertion into mitochondrial inner membrane	0.0228	TIMM13,TIMM10
GO:1903376	Regulation of oxidative stress-induced neuron intrinsic apoptotic signaling pathway	0.0228	PARP1,MCL1
GO:0048087	Positive regulation of developmental pigmentation	0.0266	BAX,BCL2
GO:0090150	Establishment of protein localization to membrane	0.0266	TIMM13,TIMM10, BAX,BID,PMAIP1
GO:0006950	Response to stress	0.029	AKAP10,LIAS,XRCC1, POLB,BAX,HSPA9,BID, PNKP,UCP3,PMAIP1, STOML2,BECN1, PARP1,MCL1,LIG3, BCL2,DNAJC4
GO:0010918	Positive regulation of mitochondrial membrane potential	0.0352	BID,STOML2
GO:2001236	Regulation of extrinsic apoptotic signaling pathway	0.039	BID,PMAIP1,MCL1, BCL2
GO:1902510	Regulation of apoptotic DNA fragmentation	0.0403	BAX,PAM16
GO:0010917	Negative regulation of mitochondrial membrane potential	0.0456	BAX,PMAIP1
GO:0051179	Localization	0.0456	TIMM21,TIMM13, AKAP10,TIMM10, GRPEL1,TIMM44,BAX, HSPA9,PAM16,BID, UCP3,PMAIP1, SLC25A42,STOML2, BECN1,TIMM17A, MCL1,AHCYL1, TIMM8A,BCL2, TIMM50,TIMM23
GO:0045739	Positive regulation of DNA repair	0.0494	XRCC1,PNKP,PARP1
Molecular Processes			
#term ID	**term description**	**p-value**	**matching proteins in network (labels)**
GO:0051434	BH3 domain binding	0.0021	BAX,MCL1,BCL2
GO:0008320	Protein transmembrane transporter activity	0.0095	TIMM17A,MCL1, TIMM23

(*continued on next page*)

Table 3 (*continued*)

Biological Processes			
#term ID	**term description**	**p-value**	**matching proteins in network (labels)**
GO:0051087	Chaperone binding	0.0286	TIMM10,GRPEL1, TIMM44,BAX
GO:0015450	P-P-bond-hydrolysis-driven protein transmembrane transporter activity	0.0406	TIMM17A,TIMM23
Cellular Components			
#term ID	**term description**	**p-value**	**matching proteins in network (labels)**
GO:0005739	Mitochondrion	1.16E-29	TIMM21,TIMM13, AKAP10,PTCD3, TIMM10,LIAS, GRPEL1,TIMM44, EXOG,BAX,HSPA9, MRPS31,PAM16,BID, YARS2,MTG1,PNKP, UCP3,PMAIP1, SLC25A42,STOML2, BECN1,PARP1, TIMM17A,MCL1, CMC4,RARS2, TIMM8A,LIG3,VWA8, BDH1,MRPS33,BCL2, TIMM50,TIMM23
GO:0005740	Mitochondrial envelope	9.81E-26	TIMM21,TIMM13, PTCD3,TIMM10, GRPEL1,TIMM44, EXOG,BAX,HSPA9, MRPS31,PAM16,BID, MTG1,UCP3,PMAIP1, SLC25A42,STOML2, BECN1,TIMM17A, MCL1,CMC4,TIMM8A, BDH1,MRPS33,BCL2, TIMM50,TIMM23
GO:0031966	Mitochondrial membrane	6.83E-25	TIMM21,TIMM13, PTCD3,TIMM10, GRPEL1,TIMM44, EXOG,BAX,HSPA9, MRPS31,PAM16,BID, MTG1,UCP3,PMAIP1, SLC25A42,STOML2, BECN1,TIMM17A, MCL1,TIMM8A,BDH1, MRPS33,BCL2, TIMM50,TIMM23
GO:0031967	Organelle envelope	2.33E-22	TIMM21,TIMM13, PTCD3,TIMM10, GRPEL1,TIMM44, EXOG,BAX,HSPA9, MRPS31,PAM16,BID, MTG1,UCP3,PMAIP1, SLC25A42,STOML2, BECN1,PARP1, TIMM17A,MCL1, CMC4,TIMM8A,BDH1, MRPS33,BCL2, TIMM50,TIMM23
GO:0005743	Mitochondrial inner membrane	8.26E-18	TIMM21,TIMM13, PTCD3,TIMM10, GRPEL1,TIMM44, EXOG,MRPS31, PAM16,MTG1,UCP3, SLC25A42,STOML2, TIMM17A,TIMM8A, BDH1,MRPS33, TIMM50,TIMM23
GO:0005744	TIM23 mitochondrial import inner membrane translocase complex	2.04E-12	TIMM21,TIMM10, GRPEL1,PAM16, TIMM17A,TIMM50, TIMM23
GO:0098798	Mitochondrial protein complex	3.25E-11	TIMM21,TIMM13, TIMM10,GRPEL1,BAX, HSPA9,MRPS31, PAM16,TIMM17A, MRPS33,TIMM50, TIMM23
GO:0031090	Organelle membrane	1.73E-09	TIMM21,TIMM13, PTCD3,TIMM10, GRPEL1,TIMM44, EXOG,BAX,HSPA9, MRPS31,PAM16,BID, MTG1,UCP3,PMAIP1, SLC25A42,STOML2, BECN1,TIMM17A, MCL1,AHCYL1, TIMM8A,BDH1, MRPS33,BCL2, TIMM50,TIMM23
GO:0005759	Mitochondrial matrix	3.94E-07	LIAS,GRPEL1, TIMM44,HSPA9, MRPS31,PAM16, YARS2,MTG1,RARS2, BDH1,MRPS33
GO:0005758	Mitochondrial intermembrane space	2.85E-06	TIMM13,TIMM10, STOML2,CMC4, TIMM8A,TIMM23
GO:0005737	Cytoplasm	2.25E-05	TIMM21,TIMM13, AKAP10,PTCD3, TIMM10,LIAS, GRPEL1,POLB, TIMM44,EXOG,BAX, HSPA9,MRPS31, PAM16,BID,YARS2, MTG1,PNKP,UCP3, PMAIP1,SLC25A42, STOML2,BECN1, PARP1,TIMM17A, MCL1,CMC4,RARS2, AHCYL1,TIMM8A, LIG3,VWA8,BDH1, MRPS33,LDHB,BCL2, TIMM50,TIMM23
GO:0043231	Intracellular membrane-bounded organelle	2.67E-05	TIMM21,TIMM13, AKAP10,PTCD3, TIMM10,LIAS,XRCC1, GRPEL1,POLB, TIMM44,EXOG,BAX, HSPA9,MRPS31, PAM16,BID,YARS2, MTG1,PNKP,UCP3, PMAIP1,SLC25A42, STOML2,BECN1, PARP1,TIMM17A, MCL1,CMC4,RARS2, TIMM8A,LIG3,VWA8, BDH1,MRPS33,BCL2, TIMM50,TIMM23
GO:0043227	Membrane-bounded organelle	3.19E-05	TIMM21,TIMM13, AKAP10,PTCD3, TIMM10,LIAS,XRCC1, GRPEL1,POLB, TIMM44,EXOG,BAX, HSPA9,MRPS31, PAM16,BID,YARS2, MTG1,PNKP,UCP3, PMAIP1,SLC25A42, STOML2,BECN1, PARP1,TIMM17A, MCL1,CMC4,RARS2, AHCYL1,TIMM8A, LIG3,VWA8,BDH1, MRPS33,LDHB,BCL2, TIMM50,TIMM23
GO:0070013	Intracellular organelle lumen	0.0001	TIMM13,PTCD3, TIMM10,LIAS,XRCC1, GRPEL1,POLB,

(*continued on next page*)

Table 3 (*continued*)

Biological Processes			
#term ID	**term description**	**p-value**	**matching proteins in network (labels)**
			TIMM44,HSPA9, MRPS31,PAM16, YARS2,MTG1,PNKP, STOML2,PARP1, TIMM17A,MCL1, CMC4,RARS2, TIMM8A,LIG3,BDH1, MRPS33,BCL2, TIMM50,TIMM23
GO:0005741	Mitochondrial outer membrane	0.00024	BAX,HSPA9,BID, PMAIP1,MCL1,BCL2
GO:0098796	Membrane protein complex	0.00089	TIMM21,TIMM10, GRPEL1,BAX,HSPA9, PAM16,BECN1, TIMM17A,BCL2, TIMM50,TIMM23
GO:0016020	Membrane	0.00092	TIMM21,TIMM13, AKAP10,PTCD3, TIMM10,GRPEL1, TIMM44,EXOG,BAX, HSPA9,MRPS31, PAM16,BID,MTG1, PNKP,UCP3,PMAIP1, SLC25A42,STOML2, BECN1,PARP1, TIMM17A,MCL1, AHCYL1,TIMM8A, BDH1,MRPS33,LDHB, BCL2,DNAJC4, TIMM50,TIMM23
GO:0005622	Intracellular	0.0033	TIMM21,TIMM13, AKAP10,PTCD3, TIMM10,LIAS,XRCC1, GRPEL1,POLB, TIMM44,EXOG,BAX, HSPA9,MRPS31, PAM16,BID,YARS2, MTG1,PNKP,UCP3, PMAIP1,SLC25A42, STOML2,BECN1, PARP1,TIMM17A, MCL1,CMC4,RARS2, AHCYL1,TIMM8A, LIG3,VWA8,BDH1, MRPS33,LDHB,BCL2, TIMM50,TIMM23

apoptosis.. It can start when damaged mitochondria release apoptosis signaling components and which would then affect insulin secretion (Prasun, 2020). These dysfunctions aid in insulin resistance, as well as decrease insulin secretion. The understanding and treatment of these mitochondrial-related problems is an active field of research in the management and prevention of diabetes. The PPI network was primarily enriched mainly in four significant molecular functions such as BH3 domain binding, protein transmembrane transporter activity, Chaperone binding, and P-P-bond-hydrolysis-driven protein transmembrane transporter activity. BH3 protein binding to BAD and BCL decreases the threshold for apoptosis to occur and inhibits the action of anti-apoptotic proteins in type 2 diabetes (Tomita, 2016). Rest of the processes are involved in protein transport and solute transport across ATP synthase. Pathway enrichment analysis (KEGG) from the network showed that 'apoptosis' is the most significantly enriched pathway both in humans and multiple species in type 2 diabetes. Base excision repair, platinum drug resistance, and p53 signaling pathways were also among others as given in Table 4.

Table 4
Pathway enrichment analysis of the identified key genes from SHAP values (KEGG Pathway).

#term ID	term description	p-value	Genes
hsa04215	Apoptosis - multiple species	2.84E-06	BAX,BID,PMAIP1,BECN1, BCL2
hsa04210	Apoptosis	5.77E-05	BAX,BID,PMAIP1,PARP1, MCL1,BCL2
hsa03410	Base excision repair	0.0001	XRCC1,POLB,PARP1,LIG3
hsa01524	Platinum drug resistance	0.0013	BAX,BID,PMAIP1,BCL2
hsa04115	p53 signaling pathway	0.0013	BAX,BID,PMAIP1,BCL2
hsa04217	Necroptosis	0.0147	BAX,BID,PARP1,BCL2
hsa05152	Tuberculosis	0.0196	BAX,HSPA9,BID,BCL2
hsa05210	Colorectal cancer	0.0291	BAX,PMAIP1,BCL2

3.5. Identification of miRNA through integrated mRNA-miRNA network in skeletal muscle of type 2 diabetes

Understanding the variables influencing gene expression variations is essential for the precise molecular pathophysiology of complex diseases like type 2 diabetes. There have been numerous reports of altered miRNA and target expressions in type 2 diabetes. Hence, we constructed the potential miRNA network of the SHAP features using miRNET 2.0 database. All 20 genes from Fig. 4B were mapped against the human reference database. As a result, the constructed network has 463 miRNA nodes and 19 gene nodes with a total of 717 edges (interactions) as shown in Fig. 7. Multiple targets were found to be controlled by different miRNAs. TIMM8A, AKAP10, TIMM17A, BAX, and LIAS have the highest number of interactions in the network. miR-375, miR-30a-5p, miR-16-5p, miR-129-5p, miR-1229-3p and miR-1224-3p have the most significant interactions with high number of targets as depicted in Fig. 8A. Further analysis based on the strong literature evidence using Mienturnet database showed in Fig. 8B, miR-375, miR-766-3p, miR-298, and miR-24-3p have high number of interactions. miR-375 and miR-298 and several other miRNAs are similar to the miRNA-mRNA network constructed previously. Also, BAX which regulate the mitochondrial apoptosis signaling is targeted by several miRNAs as shown by the Fig. 8B. Previously, we have shown that miR-128 targets BAX and is an endogenous regulator of apoptotic signaling pathway in HEK cells (Adlakha and Saini, 2011). In another study, we have shown the mitochondrial biogenesis and function is inhibited by miR-128 in the model skeletal muscle cells (Sharma et al., 2021).

4. Discussion

Insulin resistance, activated inflammation, and elevated oxidative stress are typical symptoms of type 2 diabetes. These pathways lead to mitochondrial dysfunction and protein degradation, which poses a great threat to the health of skeletal muscle tissue including muscular mass, strength, quality, and function (Huang et al., 2022). A pro-inflammatory state such as type 2 diabetes generally leads to an imbalance in redox-sensitive events. Both cytoplasmic and mitochondrial pathways are responsible for ROS in the disease. The pathogenesis of type 2 diabetes is significantly influenced by mitochondrial dysfunction in the target organs like skeletal muscle cells. Alterations in mitochondrial bioenergetics have been linked to poor glucose and fatty acid metabolism because ATP is essential for the creation and release of insulin (Patti and Corvera, 2010; Grubelnik et al., 2010). We have used machine learning as a systems biology technique to assess and predict genetic components in type 2 diabetes compared to control. BMI (Body Mass Index) has lately been recognized by Owusu Adjah et al. as a risk factor for identifying the propensity of an ethnic group. In particular, a non-linear association exists between BMI and a higher prevalence of diabetes mellitus; some people, such as those in South Asia, are predisposed to the condition even at lower BMIs (Owusu Adjah et al., 2018). Our study used the

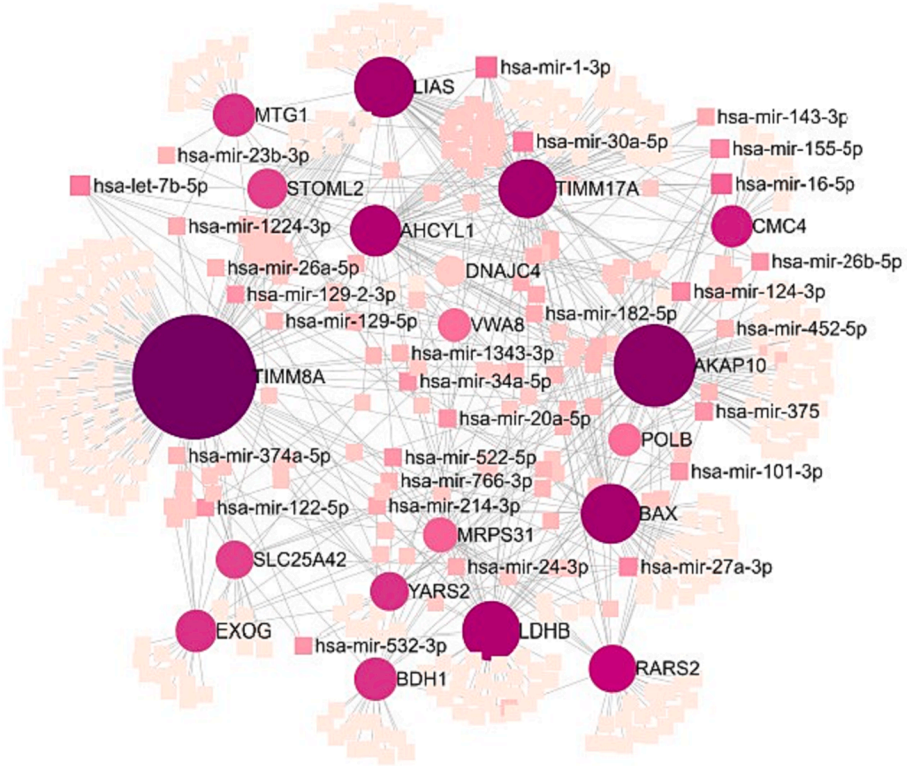

Fig. 7. miRNA-mRNA interaction of top 20 mitochondrial gene altered in skeletal muscle of type 2 diabetic patients.

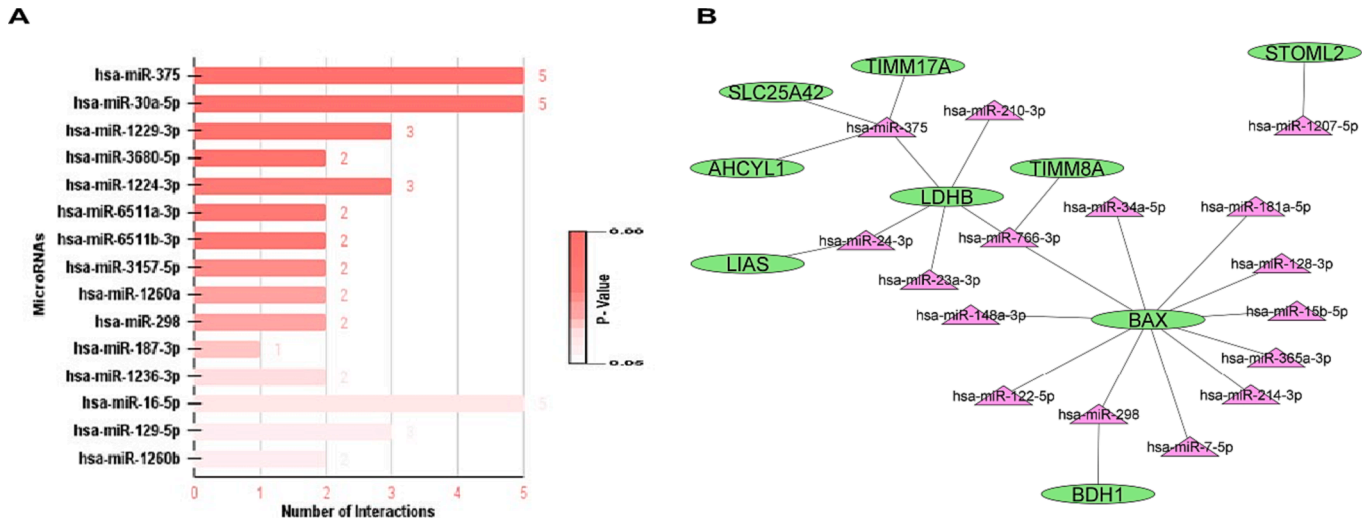

Fig. 8. (A) Significant miRNAs after the enrichment analysis are represented by a bar plot, displaying the number of its target genes. The bars color corresponds to the p-values. (B) This network represents the mRNA-miRNA interaction based on strong literature evidence is visualized using Cytoscpe.

authoritative mitochondrial proteome database MitoCarta 3.0 for the first time to identify mitochondria-related genes from the skeletal muscle expression data of 107 control patients and 70 type 2 diabetes patients. Altogether, we have identified 409 mitochondrial genes in the combined expression dataset. On the other hand, we want to point out the limitation of the study due to the difference in gene coverage by the platforms used or by experimental variations, we could have overlooked the expression of relevant mRNAs in the study. In order to confirm the validity of the conclusions reached from our study despite the differing platforms and expression of the genes, we have confirmed our findings with previously published literature. We found that there was a significant degree of consistency with the data that had been previously reported.

After applying SHAP values to quantify the machine learning predictions, the top 20 genes were finally determined as shown in Fig. 4. Results were compared before and after applying the SHAP values. The accuracy was similar in both the cases, indicating that the identified genes using feature values are equally consistent for making a prediction and provide valuable insights. Literature search using PubMed gave us clues towards involvement of the genes. Svensson et al., showed that the mitochondria of non-hepatic organs use ketone bodies, which are significant metabolic fuels produced, and that patient's skeletal muscle had lower levels of BDH1, an essential catalyst of ketone metabolism (Svensson et al., 2016; Barberio et al., 2021). YARS2 and RARS2 encode

enzymes involved in protein synthesis whereas STOML2 controls the development of mitochondrial cristae, POLB takes a role in DNA repair, and UCP3 decouples oxidative phosphorylation. The cytochrome *c* oxidase assembly process is assisted by CMC4, pyruvate metabolism is facilitated by LDHB, and disorders of the mitochondria are linked to TIMM8A. BAX regulates mitochondrial cytochrome *c* release leading to the process of apoptosis.

Next, using the String database, protein–protein interaction network was analyzed to determine the influence of top 20 genes, for both their regulation and involvement in type 2 diabetes. The KEGG pathway enrichment analysis was used to identify the pathways for base excision repair, platinum drug resistance, and p53 signaling from the protein–-protein interaction network. The base excision repair pathway is involved in DNA damage repair caused by oxidative stress due to excessive nutrients in type 2 diabetes. The development and progression of diabetes could also be accelerated by impaired base excision repair activity, which may also contribute to genomic instability. Moreover, different tissues have shown disruption of the p53 signaling pathway in type 2 diabetes. Pancreatic beta-cell function, glucose metabolism, and insulin signaling can all be affected by altered p53 activity, which can therefore influence insulin resistance and disease development.

The miRNAs are small RNAs generally single-stranded, non-coding, that are highly conserved and 18 to 25 nucleotide long. They can control gene expression by preventing the translation of their target mRNAs or decreasing their post-transcriptional stability. Studies have intensively revealed that miRNAs, which are crucial regulators in malignancies and metabolic disorders, can control one-third of the human genome. We found several miRNAs like miR-375, miR-30a-5p, miR-16-5p, miR-129-5p, miR-1229-3p, and miR-1224-3p to be significant regulating factors in the homeostasis of skeletal muscle tissue in type 2 diabetes. Zebrafish pancreatic development has been linked to the pancreatic islet alpha and beta cell number regulation by miR-375 (Poy et al., 2009). MiR-375 can inhibit myotrophin (Mtpn), which reduces insulin secretion, and inhibit the expression of pyruvate dehydrogenase kinase 1 (PDK1), which is involved in glucose metabolism (El et al., 2008). Recent study by Chigusa Higuchi et al., states that in comparison to control mice model, the levels of miR-375 are much higher in serum of type 2 diabetes mice model (Higuchi et al., 2015). Whereas inhibition of Beta 2/neurogenic differentiation D1 (BETA2/NeuroD) gene, miR-30a-5p has been discovered to be associated with ß-cell malfunction in the pancreas, resulting in glucotoxicity. Since newly diagnosed T2DM patients had higher levels of this miRNA in the first year following diagnosis compared to non-diabetic individuals (Weale et al., 2021). Furthermore, in gestational diabetes, there was a favorable correlation between miR-16-5p and insulin resistance. In animal models and in vitro mechanistic studies, miR-16-5p has at least 24 additional targets in the insulin signaling system, including genes encoding the insulin receptor (INSR), insulin receptor substrate (IRS) proteins 1 and 2, and ak strain transforming (AKT) protein 1 and 3 (Calimlioglu et al., 2015; Hubal et al., 2017; Catanzaro et al., 2021). MiR-129-5p has been linked to diabetes and shown to be elevated, which may be a factor in insulin resistance and beta-cell malfunction by inhibiting the expression of its targets PDX-1 and IRS1. Role of miR-1224-3p in type 2 diabetes is not well understood, further validation can be crucial to processes in controlling skeletal muscle homeostasis. As the topic of miRNA research in T2D is still young, it is vital to recognize that more study is required to confirm the results and establish the clinical value of miRNAs to be considered as a biomarker.

Altogether, for a better understanding of the relationship between characteristics and predictions in type 2 diabetes, machine learning, and the SHAP interpretations to the framework can be employed. By giving each attribute a value based on relevance, the model independent SHAP technique explains why certain predictions were made. Furthermore, SHAP can produce individual-level explanations that demonstrate how genetic features influence the forecast for a specific patient. This level of interpretability can aid physicians and researchers in comprehending the reasoning behind a specific prognosis and gaining knowledge of the disease's underlying causes. It can show unique connections and intricate interactions between variables that could help advance disease research and knowledge in the future.

5. Conclusion

In conclusion, the current study investigates mitochondrial dysfunction in skeletal muscle to shed some light on the molecular mechanisms causing type 2 diabetes. The mitochondrial target genes which are linked to type 2 diabetes were identified by examining gene expression data. XGBoost algorithm and SHAP interpretations were used for the identification. BDH1, YARS2, AKAP10, RARS2, MRPS31, AHCYL1, EXOG, DNAJC4, UCP3, POLB, STOML2, LDHB, CMC4, TIMM8A, BAX, SLC25A42, VWA8, TIMM17A, MTG1, and LIAS are top potential genes involved. These genes play a significant role in many different biological functions such as mitochondrial processes, including transport, structuring, controlling membrane potential, and intrinsic apoptotic signaling. The dysregulation in these processes in skeletal muscle of individuals with type 2 diabetes gives rise to the possibility that they are playing an important part in the onset and development of the condition. Our study also emphasizes the importance of miRNAs in controlling mitochondrial metabolism in type 2 diabetic patients, including miR-375, miR-30a-5p, miR-16-5p, miR-129-5p, and miR-1229-3p. These deregulated miRNAs could alter the mitochondrial processes seen in the disease, which could be essential in regulating the gene expression. Understanding these molecular pathways and interactions of the identified genes and miRNAs with the help of machine learning model can help us in better understanding of the disease. It may help with the discovery of fresh therapeutic targets and the prospective of new disease biomarkers.

Declaration of competing interest

The authors declare that they have no known competing financial interests or personal relationships that could have appeared to influence the work reported in this paper.

Acknowledgement

Kritika Sharma would like to acknowledge the fellowship from CSIR project "HCP043".

References

Abdul-Ghani, M.A., Sabbah, M., Kher, J., Minuchin, O., Vardi, P., Raz, I., 2006. Different contributions of insulin resistance and beta-cell dysfunction in overweight Israeli Arabs with IFG and IGT. Diabetes Metab. Res. Rev. 22 (2), 126–130. https://doi.org/10.1002/DMRR.595.

Abubaker, J., Tiss, A., Abu-Farha, M., Al-Ghimlas, F., Al-Khairi, I., Baturcam, E., Cherian, P., Elkum, N., Hammad, M., John, J., Kavalakatt, S., Khadir, A., Warsame, S., Dermime, S., Behbehani, K., Dehbi, M., Gallyas, F., 2013. DNAJB3/HSP-40 cochaperone is downregulated in obese humans and is restored by physical exercise. PLoS One 8 (7), e69217. https://doi.org/10.1371/JOURNAL.PONE.0069217.

Abu-Farha, M., Cherian, P., Al-Khairi, I., Tiss, A., Khadir, A., Kavalakatt, S., Warsame, S., Dehbi, M., Behbehani, K., Abubaker, J., 2015. DNAJB3/HSP-40 cochaperone improves insulin signaling and enhances glucose uptake in vitro through JNK repression. Sci. Reports 5 (1). https://doi.org/10.1038/srep14448.

Adlakha, Y.K., Saini, N., 2011. MicroRNA-128 downregulates Bax and induces apoptosis in human embryonic kidney cells. Cell Mol. Life Sci. 68 (8), 1415–1428. https://doi.org/10.1007/S00018-010-0528-Y.

Ando, F., Mori, S., Yui, N., Morimoto, T., Nomura, N., Sohara, E., Rai, T., Sasaki, S., Kondo, Y., Kagechika, H., Uchida, S., 2018. AKAPs-PKA disruptors increase AQP2 activity independently of vasopressin in a model of nephrogenic diabetes insipidus. Nat. Commun. 9 (1) https://doi.org/10.1038/s41467-018-03771-2.

Anguita-Ruiz, A., Segura-Delgado, A., Alcalá, R., Aguilera, C.M., Alcalá-Fdez, J., Althouse, B., 2020. eXplainable Artificial Intelligence (XAI) for the identification of biologically relevant gene expression patterns in longitudinal human studies, insights from obesity research. PLOS Comput. Biol. 16 (4), e1007792. https://doi.org/10.1371/JOURNAL.PCBI.1007792.

Arden, S.D., Roep, B.O., Neophytou, P.I., Usac, E.F., Duinkerken, G., de Vries, R.R., Hutton, J.C., 1996. Imogen 38: a novel 38-kD islet mitochondrial autoantigen recognized by T cells from a newly diagnosed type 1 diabetic patient. J. Clin. Invest. 97 (2), 551–561. https://doi.org/10.1172/JCI118448.

Barberio, M.D., Dohm, G.L., Pories, W.J., et al., 2021. Type 2 diabetes modifies skeletal muscle gene expression response to gastric bypass surgery. Front. Endocrinol. (Lausanne) 12, 1243. https://doi.org/10.3389/FENDO.2021.728593/BIBTEX.

Barrett, T., Wilhite, S.E., Ledoux, P., Evangelista, C., Kim, I.F., Tomashevsky, M., Marshall, K.A., Phillippy, K.H., Sherman, P.M., Holko, M., Yefanov, A., Lee, H., Zhang, N., Robertson, C.L., Serova, N., Davis, S., Soboleva, A., 2013. NCBI GEO: archive for functional genomics data sets—update. Nucleic Acids Res. 41 (D1), D991–D995. https://doi.org/10.1093/NAR/GKS1193.

Calimlioglu, B., Karagoz, K., Sevimoglu, T., Kilic, E., Gov, E., Arga, K.Y., 2015. Tissue-specific molecular biomarker signatures of type 2 diabetes: An integrative analysis of transcriptomics and protein–protein interaction data. OMICS 19 (9), 563–573. https://doi.org/10.1089/OMI.2015.0088.

Catanzaro, G., Filardi, T., Sabato, C., Vacca, A., Migliaccio, S., Morano, S., Ferretti, E., 2021. Tissue and circulating microRNAs as biomarkers of response to obesity treatment strategies. J. Endocrinol. Investig. 44 (6), 1159–1174. https://doi.org/10.1007/S40618-020-01453-9.

Cea, L.A., Vásquez, W., Hernández-Salinas, R., et al., 2023. Skeletal muscle atrophy induced by diabetes is mediated by non-selective channels and prevented by boldine. Biomolecules 13 (4), 708. https://doi.org/10.3390/BIOM13040708/S1.

Chang, L., Xia, J., 2023. MicroRNA Regulatory Network Analysis Using miRNet 2.0. Methods Mol. Biol. 2594, 185–204. https://doi.org/10.1007/978-1-0716-2815-7_14/COVER.

Cordova, C., Muñoz, R., Olivares, R., et al., 2023. HER2 classification in breast cancer cells: A new explainable machine learning application for immunohistochemistry. Oncol. Lett. 25 (2), 1–9. https://doi.org/10.3892/OL.2022.13630/HTML.

Del Vescovo, V., Meier, T., Inga, A., Denti, M.A., Borlak, J., Choi, S., 2013. A cross-platform comparison of affymetrix and agilent microarrays reveals discordant miRNA expression in lung tumors of c-Raf transgenic mice. PLoS One 8 (11), e78870. https://doi.org/10.1371/JOURNAL.PONE.0078870.

Dubé, J.J., Collyer, M.L., Trant, S., Toledo, F.G.S., Goodpaster, B.H., Kershaw, E.E., DeLany, J.P., 2020. Decreased mitochondrial dynamics is associated with insulin resistance, metabolic rate, and fitness in African Americans. J. Clin. Endocrinol. Metab. 105 (4), 1210–1220. https://doi.org/10.1210/CLINEM/DGZ272.

El, O.A., Baroukh, N., Martens, G.A., Lebrun, P., Pipeleers, D., Van Obberghen, E., 2008. miR-375 targets 3′-phosphoinositide–dependent protein kinase-1 and regulates glucose-induced biological responses in pancreatic β-cells. Diabetes 57 (10), 2708–2717. https://doi.org/10.2337/DB07-1614.

Gallagher, I.J., Scheele, C., Keller, P., et al., 2010. Integration of microRNA changes in vivo identifies novel molecular features of muscle insulin resistance in type 2 diabetes. Genome Med. 2 (2), 1–18. https://doi.org/10.1186/GM130/FIGURES/3.

Glovaci, D., Fan, W., Wong, N.D., 2019. Epidemiology of diabetes mellitus and cardiovascular disease. Curr. Cardiol. Rep. 21 (4), 21. https://doi.org/10.1007/S11886-019-1107-Y.

Grindel, A., Guggenberger, B., Eichberger, L., Pöppelmeyer, C., Gschaider, M., Tosevska, A., Mare, G., Briskey, D., Brath, H., Wagner, K.-H., Sánchez-Margalet, V., 2016. Oxidative stress, DNA damage and DNA repair in female patients with diabetes mellitus type 2. PLoS One 11 (9), e0162082. https://doi.org/10.1371/JOURNAL.PONE.0162082.

Grubelnik, V., Zmazek, J., Markovič, R., Gosak, M., Marhl, M., 2010. Mitochondrial dysfunction in pancreatic alpha and beta cells associated with type 2 diabetes mellitus. Life 10 (12), 348. https://doi.org/10.3390/LIFE10120348.

Gupte, A.A., Bomhoff, G.L., Geiger, P.C., 2008. Age-related differences in skeletal muscle insulin signaling: The role of stress kinases and heat shock proteins. J. Appl. Physiol. 105 (3), 839–848. https://doi.org/10.1152/JAPPLPHYSIOL.00148.2008/ASSET/IMAGES/LARGE/ZDG00908812300007.JPEG.

Higuchi, C., Nakatsuka, A., Eguchi, J., Teshigawara, S., Kanzaki, M., Katayama, A., Yamaguchi, S., Takahashi, N., Murakami, K., Ogawa, D., Sasaki, S., Makino, H., Wada, J., 2015. Identification of circulating miR-101, miR-375 and miR-802 as biomarkers for type 2 diabetes. Metabolism 64 (4), 489–497. https://doi.org/10.1016/J.METABOL.2014.12.003.

Hong, J., Luo, Y., Zhang, Y., Ying, J., Xue, W., Xie, T., Tao, L., Zhu, F., 2020. Protein functional annotation of simultaneously improved stability, accuracy and false discovery rate achieved by a sequence-based deep learning. Brief Bioinform. 21 (4), 1437–1447. https://doi.org/10.1093/BIB/BBZ081.

Hong, J., Luo, Y., Mou, M., Fu, J., Zhang, Y., Xue, W., Xie, T., Tao, L., Lou, Y., Zhu, F., 2020. Convolutional neural network-based annotation of bacterial type IV secretion system effectors with enhanced accuracy and reduced false discovery. Brief Bioinform. 21 (5), 1825–1836. https://doi.org/10.1093/BIB/BBZ120.

Huang, S., Xiang, C., Song, Y.i., Singh, K., 2022. Identification of the shared gene signatures and pathways between sarcopenia and type 2 diabetes mellitus. PLoS One 17 (3), e0265221. https://doi.org/10.1371/JOURNAL.PONE.0265221.

Hubal, M.J., Nadler, E.P., Ferrante, S.C., Barberio, M.D., Suh, J.-H., Wang, J., Dohm, G. L., Pories, W.J., Mietus-Snyder, M., Freishtat, R.J., 2017. Circulating adipocyte-derived exosomal MicroRNAs associated with decreased insulin resistance after gastric bypass. Obesity 25 (1), 102–110. https://doi.org/10.1002/OBY.21709.

Jin, W., Goldfine, A.B., Boes, T., Henry, R.R., Ciaraldi, T.P., Kim, E.-Y., Emecan, M., Fitzpatrick, C., Sen, A., Shah, A., Mun, E., Vokes, M., Schroeder, J., Tatro, E., Jimenez-Chillaron, J., Patti, M.-E., 2011. Increased SRF transcriptional activity in human and mouse skeletal muscle is a signature of insulin resistance. J. Clin. Invest. 121 (3), 918–929. https://doi.org/10.1172/JCI41940.

Jornayvaz, F.R., Shulman, G.I., 2010. Regulation of mitochondrial biogenesis. Essays Biochem. 47, 69–84. https://doi.org/10.1042/BSE0470069/78204.

Khin, P.P., Lee, J.H., Jun, H.S., 2023. Pancreatic beta-cell dysfunction in type 2 diabetes. Eur. J. Inflamm. 21. https://doi.org/10.1177/1721727X231154152/ASSET/IMAGES/LARGE/10.1177_1721727X231154152-FIG2.JPEG.

Kotagama, K., McJunkin, K., 2024. Recent advances in understanding microRNA function and regulation in C. elegans. Semin. Cell Dev. Biol. 154, 4–13. https://doi.org/10.1016/J.SEMCDB.2023.03.011.

Kumar, S., Das, A., 2023. Peripheral blood mononuclear cell derived biomarker detection using eXplainable Artificial Intelligence (XAI) provides better diagnosis of breast cancer. Comput. Biol. Chem. 104, 107867 https://doi.org/10.1016/J.COMPBIOLCHEM.2023.107867.

Lecker, S.H., Goldberg, A.L., Mitch, W.E., 2006. Protein degradation by the ubiquitin-proteasome pathway in normal and disease states. J. Am. Soc. Nephrol. 17 (7), 1807–1819. https://doi.org/10.1681/ASN.2006010083.

Leenders, M., Verdijk, L.B., van der Hoeven, L., Adam, J.J., van Kranenburg, J., Nilwik, R., van Loon, L.J.C., 2013. Patients with type 2 diabetes show a greater decline in muscle mass, muscle strength, and functional capacity with aging. J. Am. Med. Dir. Assoc. 14 (8), 585–592. https://doi.org/10.1016/J.JAMDA.2013.02.006.

Li, M.X., Sun, X.M., Cheng, W.G., et al., 2021. Using a machine learning approach to identify key prognostic molecules for esophageal squamous cell carcinoma. BMC Cancer 21 (1), 1–11. https://doi.org/10.1186/S12885-021-08647-1/FIGURES/3.

Licursi, V., Conte, F., Fiscon, G., Paci, P., 2019. MIENTURNET: An interactive web tool for microRNA-target enrichment and network-based analysis. BMC Bioinf. 20 (1), 1–10. https://doi.org/10.1186/S12859-019-3105-X/TABLES/1.

Liu, J., Li, J.i., Li, W.-J., Wang, C.-M., 2013. The role of uncoupling proteins in diabetes mellitus. J. Diabetes Res. 2013, 1–7. https://doi.org/10.1155/2013/585897.

López-Soldado, I., Torres, A.G., Ventura, R., Martínez-Ruiz, I., Díaz-Ramos, A., Planet, E., Cooper, D., Pazderska, A., Wanic, K., O'Hanlon, D., O'Gorman, D.J., Carbonell, T., de Pouplana, L.R., Nolan, J.J., Zorzano, A., Hernández-Alvarez, M.I., 2023. Decreased expression of mitochondrial aminoacyl-tRNA synthetases causes downregulation of OXPHOS subunits in type 2 diabetic muscle. Redox. Biol. 61, 102630. https://doi.org/10.1016/J.REDOX.2023.102630.

Meena, J., Hasija, Y., 2022. Application of explainable artificial intelligence in the identification of Squamous Cell Carcinoma biomarkers. Comput. Biol. Med. 146, 105505 https://doi.org/10.1016/J.COMPBIOMED.2022.105505.

Mitsopoulos, P., Chang, Y.-H., Wai, T., König, T., Dunn, S.D., Langer, T., Madrenas, J., 2015. Stomatin-like protein 2 is required for in vivo mitochondrial respiratory chain supercomplex formation and optimal cell function. Mol. Cell Biol. 35 (10), 1838–1847. https://doi.org/10.1128/MCB.00047-15.

Montgomery, M.K., Turner, N., 2015. Mitochondrial dysfunction and insulin resistance: an update. Endocr. Connect. 4 (1), R1–R15. https://doi.org/10.1530/EC-14-0092.

Moon S, Jang JY, Kim Y, Oh CM. Development and validation of a new diabetes index for the risk classification of present and new-onset diabetes: multicohort study. *Sci Reports 2021 11*. 2021;11(1):1-10. doi:10.1038/s41598-021-95341-8.

Nelson, C.A., Pérez-Chada, L.M., Creadore, A., Li, S.J., Lo, K., Manjaly, P., Pournamdari, A.B., Tkachenko, E., Barbieri, J.S., Ko, J.M., Menon, A.V., Hartman, R. I., Mostaghimi, A., 2020. Patient perspectives on the use of artificial intelligence for skin cancer screening: A qualitative study. JAMA Dermatol. 156 (5), 501. https://doi.org/10.1001/JAMADERMATOL.2019.5014.

Owusu Adjah, E.S., Bellary, S., Hanif, W., Patel, K., Khunti, K., Paul, S.K., 2018. Prevalence and incidence of complications at diagnosis of T2DM and during follow-up by BMI and ethnicity: A matched case-control analysis. Cardiovasc. Diabetol. 17 (1), 1–9. https://doi.org/10.1186/S12933-018-0712-1/FIGURES/2.

Padmalayam, I., Hasham, S., Saxena, U., Pillarisetti, S., 2009. Lipoic Acid Synthase (LASY)A novel role in inflammation, mitochondrial function, and insulin resistance. Diabetes 58 (3), 600–608. https://doi.org/10.2337/DB08-0473.

Painter, H.J., Altenhofen, L.M., Kafsack, B.F.C., Llinás, M., 2013. Whole-genome analysis of Plasmodium spp. Utilizing a new agilent technologies DNA microarray platform. Methods Mol. Biol. 923, 213–219. https://doi.org/10.1007/978-1-62703-026-7_14.

Palsgaard, J., Brøns, C., Friedrichsen, M., Dominguez, H., Jensen, M., Storgaard, H., Spohr, C., Torp-Pedersen, C., Borup, R., De Meyts, P., Vaag, A., Williams, S., 2009. Gene expression in skeletal muscle biopsies from people with type 2 diabetes and relatives: differential regulation of insulin signaling pathways. PLoS One 4 (8), e6575. https://doi.org/10.1371/JOURNAL.PONE.0006575.

Pardo, R., Blasco, N., Vilà, M., Beiroa, D., Nogueiras, R., Cañas, X., Simó, R., Sanchis, D., Villena, J.A., 2016. EndoG knockout mice show increased brown adipocyte recruitment in white adipose tissue and improved glucose homeostasis. Endocrinology 157 (10), 3873–3887. https://doi.org/10.1210/EN.2015-1334.

Patti, M.E., Corvera, S., 2010. The role of mitochondria in the pathogenesis of type 2 diabetes. Endocr. Rev. 31 (3), 364. https://doi.org/10.1210/ER.2009-0027.

Pedregosa F, Varoquaux G, Gramfort A, et al. Scikit-learn: Machine Learning in Python. *J Mach Learn Res*. 2012;12:2825-2830. Accessed June 5, 2023. https://arxiv.org/abs/1201.0490v4.

Poy, M.N., Hausser, J., Trajkovski, M., et al., 2009. miR-375 maintains normal pancreatic α- and β-cell mass. Proc. Natl. Acad. Sci. U. S. A. 106 (14), 5813–5818. https://doi.org/10.1073/PNAS.0810550106/SUPPL_FILE/0810550106SI.PDF.

Prasun, P., 2020. Role of mitochondria in pathogenesis of type 2 diabetes mellitus. J. Diabetes Metab. Disord. 19 (2), 2017–2022. https://doi.org/10.1007/S40200-020-00679-X/METRICS.

Rath, S., Sharma, R., Gupta, R., Ast, T., Chan, C., Durham, T.J., Goodman, R.P., Grabarek, Z., Haas, M.E., Hung, W.H.W., Joshi, P.R., Jourdain, A.A., Kim, S.H., Kotrys, A.V., Lam, S.S., McCoy, J.G., Meisel, J.D., Miranda, M., Panda, A., Patgiri, A., Rogers, R., Sadre, S., Shah, H., Skinner, O.S., To, T.-L., Walker, M., Wang, H., Ward, P.S., Wengrod, J., Yuan, C.-C., Calvo, S.E., Mootha, V.K., 2021. MitoCarta3.0: an updated mitochondrial proteome now with sub-organelle localization and pathway annotations. Nucleic Acids Res. 49 (D1), D1541–D1547.

Savage N. Breaking into the black box of artificial intelligence. *Nature*. Published online March 29, 2022. doi:10.1038/D41586-022-00858-1.

Savas, S., Azorsa, D.O., Jarjanazi, H., Ibrahim-Zada, I., Gonzales, I.M., Arora, S., Henderson, M.C., Choi, Y.H., Briollais, L., Ozcelik, H., Tuzmen, S., Bernhard, E., 2011. NCI60 cancer cell line panel data and RNAi analysis help identify EAF2 as a modulator of simvastatin and lovastatin response in HCT-116 cells. PLoS One 6 (4), e18306. https://doi.org/10.1371/JOURNAL.PONE.0018306.

Schrauwen, P., Mensink, M., Schaart, G., Moonen-Kornips, E., Sels, J.-P., Blaak, E.E., Russell, A.P., Hesselink, M.K.C., 2006. Reduced skeletal muscle uncoupling protein-3 content in prediabetic subjects and type 2 diabetic patients: Restoration by rosiglitazone treatment. J. Clin. Endocrinol. Metab. 91 (4), 1520–1525. https://doi.org/10.1210/JC.2005-1572.

Shannon, P., Markiel, A., Ozier, O., Baliga, N.S., Wang, J.T., Ramage, D., Amin, N., Schwikowski, B., Ideker, T., 2003. Cytoscape: A software Environment for integrated models of biomolecular interaction networks. Genome Res. 13 (11), 2498–2504. https://doi.org/10.1101/GR.1239303.

Sharma, K., Chandra, A., Hasija, Y., Saini, N., 2021. MicroRNA-128 inhibits mitochondrial biogenesis and function via targeting PGC1α and NDUFS4. Mitochondrion 60, 160–169. https://doi.org/10.1016/J.MITO.2021.08.008.

Stumvoll, M., Goldstein, B.J., Van Haeften, T.W., 2005. Type 2 diabetes: principles of pathogenesis and therapy. Lancet (London, England) 365 (9467), 1333–1346. https://doi.org/10.1016/S0140-6736(05)61032-X.

Svensson, K., Albert, V., Cardel, B., Salatino, S., Handschin, C., 2016. Skeletal muscle PGC-1α modulates systemic ketone body homeostasis and ameliorates diabetic hyperketonemia in mice. FASEB J. 30 (5), 1976–1986. https://doi.org/10.1096/FJ.201500128/-/DC1.

Szklarczyk, D., Gable, A.L., Nastou, K.C., Lyon, D., Kirsch, R., Pyysalo, S., Doncheva, N. T., Legeay, M., Fang, T., Bork, P., Jensen, L.J., von Mering, C., 2021. The STRING database in 2021: customizable protein–protein networks, and functional characterization of user-uploaded gene/measurement sets. Nucleic Acids Res. 49 (D1), D605–D612. https://doi.org/10.1093/NAR/GKAA1074.

Thai, P.N., Miller, C.V., King, M.T., Schaefer, S., Veech, R.L., Chiamvimonvat, N., Bers, D. M., Dedkova, E.N., 2021. Ketone ester D-β-hydroxybutyrate-(R)-1,3 butanediol prevents decline in cardiac function in type 2 diabetic mice. J. Am. Heart Assoc. 10 (19) https://doi.org/10.1161/JAHA.120.020729.

Tomita, T., 2016. Apoptosis in pancreatic β-islet cells in Type 2 diabetes. Biomol. Biomed. 16 (3), 162–179. https://doi.org/10.17305/bjbms.2016.919.

Wang, S., Zhao, H., Lin, S., et al., 2023. New therapeutic directions in type II diabetes and its complications: mitochondrial dynamics. Front. Endocrinol. (Lausanne) 14, 1230168. https://doi.org/10.3389/FENDO.2023.1230168/BIBTEX.

Weale, C.J., Matshazi, D.M., Davids, S.F.G., et al., 2021. Expression profiles of circulating microRNAs in South African Type 2 diabetic individuals on treatment. Front. Genet. 12, 1646. https://doi.org/10.3389/FGENE.2021.702410/BIBTEX.

Wu, X., Wang, J., Cui, X., et al., 2007. The effect of insulin on expression of genes and biochemical pathways in human skeletal muscle. Endocrine 31 (1), 5–17. https://doi.org/10.1007/S12020-007-0007-X/METRICS.

Yap, K.H., Yee, G.S., Candasamy, M., Tan, S.C., Md, S., Abdul Majeed, A.B., Bhattamisra, S.K., 2020. Catalpol ameliorates insulin sensitivity and mitochondrial respiration in skeletal muscle of type-2 diabetic mice through insulin signaling pathway and AMPK/SIRT1/PGC-1α/PPAR-γ activation. Biomolecules 10 (10), 1360. https://doi.org/10.3390/BIOM10101360.

Zhu H, Leung S wai. MicroRNA biomarkers of type 2 diabetes: evidence synthesis from meta-analyses and pathway modelling. *Diabetologia*. 2023;66(2):288-299. doi: 10.1007/S00125-022-05809-Z/FIGURES/4.